Simultaneous fluorescence-interference detection for dissecting 2-dimensional protein-protein interactions on membranes

Dissertation

zur Erlangung des Doktorgrades

der Naturwissenschaften

vorgelegt beim Fachbereich

Biochemie, Chemie und Pharmazie

der Johann Wolfgang Goethe-Universität in Frankfurt am Main

von

Martynas Gavutis

Frankfurt, 2005

vom Fachbereich Biochemie, Chemie und Pharmazie der Johann Wolfgang Goethe-Universität als Dissertation angenommen.

Dekan:

1. Gutachter: Dr. Jacob Piehler

2. Gutachter: Prof. Dr. Ernst Bamberg

Datum der Disputation:

Acknowledgements

During my PhD education, I have had the pleasure to work in an interdisciplinary environment within the Institute for Biochemistry. These years have been very challenging, yet rewarding. I have greatly broadened my scientific horizons and have been able to mature into an independent researcher. For this I would like to thank a bunch of people:

First of all, my supervisor Dr. Jacob Piehler who struggled to make me understand the way Chemists and Biochemists think. He always took time to discuss the big and small things even though sometimes no answers were found (or maybe often …). He is always full of new ideas, unfortunately the time is too short to try them all.

This work has also not been possible without excellent contribution from other members of the group. I kindly thank Suman Lata for developing and optimizing membrane tethering protocols, Peter Lamken for different ifnar1-EC constructs, Pia Müller for constant supply of differently labeled IFNα2 mutants, Eva Jaks for purifying large amounts of IFNα2 HEQ mutant.

I thank these and all the other members of the institute for creating a wonderful atmosphere, so that I did not want to leave the lab until the very late evening or the early morning hours. Midnight conversations with Ali Tinazli deserve a special mention.

Finally, I thank Prof. Dr. R.Tampé for the unique infrastructure and scientific environment in his institute.

Table of Contents

1. Summary

Protein-protein interactions within the plane of cellular membranes play a key role for many biological processes and in particular for transmembrane signaling. A prominent example is the ligand-induced crosslinking of cytokine receptors, where 3-dimensional cytokine binding followed by 2-dimensional interaction between the receptor subunits have been recognized to be important for regulating signaling specificity. The fundamental importance of such coupled interactions for cell-surface receptor activation has stimulated numerous theoretical studies, which have hardly been confirmed experimentally. An experimental approach to measure interactions and real time kinetics of type I interferon (IFN) induced assembly between interferon receptor subunits ifnar2 and ifnar1 on membrane was developed and determinants of the 2-dimensional interactions, such as dimensionality, size, valency, orientation, membrane fluidity and receptor density were quantitatively addressed

The C-terminal decahistidine tagged extracellular domains (EC) of ifnar1 and ifnar2 were site- specifically tethered onto solid-supported fluid lipid membrane, which carried covalently attached chelator bis-nitrilotriacetic acid (bis-NTA) groups. Interactions on the lipid bilayer were detected with a novel solid phase detection technique, which allows simultaneous detection of ligand binding to a membrane anchored receptors and lateral interaction between them in the real time. This was achieved by combining two optical techniques: label-free reflectance interferometry (RIf) and total internal reflection fluorescence spectroscopy (TIRFS). Fluorescence signals, in the order of 10 fluorophores/μm^2, were detected without substantial photobleaching. The sensitivity of the label-free interferometric detection was in the range of 10 pg/mm^2. The crosstalk between the two signals was eliminated by means of spectral separation. Fluorescence was detected in the visible region and RIf was performed at 800 nm in the near infrared. Flow through conditions allowed to automate experiments and measure binding events as fast as ~ 5 s^{-1}.

Using this technique we have dissected the interactions involved in IFN-induced ifnar crosslinking. 2-dimensional association and dissociation rate constants were independently determined by tethering high stoichiometric excess of one of the receptor subunits and comparing dissociation of the labelled ligand away from the membrane in the absence and presence of the non-labelled high affinity competitor. Dissociation traces were fitted with the two-step dissociation model: the first step

being the 2-dimensional separation of the ternary complex followed by the 3-dimensional ligand dissociation into solution. Label-free RIf detection allowed absolute parameterization of the 2-dimensional concentrations of the ifnar subunits on the membrane. The TIRFS signal provided high sensitivity of the ligand dissociation and was correlated against the RIf signal before fitting. These features of the detection system allowed us to parameterize the model, and the 2-dimensional association or dissociation rate constants were the only variables during the fitting.

Another FRET based binding assay was developed to determine the 2-dimensional dissociation rate constant using a pulse-chase approach. The donor fluorescence from ifnar2-EC was quenched upon the ternary complex formation with the acceptor-labelled IFN and the nonlabelled ifnar1-EC. The equilibrium was perturbed by rapid tethering of substantial excess of the nonlabelled ifnar2-EC onto the membrane. The exchange of the labelled ifnar2-EC with the nonlabelled one was monitored as the decrease in the FRET signal with the 2-dimensional dissociation of ifnar2-EC from the ternary complex being the rate limiting step.

Based on the several mutants and variants of the interacting proteins, the effect of different rate constants and receptor orientation on the 2-dimensional crosslinking dynamics was studied. We have identified several critical features of the 2-dimensional interactions on membranes, which cannot be readily concluded from the solution binding assays. The restricted rotation and the increased lifetime of the encounter complex due to high membrane viscosity are the main determinants of the 2-dimensional association. Tethering ifnar1-EC to the membrane via N-terminal decahistidine tag decreased the 2-dimensional association rate constant 4-5 fold. Electrostatic attraction and steering, the important mechanism to enhance association rate constant between the soluble proteins, are not pronounced for interactions on the membrane. Protein orientation due to membrane anchoring dominates over electrostatic effects and together with the increased lifetime of the encounter complex consequence that 2-dimensional association rate constants are quite similar and do not correlate with association rate constants in solution. The 2-dimensional dissociation rate constants were generally 2-5-fold lower compared to the corresponding 3-dimensional dissociation rate constants in solution. Possible explanations for this are that long lifetime of the encounter complex stabilizes the ternary complex or that membrane tethering affects the interaction diagram. In conclusion, combined TIRFS-RIf detection turn to be powerful and versatile technique to characterize protein-protein interactions on membranes.

2. Zusammenfassung

Inter-zelluläre Kommunikation basiert häufig auf Liganden, welche selektiv von Rezeptoren auf der Plasmamembran erkannt werden, und durch Wechselwirkung mit diesen Rezeptoren Signaltransduktion im Zytoplasma aktivieren. Die molekularen Mechanismen der Signalvermittlung durch die Membran sind noch wenig verstanden. Die wichtigen Klassen der Zytokinrezeptoren und der Rezeptortyrosinkinasen werden durch Liganden aktiviert, die zu einer Di- oder Oligomerisierung von Rezeptoruntereinheiten führt, welche offenbar für die Aktivierung zytoplasmatischer Effektoren notwendig ist. Diese laterale Interaktion zwischen Rezeptoruntereinheiten lässt sich aus mehreren Gründen nicht mit der Interaktion der Proteine in Lösung vergleichen. Zum einen handelt es sich um eine Wechselwirkung in 2 anstatt von 3 Dimensionen, d.h. die Interaktionspartner haben durch die Verankerung auf der Membrane weniger Freiheitsgrade als in Lösung. Dabei spielt die eingeschränkte Rotation ein besondere Rolle, da sie zu einer Vor-Orientierung der Interaktionspartner führt. Ein weiterer wichtiger Unterschied ist die dramatisch langsamere Diffusion von Membran-verankerten Proteinen im Vergleich zu Proteinen in Lösung. Über die Einflüsse dieser Faktoren auf die Bildung von Proteinkomplexen an der Membran wurde sehr viel spekuliert, aber es liegen bis *dato* kaum systematische experimentelle Untersuchungen vor.

In der vorliegenden Arbeit sollten Detektionsmethoden und Bindungsassays etabliert werden, mit welchen die Gleichgewichtskonstanten und die Ratenkonstanten von Ligand-Rezeptor Interaktionen auf Membranen *in vitro* bestimmt werden können. Als biologisches Testsystem wurde der Typ I Interferonrezeptor gewählt. Typ I Interferone (IFN) sind wichtige Zytokine in der angeborenen Immunabwehr von viralen Infektionen, und haben weitere wichtige Funktionen für die Aktivierung des adaptiven Immunsystems. Interessanterweise binden verschiedene IFN an den gleichen Rezeptor, aber führen zu unterschiedlichen Wirkungsmustern. Diese Unterschiede müssen in der Wechselwirkung mit den Rezeptoruntereinheiten ifnar1 und ifnar2 kodiert sein. Intensive Struktur-Funktions-Untersuchungen konnten keine Unterschiede in der Struktur oder Stöchiometrie der Ligand-Rezeptor Komplexen identifizieren, die durch verschiedene IFN rekrutiert werden. Allerdings unterscheiden sich für verschiedene IFN die Bindungskonstanten und die Ratenkonstanten der Wechselwirkung mit den Rezeptoruntereinheiten außerordentlich. Daher sind vermutlich die Effinzienz der

Rekrutierung der Rezeptoruntereinheiten und die Dynamik des ternären Komplexes von zentraler Bedeutung für die differentielle Wirkung verschiedener IFN. Da der Ligand die beiden Untereinheiten auf der Membran verbrückt, sind hier 2-dimensionale Wechselwirkungen Membran-verankerter Proteine vermutlich die Grundlage unterschiedlicher Wirkung. Um diese Szenario zu emulieren, wurden die extrazellulären Domänen von ifnar1 (ifnar1-EC) und ifnar2 (ifnar2-EC) über C-terminale Histidin-*tags* an Festkörper-unterstützten Membranen mit Chelatorlipiden angebunden. FRAP-Experimente haben gezeigt, dass die so angebundenen Proteine lateral mit einer Geschwindigkeit von ca. 1 μm²/s diffundieren, also ähnlich der (lokalen) Diffusion auf der Plasmamembran.

Zur Untersuchung der Ligand-induzierten Hetero-Dimerisierung von ifnar1-EC und ifnar2-EC auf Festkörper-unterstützten Membranen wurde ein Versuchsaufbau zur simultanen Detektion von Fluoreszenz und von Massenänderungen an Oberflächen implementiert. Dazu wurde die totalinterne Reflexions-Fluoreszenz Spektroskopie (TIRFS) mit der reflektometrischen Interferenzspektroskopie (RIf) kombiniert. TIRFS basiert auf der selektiven Anregung von Oberflächen-nahen Fluorophoren durch das evaneszente Feld, welches bei Totalreflexion an Grenzflächen wenige 100 nm mit dem benachbarten Medium wechselwirkt. Über Faseroptik wurde zusätzlich eine Illuminierung senkrecht zur Transducer-Oberfläche implementiert, über welche die Dicke einer Interferenzschicht reflektometrisch gemessen werden kann. Durch diese Methode können Bindungsereignisse an Oberflächen markierungsfrei quantifiziert werden. Da die Schichtdickenmessung bei 800 nm im NIR Bereich erfolgt, ist sie von der Fluoreszenzmessung im sichtbaren Bereich (500-700 nm) spektral separiert. Die Detektion von Fluoreszenz- und Massenänderungen an der Oberfläche wurde über die Fusion von Vesikeln mit Fluoreszenzmarkierten Lipiden charakterisiert. So konnte gezeigt werden, dass in der Tat beide Signale voneinander unabhängig voneinander und ohne detektierbares Übersprechen detektiert wurden. Das massensensitive Interferenzsignal wurde mittels Vesikelfusion kalibriert, da die dabei entstehende Lipiddoppelschicht eine definierte, reproduzierbare Masse auf der Oberfläche abscheidet. Für die massensensitive Interferenzdetektion ergab sich so ein Detektionslimit von etwa 10 pg/mm². Mittels Fluoreszenzdetektion konnten Oberflächenbeladungen von wenigen Molekülen/μm² detektiert werden. Durch Kombination mit einer automatisierten Fluidik konnten schnelle Injektionsschemata realisiert werden, so dass Ratenkonstanten von bis zu 5 s^{-1} aufgelöst werden konnten.

Diese kombinierte Detektionsmethode wurde zunächst eingesetzt, um die einzelnen Interaktionen von Fluoreszenz-markiertem IFNα2 sowie anderen IFN mit ifnar1-EC bzw. ifnar2-EC zu charakterisieren. So konnten die Ratenkonstanten dieser Interaktionen bei sehr geringen Oberflächenkonzentrationen charakterisiert werden, was für eine genaue Bestimmung ohne Einfluss von Massentransport-Effekten notwendig ist. Durch simultane Detektion der Bindung über das Massensignal und das Fluoreszenzsignal wurde die Orts-spezifische Fluoreszenzmarkierung des Liganden IFNα2 untersucht, und gezeigt, dass die Bindung an die Rezeptoruntereinheiten durch die Fluoreszenzmarkierung nicht beeinflusst wurde. Zudem konnte kompetitive Bindung von IFN nicht nur an die hoch-affine Untereinheit ifnar2, sondern auch an ifnar1, welche IFN nur mit sehr geringer Affinität erkennt, gezeigt werden. Im nächsten Schritt wurde die Ligand-induzierte Assemblierung des ternären Komplexes mit ifnar1-EC und ifnar2-EC auf fluiden Membranen untersucht. Dabei wurde bei hohen Rezeptorbeladungen sehr langsame Dissoziation des Liganden beobachtet, die bei niedrigen Rezeptorbeladungen deutlich schneller war. Diese Beobachtung deutete auf eine kinetische Stabilisierung des ternären Komplexes hin. Über *Chasing*-Experimente mit unmarkiertem Liganden konnte diese Vermutung bestätigt werden, da ein deutlich beschleunigter Austausch des Liganden beobachtet wurde. Da über das RIf-Signal die absoluten Oberflächenkonzentrationen von ifnar1-EC und ifnar2-EC bestimmt werden konnten, wurde so auch eine strikte 1:1:1 Stöchiometrie des ternären Komplexes gezeigt: war eine der Untereinheiten im Überschuss, dissozierte der überschüssige Ligand zunächst mit einer Kinetik, die dem entsprechenden 1:1-Komplex entsprach, bis sich ein stabiler 1:1:1-Komplex gebildet hatte.

Die Bildung des ternären Komplexes wurde im Folgenden detailliert charakterisiert. Zunächst wurde die Dissoziationskinetik bei verschiedenen Oberflächenkonzentrationen der Rezeptoruntereinheiten in stöchiometrischem Verhältnis vermessen. Diese Kurven konnten durch ein 2-stufiges Assoziations- bzw. Dissoziationsmodell angepasst werden, in dem der Ligand im ersten Schritt an ifnar2-EC bindet und im zweiten Schritt mit ifnar1 auf der Membran einen ternären Komplex bildet. Dadurch, dass die Oberflächenkonzentrationen von ifnar1-EC und ifnar2-EC genau quantifiziert werden konnten, musste nur ein Parameter in diesem Modell angepasst werden, welcher der Gleichgewichts-Dissoziationskonstante der 2-dimensionalen Interaktion des binären IFN/ifnar2-EC Komplexes mit ifnar1-EC beschreibt. Aus allen Experimenten mit Oberflächenbeladungen, die über einen

Konzentrationsbereich von zwei Größenordnungen variierte, konnte reproduzierbar eine Bindungskonstante von ca. 40 Molekülen/µm² bestimmt werden. Erstaunlicherweise liegt diese Bindungskonstante deutlich über der typischen Konzentration von Rezeptoren auf der Zelloberfläche (ca. 1000/Zelle). Damit ist es wahrscheinlich, dass die Bildung des ternären Komplexes auf der Zelloberfläche durch die Bindungsaffinität bzw. die Rezeptorkonzentration limitiert ist. Diese Affinität lässt sich nicht durch Steigerung der Dosis kompensieren. Interessanterweise gibt es zudem IFN mit deutlich höherer Affinität zu ifnar1. Damit könnte diese Interaktion eine Schlüsselrolle bei der Regulation des Ansprechverhaltens verschiedener Zellen spielen.

Weitere Untersuchungen zur Bildung des ternären Komplexes wurden mit IFNα2 Mutanten durchgeführt, welche eine niedrigere Bindungsaffinität zu ifnar2-EC zeigten. Die Dissoziationskinetiken dieser Mutanten aus dem ternären Komplex mit ifnar1-EC und ifnar2-EC ergaben, dass selbst bei stöchiometrischen Konzentrationen der Rezeptoruntereinheiten durchaus auch die Bindung an ifnar1 im ersten Schritt erfolgen kann. Da die Ligandenbindung der Geschwindingkeits-bestimmende Schritte der Rezeptorassembliert darstellt, entscheidet die relative Assoziationswahrscheinlichkeit, inwieweit welcher dieser beiden Wege populiert ist. Damit ist nicht nur die Assoziationsratenkonstante, sondern auch die relative Konzentration der Rezeptoruntereinheiten für den Assemblierungsmechanismus wichtig. Da unterschiedliche IFN verschiedene Assoziationsratenkonstanten haben, sind durchaus verschiedene Assemblierungssmechanismen für verschiedene IFN denkbar.

Um die Dynamik des ternären Ligand-Rezeptor-Komplexes auf der Membran zu charakterisieren wurden Assays etabliert, um die 2-dimensionale Interaktionskinetik direkt zu messen. Hier wurden zwei Strategien verfolgt. Zunächst wurde der Förster-Resonanzenergietransfer (FRET) zwischen Donor-markiertem ifnar2-EC und Akzeptor-markiertem ifnar1-EC eingesetzt, um die Ligand-Rezeptor Interaktion auf der Membran zu verfolgen. Durch schnelles Beladen mit einem Überschuss von unmarkiertem ifnar2-EC auf die Membran wurde ein Austausch von markiertem gegen unmarkierten ifnar2-EC über das Abklingen des FRET gemessen. Dieser Austausch wird bestimmt durch die 2-dimensionale Dissoziazionskinetik des ifnar2-EC/IFNα2 Komplexes die aus der Änderung des FRET-Signals bestimmt werden kann. Interessanterweise war die Dissoziationsratenkonstante, die aus dieser Kinetik

bestimmt wurde, um einen Faktor 3-5 höher als die Dissoziationsratenkonstante des ifnar2-EC/IFNα2 Komplexes mit dem freien Liganden. Da die Bindung von ifnar1-EC keinen Einfluss auf die ifnar2-EC/IFNα2 Interaktion hat, müssen diese Unterschiede auf die Verankerung an der Membran zurückgeführt werden. Wahrscheinlich spielt die langsamere Diffusionskinetik hier eine entscheidende Rolle, die zu einer langsameren Separation der dissoziierten Komponenten führt.

Diese Beobachtungen wurden bestätigt durch Bindungsassays, in denen die Austauschkinetik des Liganden im ternären Komplex bei Zugabe von unmarkiertem Liganden vermessen wurde. Dazu wurde eine der Rezeptoruntereinheiten im stöchiometrischen Überschuss auf die Membran geladen. Nach Bildung des ternären Komplexes mit Fluoreszenz-markiertem IFNα2 wurde der Überschuss an Rezeptoruntereinheit mit unmarkiertem Liganden in hoher Konzentration beladen. Der nun erfolgende Austausch von markiertem gegen unmarkierten Liganden wurde über das Fluoreszenzsignal verfolgt. Bei Verwendung geeigneter Mutanten ist diese Austauschkinetik wiederum durch die 2-dimensionale Dissoziationskinetik der Ligand-Rezeptor-Interaktion bestimmt. Mit diesen Bindungsassays wurden die Dissoziationskinetiken für ifnar1-EC und ifnar2-EC, sowie verschiedene Mutanten bestimmt. Aus der Gleichgewichts-Dissoziationskonstante und der Dissoziationsratenkonstante konnte auch die 2-dimensionale Assoziationsratenkonstante berechnet werden. Basierend auf systematischen Untersuchungen konnten einige prinzipielle Eigenschaften von 2-dimensionalen Protein-Protein Interaktionen identifiziert werden. So bestätigte sich für alle Ligand-Rezeptor Interaktionspaare, dass die 2-dimensionale Dissoziationskinetik um einen Faktor 3-5 langsamer war als die entsprechende 3-dimensionale Dissoziation. Weiterhin ist konnte für die Assoziationskinetik beobachtet werden, dass die großen Unterschiede in der Assoziationsratenkonstante in Lösung, die durch elektrostatisches Wechselwirkungen zu erklären sind (*electrostatic steering*), nicht für die 2-dimensionale Interaktion auf der Membran beobachtet wurde. Weit wichtiger als elektrostatische Steuerung ist dagegen die „richtige“ Orientierung der Proteine an der Oberfläche: Durch Änderung der Orientierung von ifnar1-EC auf der Membran über ein N-terminales Histidin-*tag* sank die Assoziationratenkonstante um einen Faktor von >5. Dies ist insbesondere überraschend, weil ifnar1-EC eine flexible multi-Domänenstruktur hat und zudem relativ flexibel über das Histidin-tag an der Membrane angebunden ist. Diese Ergebnisse zeigen, dass die Membran-verankerung, die Flexibilität, die laterale Diffusionskinetik und die

Oberflächenkonzentration zentrale Parameter für die Bildung und die Dynamik Zytokin-Rezeptorkomplexen auf Membranen sind. Diese Eigenschaften hängen auch von der lokalen Umgebung auf der Plasmamembran ab, die sich auch durch die Komplexbildung ändern können. Damit lässt sich erwarten, dass Rezeptorassemblierung in Zellen einen noch durchaus komplexeren Verlauf nehmen kann. In dieser Arbeit konnten diese Prozesse unter kontrollierten Bedingungen charakterisiert werden. Dabei erwies sich die neu etablierte Methode der simultanen TIRFS-RIf Detektion als äußerst versatil. Die komplementären Messgrößen dieser Detektionsmethode waren insbesondere nützlich, um die multiplen Parameter (Membran-Assemblierung, Rezeptorkonzentrationen) zu kontrollieren, und gleichzeitig komplexe Bindungsassays mit hoher Zeitauflösung durchzuführen. Eine breite Anwendung dieser Methode, um komplexe Prozesse an Membranen und an nicht-fluiden Oberflächen zu charakterisieren, ist vorauszusehen.

3. Preface

A cell uses cell surface receptors to constantly monitor its environment and initiate responses to environmental cues, e.g., signals such as hormones, growth factors and cytokines. The range of signals, typically ligands, a cell can detect and the concentrations at which ligands can be detected are determined by the array of receptors on the cell's surface. When a receptor encounters an agonist ligand, ligand-receptor interaction triggers a cascade of intracellular signaling reactions that can lead to a variety of cellular responses, such as the secretion of mediators of cell–cell communication, changes in gene expression, and cell proliferation. Protein-protein interactions between cell surface receptors, triggered by ligand binding play crucial roles in signal transduction. Kinetic and equilibrium properties, stoichiometry and conformational states of the signaling complexes are suggested to be largely responsible for signaling amplitude and specificity. Type I interferons (IFNs) elicit their antiviral, antiproliferative and immunmodulatory responses through binding to a shared receptor consisting of the transmembrane proteins ifnar1 and ifnar2. Differential signaling by different interferons emphasize the importance of 2-dimensional interactions between ifnar subunits in signal propagation. Therefore, understanding the determinants of protein-protein interactions on the biological membranes are important not only from the fundamental point of view, but also has a number of important practical applications. In 1968 Adam and Delbruck [1] introduced the concept of "reduction of dimensionality" which suggested that organisms handle some of the problems of timing, efficiency and sensitivity, in which small numbers of molecules and their diffusion are involved, by reducing the dimensionality in which diffusion takes place from the 3-dimensional space into 2-dimensional surface diffusion. Later, the initial concept was expanded, and the consequences of dimensionality, diffusion, orientation, electrostatics and other variables on 2-dimensional association and dissociation rate constants and equilibrium dissociation constants were subject of intensive theoretical treatment. It was realized, that in some cases interaction between membrane anchored proteins can be much more potent than between their soluble counterparts. In general, 2-dimensional interaction rate constants and equilibrium dissociation constants can not be deduced by measuring their 3-dimensional interaction in solution. Despite advances in experimental techniques little has been done to experimentally confirm

theoretical predictions and quantitatively understand determinants of protein-protein interactions in 2-dimensions.

4. Interactions in three dimensions

4.1. Basic description of biomolecular interactions

When two molecular species, receptor R and ligand L with mutual affinity are mixed in a solution, a time-dependent association between these molecules is expected to occur following the simple model:

$$R + L \underset{k_d}{\overset{k_a}{\rightleftharpoons}} RL \qquad \text{Eq. 1}$$

Where k_a and k_d are the association and the dissociation rate constants.

This interaction mechanism is described by the differential equation of the type:

$$\begin{aligned} \frac{d[RL]}{dt} &= k_a[R][L] - k_d[RL] \\ [R]_0 &= [R] + [RL] \\ [L]_0 &= [L] + [RL] \end{aligned} \qquad \text{Eq. 2}$$

where *[R]*, *[L]* and *[RL]* are concentrations of the reactants, $[R]_0$ and $[L]_0$ are the total amount of the receptor and the ligand respectively.

After certain time, the reaction reaches equilibrium and concentrations of the reactants does not change during the time. Therefore $\frac{d[RL]}{dt} = 0$ and Eq.2 can be simplified to

$$k_a[R][L] = k_d[RL] \qquad \text{Eq. 3}$$

The principle of microscopic reversibility at equilibrium states that, in a system at equilibrium, a number of association events is equal to the number of dissociation events. The equilibrium dissociation constant is defined as the ratio of concentrations between reagents and products at equilibrium:

$$K_D = \frac{[R][L]}{[RL]} = \frac{k_d}{k_a} \qquad \text{Eq. 4}$$

As can be seen from Eq.4, the concentration of the free ligand *[L]*, when half of the receptors are occupied is equal K_D.

$$K_D = [L]_{[R]=[RL]} \quad \text{Eq. 5}$$

The relationship between the thermodynamic parameters characterizing complex formation, such as the Gibbs free energy ΔG^0, and K_D is described by following equation:

$$\Delta G^0 = R^{gas} T \cdot ln(K_D) \quad \text{Eq. 6}$$

Where R^{gas} is the gas constant, T – the absolute temperature.

Eq.6 is the most important equation to predict the direction and the extent of an interaction. For spontaneous reaction the change in Gibbs free energy is negative $\Delta G<0$. The sequence of the several interactions will spontaneously proceed only if the overall change in free energy is negative. In the cell, thermodynamically unfavorable interactions are coupled with ATP hydrolysis and proceed spontaneously if $\Delta G+\Delta G_{ATP}<0$. K_D has a very strong dependence on ΔG^0, because of the logarithmic relationship. This emphasizes the importance of weak interactions, since small changes in ΔG^0 imply large changes in K_D. For example, at room temperature an additional hydrogen bond of 5 kcal/mol would decrease K_D more than three orders of magnitude.

ΔG^0 can be divided into enthalpic, ΔH^0, and entropic, ΔS^0, contributions:

$$\Delta G^0 = \Delta H^0 - T\Delta S^0 \quad \text{Eq. 7}$$

Change in enthalpy depends on hydrogen bond formation, electrostatic and Van der Waals interactions, steric hindrance, solvation and other effects. Change in entropy is primarily associated with randomness and rigidness of the system, restrictions of its translational, rotational or vibrational motions upon complex formation.

Most of the biological interactions happen in aqueous solutions and water does not act as the inert space filler, but is significantly involved during the course of complex formation. This is especially true when ions or dipolar molecules are involved. Water dipoles orient themselves in the electrostatic field generated by ions or dipoles and this contributes to a large negative change in solution entropy. The mobility of the hydrated proteins is further decreased bringing additional change in entropy. Water forms weak bonds with proteins resulting in positive enthalpy. Thus, changes in enthalpy and entropy tend to compensate each other. The free energy

difference of the hydration shell between R, L and their complex RL can have substantial contribution to the interaction ΔG^0.

4.2. Interaction diagram

The potential energy surface of an interaction is a geometrical hypersurface on which the potential energy of a set of reactants is plotted as a function of coordinates representing the molecular geometries (for example, a bond length or bond angle) of the system. The energetically easiest route from reactants to products on the potential energy contour map defines the interaction potential-energy profile. The interaction coordinate is typically chosen to follow the potential energy profile from the reactants to the products. The potential energy profile plotted against interaction coordinate is called the interaction diagram. The diagram for elementary interactions is presented in Figure 1A. In 1935 Eyring [2] and others described the theory that an interaction proceeds through a transition state or an activated complex. The reactants are in rapid equilibrium with the transition state. The activated complex can go forward to produce the product, the complex RL, or reverse to re-generate the reactants R and L. Only molecules, which have enough energy to reach the transition state can form a complex.

Most biological interactions can not be explained by elementary interaction diagram presented in Figure 1A. The course from R and L to RL often involve multiple sequential elementary steps. These steps are bringing proteins to close proximity state, removal of interfacial water, bond breakage and conformational optimization of binding sites to form a complex, formation of the interaction bonds between the receptor and the ligand chains and formation of a new hydration shell around the complex. These steps appear on different time and length scales. If proteins are very flexible, multiple conformational optimization, bond formation and hydration / dehydration cycles are required to form the functional complex. This type of complex formation is also called “induced fit” interaction. During the course of sequential elementary interactions the local free energy minimums with a depth greater than the RT can be formed. Protein complexes in these local energy wells are called interaction intermediates and these states can be detected with modern ultrafast spectroscopic detection techniques. The interaction diagram for two proteins (Figure 1B) is a complex curve with multiple transition states ($RL^{\ddagger}$, $RL^{\ddagger\ddagger}$ and $RL^{\ddagger\ddagger\ddagger}$) and reaction intermediates (RL*and RL**). The energy barrier receptor and ligand

have to cross to associate is called activation energy or association free energy $\Delta G^{\ddagger}_{on}$. Similarly, the energy barrier for dissociation is called $\Delta G^{\ddagger}_{off}$. The free energy difference between reactants R and L and their complex RL is the interaction free energy ΔG^{0}.

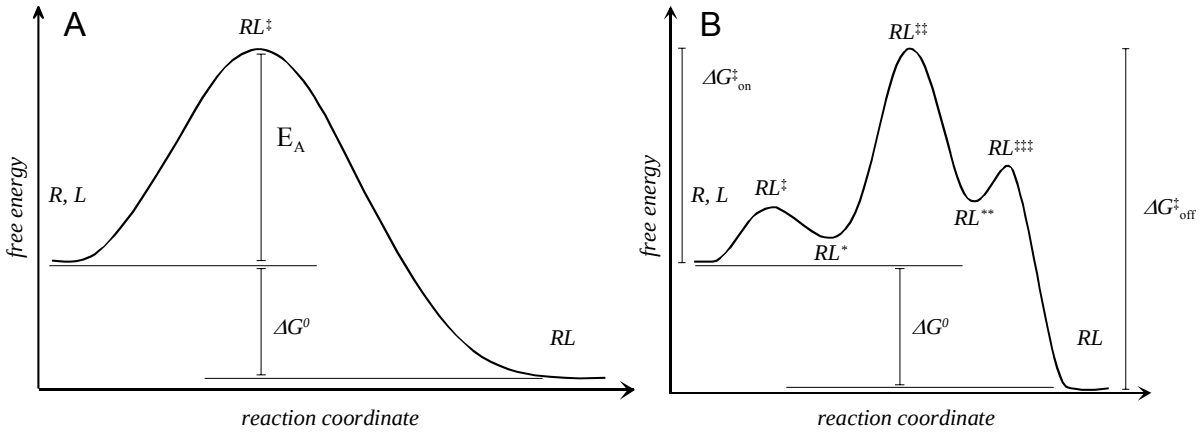

Figure 1. Interaction diagram for (**A**) elementary reaction and (**B**) for receptor-ligand complex formation.

4.3. Factors affecting association rate constant

The association rate constant for protein-protein interactions was intensively studied and summarized in numerous books and reviews [3-5]:

$$k_a = p \cdot Z \cdot exp(-\Delta G_{on} / R^{gas} T) \qquad \text{Eq. 8}$$

where p is the orientation factor and Z is the collision frequency;

The collision frequency for neutral spherical and uniformly reactive particles, R and L, in solution can be calculated from the Smoluchowski equation:

$$Z^{3D} = 4\pi C_R^{3D} C_L^{3D} (D_R^{3D} + D_L^{3D}) r \qquad \text{Eq. 9}$$

where C_R^{3D} and C_L^{3D} – the concentrations of the R and the L respectively, D_R^{3D} and D_L^{3D} – the diffusion coefficients of the R and the L respectively, r – the encounter radius;

The state of close proximity between the receptor and the ligand during collision is called diffusional encounter. Eq.8 shows that not every collision or not every diffusional encounter between R and L proteins leads to complex formation. First, $exp(-\Delta G_{on}/RT)$ represent fraction of collision pairs that have the necessary activation energy for biological interaction to take place. It should be noted, that only the activation energy which is localized in the protein binding site is important for association. Second, "p" is a steric or orientation factor, describing the probability that

energized collisions would have a geometry suitable for interaction. "*p*" values are difficult to predict and exact solutions can be found only in special cases [6,7].

The long-range electrostatic interaction between R and L can change the association rate constant by increasing or decreasing collision frequency. Due to the attractive potential between opositively charged proteins, they will stay in the vicinity to each other and will collide several times before full separation. Additionally, charge distribution on protein interface affects the orientation at which they collide. This optimization of long range electrostatic interactions prior collision, also called electrostatic steering, can dramatically increase orientation factor "*p*" and corresponding association rate constant [8-10].

The solvent environment can influence the association rate constant and even the mechanism of complex formation by changing the force between the interacting proteins and hence altering the readiness with which they approach each other. Such phenomenon is illustrated by effect of solvent's dielectric constant on electrostatic and Van der Walls forces among interacting proteins. Dissolved salts additionally minimize electrostatic and Van der Waals interactions affecting the orientation factor, the collision frequency and the activation energy barrier which needs to be overcome. Solvent viscosity affects the diffusion coefficients of proteins and hence alters the collision frequency "*Z*" between reacting species with possible effect on the association rate constant. Proteins are randomly activated / deactivated by solvent molecules during their collision. The translational energy of the solvent molecules can be converted to protein's vibrational energy. Additionally, the energy between different vibration modes can be redistributed during collision. In favorable cases, these changes are delivered to the binding site, the protein gets activated and ready to form a complex. If no interaction partner is available in the vicinity of an activated protein, further collisions with solvent molecules will deactivate the protein until the next activation.

4.4. Factors affecting dissociation rate constant

Similarly to the association kinetics, dissociation kinetics theory also deals with the problem of diffusion in the presence of forces. Dissociation can be imagined as thermally activated particle escape from the potential well [2,11,12]:

$$k_d = A\,exp(\Delta G_{off}/RT) \qquad \text{Eq. 10}$$

where *A* is the preexponential factor.

In case of a receptor-ligand complex, dissociation involves bond breaking, dehydration, conformational changes of R and L, new bond and solvent shell formation and spatial separation. In high viscosity solvents, spatial separation of the reactants can become a rate-limiting step. If proteins will get activated, while being in close proximity state, they will reassociate back to the complex. Therefore, the observed dissociation rate constant will be lower than predicted from Eq.10.

5. Comparison of interactions in two and three dimensions

Interactions in two dimensions can be described using the same basic equations (Eq.4, Eq.6, Eq.8 and Eq.10) as used to analyze 3-dimensional interactions. However, the limitations introduced by the membrane interface affect the interaction rates and equilibrium constants. Therefore, the parameters, such as p, Z or ΔG^0 will be different for membrane anchored proteins in comparison to the same proteins in aqueous solution.

5.1. Collision frequency in 2D

The collision frequency for neutral, spherical and uniformly reactive particles, R and L distributed on the membrane was calculated and reviewed by several authors [3,13-15] to be:

$$Z^{2D} = \frac{4\pi(D_R^{2D} + D_L^{2D})}{ln(b/r)} C_R^{2D} C_L^{2D} \qquad \text{Eq. 11}$$

where b is the average distance between R and L and r is the encounter radius. C_R^{2D} and C_L^{2D} are the concentrations of the receptor and ligand respectively, D_R^{2D} and D_L^{2D} – the diffusion coefficients of receptor and ligand respectively.

It has been suggested that reactions between ligands and cell surface receptors can be speeded up by nonspecific adsorption of the ligand to the surface followed by 2-dimensional surface diffusion to the receptor, a mechanism called “reduction of dimensionality rate enhancement” [16-21]. While this is certainly true for certain interactions [18] available data on lateral diffusion rates, membrane-substrate affinities and calculations have suggested that the encounter rates of membrane-linked proteins, compared to cytosol-located proteins are actually very similar [22,23]. The reduction of dimensionality rate enhancement is getting significant only when the reactants are much diluted and the average distance between them exceeds well above the dimensions of an average cell.

Eq.11 was derived assuming infinitely large plane and homogeneous protein distribution on the membrane. Membrane proteins *in vivo* are often localized in membrane microdomains stabilized by the cytoskeleton, segregated lipids and special raft proteins [24-29]. Also because of high protein concentration in the membrane, temporal domains with moving boundaries can form. This effect is often described as macromolecular crowding [30-35]. Extensive computer simulations have shown that the long-distance molecular mobility is reduced when a particle diffuses in an environment with various size mobile or immobile obstacles [36,37]. Even if the translational diffusion coefficient is reduced, collision frequency within a domain can increase, depending on the domain size, in comparison to infinite plane situation [38].

5.2. The effect of surface exclusion

Theoretical and experimental studies of the effect of excluded surface indicate that when the fraction of membrane surface occupied by membrane receptors exceeds a few percent, the equilibrium dissociation constant K_D^{exc}, characterizing the interaction between macromolecules, may be markedly different than in the limit of high dilution $K_D^{diluted}$ [39]. For a simple bimolecular interaction the correction factor, k_{exc}, is defined:

$$\frac{K_D^{exc}}{K_D^{diluted}} = k_{exc} = \frac{\gamma_R \gamma_L}{\gamma_{RL}} \qquad \text{Eq. 12}$$

where γ_R, γ_L and γ_{RL} are the activity coefficients of receptor, ligand and receptor-ligand complex, respectively.

At the limit of 50% surface occupancy K_D^{exc} is one order of magnitude higher in comparison to $K_D^{diluted}$. This effect scales up with number of membrane proteins involved in complex formation. For tetramer k_{exc}>100 at 50% surface occupancy. Effect of excluded surface is present on the membranes as well as for soluble proteins (the effect of excluded volume). However, excluded surface conditions are readily realized for membrane anchored proteins. A relatively low number of receptors on the membrane or membrane microdomain is needed to occupy substantial fraction of membrane or membrane domain surface area. This situation is very hard to achieve in solution.

5.3. Lifetime of the diffusional encounter complex

The translational diffusion coefficient of membrane-anchored proteins is reduced as much as two orders of magnitude compared to soluble proteins because of the high membrane viscosity. This means that the lifetime of the diffusional encounter complex is also hundred times longer. Extracellular or cytoplasmic parts of the transmembrane protein are exposed to aqueous (low viscosity) solution, so vibrations and movements of these protein domains are not affected. Flexible proteins will have more time to optimize their structure to form a complex; therefore the orientation factor "*p*" will increase. Increased lifetime of the diffusional encounter also means that probability of receptor and ligand activation by solvent molecules during collision is much higher compare to the situation in solution.

Cells can fine tune interaction efficiency by varying the viscosity of the membrane and corresponding diffusion coefficient of membrane anchored proteins by localizing them in different microdomains. Depending on membrane composition diffusion coefficients can vary between (1-10)E-8 cm^2/s [40]. It decreases with increasing fraction of saturated alkyl chain lipids. Membranes in the gel phase are essentially immobile with diffusion coefficient in the order of 1E-11 cm^2/s. In microdomain caveolae [41-43], integral membrane protein caveolin is attached to the actin cytoskeleton. This immobilization has many biologically important consequences including reduced membrane fluidity and the diffusion coefficient.

5.4. Orientation

The presence of the membrane anchors has only a minute effect on vibrational modes of the membrane anchored receptor side chains in comparison with soluble protein case. The situation is completely different for rotational movement. Soluble receptor chains freely rotate and collide with random orientation against each other. The membrane introduces a high potential energy barrier for rotation about the membrane anchor. This effect, also called hindered or restricted rotation, reduces the range of available rotation angles and orients membrane-anchored receptors. In contrast to the soluble protein case, the membrane anchored receptor and the ligand will not collide randomly oriented to each other, but with the preferred orientation. If this preorientation brings their binding sites to the interaction favorable positions, the orientation factor "*p*" will be drastically higher in comparison to the soluble protein case. The degree of "*p*" enhancement depends on residual rotational flexibility [39].

For the very inflexible proteins "*p*" enhancement due to membrane anchoring can be as much as two orders of magnitude compare to the soluble protein case. The opposite scenario is also possible. If the binding sites are not positioned in the interaction favorable way, membrane anchored proteins will always collide with wrong geometrical orientation and complex will not form. In this case "*p*" will be lower than in interaction between soluble proteins. The unfavorable orientation constrains of some membrane receptors (epidermal growth factor receptor, insulin receptor) in the cell can be eliminated by ligand binding from solution. This is the effective way to switch receptors on and off and activate them only when it is required.

The electrostatic steering, mechanism to enhance association rate constant between the soluble proteins, will not be strongly pronounced for interactions on membranes. Membrane anchored proteins are already oriented and additional orientation due to electrostatic steering should have only minor effect on "*p*" and association rate constant in general.

5.5. Activation energy and $\Delta G°$

The effect of dimensionality on the potential energy landscape and the interaction diagram has not been systematically addressed. It was suggested, that anchoring the receptor and the ligand to the membrane would restrict their rotational and translational freedom as well as the diffusional properties, altering the reaction thermodynamics and binding kinetics. The ΔH^0, which is related to the bond formation, is probably the same. But the entropic contribution, ΔS^0, related to loss of degrees of freedom is clearly higher (less negative) in 2-dimensional case [39]. For example, formation of the RL complex between soluble R and L would result in the loss of six translational and rotational degrees of freedom in contrast to five for the membrane anchored proteins. Therefore, the change in system randomness and flexibility will be lower for 2-dimensional interactions. Rigidness of the polypeptide chain in solution and on the membrane can also be different, but these effects are difficult to quantify.

Favorable orientation and increased lifetime of the encounter complex can drastically increase the collision efficiency and decrease the effective activation energy needed for interaction. Together with the movement restrictions imposed by presence of the membrane, Gibbs free energy landscape and a corresponding

interaction diagram can have different profile comparing soluble and membrane anchored proteins.

5.6. Concluding remarks

It is very likely, that cells use effects caused by receptor membrane anchoring to optimize interactions between membrane proteins. It is apparent that solubilization with detergents may disrupt the membrane protein-protein interactions of interest. Elimination of preferred orientation, shorter lifetime of the encounter complex and the substantial dilution can markedly shift the equilibrium towards dissociation. The change in entropy (and corresponding ΔG^0) associated with complex formation will be different for proteins confined to a membrane than for proteins in solution. From what was said above it is clear that the binding affinity between receptor and ligand, localized on the membrane, cannot be easily determined by using soluble forms of the membrane proteins.

6. Coupled three and two dimensional interactions

When the receptors and the ligand are distributed both on the surface of the membrane and in the aqueous phase, two alternative mechanisms of bimolecular reactions differing in the dimensionality of reaction space are possible. These are the 3-dimensional ligand binding to the membrane receptor and the 2-dimensional interaction between membrane receptors. Although both monovalent and multivalent ligands can bind to cell surface receptors, only multivalent ligands have the ability to simultaneously bind multiple receptors, that is, to crosslink receptors. The amount of crosslinked receptors, in contrast to ligand binding, is recognized to be the basic principle for signal transduction through cytokine receptors and growth factors [44-48]. Crosslinked receptors can be considered a signaling unit.

6.1. Bivalent ligand induced receptor crosslinking

The ability of bivalent ligands to aggregate receptors is shown schematically in Figure 2. Receptors, which are linked to other receptors, are said to be crosslinked or dimerized. The apparent K_D of bivalent ligand binding to membrane anchored receptors is increased due to multivalent interactions [13,49-55] and this affinity increase is modulated by the receptor density on the membrane [49,50,56-63].

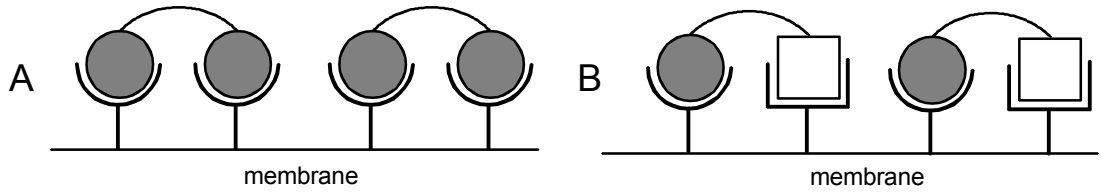

Figure 2 Ligand induced receptor crosslinking. (**A**) Homodimeric ternary complex: ligand crosslinks two identical membrane anchored receptors. (**B**) Heterodimeric ternary complex: ligand crosslinks different membrane anchored receptors.

6.2. Homodimerization

Ligand induced receptor crosslinking occurs in two steps. The ligand binds to one receptor chain, with the equilibrium dissociation constant K_1^{3D}, to form a binary complex RL. In a subsequent step RL recruits a second receptor chain to form the ternary complex RLR (Figure 3). The affinity of the second step, which is a bimolecular association event constrained to the two dimensions of the membrane, is given by dissociation constant K_2^{2D}, which has units of molecules/μm² [64].

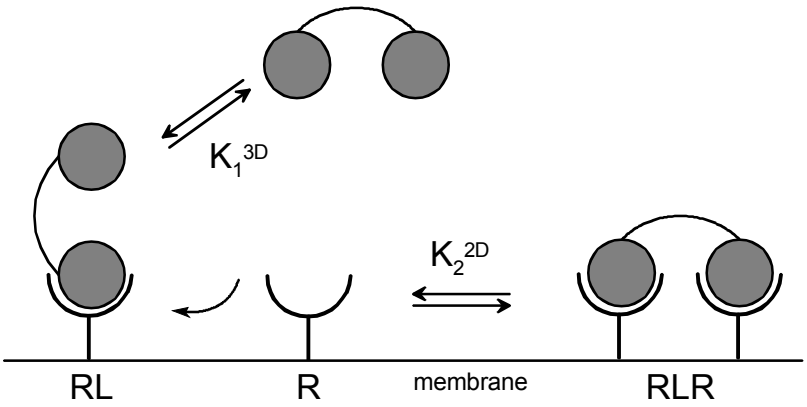

Figure 3 Schematic of two step ligand induced receptor homodimerization

The two interactions at equilibrium can be described:

$$K_1^{3D} = \frac{[R][L]}{[RL]} \quad K_2^{2D} = \frac{[RL][R]}{[RLR]} \qquad [R] = [R]_0 - 2 * [RLR] - [RL] \quad \text{Eq. 13}$$

Where *[L]* is the 3-dimensional concentration [mol/l] of the ligand and *[R]*, *[RL]*, *[RLR]* and $[R]_0$ are the 2-dimensional concentrations [mol/mm²] of the receptor, the receptor-ligand complex, the crosslinked receptors and the total amount of receptor, respectively.

Simulated *[RLR]*, *[RL]* and *[R]* populations as a function of ligand concentration *[L]* are presented in Figure 4. Bell-shaped crosslinking curve is a characteristic

feature of homo and heterodimeric receptors that are activated by ligand induced dimerization. At low concentration of soluble ligand, most of the receptors are not occupied and the singly-bound ligand has a lot of free receptors available for crosslinking (Figure 4A and B). The amount of receptor crosslinking increases with increasing ligand concentration. When the concentration of soluble ligand increases even more, free receptor can be either occupied by ligand binding from solution or crosslinked by binary receptor-ligand complex. The two receptor chains involved in signaling complex are identical, so at very high concentration of the ligand, the system is forced to the state in which each receptor molecule is occupied by separate molecule of ligand (Figure 4C), such that, at equilibrium, virtually all receptor molecules are present in RL complexes. High concentration of the soluble ligand has a self-inhibiting effect, because receptor crosslinking, which initiates signaling, is prevented and receptor is present in the inactive state of binary complex (Figure 4C). There is, therefore, little formation of the ternary complex at either very low or very high concentration of ligand in solution. The concentration of the ligand that corresponds to the peak or mid point of the bell shaped curve equals K_1^{3D}, the affinity of ligand binding to the first receptor chain. Figure 4C shows that initial binding of L to R and the self-inhibition, which occurs at very high concentrations of L are both governed by K_1^{3D}, so at $[L]= K_1^{3D}$ these effects are equally balanced and the concentration of *[RLR]* is maximal.

The amount of *[RLR]* at the peak of the bell shaped curve is another measure of how effective ligand induced receptor dimerization is. Equations from [60] predicts that the height of the peak is a function of K_2^{2D} and $[R]_0$ but not K_1^{3D}. $[R]_0$ has to be high relative to K_2^{2D} to induce majority of the receptors to dimerize. For example, to dimerize 80% of the receptor molecules at $[L]= K_1^{3D}$, $[R]_0/ K_2^{2D}$, must be equal 80.

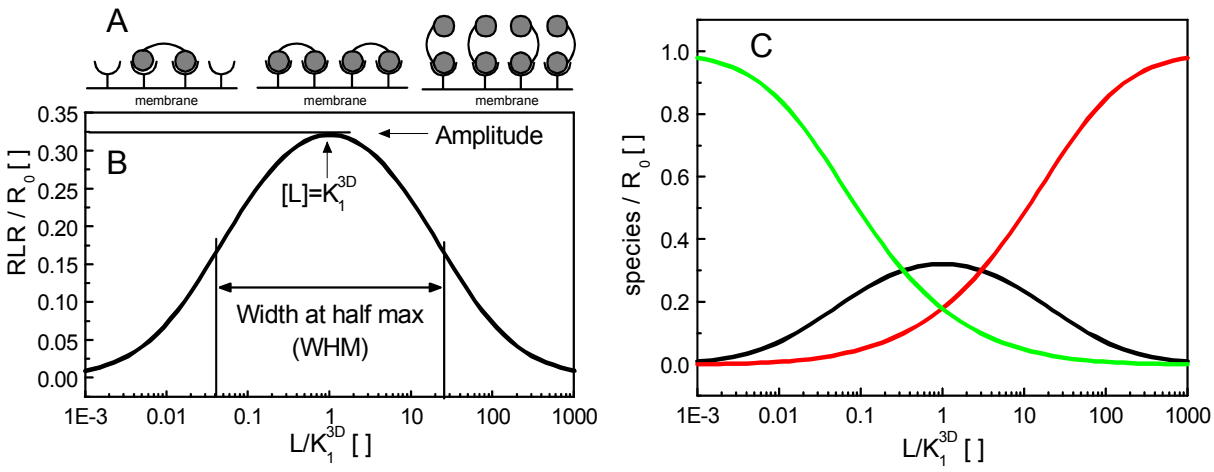

Figure 4 Dependence of the concentration of the RLR complex, expressed as a fraction of total receptor, $[R]_0$, on the ligand concentration for a value $[R]_0/K_2^{2D} = 10$. (**A**) Schematic of the dominant receptor states at different ligand concentration. (**B**) The ligand concentration that produces maximal level of RLR and therefore defines the peak of the bell shaped curve is equivalent to K_1^{3D}, the width at half maximal RLR is designated as WHM. (**C**) The same simulation as shown in (A), but showing how each of the forms of the receptor, RLR (black), RL (red) and R (green) varies with the ligand concentration.

The width of the bell-shaped curve at half maximum (WHM) is a measure of the ligand concentration range at which at least half maximal amount of crosslinked receptors is present. As it was calculated by Perelson and Delisi [60], the magnitude of the WHM is governed by the effective affinity of the second step in receptor crosslinking, which is the affinity of RL binding to R on the membrane. It is a function of $[R]_0 * K_2^{2D}$, but not of K_1^{3D} (Figure 5A). A low K_2^{2D} and a high $[R]_0$ both favor a wide WHM (Figure 5B). This is because the more thermodynamically stable RLR, the lower concentration of RL is required to form it, and the higher concentration of L is required to disrupt the RLR complex. The experimental observation of a very broad WHM would therefore indicate that the total concentration of receptor on the cell membrane, $[R]_0$, is much larger than K_2^{2D}.

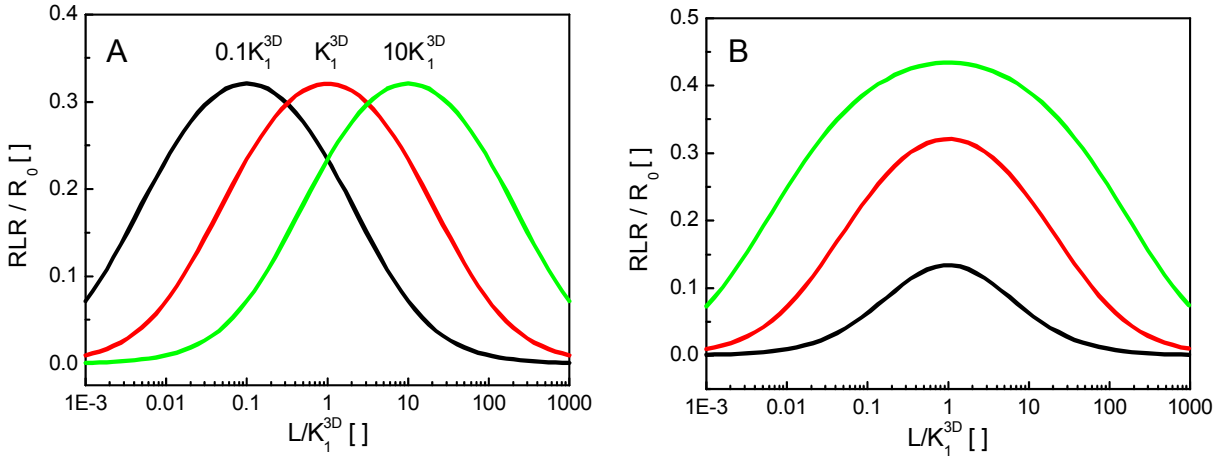

Figure 5 Influence of K_1^{3D} and K_2^{2D} on the shape of the RLR crosslinking curves. (**A**) For fixed values of K_2^{2D} and $[R]_0$ ($[R]_0$=10*K_2^{2D}), increasing or decreasing K_1^{3D} by a factor of 10 causes the mid point to shift to correspondingly higher or lower ligand concentrations. The width and the amplitude of the curve are unaffected. (**B**) For a fixed value of K_1^{3D} and $[R]_0$, decreasing K_2^{2D} by increments of 10 over the range of values $[R]_0/K_2^{2D}$ = 1 (black); 10 (red); 100 (green) increases the width and amplitude of the RLR curve without altering the mid point. (An identical result would be obtained if $[R]_0$ were increased at constant K_2^{2D}.)

Only very few studies analyzed bivalent fluorescent ligand binding titration curves with above discussed two-step interaction model (Figure 3) [21,65-68]. The major difficulty associated with this type of data analysis is the requirement to parameterize the surface density of unoccupied receptors. In these studies, the density was calculated by using fluorescent standard or correlating the fluorescence signal with radioimmunoassay.

6.3. Heterodimerization

The same line of arguing is valid in the case when the ligand crosslinks different receptors, R1 and R2. Receptor crosslinking can be imagined as a two step process: 3-dimensional ligand binding to R1 or R2 from solution and 2-dimensional crosslinking as depicted in Figure 6.

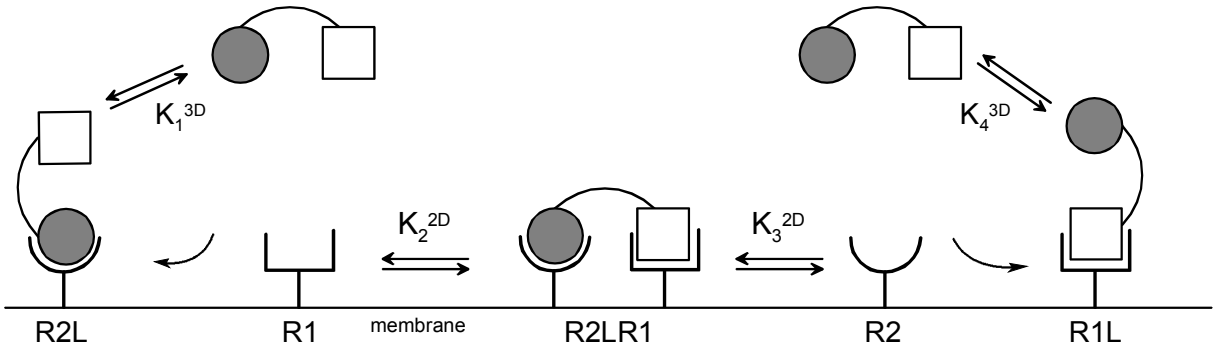

Figure 6 Schematic of two step ligand induced receptor heterodimerization.

The equilibrium dissociation constants of this system are defined as:

$$K_1^{3D} = \frac{[R2][L]}{[R2L]} \quad K_2^{2D} = \frac{[R2L][R1]}{[R2LR1]} \quad K_3^{2D} = \frac{[R1L][R2]}{[R2LR1]} \quad K_4^{3D} = \frac{[R1][L]}{[R1L]}$$

$$[R2] = [R2]_0 - [T] - [R2L] \qquad [R1] = [R1]_0 - [T] - [R1L] \qquad \text{Eq. 14}$$

Where *[L]* is the 3-dimensional concentration [mol/l] of the ligand and *[R1]*, *[R2]*, *[R1L]*, *[R2L]*, *[R2LR1]*, $[R2]_0$ and $[R1]_0$ are the 2-dimensional concentrations [mol/mm²] of the receptors, the receptor-ligand complexes, the crosslinked receptors and the total amount of the receptors, respectively.

Let us assume, without simplifying the system, that the ligand affinity towards R2 is hundred times higher than for R1, i.e. K_1^{3D}=0.01 K_4^{3D}. Simulated *[R2LR1]*, *[R2L]*, *[R1L]*, *[R2]* and *[R1]* populations as a function of the ligand concentration *[L]* at stoichiometric concentrations of $[R1]_0$ and $[R2]_0$ are presented in Figure 7. Similarly to the situation, where ligand crosslinks identical receptors, the receptor crosslinking curve for non-identical receptors is also bell-shaped. At low ligand concentration, bound ligand can crosslink many unoccupied receptors and preferably will be present in R2LR1 state. When the ligand concentration continues to increase unoccupied receptor R2 or R1 can bind ligand L from solution or they can be crosslinked by singly bound receptor-ligand complex R2L and R1L. As *[L]* continues to increase, 3-dimensional binding will more and more dominate over 2-dimensional crosslinking, and finally only monovalently bound R2L and R1L complexes will be present. As can be seen from the Figure 7B and proven mathematically [69], peak of ligand induced R2 and R1 crosslinking appears at ligand concentration sqrt(K_1^{3D}*K_4^{3D}). Initial binding of L to the membrane is governed by the high affinity interaction with R2 (K_1^{3D}) self-inhibition of receptor crosslinking is governed by low affinity interaction K_4^{3D} between L and R1. So at *[L]*= sqrt(K_1^{3D}*K_4^{3D}) these effects are balanced and the concentration of RLR is maximal.

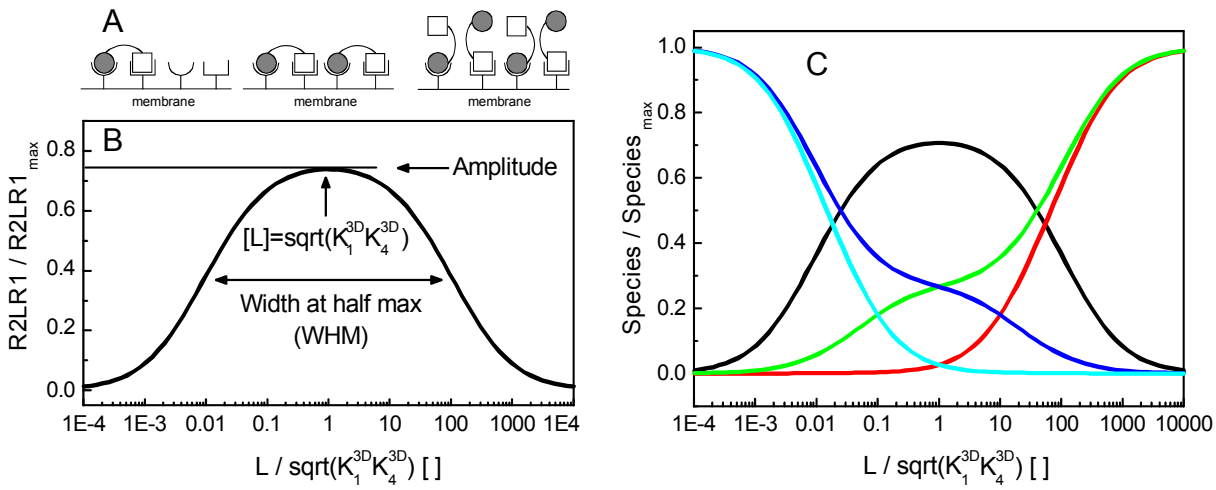

Figure 7 Dependence of the concentration of the R2LR1 complex, expressed as a fraction of the maximum theoretical value, on the ligand concentration for a value $[R1]_0=[R2]_0= 10*K_2^{2D}$ and $K_1^{3D}=0.01\ K_4^{3D}$. (**A**) Schematic of the dominant receptor states at different ligand concentration. (**B**) The ligand concentration that produces maximal level of RLR and therefore defines the peak of the bell shaped curve is equivalent to square root of $(K_1^{3D}*K_4^{3D})$, the width at half maximal R2LR1 is designated as WHM. (**C**) The same simulation as shown in (A), but showing how each of the forms of the receptor, R2LR1 (black), R1L (red), R2L (green), R1 (blue) and R2 (cyan) varies with the ligand concentration.

Homo- and heterodimerization curves share similar features. For example, at fixed K_2^{2D}, K_3^{2D} and $[R2]_0=[R1]_0$ increasing or decreasing K_1^{3D} and K_4^{3D} by the same factor shifts the mid point of the crosslinking curve without altering the amplitude and width at half maximum (Figure 8A). Similarly, at fixed K_1^{3D}, K_4^{3D} and $[R2]_0=[R1]_0$, decrease of K_2^{2D} increases the amplitude and WHM of the crosslinking curve without altering the mid point (Figure 8B)

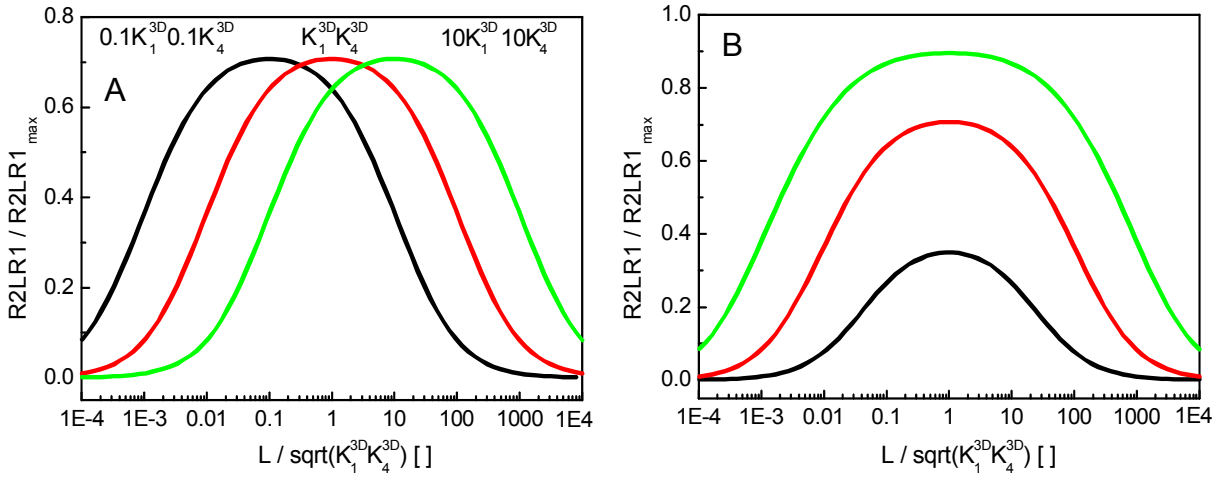

Figure 8 Influence of equilibrium dissociation constants on the shape of the R2LR1 crosslinking curves. (**A**) For the fixed values of K_2^{2D}, K_3^{2D} and $[R2]_0=[R1]_0=10*K_2^{2D}$, increasing or decreasing K_1^{3D} and K_4^{3D} by a factor of 10 causes the mid point to shift to correspondingly higher or lower ligand concentrations. The width and the amplitude of the curve are unaffected. (**B**) For fixed values of K_1^{3D}, K_4^{3D} and $[R2]_0=[R1]_0$, decreasing K_2^{2D} by increments of 10 over the range of values $[R1]_0/K_2^{2D}$ = 1 (black); 10 (red); 100 (green) increases the width and amplitude of the crosslinking curve without altering the mid point.

However, there are a few important differences between ligand induced homo- and heterodimerization. At fixed 2-dimensional equilibrium dissociation constants and receptor surface densities, the rise of the bell shaped curve is dominated by the affinity towards the high affinity receptor R2. The second part, crosslinking self-inhibition, is dominated by affinity towards low affinity receptor R1. Therefore, WHM can be effectively varied by decreasing K_1^{3D} and increasing K_4^{3D} (Figure 9A). The broader the WHM, the lower the maximum response sensitivity to ligand concentration. The position of the mid point is not affected and the amplitude is only slightly higher for different combinations of K_1^{3D} and K_4^{3D} (Figure 9A).

Another important difference between homo- and heterodimerization is that the fraction of crosslinked receptors can be maximized by increasing the 2-dimensional concentration of only one of the subunits (Figure 9B). For example, an excess of R1 in comparison to R2 shifts the K_2^{2D} equilibrium towards ternary complex. Additionally, self-inhibition at high ligand concentrations will be buffered by excess R1 and higher *[L]* will be required to compete 2-dimensional interaction between receptors by 3-dimensional ligand binding from solution (Figure 9B).

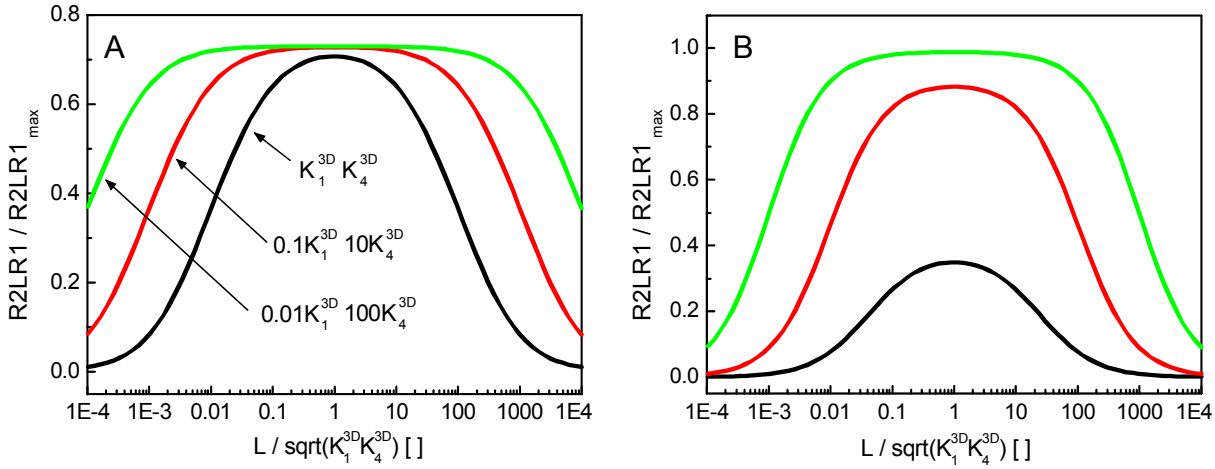

Figure 9 Influence of equilibrium dissociation constants on the shape of the R2LR1 titration curves. (**A**) For fixed value of K_2^{2D}, K_3^{2D} and $[R2]_0=[R1]_0=10*K_2^{2D}$, decreasing K_1^{3D} and increasing K_4^{3D} by a factor of 10 or 100 increases WHM of the crosslinking curve without altering the mid point. The amplitude is almost unaffected. (**B**) For fixed values of K_1^{3D}, K_4^{3D} and $[R2]_0=K_2^{2D}$, increasing $[R1]_0$ by increments of 10 over the range of values $[R1]_0/K_2^{2D}$ = 1 (black); 10 (red); 100 (green) increases the WHM and amplitude of the crosslinking curve without altering the mid point. An identical result would be obtained if $[R2]_0$ was increased at constant $[R1]_0$.

6.4. Concluding remarks

The dependency of the ligand-induced receptor crosslinking on logarithm of ligand concentration is a bell shaped curve. The position of the mid point is effectively varied by 3-dimensional equilibrium dissociation constants. The amplitude and width at half maximum are mainly governed by 2-dimensional interactions. Significant amounts of ternary complexes are achieved only if receptor density on the membrane is much higher than 2-dimensional equilibrium dissociation constant. This situation is readily realized in case of membrane anchored proteins. The relatively low number of receptors on the membrane or membrane microdomain is needed to reach situation, where average distance between receptors gets comparable with their dimensions. This situation is very hard to achieve in solution.

Ternary complex between different receptors gives additional flexibility to the system and provides possibility to manipulate the shape of the crosslinking curve. If ligand affinity towards R2 and R1 is different by several orders of magnitude, the amount of crosslinked receptors in the area of few log units around the mid point will be essentially independent on the ligand concentration. This is an attractive feature

for pharmaceutical applications. Large excess of one of the receptors has a buffering effect, which leads to a increased amplitude and WHM of the crosslinking curve.

The crosslinking of the cell surface receptors by interaction with cytokines has been shown to be an important event in triggering cellular responses. It is very likely that cells use above-described crosslinking properties to optimize their communication and transmembrane signaling. For example, it can explain how differential signaling is realized by different cytokines through shared receptors. High affinity ligands will crosslink more receptors and initiate stronger cellular responses in comparison to low affinity ones. If different threshold values of receptor crosslinking are required to initiate different responses, lower concentrations of high affinity ligands will be required to activate them. It should be emphasized that amount of receptor crosslinking can not be higher than maximum value determined by receptor densities on the membrane and 2-dimensional equilibrium dissociation constants. Therefore some low affinity ligands will not be able to initiate responses, which require high crosslinking threshold; no matter how much ligand concentration (dose) is increased. Additionally, different densities of receptors in the membrane can explain why different cells or cells at different stage of differentiation respond differently to the same cytokine. For a given ligand concentration, the amount of receptor crosslinking will depend on the 2-dimensional density of receptors on the membrane. Different cells can have different receptor densities and will start different responses or same responses with different signaling intensity.

Thus, it is essential to measure 2-dimensional interaction rate and equilibrium dissociation constants in order to understand receptor crosslinking and differential signaling. Experimental observation of membrane receptors *in vitro* and *in vivo,* differentiation between free and crosslinked state is of primary importance in the field of cellular signaling.

7. Experimental techniques to study interactions on membranes

In recent years, the combined advances in fluorescence labeling, imaging methods and technical equipment provided the possibility for detecting and analyzing protein-protein interactions on membranes in real time with high sensitivity and high temporal as well as spatial resolution. Cost-effective computing resources have become available to handle large amounts of data, and powerful software packages are easily obtainable for analyzing digital information. Therefore, biomolecular

interactions and translocations on membranes now can be routinely observed in living cells or on model membranes.

7.1. Diffusion and mobility techniques

Fluorescence recovery after photobleaching (FRAP) [40,70-77], fluorescence correlation spectroscopy (FCS) [29,40,77-90] and single particle tracking (SPT) [91-97], belongs to the family of methods that yield rates of diffusion and active transport from measurements of spontaneous thermally driven microscopic fluctuations in the positions of molecules or their local densities. The diffusion coefficient (D) of the freely diffusing membrane protein is dominated by the high viscosity of the membrane and the radius of the transmembrane segment. The aqueous portion usually does not significantly contribute to the D value [98]. Protein–protein interactions or binding to a scaffold may slow down or immobilize a protein, and collisions with other membrane-anchored receptors hinder free diffusion. Commonly, above-mentioned techniques allow to determine whether protein mobility is rapid or slow, whether binding interactions are present, whether an immobile fraction exists, or how a particular treatment (such as ligand binding or a mutation in the protein of interest) affect these properties. Proper interpretation of the data also yields information about binding interactions of fluorescently tagged molecules, including the number of binding states and the binding strength of each state.

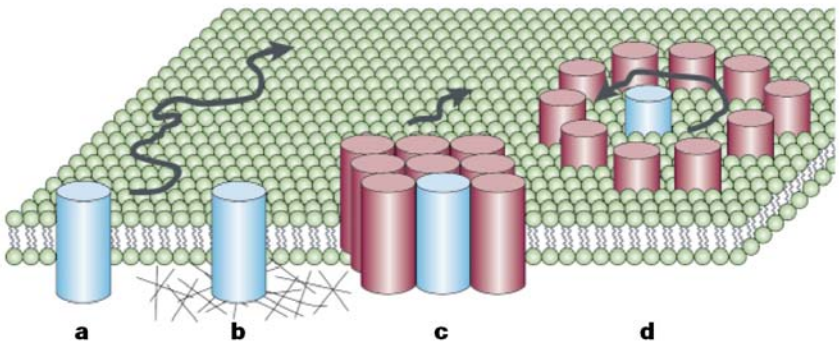

Figure 10 Mechanisms that reduce the mobility of membrane proteins. (**a**) An unrestricted membrane protein freely diffuses in the lipid bilayer of the membrane. (**b**) Membrane proteins bound to an immobile matrix (e.g. cytoskeleton) become immobilized. (**c**) Large multimeric protein complexes diffuse at significantly reduced rates within the bilayer compared with monomeric proteins with small transmembrane radii. (**d**) Corralling of a membrane protein by aggregated or matrix bound membrane proteins effectively reduces the long distance mobility of the protein. (taken from [40])

However, it is rather challenging and imprecise to determine interaction rate constants and equilibrium constants based on diffusion coefficients of membrane proteins. First, the unknown geometry of the membrane leads to a uncertainty in protein mobility by a factor of two or more. Second, the diffusion of membranes is often anomalous and measurement usually does not permit to distinguish between subdiffusion (Figure 10d) and a mixture of fast moving monomers and/or slow moving complexes (i.e. multiple populations having different diffusion coefficients) (Figure 10a and c).

7.2. Direct interaction detection using spectroscopic probes

Interaction between membrane proteins can be sensed more reliably by labeling both proteins with the spectroscopic probes or fluorescent proteins. Interactions can be detected using various experimental approaches. (i) During the course of the interaction both fluorescent labels are colocalized in the same membrane area and can be detected by standard fluorescence microscopy. However, colocalization does not necessarily mean interaction. (ii) Dual-colour cross-correlation analysis [78,81,89,99], a conceptual modification of FCS using two spectrally separable fluorescent labels, yields a considerable improvement in signal specificity for heterogeneous systems where molecular interactions of different species are to be observed. In principle, any molecular association and dissociation can be studied by simultaneous detection of two spectrally separated fluorophores, following the amplitude of the cross-correlation function in real time during the reaction. (iii) Fluorescence resonance energy transfer (FRET) [80,100-102] is one of the most elegant methods to quantify protein-protein interactions by measuring the rate of non-radiative transfer from the excited state of a fluorophore attached to one protein (donor) to another fluorophore attached to a binding partner (acceptor). The rate of energy transfer strongly depends on the distance between the donor and acceptor probes and their relative orientation. The FRET efficiency is usually determined by measuring the quantum yield or the fluorescence lifetime of the donor probe in the absence and presence of the acceptor probe, respectively. FRET proved particularly suitable for detecting dimerization and complex formation events in signaling networks [103-109]. FRET techniques usually provide qualitative information about dimerization events. Experimental limitations such as relatively high background of cellular autofluorescence, direct excitation of the acceptor, sensitivity to

photobleaching frequently biases the interaction experiments and require extensive correction factors [110-112].

8. Problem of quantitative detection

The interaction between receptor chains on the cell surface is constrained to the 2-dimensions of the membrane and thus the K_D has a dimension [molecules/μm²] or [mol/μm²]. Parameterization of receptor concentration on the membrane is a necessary requirement for quantitative studies. Different mathematical ways were suggested how to relate 2-dimensional interaction rate constants with readily measurable 3-dimensional rate constants. These are: (i) Introducing dimensionless rate constants [19] and corresponding equilibrium dissociation constants [113]; (ii) introducing 3D to 2D conversion coefficient [13,23,58,59]; (iii) use of interaction rate constant dimension [s^{-1}] for 2-dimensional association rate constant [62,114] or 3-dimensional units like [M^{-1}] for species placed in vesicles or cells, which are dispersed in aqueous solution [115]. Therefore, theoretical results concerning interactions in 2-dimensions were hardly confirmed experimentally. The complexity of in vivo systems usually does not allow drawing solid conclusions about determinants of protein-protein interactions on membranes. The requirement to parameterize 2-dimensional concentrations of interacting proteins as well as their complex was a big obstacle to determine 2-dimensional equilibrium dissociation constants (Eq.4). Fluorescent standards and correlation with radioimmunoassay are not readily available and does not offer real time monitoring.

Quantitative understanding of how membrane proteins function requires that the interactions of their components are monitored as they occur. Perturbations of the environment in which they operate, either before, during or after their assembly, may also give mechanistic insight. The possibility not only to monitor, but also to change 2-dimensional concentrations of receptors during the course of the experiment would be a powerful approach to dissect interactions on membranes. A systematic study of protein-protein interactions in well defined in vitro lipid bilayer would provide a firmer basis for the interpretation of experimental results in cells. Solid phase detection techniques, measuring time-resolved kinetics on a surface or in a layer, allow questions of size, valency, orientation and receptor density to be experimentally addressed.

9. Objectives

Protein-protein interactions on and within biological membranes play crucial roles in variety of cellular processes, and in particular in signal transduction. Despite advances in experimental techniques little has been done to quantitatively asses determinants of protein-protein interactions in two dimensions. The objective of this work was to establish detection techniques for studying ligand induced receptor assembling on a mechanistic and quantitative level *in vitro*. Based on this approach, the role of dimensionality and receptor orientation on interferon (IFN) induced interferon receptor (ifnar) crosslinking was quantitatively addressed. This study can be divided into following steps:

● Establishing an optical solid phase detection approach to quantitatively study lateral interactions on model lipid membranes *in vitro*.

● Applying this detection technique to study type I interferon (IFN) induced heterodimerization of the interferon receptor (ifnar) extracellular domains.

● Development of the mechanistic model for IFN induced ifnar assembling and determination of the 2-dimensional interaction rate and equilibrium dissociation constants involved in complex assembling.

● Exploring the influence of ifnar orientation on the 2-dimensional interaction rate and equilibrium dissociation constants.

10. Biological model system

10.1. Ifnar and differential signaling

Type I interferons (IFNs), first discovered by Isaacs [116,117], are a family of cytokines which act early in the innate immune response. IFNs initiate different signal transduction pathways leading to a pleiotropic response with antiviral, antiproliferative and immunmodulatory effects [118-129].

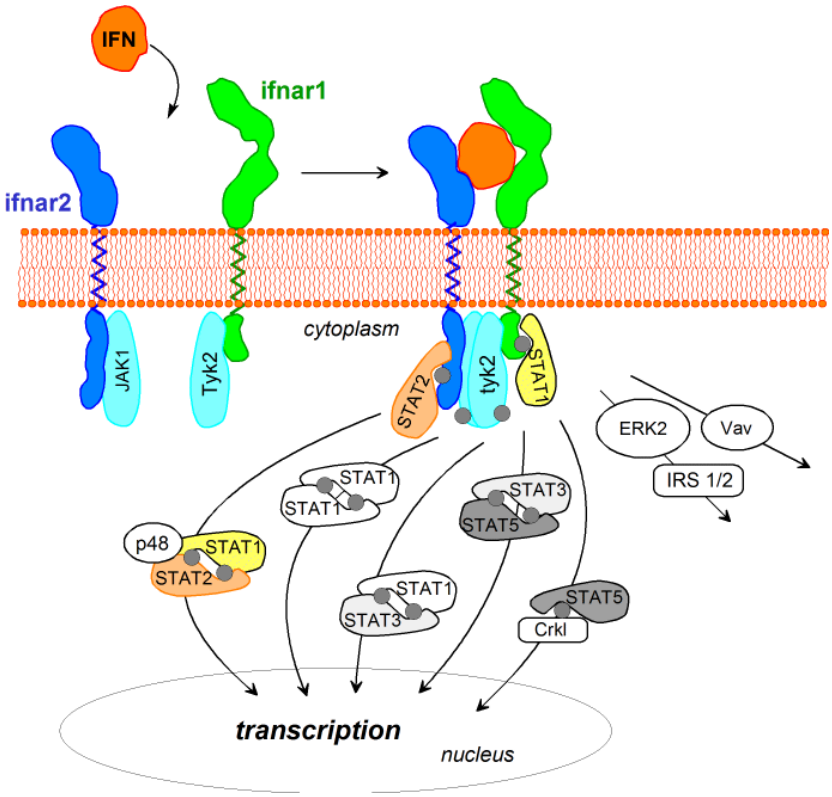

Figure 11 Schematic of type I interferon signaling. Binding of IFN crosslinks its common receptor chains, ifnar2 and ifnar1, and induces trans-phosphorylation of cytoplasmic domains, JAK kinases and associated STAT transcription factors. This leads to the activation of several signal transduction pathways.

The type I IFN receptor (ifnar) consists of 2 subunits: the high affinity subunit ifnar2 and the low affinity subunit ifnar1 (Figure 11). Ligand binding induces the assembling of the active receptor complex, which leads to the phosphorylation of tyrosine residues located in the intracellular domain of each receptor chain. These tyrosine phosphorylation events are carried out by Janus kinases (JAKs), JAK1 and TYK2, which are themselves activated by tyrosine phosphorylation. The subsequent substrates of the JAK1 and TYK2 are the signal transducer and activator of

transcription (STAT) proteins that are recruited and phosphorylated at the phosphotyrosines located at the cytoplasmic tail of receptor. Modified STATs are released from the cytoplasmic region of the receptor subunits to form homo- or heterodimers. Dimerized STATs are rapidly translocated to the cell nucleus and interact with specific regulatory elements to induce target gene transcription. The interferon-induced heterodimerization of ifnar2 and ifnar1 appears to have two purposes: to bring the JAKs into proximity and allow transphosphorylation, and to form a scaffold for the binding of STAT proteins.

10.2. Differential signaling

There are more than 10 different type I interferons [121] and all of them initiate different activity patterns by recruiting the same pair of receptor subunits. Different cell lines or cells at different stages of differentiation respond differently to the same interferon. Type I interferons do not enter the cell, so ifnar receptor crosslinking is essential in determining which signal transduction pathway will be initiated [13,130-132]. Initially it was suggested that different interferons form structurally different complexes with its shared receptor. The ifnar subunits crosslinked with different interferons bring cytoplasmic domains to different degree of proximity and orientation against each other. This results in different tyrosine phosphorylation pattern and different times will be required to phosphorylate them. Finally, different STATs will be recruited and different cellular responses initiated. Additionally, signaling complexes with different stoichiometry of ligand and receptor subunits have been suggested to be responsible for differential signaling. Also it was found that in some cases after receptor crosslinking large signaling complexes are formed on the intracellular side with scaffold, signaling, docking and effector proteins. Different combinations of these proteins were proposed to initiate different signals. Each cell can have a different set and different concentration of these proteins, which would define signaling specificity [131,133-136] and explain why different cell lines respond differently to the same interferon. However, the crystal structures of different interferons appeared to be very similar and the main difference between them were different affinities and interaction rate constants towards receptor subunits. Therefore, kinetics and equilibrium properties of crosslinking dynamics on membranes were suggested to be responsible for differential signaling. Signaling intensity is proportional to the amount of phosphorylated STATs and probably different threshold concentrations are required to initiate different responses. The amount of phosphorylated STATs depends on the

amount of crosslinked receptor. As it was presented in chapter 5.3, it depends on ligand concentration in solution, concentrations of the receptor subunits on the membrane and corresponding 3- and 2-dimensional equilibrium dissociation constants. Having receptors in different compartments with different densities could help to code the response to ligand concentration. Membrane compartments with high and low receptor density will have different amounts of crosslinked receptors at the same ligand concentration [137-139]. The kinetics of receptor assembling and the lifetime of the ternary complex explain differential signaling in terms of kinetic proofreading [140-144]. The cytoplasmic receptor domains must undergo a series of modifications before generating a productive signal. If a ligand dissociates before these modifications are completed, the generation of a productive signal is prevented. When many steps are involved, then slowly dissociating ligands will generate stronger cellular responses than rapidly dissociating ones. In case of fewer modification steps ligands with different kinetic properties may trigger similar responses or even responses in which the expected sensitivity to ligand-receptor binding kinetics is reversed. In conclusion, the 2-dimensional interactions between ifnar subunits can be largely responsible for defining specificity of differential signaling. Therefore, investigation of IFN induced ifnar crosslinking is important not only from fundamental understanding of 2-dimensional interactions point of view, but it is also a prerequisite for systematic manipulation of receptor mediated responses in therapeutical applications.

10.3. Model in vitro system

Several striking features make the IFN-ifnar interaction a particularly suitable model system for studying 2-dimensional interactions: First, the receptor subunits interact independently from each other with the ligand, and do not interact in the absence of the ligand as proposed for other cytokine receptors. Second, only a heterodimeric ternary complex was detectable, involving ifnar2, ifnar1 and IFN in a 1:1:1 stoichiometry. Thus, the receptor heterodimerization is triggered by a ligand binding from solution and 2-dimensional interactions can be probed by the dissociation kinetics of the ligand away from the membrane.

There is no interaction between ifnar intracellular and extracellular domains. One transmembrane helix allows reducing overall complexity to only the extracellular

domains (Figure 12). A decahistidine-tag was fused to the C-terminus instead of the transmembrane helix for tethering the proteins to the membrane (**see chapter 11**).

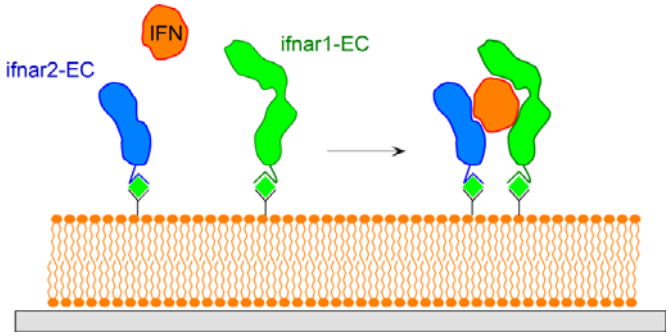

Figure 12 Model in vitro system to study IFN induced ifnar assembling.

11. Solid phase detection

2-dimensional concentrations of the biomolecules on surfaces are quantitatively detected in a straightforward manner by solid phase label-free detection techniques. These techniques sense changes in optical or acoustic properties at the interface layer above the surface induced by molecules binding to or dissociating from the surface, and are particularly suitable to study interactions between soluble and membrane-anchored proteins.

Solid phase detection of molecular interactions offers a substantial advantage over investigations in bulk solution. If a receptor is immobilised on the sensor surface, the subsequent binding of the ligand is detected by a change of the optical or acoustic properties of the sensor surface, without an additional separation step. From the practical point of view, additional important advantages come into play. These techniques can be combined with modern fluid handling devices, thus not only equilibrium signals, but also interaction kinetics can be measured and quantitatively analyzed. Measurements require minimal sample volumes and receptor quantities and furthermore can be fully automated resulting in a substantial increase of sensitivity and reproducibility of signal detection.

Different physical phenomenons are employed to detect molecular binding to the surface, which will be discussed in more detail in the following chapters.

11.1. Quartz crystal microbalance with dissipation monitoring

The quartz crystal microbalance with dissipation monitoring (QCM-D) [145,146] measures mass and viscosity changes in processes occurring at or near surfaces, or within thin films. The instrument measures the resonance frequency and energy dissipation of a piezoelectric quartz crystal. The resonance frequency changes linearly with the amount of biomolecules deposited on the crystal surface. The energy dissipation at the resonance frequency changes with the viscosity / elasticity of the material in contact with the crystal surface. Adsorbed biomolecular film may consist of a considerably high amount of water, which is sensed as an additional mass. By measuring the dissipation it becomes possible to judge if the adsorbed film is rigid or water rich (soft) which is not possible by detecting at the frequency response alone. The amount of water may be very different depending on the kind of molecule and the type of surface studied.

QCM-D is one of the few solid phase detection techniques, where kinetics of protein adsorption and subsequent structural rearrangements can be directly measured and analyzed simultaneously in real time [147]. However, the resonance frequency and the energy dissipation are not independent parameters. The resonance frequency is dependent on the buffer viscosity and conformational changes change not only the dissipation but also the resonant frequency. Commercial QCM-D devices have lower detection limit of 50 pg/mm² and can detect submonolayer surface coverage by small molecules or protein films. At the upper end, they are capable of detecting whole cells bound to the surface [148] or biomolecular layers with thicknesses up to 10μm.

11.2. Optical reflectometric techniques

Optical techniques are relatively simple, non-destructive and non-invasive, do not require vacuum and can be applied in any transparent media and are the natural choice to study real time protein-protein interactions *in vitro* and *in vivo*. Optical label-free detection is based on the fact that biomolecules have different refractive index than aqueous solution. Proteins, bound to the surface, replace the buffer and change effective refractive index of the solid-liquid interface. This refractive index change is the main parameter which is used to sense biological interactions by variety of optical detection schemes. Additionally, the thickness of the biomolecular layer and the

absorption of adsorbed molecules can be used as readout to monitor biomolecular interactions in real time.

11.2.1. Ellipsometry

Historically ellipsometry was the first method introduced to quantitatively investigate thin layers of adsorbed biomolecules at solid-liquid interfaces. Ellipsometry is a technique that can be used to measure the thickness and refractive index of the thin transparent or semi-transparent films [149]. The technique utilizes the polarization change of light upon reflection from a surface (Figure 13). The polarization change is defined by the ratio of the total reflectance coefficients, R_p and R_s, for light polarized parallel (p) and perpendicular (s) to the plane of incidence, respectively.

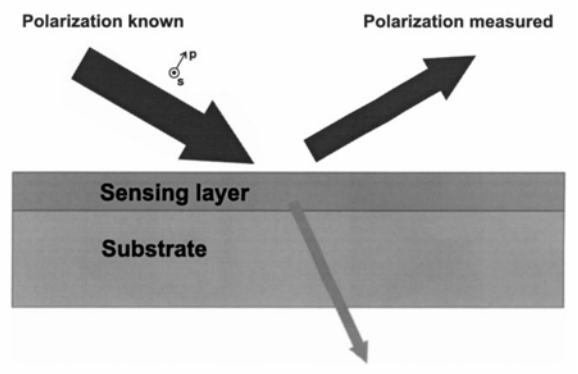

Figure 13 Principle of ellipsometry. Properties of biomolecular film are calculated by measuring polarization changes before and after reflection from the surface.

This ratio can also be expressed in terms of ellipsometric angles Ψ and Δ.

$$\frac{R_p}{R_s} = \tan\Psi \cdot \exp(i\Delta) \qquad \text{Eq. 15}$$

In short, Δ is the difference in phase shift between p-wave and s-wave of the light before reflection from the surface minus the difference in the phased shift after reflection from the surface. TanΨ is the corresponding amplitude ratio of R_p and R_s. Ellipsometry is not a direct technique. Thickness and refractive indexes are calculated from measured ellipsometric angles Ψ and Δ using optical models. The final result depends on the model used for data evaluation.

The surface mass density, Γ, for an adsorbed protein layer can be calculated from the thickness and refractive index using de Feijtert's formula [150]:

$$\Gamma = \frac{d \cdot (n_1 - n_2)}{dn/dc} \qquad \text{Eq. 16}$$

where d is the thickness of the layer, n_1 is the refractive index of the adsorbed layer, n_2 is the refractive index of the solution and dn/dc is the refractive index increment of the solute. For proteins, dn/dc is 0.18 cm^3g^{-1} and for lipid layers 0.16 cm^3g^{-1} [151].

The traditional technique used in real-time ellipsometric studies is null ellipsometry presented in Figure 14. Positions of the polarizer, compensator and analyzer (another polarizer) are adjusted to get minimum (null) signal to the detector and these values are used to calculate the ellipsometric angles [149] and the corresponding thickness of the biomolecular layer.

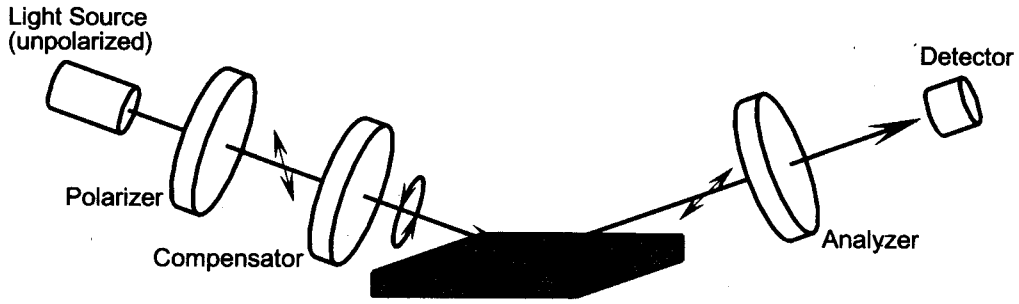

Figure 14 Schematic of a nulling ellipsometer. The optical components are adjusted to minimize (null) the signal reaching the detector.

In more advanced studies such parameters as tilt angle of molecules in a monolayer, density of a protein layer, mass distribution (density gradient) over a protein layer, lateral mass distribution (surface clustering) can be determined. Such studies require state of the art spectroscopic and imaging ellipsometers [152,153] as well as advanced optical modeling.

11.2.2. Interferometry

Reflectance interferometry (RIf) measures the intensity of the reflected light, which is modulated by the thin layer interference (Figure 15A) [154-158].

For perpendicular incidence and a single non-absorbing layer the reflected intensity I is equal:

$$I = I_1 + I_2 + 2\sqrt{I_1 I_2}\cos(4\pi nd / \lambda) \qquad \text{Eq. 17}$$

where I_1 and I_2 are the reflected intensities from the bottom and top interfaces of the thin film, d is the physical thickness of the film, n is the refractive index and λ is the wavelength of the incident light.

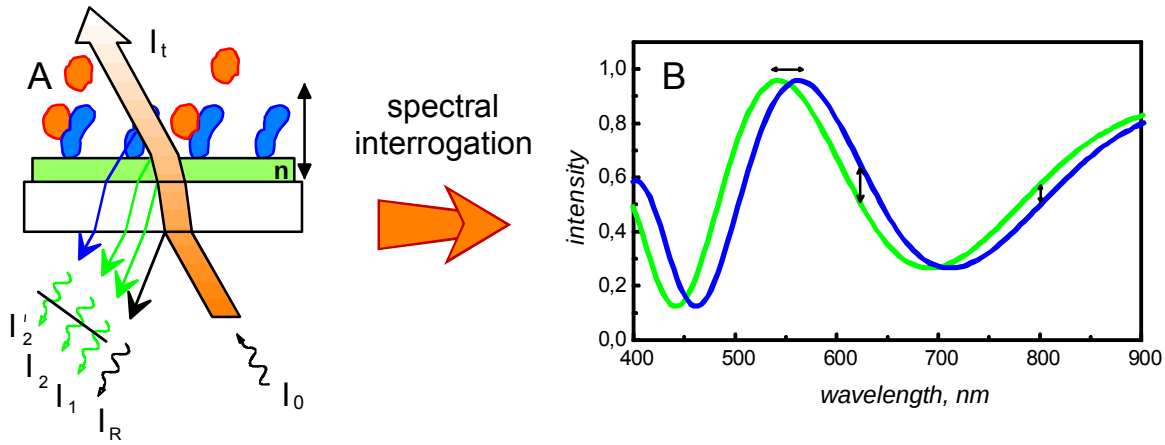

Figure 15 (**A**) Principle of the detection of affinity interactions by reflectance interferometry. n and d are the refractive index and the average physical thickness of the layer, respectively, I_1 and I_2 are the intensities of the light beams, reflected at the interfaces of the layer. (**B**) Spectral reflectance pattern due to constructive and destructive interference of the reflected radiation (green). Upon ligand binding, interference pattern shifts to the longer wavelengths (blue). The interaction is detected by monitoring the position of the extremum (horizontal arrow) of the interference pattern or by change in intensity at a given wavelength (vertical arrows).

A typical spectral interference pattern showing the modulation of intensity with *cos(1/λ)* is presented in Figure 15B. During the protein deposition on the surface, the optical thickness *(n*d)* of the interference layer increases and interference pattern shifts to longer wavelengths (Figure 15B). This shift can be detected by measuring the position of the interference pattern maximum or by change in intensity at given wavelength.

Interferometric detection can be readily realized with standard light sources, detectors and fiber optic components (Figure 16A). White light from a tungsten halogen lamp is delivered to the surface via a bifurcated optical fiber. The intensity of the reflected light is detected by a spectral or non-spectral detector. Flow through conditions allows real time detection of binding kinetics. Spectral shifts or intensity changes, monitored in real time, are converted into a binding curve (Figure 16B).

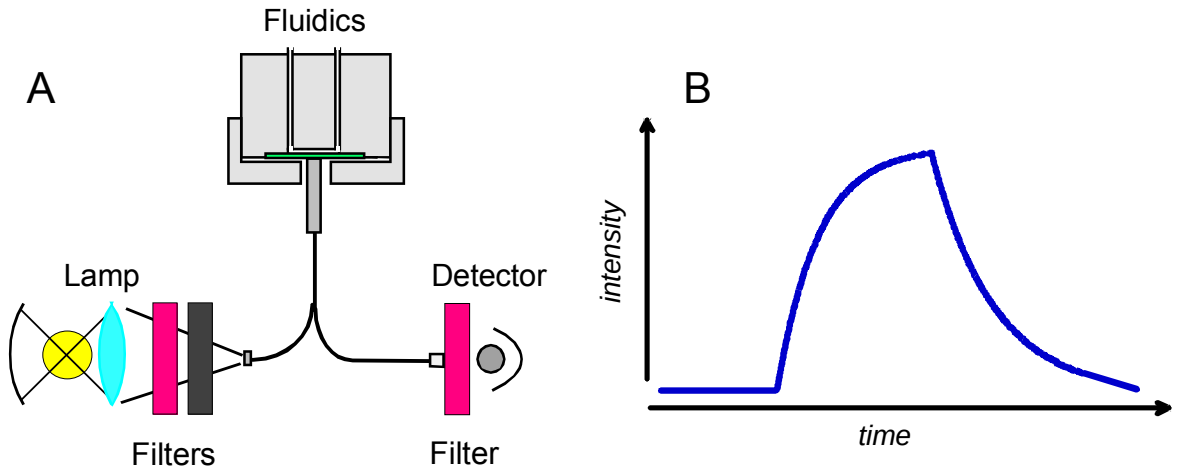

Figure 16 (**A**) Schematic of reflectance interferometric detection. (**B**) Typical example of the binding curve.

11.3. Evanescent field techniques

When light reaches the interface between two mediums, it is reflected and refracted. The incidence and refraction angles are related by Snell's law:

$$n_1 \sin\theta_1 = n_2 \sin\theta_2 \qquad \text{Eq. 18}$$

If the refractive index of the first medium is higher than for the second, $n_1 > n_2$, then $\theta_1 < \theta_2$. The incidence angle when $\theta_2 = 90°$ is called the critical angle θ_c.

$$\theta_c = \sin^{-1}(n_2 / n_1) \qquad \text{Eq. 19}$$

If the angle of incidence is higher than θ_c, then the light is totally internally reflected and does not propagate into the second medium. Even so, some of the light still penetrates the medium of lower diffractive index as an electromagnetic field called the "evanescent wave" [159,160]. A key characteristic of the evanescent wave is that it propagates parallel to the interface, vanishing exponentially with distance. The decay length (d_p) of the evanescent wave along the depth of field depends on the incident angle (θ), the wavelength of the excitation beam (λ) and the diffractive indices of both media:

$$I_z = I_0 \exp(-z / d_p)$$
$$d_p = \frac{\lambda}{4\pi\sqrt{n_1^2 \sin^2\theta_1 - n_2^2}} \qquad \text{Eq. 20}$$

It should be emphasized that when the incident light is s-(perpendicular) polarized the evanescent field is purely transverse to the direction of propagation. In the p-(parallel) polarization case, the evanescent field has two non-zero components with a

phase difference equal to $\pi/2$. Therefore the extremity of the field vector will describe ellipse as time evolves.

An evanescent field can be generated also by diffraction from a sub wavelength size aperture or a grating. The smaller the diameter of the aperture, the large the bending of the diffracted beam. When the width of a slot is equal to $\lambda/2$, the emerging beam fills the entire half space (Figure 17). If the aperture size is reduced below this value evanescent waves will be generated at the interface and their intensity will decay exponentially with the distance from the interface.

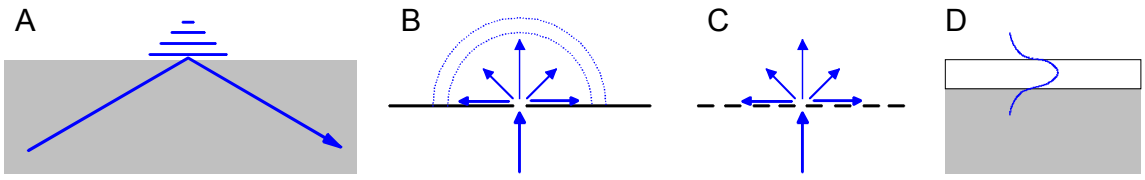

Figure 17 The systems generating an evanescent field. (**A**) total internal reflection of a light beam; (**B**) diffraction of a beam from an aperture; (**C**) diffraction from the grating; (**D**) evanescent field of a guided mode. (Adapted from [160])

The phenomenon of TIR, it be generated by a prism or by a waveguide, is highly sensitive to all parameters involved, namely to the wavelength, refractive indices of the media, surface roughness, etc. This sensitivity has given rise to the production of several different types of sensors, especially in the field of optics and nanobiotechnology. The exploitation of evanescent properties of light has led to impressive progress in such areas as fibre optics, near-field microscopy and biomolecular interaction analysis.

11.3.1. Evanescent field interferometric techniques

The evanescent wave velocity is sensitive to the refractive indices of both materials at the interface. This effect was used to construct interferometric sensors. The basic principle of fiber optic Mach-Zehnder type interferometer is depicted in Figure 18. A linear waveguide (I) is divided into two arms at a Y junction (II), where light is distributed equally between the waveguides (III) and (IV). Branch (III) presents locally a depression where the waveguide is in contact with the buffer. Upon protein binding to the waveguide, the refractive index at the waveguide-buffer interface will change and will be different from the one in branch 2 (IV). For the same geometrical distance travelled inside the waveguide, the optical path in each branch will be

different. After the second Y junction (V), the two modes recombine. Depending on the phase difference they will produce constructive or destructive interference, which is used as the readout for binding or dissociation events from the waveguide surface.

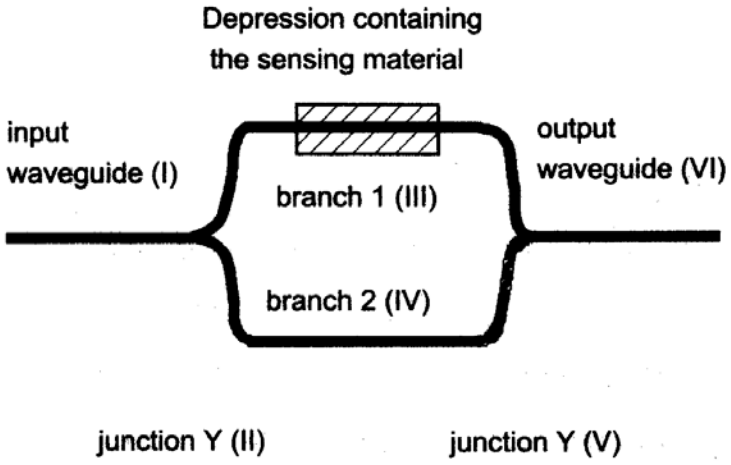

Figure 18 Evanescent field Mach-Zehnder interferometer. (taken from [160])

11.3.2. Resonant mirror.

Resonant mirror is a optical biosensor design [161,162], which uses the evanescent wave associated with a dielectric resonant structure to probe binding events occurring in a sensing layer, deposited within few hundred nanometers of the device surface (Figure 19). The evanescent field, generated upon light reflection from the prism is perturbed by a high refractive index waveguide layer. Light may couple to the resonant layer via the evanescent field. Efficient coupling occurs only for certain incident angles, where phase matching between in incident beam and the resonant modes of the high index layer is achieved. At the resonant point, light couples into the high refractive index layer and propagate some distance along the sensing interface before coupling back to the prism. The resonant angles are different for p and s polarisations. Therefore interference between them is used for readout. Binding of the protein to the sensing layer increases the angle of incidence, at which resonance coupling occurs.

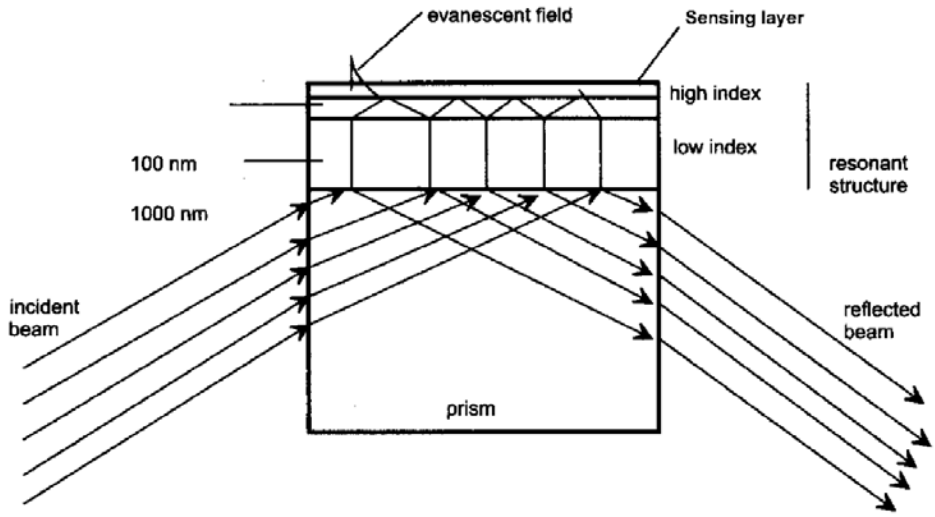

Figure 19 Structure of the resonant mirror biosensor (taken from [160])

11.3.3. Internal reflection spectroscopy

Another application of great importance concerns the possibility of producing spectroscopic measurements by total internal reflection. Evanescent light, like propagating light, can be absorbed, depending on the material deposited at the interface where it arises. This property is used to obtain absorption spectrums of the deposited materials. Sensitivity can be enhanced by using multiple internal reflections in optical fibers, waveguides or other optical elements and by means of Fourier transforms. Binding of the proteins to the interface can be followed as an increase in the absorption at a specific wavelength in the infrared. This combination is also widely used to detect conformational state and conformational changes of the proteins adsorbed to the interface or to biological membrane.

11.3.4. Surface plasmon resonance-based detection

When there is a thin gold (or other noble metal) layer at the interface between two dielectric materials then the evanescent field interacts with free electrons and a charge density wave, also called surface plasmon is generated. Under resonance conditions, the energy from the evanescent light is efficiently transferred to these charge oscillations, which cause drastic reduction in the intensity of the reflected light. The resonance angle, at which the intensity minimum occurs, is a function of the refractive index of the solution close to the gold layer (Figure 20).

As biomolecules are immobilized on a sensor surface, the refractive index at the interface between the gold surface and a solution flowing over the surface changes,

altering the angle, at which reduced intensity light is reflected from a supporting glass plane. The change in the resonance angle, caused by binding or dissociation of molecules from the sensor surface, is proportional to the mass of bound material. Surface plasmon resonance detection is the most sensitive and most popular commercially available label free solid phase detection technique today.

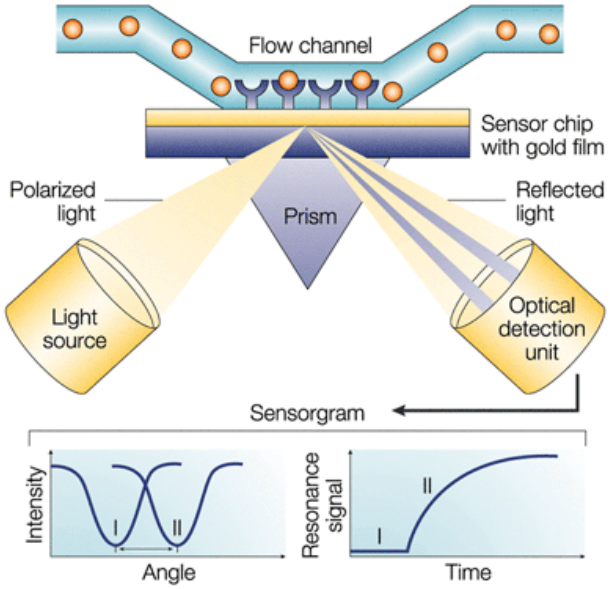

Figure 20 Surface plasmon resonance (SPR) detects changes in the refractive index in the immediate vicinity of the surface layer of a sensor chip. SPR is observed as a sharp decrease in the reflected light from the surface at an angle that is dependent on the mass of material at the surface. The SPR angle shifts (from I to II in the lower left-hand diagram) when biomolecules bind to the surface and change the mass of the surface layer. This change in resonant angle can be monitored non-invasively in real time (taken from [163]).

11.3.5. Total internal reflection fluorescence spectroscopy (TIRFS)

Fluorescent molecules in the medium with the lower refractive index that are on or near interface are selectively excited by the evanescent illumination (Figure 21A) [164-171]. This type of excitation is particularly suitable to analyze interactions at membranes because only fluorophores at the interface will be excited and others in solution remain dark. This feature drastically reduces the background level, and even single molecule fluorescence detection becomes possible [96,171,172]. TIR is realized with different prism (Figure 21B) [173-180] and objective type [168,171,181] optical geometries and can be combined with many fluorescence detection modes like FRAP [182,183], FCS [82,184], and FRET [174].

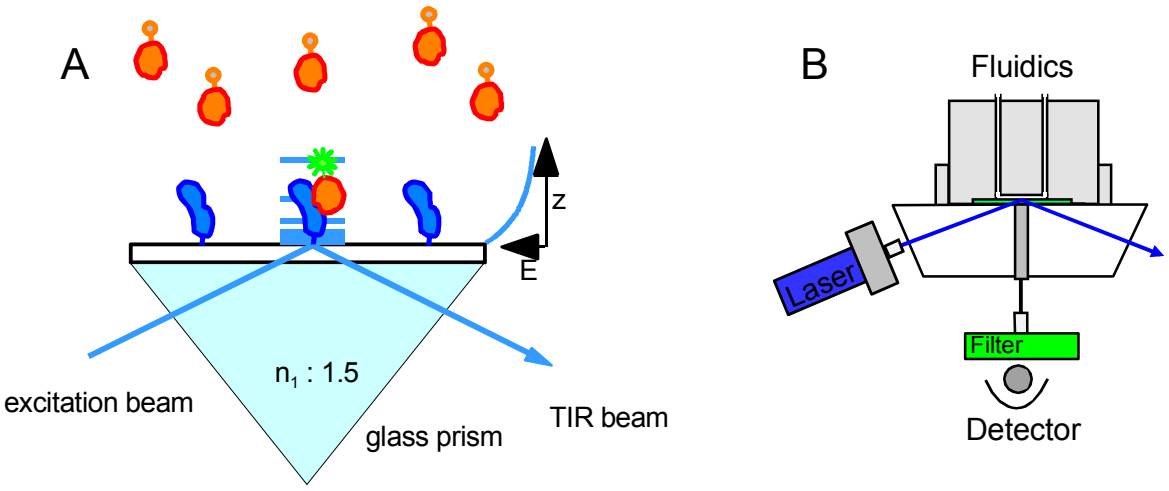

Figure 21 (**A**) Principle of total internal reflection fluorescence spectroscopy. (**B**) Schematic of prism based TIRFS detection.

In contrast to the relatively constant fluorescence emission rates in free solution, it is known that the radiative emission rates can be modified by placing the fluorophores at suitable distances from metallic surfaces and particles [185-190]. The effects of metallic surfaces are complex and include quenching at short distances, spatial variation of the incident light field, and change the fluorescence lifetime rates. The evanescent field, amplified by the surface plasmons will enhance fluorescence intensity of the fluorophores at the interface. Due to fluorophore dipole interaction with free electrons in the thin metal layer, normally isotropic emission is converted into highly directional emission at a well-defined angle from the normal axis (Figure 22). Therefore, surface plasmon enhanced and directional fluorescence emission increases signal to noise, simplifies detection and provides numerous opportunities for new approaches in surface sensitive fluorescence spectroscopy.

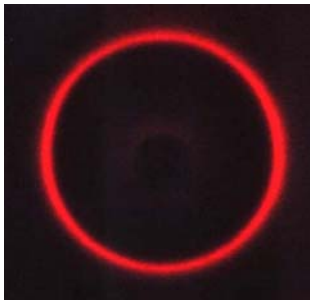

Figure 22 Cone of the surface plasmon coupled directional fluorescence emission of the fluorophores at the surface of the thin metallic film. (taken from [188])

11.4. Combined label and label-free solid phase detection

Label free detection allows absolute quantification of adsorbed biomolecules on the surface. However, the response is directly related to the molecular mass of the species bound to the sensor surface, and it is difficult or sometimes impossible to detect small analytes or do measurements at very low surface concentrations of the immobilized receptor. The sensitivity of signal detection is in general far below that of fluorescence measurements. Fluorescence detection is very sensitive, and with modern detectors single fluorophore sensitivity can be achieved. However, the amplitude of fluorescence signal is difficult to quantify absolutely because it depends on the excitation power, the light collection efficiency, the excitation and the detection filters, the labeling degree and other experimental parameters. In complex receptor-ligand interactions it is not always possible to have all interacting proteins labeled and to exclude that labeling has no effect on protein function. Therefore the combination of fluorescence and label free-techniques is an ideal solution to study ligand induced receptor crosslinking. Label-free detection allows to absolutely quantify the amount of interacting proteins on the surface and simultaneously provides possibility to convert arbitrary fluorescence signal into absolute units like ng/mm² or mol/mm². Simultaneous fluorescence detection allows to measure interaction kinetics with high signal to noise ratio and automatically solves sensitivity the problem associated with label free detection. Additionally, effects of local probe environment on the fluorescent probe brightness and energy transfer between donor and acceptor probes can serve as the readout for receptor crosslinking and allow differentiating between different conformational states.

Typical experiment of combined label and label free detection is showed in Figure 23. All steps of surface architecture formation are detected by label-free detection: vesicle fusion on the surface, bilayer conditioning, immobilization of the receptor. None of these molecules are labeled, so fluorescence channel shows no signal. The labelled ligand binding to surface anchored receptor is simultaneously detected on both channels. Due to higher sensitivity, the fluorescence signal provides much higher signal-to-noise ratio.

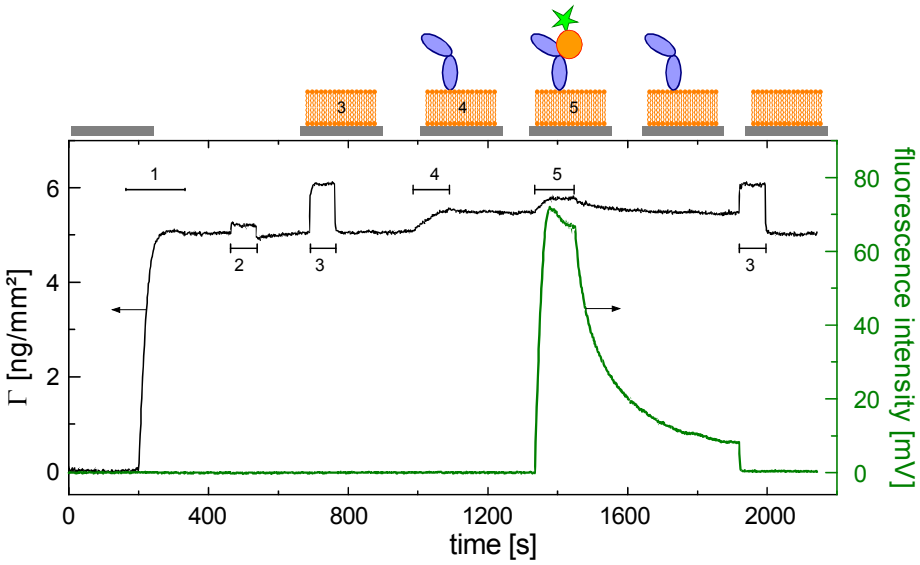

Figure 23 Course of a typical binding experiment on supported lipid bilayers as detected by label-free (black) and fluorescence (green) detection. Injection of (1) vesicle fusion, (2) and (3) – membrane conditioning, (4) receptor immobilization and (5) binding of the fluorescently labeled ligand.

From technical point of view, the combination of fluorescence and label-free detection techniques is a straightforward approach. The same light beam can be used to probe refractive index changes due to protein binding to the surface and excite fluorophores which are present at the interface. Fluorescence can be emitted directly to the optical fiber or waveguide and later spectral detector will be used to independently detect changes of refractive index and measure fluorescence intensity (Figure 24).

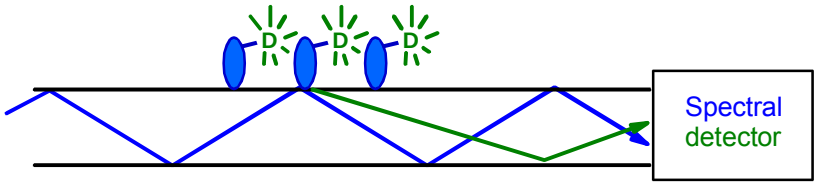

Figure 24 Combination of evanescent field fluorescence and label free detection techniques. The same light beam (blue) is used to probe the amount of proteins on the surface and to excite fluorophores present at the interface. The fluorescence is emitted to the same optical fiber or waveguide (green) and both signals are independently detected by spectral detector (not shown).

Another detection scheme would be to use interferometric, resonant mirror or surface plasmon resonance biosensors and collect fluorescence signal from the top of the surface (Figure 25). Combination of evanescent field excited fluorescence with

SPR, called surface plasmon field-enhanced fluorescence spectroscopy, has been shown to be a powerful tool for characterizing processes at interfaces (Liebermann and Knoll, 2000; Neumann et al., 2002).

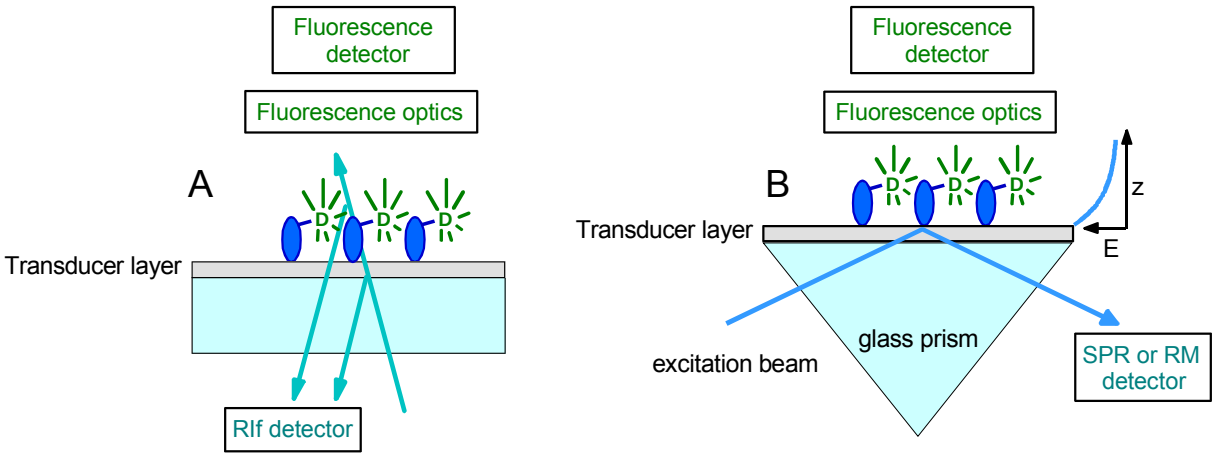

Figure 25 Combination of fluorescence and label-free detection techniques. The same light beam (cyan) is used to probe the amount of proteins on the surface and excite fluorophores present at the interface. Fluorescence is collected from the top of the surface. (**A**) Interferometric – epifluorescence approach; light beam comes perpendicular to the surface. Optical thickness of the biomolecular layer is probed interferometrically by RIf detection. Fluorescence is detected from the top of the surface. (**B**) Combined SPR or resonant mirror and TIRFS approach. Changes in refractive index are probed by measuring intensity of the reflected light. Evanescent field excited fluorescence is collected and detected from the top of the surface.

All presented detection schemes use the same light source for fluorescence excitation as for label-free detection, thus limiting the flexibility of each technique. Additionally, absorption by the fluorophores affects the intensity and phase difference of TIR beam, thus, introducing a crosstalk between the two detection techniques. The refractive index close to the absorption band differs from the one far from absorption peak; it has a different absolute value and a sharp negative dispersion profile. Furthermore, strong light intensity required for label-free detection can bleach fluorophores and complicate fluorescence experiments. The metal layers required for SPR are furthermore disadvantageous due to their strongly surface distance-dependent fluorescence quenching. Ideally, combined fluorescence and label-free detection should be simultaneous, independent and without crosstalk.

We combined reflection interferometry (RIf) and total internal reflection fluorescence spectroscopy (TIRFS) detection techniques into a single experimental

set-up which fully implements above-mentioned features and is schematically presented in Figure 26. Fluorescence excitation and emission were kept independent of RIf illumination by implementing monochromatic RIf detection in the near infrared region. Complete spectral separation of the two techniques proved valuable as high-power illumination for optimum RIf detection could be applied without photobleaching the fluorophores absorbing in the visible region. This allowed us to fully eliminate crosstalk between two techniques by using proper combinations of detection filters. Flow through conditions allowed real-time detection of ligand binding and receptor crosslinking events.

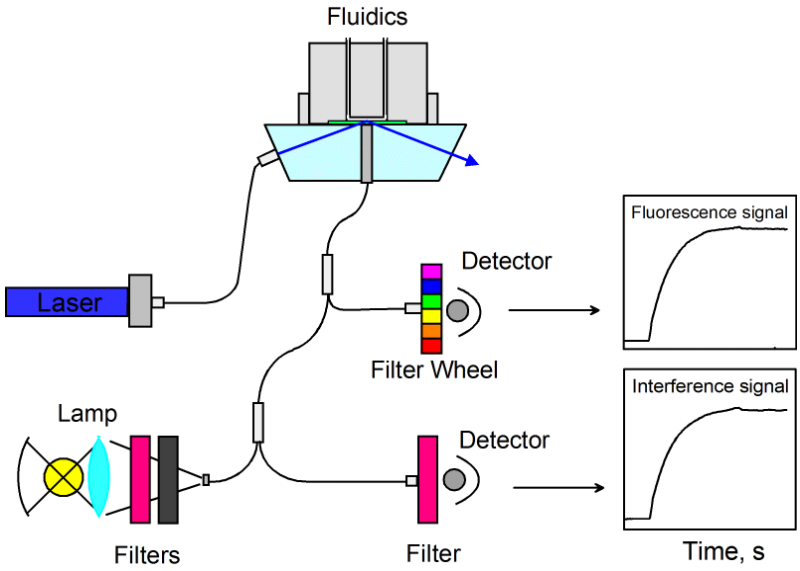

Figure 26 Schematic of combined reflectance interferometric and total internal reflection fluorescence spectroscopic detection.

12. Solid-supported lipid bilayers

It is known that membrane environment is important, if not essential, for membrane receptor function and reconstitution of membrane proteins in model lipid membranes is a necessary requirement to study their interactions *in vitro*. The combination of optical biosensor (label and label free) techniques with fluid lipid membranes fused on a solid support [191-197] offers the advantages of surface sensitive solid phase detection with keeping membrane proteins in their natural environment. Small unilamelar vesicles (SUV) fused on hydrophilic surfaces form solid supported bilayer with well-defined composition, electrostatic and fluidic properties. SUV fusion and bilayer formation was intensively studied with many techniques including QCM-D [198,199], ellipsometry [200], interferometry [201], surface plasmon resonance [202], fluorescence microscopy [203] and atomic force

microscopy [204,205]. Solid supported membranes offer the platform to reconstitute membrane receptors and quantitatively study effects of dimensionality, fluidity and electrostatics on 2-dimensional interactions under defined conditions.

Specific and oriented tethering of C-terminal decahistidine-tagged extracellular domains of ifnar2 and ifnar1 was achieved using lipid molecules which carry covalently attached chelator bis-nitrilotriacetic acid (bis-NTA) groups (figure 26A) [206]. The formation of the decahistidine and bis-NTA complex is highly specific. Furthermore it is fully reversible upon addition of a competitive ligand (imidazole), protonation of the histidines, or removal of the metal ions by EDTA complexation. FRAP measurements confirmed that bis-NTA lipids do not phase segregate and bilayer fluidity is not affected by bis-NTA attachment or decahistidine tagged protein immobilisation (figure 26B).

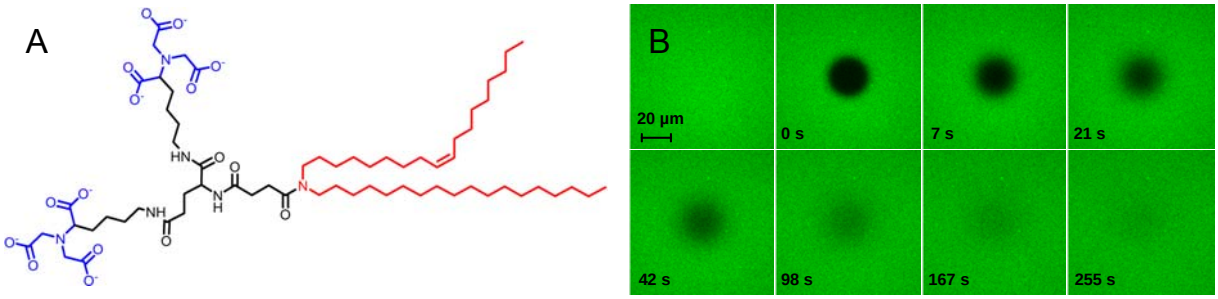

Figure 27 (**A**) structure of bis-NTA lipids. (**B**) FRAP experiment confirm bilayer fluidity and homogeneity of bis-NTA lipid bilayer.

13. Approach summary

Solid supported lipid bilayer provided 2-dimensional interaction environment for membrane receptors. Ifnar2-EC and ifnar1-EC were reconstituted in the specific, oriented and stable yet reversible manner on fluid lipid bilayer via decahistidine and bis-NTA interaction. The 2-dimensional concentrations were absolutely quantified by label-free interferometric detection and ligand induced receptor crosslinking kinetics were sensitively and simultaneously detected by total internal reflection fluorescence spectroscopy. Binding curves were fitted with 2-step interaction model and 2-dimensional dissociation and association rate constants of ifnar crosslinking were independently determined. Detection system allowed parameterizing all variables in the model leaving 2-dimensional interaction rate constants the only variables during the fitting.

14. Papers

14.1. Paper I.

Lamken P, Lata S, Gavutis M Jacob Piehler: **Ligand-induced Assembling of the Type I Interferon Receptor on Supported Lipid Bilayers.** *Journal of Molecular Biology*, 2004, **341**: 303-318

This paper presents the in vitro approach to study type I interferon (IFN)-induced crosslinking of its receptor subunits, ifnar2 and infar1. SOPC lipid vesicles doped with bis-NTA chelator groups were fused on to silica transducer surface and formed fluid solid supported lipid bilayer. Membrane fluidity was confirmed by FRAP experiments. The extracellular domains of the interferon receptor subunits ifnar2-EC and ifnar1-EC carrying C terminal decahistidine tag were anchored to solid-supported membranes via C-terminal decahistine tag and bis-NTA chelator interaction. The high stability and specificity of this interaction ensured stable and oriented reconstitution of receptor subunits. Interactions on solid supported membrane were optically detected using novel combination of two solid phase detection techniques: label-free reflectance interferometry (RIf) and total internal reflection fluorescence spectroscopy (TIRFS). Flow through conditions allowed monitoring of interaction events in real time.

Main results:

● Equilibrium dissociation constants and association / dissociation rate constants of individual interactions between IFNα2 and individual subunits were measured and parameterized.

● No interaction between the receptor subunits in absence of the ligand was detected.

● The stoichiometry of the ternary complex between ligand and receptor subunits was estimated to be 1:1:1.

● Stoichiometric coimmobilization of receptor subunits on solid supported membrane decreased observed ligand dissociation rate constant 2-200 times depending on 2-dimensional concentrations of the membrane-anchored receptor subunits.

● Dissociation rate constant of fluorescence labelled IFNα2 is increased in presence of nonlabelled ligand indicating kinetic nature of interactions between membrane anchored ifnar subunits.

● Based on experimental data an IFN-induced 2-step ifnar assembling model was proposed.

14.2. Paper II.

Gavutis M, Lata S, Lamken P, Müller P, Piehler J: **Lateral Ligand-Receptor Interactions on Membranes Probed by Simultaneous Fluorescence-Interference Detection.** *Biophysical Journal*, 2005, **88**: 4289–4302

This paper describes in detail simultaneous, real-time RIf-TIRFS detection, introduced in paper 1 and its potential for quantitative studying interactions on membranes. RIf and TIRFS techniques were combined in single experimental setup and allowed simultaneous real-time detection of both signals without crosstalk between them. This was achieved by using separated excitation and detection modules for both techniques and spectrally separating them. RIf detection was performed in NIR and TIRFS in VIS spectral regions. Flow-through conditions allowed to monitor binding assays in real time.

Main results:

● The RIf-TIRFS setup was characterized and calibrated with respect to noise and detection limits using Oregon Green 488 labelled lipid bilayer and Oregon Green 488 fluorophore solution as a model systems. Detection limits were determined to be 10 pg/mm² for RIf and 10 fluorophores/µm² for TIRFS. The flow through system allowed measuring interaction rate constants up to 5 s^{-1}.

● Sensitive fluorescence detection allowed measuring binding kinetics at very low surface concentrations of immobilized receptor subunits. Dissociation rate constants of IFNα2 were found to be 0.013 s^{-1} and 1 s^{-1} for ifnar2-EC and ifnar1-EC respectively.

● The observed ligand dissociation rate constant depends on absolute as well as relative 2-dimensional concentrations of co-immobilized receptor subunits ifnar2-EC and ifnar1-EC on the membrane

● 2-step dissociation model based on an interaction model presented in paper 1 was used to fit the ligand dissociation curves at different stoichiometric amounts of immobilized receptor subunits. The detection system allowed parameterizing all variables in the model except the 2-dimensional association rate constant k_a^T between ifnar1-EC and binary complex between ifnar2-EC and IFNα2.

● k_a^T was found to be 16 mm²fmol^{-1}s^{-1} and the corresponding 2-dimensional equilibrium dissociation rate constant K_D^T 0.06 fmol/mm². Experiments with IFNα2 mutants M148A and R144A showed that deviations from the model appear when association rate constants of IFN towards the individual ifnar subunits gets comparable.

14.3. Paper III

Lamken P, Gavutis G, Peters I, Van der Heyden J, Uzé G, Jacob Piehler: **Functional Cartography of the Ectodomain of the Type I Interferon Receptor Subunit ifnar1.** *Journal of Molecular Biology*, 2005, **350**: 476-488

In this paper, the role of ifnar1-EC subdomains with respect to ligand binding and receptor crosslinking was investigated using the experimental approach described in paper 1 and 2, and by FACS analysis. Different C and N terminal decahistidine tagged Ifnar1-EC fragments were expressed in *Sf9* insect cells and purified to homogeneity.

Main results:

● From binding assays with IFNα2 and IFNβ it was concluded that all the three N terminal ifnar1-EC subdomains are involved in ligand binding.

● IFNα2 and IFNβ bind competitively to ifnar1-EC and the fragments with three N terminal subdomains indicating the same binding site for both IFNs.

● The role of orientation in ternary complex assembling was qualitatively compared for different constructs by comparing observed ligand dissociation rate constant at similar (e.g. same surface concentrations of receptor subunits on the membrane) conditions. N terminal ifnar1-EC was crosslinked with ifnar2-EC with much lower efficiency in comparison to C terminal ifnar1-EC. Deletion of the membrane-proximal domain increased the observed ligand dissociation rate costant even more and no difference was observed for C and N terminal constructs.

● The membrane proximal subdomain, SD4, is not involved in ligand binding, but is important in IFN-induced receptor assembling and signal transduction in vivo. Cells expressing ifnar1 without membrane proximal domain were not able to transmit the cellular signal.

14.4. Paper IV

Lata S, Gavutis M, Piehler J: **Monitoring the Dynamics of Ligand-Receptor Complexes on Model Membranes.** *submitted*

This letter describes the synthesis of bis-NTA lipids and presents binding assay to calculate 2-dimensional dissociation rate constant of ifnar2-EC leaving ternary complex using the experimental approach described in paper 1 and 2.

Fluorescence from donor (OG488) labelled ifnar2-EC is quenched upon ternary complex formation with acceptor (Cy3) labelled IFNα2 and unlabeled ifnar1-EC. Upon pulse-chasing the ternary complex by rapidly tethering an excess of unlabeled ifnar2-EC to the membrane, donor-labeled ifnar2-EC is competed out of the complex, leading to a recovery of the fluorescence. The rate-limiting step of donor dequenching is the 2-dimensional dissociation rate constant of labelled ifnar2-EC from the ternary complex.

Strikingly, the 2-dimensional dissociation rate constant was about 5 times lower than the corresponding 3-dimensional dissociation rate constant. The reasons for this could be slower diffusion of the proteins in the membrane, the reduced degree of freedom affecting the reaction coordinate or cooperative interaction with ifnar1-H10.

14.5. Paper V

Gavutis M, Jaks E, Lamken P, Jacob Piehler: **Determination of the 2-dimensional interaction rate constants of a cytokine receptor complex.** *Biophysical Journal*, *accepted*

This paper describes binding assays, based on the experimental approach presented in paper 1 and 2, to independently determine 2-dimensional association and dissociation rate constants of ifnar2-EC and ifnar1-EC crosslinking.

Main results:

● Ligand dissociation from the ternary complex is a 2-step process with sequential dissociation of ifnar1-EC and ifnar2-EC from IFN. The concentration of the receptor subunits on the membrane and their affinity towards the ligand define, which subunit will dissociate first.

● The 2-dimensional dissociation and association rate constants of ifnar2-EC with ifnar1-EC-IFN complex were determined comparing IFN dissociation into solution at 10 fold excess of ifnar1-EC on the membrane in presence and absence of the high

affinity competitor IFNα2 HEQ. Dissociation traces were fitted with a monoexponential function and the 2-step dissociation model described in paper 2. Strikingly, the 2-dimensional dissociation rate constant was 3-5 times slower than the corresponding 3-dimensional rate constant which was in good agreement with FRET based binding assay described in paper 4.

- The same type of binding assay with 10 fold excess of ifnar2-EC was performed to calculate 2D dissociation and association rate constant between the ifnar1-EC and the ifnar2-EC-IFN complex.

- The 2-dimensional interaction rate constants were determined for several combinations of IFNα2 and ifnar2-EC mutants and ifnar1-EC tethered to the membrane via C and N terminal decahistidine tag. In contrast to the interaction in solution, the association rate constants depended on the orientation of the receptor components. Furthermore, the large differences in association kinetics observed in solution were not detectable on the surface. The key roles of orientation and lateral diffusion on the kinetics of protein interactions in plane of the membrane are emphasized and discussed.

15. References

1. Adam GD, M.: **Reduction of dimensionality in biological diffusion processes**. In *Structural chemistry and molecular biology*. Edited by Rich AD, N.: W.H. Freeman and Co; 1968.
2. Eyring H: **The Activated Complex in Chemical Reactions**. *Journal of Chemical Physics* 1935, **3**:107-115.
3. DeLisi C: **The biophysics of ligand-receptor interactions**. *Q Rev Biophys* 1980, **13**:201-230.
4. Gutfreund H: *Kinetics for life sciences, Receptors, transmitters and catalysis*: Cambrige University Press; 1995.
5. Bongrand P: **Ligand-receptor interactions**. *Reports on Progress in Physics* 1999, **62**:921-968.
6. Schmitz KS, Schurr JM: **Role of Orientation Constraints and Rotational Diffusion in Bimolecular Solution Kinetics**. *Journal of Physical Chemistry* 1972, **76**:534-&.
7. Hill TL: **Effect of rotation on the diffusion-controlled rate of ligand-protein association**. *Proc Natl Acad Sci U S A* 1975, **72**:4918-4922.
8. Vijayakumar M, Wong KY, Schreiber G, Fersht AR, Szabo A, Zhou HX: **Electrostatic enhancement of diffusion-controlled protein-protein association: comparison of theory and experiment on barnase and barstar**. *J Mol Biol* 1998, **278**:1015-1024.
9. Frisch C, Fersht AR, Schreiber G: **Experimental assignment of the structure of the transition state for the association of barnase and barstar**. *J Mol Biol* 2001, **308**:69-77.
10. Kiel C, Selzer T, Shaul Y, Schreiber G, Herrmann C: **Electrostatically optimized Ras-binding Ral guanine dissociation stimulator mutants increase the rate of association by stabilizing the encounter complex**. *Proc Natl Acad Sci U S A* 2004, **101**:9223-9228.
11. Hanggi P, Talkner P, Borkovec M: **Reaction-Rate Theory - 50 Years after Kramers**. *Reviews of Modern Physics* 1990, **62**:251-341.
12. Kramers HA: **Brownian motion in a field of force and the diffusion model of chemical reactions**. *Physica* 1940, **7**:284-304.
13. Lauffenburger DAL, J.J: *Receptors, models for binding, trafficking and signaling*: Oxford University press; 1993.
14. Hardt SL: **Rates of diffusion controlled reactions in one, two and three dimensions**. *Biiophysical Chemistry* 1979, **10**:239-243.
15. Torney DC, Mcconnell HM: **Diffusion-Limited Reaction-Rate Theory for Two-Dimensional Systems**. *Proceedings of the Royal Society of London Series a-Mathematical Physical and Engineering Sciences* 1983, **387**:147-170.
16. Cukier RI: **The Effect of Surface-Diffusion on Surface-Reaction Rates**. *Journal of Chemical Physics* 1983, **79**:2430-2435.
17. Axelrod D: **Lateral motion of membrane proteins and biological function**. *J Membr Biol* 1983, **75**:1-10.
18. Mccloskey MA, Poo MM: **Rates of Membrane-Associated Reactions - Reduction of Dimensionality Revisited**. *Journal of Cell Biology* 1986, **102**:88-96.
19. Wang D, Gou SY, Axelrod D: **Reaction rate enhancement by surface diffusion of adsorbates**. *Biophys Chem* 1992, **43**:117-137.
20. Axelrod D, Wang MD: **Reduction-of-dimensionality kinetics at reaction-limited cell surface receptors**. *Biophys J* 1994, **66**:588-600.

21. Li P, Selvaraj P, Zhu C: **Analysis of competition binding between soluble and membrane-bound ligands for cell surface receptors**. *Biophys J* 1999, **77**:3394-3406.
22. Kholodenko BN: **Four-dimensional organization of protein kinase signaling cascades: the roles of diffusion, endocytosis and molecular motors**. *J Exp Biol* 2003, **206**:2073-2082.
23. Kholodenko BN, Hoek JB, Westerhoff HV: **Why cytoplasmic signalling proteins should be recruited to cell membranes**. *Trends Cell Biol* 2000, **10**:173-178.
24. Edidin M: **Lipids on the frontier: a century of cell-membrane bilayers**. *Nat Rev Mol Cell Biol* 2003, **4**:414-418.
25. Edidin M: **The state of lipid rafts: from model membranes to cells**. *Annu Rev Biophys Biomol Struct* 2003, **32**:257-283.
26. Devaux PF, Morris R: **Transmembrane asymmetry and lateral domains in biological membranes**. *Traffic* 2004, **5**:241-246.
27. Lommerse PH, Spaink HP, Schmidt T: **In vivo plasma membrane organization: results of biophysical approaches**. *Biochim Biophys Acta* 2004, **1664**:119-131.
28. Mukherjee S, Maxfield FR: **Membrane domains**. *Annu Rev Cell Dev Biol* 2004, **20**:839-866.
29. Kahya N, Scherfeld D, Bacia K, Schwille P: **Lipid domain formation and dynamics in giant unilamellar vesicles explored by fluorescence correlation spectroscopy**. *J Struct Biol* 2004, **147**:77-89.
30. Cherry RJ, Smith PR, Morrison IE, Fernandez N: **Mobility of cell surface receptors: a re-evaluation**. *FEBS Lett* 1998, **430**:88-91.
31. Rohwer JM, Postma PW, Kholodenko BN, Westerhoff HV: **Implications of macromolecular crowding for signal transduction and metabolite channeling**. *Proc Natl Acad Sci U S A* 1998, **95**:10547-10552.
32. Ellis RJ: **Macromolecular crowding: obvious but underappreciated**. *Trends Biochem Sci* 2001, **26**:597-604.
33. Ellis RJ, Minton AP: **Cell biology: join the crowd**. *Nature* 2003, **425**:27-28.
34. Hall D, Minton AP: **Macromolecular crowding: qualitative and semiquantitative successes, quantitative challenges**. *Biochim Biophys Acta* 2003, **1649**:127-139.
35. Schnell S, Turner TE: **Reaction kinetics in intracellular environments with macromolecular crowding: simulations and rate laws**. *Prog Biophys Mol Biol* 2004, **85**:235-260.
36. Levin MD, Shimizu TS, Bray D: **Binding and diffusion of CheR molecules within a cluster of membrane receptors**. *Biophys J* 2002, **82**:1809-1817.
37. Berry H: **Monte carlo simulations of enzyme reactions in two dimensions: fractal kinetics and spatial segregation**. *Biophys J* 2002, **83**:1891-1901.
38. Shea LD, Linderman JJ: **Compartmentalization of receptors and enzymes affects activation for a collision coupling mechanism**. *Journal of Theoretical Biology* 1998, **191**:249-258.
39. Grasberger B, Minton AP, DeLisi C, Metzger H: **Interaction between proteins localized in membranes**. *Proc Natl Acad Sci U S A* 1986, **83**:6258-6262.
40. Lippincott-Schwartz J, Snapp E, Kenworthy A: **Studying protein dynamics in living cells**. *Nat Rev Mol Cell Biol* 2001, **2**:444-456.
41. van Deurs B, Roepstorff K, Hommelgaard AM, Sandvig K: **Caveolae: anchored, multifunctional platforms in the lipid ocean**. *Trends Cell Biol* 2003, **13**:92-100.
42. Parton RG: **Caveolae and caveolins**. *Curr Opin Cell Biol* 1996, **8**:542-548.

43. Anderson RG: **The caveolae membrane system**. *Annu Rev Biochem* 1998, **67**:199-225.
44. Weiss A, Schlessinger J: **Switching signals on or off by receptor dimerization**. *Cell* 1998, **94**:277-280.
45. Bray D: **Signaling complexes: biophysical constraints on intracellular communication**. *Annu Rev Biophys Biomol Struct* 1998, **27**:59-75.
46. Heldin CH: **Dimerization of cell surface receptors in signal transduction**. *Cell* 1995, **80**:213-223.
47. Klemm JD, Schreiber SL, Crabtree GR: **Dimerization as a regulatory mechanism in signal transduction**. *Annu Rev Immunol* 1998, **16**:569-592.
48. Marianayagam NJ, Sunde M, Matthews JM: **The power of two: protein dimerization in biology**. *Trends Biochem Sci* 2004, **29**:618-625.
49. Dower SK, DeLisi C, Titus JA, Segal DM: **Mechanism of binding of multivalent immune complexes to Fc receptors. 1. Equilibrium binding**. *Biochemistry* 1981, **20**:6326-6334.
50. Dower SK, Titus JA, DeLisi C, Segal DM: **Mechanism of binding of multivalent immune complexes to Fc receptors. 2. Kinetics of binding**. *Biochemistry* 1981, **20**:6335-6340.
51. Tamm LK, Bartoldus I: **Antibody-Binding to Lipid Model Membranes - the Large-Ligand Effect**. *Biochemistry* 1988, **27**:7453-7458.
52. Nice EC, McInerney TL, Jackson DC: **Analysis of the interaction between a synthetic peptide of influenza virus hemagglutinin and monoclonal antibodies using an optical biosensor**. *Mol Immunol* 1996, **33**:659-670.
53. Mattes MJ: **Binding parameters of antibodies reacting with multivalent antigens: functional affinity or pseudo-affinity**. *J Immunol Methods* 1997, **202**:97-101.
54. Muller KM, Arndt KM, Pluckthun A: **Model and simulation of multivalent binding to fixed ligands**. *Anal Biochem* 1998, **261**:149-158.
55. Dmitriev DA, Massino YS, Segal OL: **Kinetic analysis of interactions between bispecific monoclonal antibodies and immobilized antigens using a resonant mirror biosensor**. *J Immunol Methods* 2003, **280**:183-202.
56. DeLisi C, Chabay R: **The influence of cell surface receptor clustering on the thermodynamics of ligand binding and the kinetics of its dissociation**. *Cell Biophys* 1979, **1**:117-131.
57. Chabay R, DeLisi C, Hook WA, Siraganian RP: **Receptor cross-linking and histamine release in basophils**. *J Biol Chem* 1980, **255**:4628-4635.
58. DeLisi C: **Role of diffusion regulation in receptor--ligand interactions**. *Methods Enzymol* 1983, **93**:95-109.
59. Sulzer B, Perelson AS: **Equilibrium binding of multivalent ligands to cells: Effects of cell and receptor density**. *Mathematical Biosciences* 1996, **135**:147-185.
60. Perelson AS, Delisi C: **Receptor Clustering on a Cell-Surface .1. Theory of Receptor Cross-Linking by Ligands Bearing 2 Chemically Identical Functional-Groups**. *Mathematical Biosciences* 1980, **48**:71-110.
61. Posner RG, Wofsy C, Goldstein B: **The kinetics of bivalent ligand-bivalent receptor aggregation: ring formation and the breakdown of the equivalent site approximation**. *Math Biosci* 1995, **126**:171-190.
62. VandenBroek W, Thompson NL: **When bivalent proteins might walk across cell surfaces**. *Journal of Physical Chemistry* 1996, **100**:11471-11479.
63. Goldstein B, Wofsy C: **Why is it so hard to dissociate multivalent antigens from cell-surface antibodies?** *Immunol Today* 1996, **17**:77-80.

64. Whitty A, Borysenko CW: **Small molecule cytokine mimetics**. *Chem Biol* 1999, **6**:R107-118.
65. Yang T, Baryshnikova OK, Mao H, Holden MA, Cremer PS: **Investigations of bivalent antibody binding on fluid-supported phospholipid membranes: the effect of hapten density**. *J Am Chem Soc* 2003, **125**:4779-4784.
66. Dustin ML, Ferguson LM, Chan PY, Springer TA, Golan DE: **Visualization of CD2 interaction with LFA-3 and determination of the two-dimensional dissociation constant for adhesion receptors in a contact area**. *J Cell Biol* 1996, **132**:465-474.
67. Chesla SE, Selvaraj P, Zhu C: **Measuring two-dimensional receptor-ligand binding kinetics by micropipette**. *Biophys J* 1998, **75**:1553-1572.
68. Piper JW, Swerlick RA, Zhu C: **Determining force dependence of two-dimensional receptor-ligand binding affinity by centrifugation**. *Biophys J* 1998, **74**:492-513.
69. Perelson AS: **Receptor Clustering on a Cell-Surface .2. Theory of Receptor Cross-Linking by Ligands Bearing 2 Chemically Distinct Functional-Groups**. *Mathematical Biosciences* 1980, **49**:87-110.
70. Reits EA, Neefjes JJ: **From fixed to FRAP: measuring protein mobility and activity in living cells**. *Nat Cell Biol* 2001, **3**:E145-147.
71. Carrero G, McDonald D, Crawford E, de Vries G, Hendzel MJ: **Using FRAP and mathematical modeling to determine the in vivo kinetics of nuclear proteins**. *Methods* 2003, **29**:14-28.
72. Giese B, Au-Yeung CK, Herrmann A, Diefenbach S, Haan C, Kuster A, Wortmann SB, Roderburg C, Heinrich PC, Behrmann I, et al.: **Long term association of the cytokine receptor gp130 and the Janus kinase Jak1 revealed by FRAP analysis**. *J Biol Chem* 2003, **278**:39205-39213.
73. Tang Q, Edidin M: **Lowering the barriers to random walks on the cell surface**. *Biophys J* 2003, **84**:400-407.
74. Sprague BL, Pego RL, Stavreva DA, McNally JG: **Analysis of binding reactions by fluorescence recovery after photobleaching**. *Biophys J* 2004, **86**:3473-3495.
75. Lagerholm BC, Weinreb GE, Jacobson K, Thompson NL: **Detecting Microdomains in Intact Cell Membranes**. *Annu Rev Phys Chem* 2005, **56**:309-336.
76. Sprague BL, McNally JG: **FRAP analysis of binding: proper and fitting**. *Trends Cell Biol* 2005, **15**:84-91.
77. Wachsmuth M, Weidemann T, Muller G, Hoffmann-Rohrer UW, Knoch TA, Waldeck W, Langowski J: **Analyzing intracellular binding and diffusion with continuous fluorescence photobleaching**. *Biophys J* 2003, **84**:3353-3363.
78. Heinze KG, Koltermann A, Schwille P: **Simultaneous two-photon excitation of distinct labels for dual-color fluorescence crosscorrelation analysis**. *Proc Natl Acad Sci U S A* 2000, **97**:10377-10382.
79. Elson EL: **Fluorescence correlation spectroscopy measures molecular transport in cells**. *Traffic* 2001, **2**:789-796.
80. Hink MA, Bisselin T, Visser AJ: **Imaging protein-protein interactions in living cells**. *Plant Mol Biol* 2002, **50**:871-883.
81. Bacia K, Schwille P: **A dynamic view of cellular processes by in vivo fluorescence auto- and cross-correlation spectroscopy**. *Methods* 2003, **29**:74-85.

82. Lieto AM, Cush RC, Thompson NL: **Ligand-receptor kinetics measured by total internal reflection with fluorescence correlation spectroscopy**. *Biophys J* 2003, **85**:3294-3302.
83. Weiss M, Hashimoto H, Nilsson T: **Anomalous protein diffusion in living cells as seen by fluorescence correlation spectroscopy**. *Biophys J* 2003, **84**:4043-4052.
84. Lieto AM, Thompson NL: **Total internal reflection with fluorescence correlation spectroscopy: nonfluorescent competitors**. *Biophys J* 2004, **87**:1268-1278.
85. Mei EW, Sharonov A, Gao F, Ferris JH, Hochstrasser RA: **Anomalously slow diffusion of single molecules near a patterned surface**. *Journal of Physical Chemistry A* 2004, **108**:7339-7346.
86. Ruan Q, Cheng MA, Levi M, Gratton E, Mantulin WW: **Spatial-temporal studies of membrane dynamics: scanning fluorescence correlation spectroscopy (SFCS)**. *Biophys J* 2004, **87**:1260-1267.
87. Weiss M, Elsner M, Kartberg F, Nilsson T: **Anomalous subdiffusion is a measure for cytoplasmic crowding in living cells**. *Biophys J* 2004, **87**:3518-3524.
88. Chattopadhyay K, Saffarian S, Elson EL, Frieden C: **Measuring unfolding of proteins in the presence of denaturant using fluorescence correlation spectroscopy**. *Biophys J* 2005, **88**:1413-1422.
89. Heinze KG, Jahnz M, Schwille P: **Triple-color coincidence analysis: one step further in following higher order molecular complex formation**. *Biophys J* 2004, **86**:506-516.
90. Weiss M, Nilsson T: **In a mirror dimly: tracing the movements of molecules in living cells**. *Trends Cell Biol* 2004, **14**:267-273.
91. Saxton MJ, Jacobson K: **Single-particle tracking: applications to membrane dynamics**. *Annu Rev Biophys Biomol Struct* 1997, **26**:373-399.
92. Forstner MB, Kas J, Martin D: **Single lipid diffusion in Langmuir monolayers**. *Langmuir* 2001, **17**:567-570.
93. Nie S, Zare RN: **Optical detection of single molecules**. *Annu Rev Biophys Biomol Struct* 1997, **26**:567-596.
94. Weiss S: **Fluorescence spectroscopy of single biomolecules**. *Science* 1999, **283**:1676-1683.
95. Ishii Y, Yanagida T: **Single Molecule Detection in Life Science**. *Single molecules* 2000, **1**:5-16.
96. Sako Y, Minoghchi S, Yanagida T: **Single-molecule imaging of EGFR signalling on the surface of living cells**. *Nat Cell Biol* 2000, **2**:168-172.
97. Moerner WE, Fromm DP: **Methods of single-molecule fluorescence spectroscopy and microscopy**. *Review of Scientific Instruments* 2003, **74**:3597-3619.
98. Livneh E, Benveniste M, Prywes R, Felder S, Kam Z, Schlessinger J: **Large deletions in the cytoplasmic kinase domain of the epidermal growth factor receptor do not affect its laternal mobility**. *J Cell Biol* 1986, **103**:327-331.
99. Kettling U, Koltermann A, Schwille P, Eigen M: **Real-time enzyme kinetics monitored by dual-color fluorescence cross-correlation spectroscopy**. *Proc Natl Acad Sci U S A* 1998, **95**:1416-1420.
100. Matyus L: **Fluorescence resonance energy transfer measurements on cell surfaces. A spectroscopic tool for determining protein interactions**. *J Photochem Photobiol B* 1992, **12**:323-337.

101. Wouters FS, Bastiaens PI: **Fluorescence lifetime imaging of receptor tyrosine kinase activity in cells**. *Curr Biol* 1999, **9**:1127-1130.
102. Haustein E, Jahnz M, Schwille P: **Triple FRET: a tool for studying long-range molecular interactions**. *Chemphyschem* 2003, **4**:745-748.
103. Guo C, Dower SK, Holowka D, Baird B: **Fluorescence resonance energy transfer reveals interleukin (IL)-1-dependent aggregation of IL-1 type I receptors that correlates with receptor activation**. *J Biol Chem* 1995, **270**:27562-27568.
104. Broudy VC, Lin NL, Buhring HJ, Komatsu N, Kavanagh TJ: **Analysis of c-kit receptor dimerization by fluorescence resonance energy transfer**. *Blood* 1998, **91**:898-906.
105. Overton MC, Blumer KJ: **Use of fluorescence resonance energy transfer to analyze oligomerization of G-protein-coupled receptors expressed in yeast**. *Methods* 2002, **27**:324-332.
106. Krause CD, Mei E, Xie J, Jia Y, Bopp MA, Hochstrasser RM, Pestka S: **Seeing the light: preassembly and ligand-induced changes of the interferon gamma receptor complex in cells**. *Mol Cell Proteomics* 2002, **1**:805-815.
107. Dinger MC, Bader JE, Kobor AD, Kretzschmar AK, Beck-Sickinger AG: **Homodimerization of neuropeptide y receptors investigated by fluorescence resonance energy transfer in living cells**. *J Biol Chem* 2003, **278**:10562-10571.
108. Miyawaki A: **Visualization of the spatial and temporal dynamics of intracellular signaling**. *Dev Cell* 2003, **4**:295-305.
109. Peter M, Ameer-Beg SM, Hughes MK, Keppler MD, Prag S, Marsh M, Vojnovic B, Ng T: **Multiphoton-FLIM quantification of the EGFP-mRFP1 FRET pair for localization of membrane receptor-kinase interactions**. *Biophys J* 2005, **88**:1224-1237.
110. Gordon GW, Berry G, Liang XH, Levine B, Herman B: **Quantitative fluorescence resonance energy transfer measurements using fluorescence microscopy**. *Biophys J* 1998, **74**:2702-2713.
111. Berney C, Danuser G: **FRET or no FRET: a quantitative comparison**. *Biophys J* 2003, **84**:3992-4010.
112. Rizzo MA, Piston DW: **High-contrast imaging of fluorescent protein FRET by fluorescence polarization microscopy**. *Biophys J* 2005, **88**:L14-16.
113. Whitty A, Raskin N, Olson DL, Borysenko CW, Ambrose CM, Benjamin CD, Burkly LC: **Interaction affinity between cytokine receptor components on the cell surface**. *Proc Natl Acad Sci U S A* 1998, **95**:13165-13170.
114. Goldstein B, Faeder JR, Hlavacek WS, Blinov ML, Redondo A, Wofsy C: **Modeling the early signaling events mediated by FcepsilonRI**. *Mol Immunol* 2002, **38**:1213-1219.
115. Frank AJ, Gratzel M, Kozak JJ: **Reduction of Dimensionality in Radical Decay Kinetics Induced by Micellar Systems**. *Journal of the American Chemical Society* 1976, **98**:3317-3321.
116. Isaacs A, Lindenmann J: **Virus interference. I. The interferon**. *Proc R Soc Lond B Biol Sci* 1957, **147**:258-267.
117. Isaacs A, Lindenmann J, Valentine RC: **Virus interference. II. Some properties of interferon**. *Proc R Soc Lond B Biol Sci* 1957, **147**:268-273.
118. Caraglia M, Marra M, Pelaia G, Maselli R, Caputi M, Marsico SA, Abbruzzese A: **Alpha-interferon and its effects on signal transduction pathways**. *J Cell Physiol* 2005, **202**:323-335.
119. Biron CA: **Interferons alpha and beta as immune regulators--a new look**. *Immunity* 2001, **14**:661-664.

120. Platanias LC, Fish EN: **Signaling pathways activated by interferons**. *Exp Hematol* 1999, **27**:1583-1592.
121. Smith PL, Lombardi G, Foster GR: **Type I interferons and the innate immune response-more than just antiviral cytokines**. *Mol Immunol* 2005, **42**:869-877.
122. Prejean C, Colamonici OR: **Role of the cytoplasmic domains of the type I interferon receptor subunits in signaling**. *Semin Cancer Biol* 2000, **10**:83-92.
123. Stark GR, Kerr IM, Williams BR, Silverman RH, Schreiber RD: **How cells respond to interferons**. *Annu Rev Biochem* 1998, **67**:227-264.
124. Liu KD, Gaffen SL, Goldsmith MA: **JAK/STAT signaling by cytokine receptors**. *Curr Opin Immunol* 1998, **10**:271-278.
125. Ihle JN: **STATs: signal transducers and activators of transcription**. *Cell* 1996, **84**:331-334.
126. Hill CS, Treisman R: **Transcriptional regulation by extracellular signals: mechanisms and specificity**. *Cell* 1995, **80**:199-211.
127. Karpusas M, Whitty A, Runkel L, Hochman P: **The structure of human interferon-beta: implications for activity**. *Cell Mol Life Sci* 1998, **54**:1203-1216.
128. Takaoka A, Taniguchi T: **New aspects of IFN-alpha/beta signalling in immunity, oncogenesis and bone metabolism**. *Cancer Sci* 2003, **94**:405-411.
129. Platanias LC: **Mechanisms of type-I- and type-II-interferon-mediated signalling**. *Nat Rev Immunol* 2005, **5**:375-386.
130. Hunter T: **Signaling--2000 and beyond**. *Cell* 2000, **100**:113-127.
131. Schlessinger J: **Cell signaling by receptor tyrosine kinases**. *Cell* 2000, **103**:211-225.
132. Asthagiri AR, Lauffenburger DA: **Bioengineering models of cell signaling**. *Annu Rev Biomed Eng* 2000, **2**:31-53.
133. Ishihara K, Hirano T: **Molecular basis of the cell specificity of cytokine action**. *Biochim Biophys Acta* 2002, **1592**:281-296.
134. Burack WR, Shaw AS: **Signal transduction: hanging on a scaffold**. *Curr Opin Cell Biol* 2000, **12**:211-216.
135. Burack WR, Cheng AM, Shaw AS: **Scaffolds, adaptors and linkers of TCR signaling: theory and practice**. *Curr Opin Immunol* 2002, **14**:312-316.
136. Levchenko A, Bruck J, Sternberg PW: **Scaffold proteins may biphasically affect the levels of mitogen-activated protein kinase signaling and reduce its threshold properties**. *Proc Natl Acad Sci U S A* 2000, **97**:5818-5823.
137. Kholodenko BN, Hoek JB, Westerhoff HV, Brown GC: **Quantification of information transfer via cellular signal transduction pathways**. *FEBS Lett* 1997, **414**:430-434.
138. Ferrell JE, Jr.: **How regulated protein translocation can produce switch-like responses**. *Trends Biochem Sci* 1998, **23**:461-465.
139. Getz WM, Lansky P: **Receptor dissociation constants and the information entropy of membranes coding ligand concentration**. *Chem Senses* 2001, **26**:95-104.
140. McKeithan TW: **Kinetic proofreading in T-cell receptor signal transduction**. *Proc Natl Acad Sci U S A* 1995, **92**:5042-5046.
141. Hlavacek WS, Redondo A, Metzger H, Wofsy C, Goldstein B: **Kinetic proofreading models for cell signaling predict ways to escape kinetic proofreading**. *Proc Natl Acad Sci U S A* 2001, **98**:7295-7300.

142. Hlavacek WS, Redondo A, Wofsy C, Goldstein B: **Kinetic proofreading in receptor-mediated transduction of cellular signals: receptor aggregation, partially activated receptors, and cytosolic messengers**. *Bull Math Biol* 2002, **64**:887-911.
143. Hlavacek WS, Faeder JR, Blinov ML, Perelson AS, Goldstein B: **The complexity of complexes in signal transduction**. *Biotechnol Bioeng* 2003, **84**:783-794.
144. O'Rourke L, Ladbury JE: **Specificity is complex and time consuming: mutual exclusivity in tyrosine kinase-mediated signaling**. *Acc Chem Res* 2003, **36**:410-416.
145. Marx KA: **Quartz crystal microbalance: a useful tool for studying thin polymer films and complex biomolecular systems at the solution-surface interface**. *Biomacromolecules* 2003, **4**:1099-1120.
146. Buttry DA, Ward MD: **Measurement of Interfacial Processes at Electrode Surfaces with the Electrochemical Quartz Crystal Microbalance**. *Chemical Reviews* 1992, **92**:1355-1379.
147. Hook F, Kasemo B, Nylander T, Fant C, Sott K, Elwing H: **Variations in coupled water, viscoelastic properties, and film thickness of a Mefp-1 protein film during adsorption and cross-linking: a quartz crystal microbalance with dissipation monitoring, ellipsometry, and surface plasmon resonance study**. *Anal Chem* 2001, **73**:5796-5804.
148. Marx KA, Zhou T, Montrone A, McIntosh D, Braunhut SJ: **Quartz crystal microbalance biosensor study of endothelial cells and their extracellular matrix following cell removal: Evidence for transient cellular stress and viscoelastic changes during detachment and the elastic behavior of the pure matrix**. *Anal Biochem* 2005, **343**:23-34.
149. Tompkins HGM, W.A.: *Spectroscopic ellipsometry and reflectometry*: John Wiley & Sons Inc.; 1999.
150. J. A. De Feijter JB, F. A. Veer,: **Ellipsometry as a tool to study the adsorption behavior of synthetic and biopolymers at the air-water interface**. *Biopolymers* 1978, **17**:1759-1772.
151. Stora T, Dienes Z, Vogel H, Duschl C: **Histidine-tagged amphiphiles for the reversible formation of lipid bilayer aggregates on chelator-functionalized gold surfaces**. *Langmuir* 2000, **16**:5471-5478.
152. Arwin H: **Ellipsometry on thin organic layers of biological interest: characterization and applications**. *Thin Solid Films* 2000, **377**:48-56.
153. Arwin H: **Spectroscopic ellipsometry and biology: recent developments and challenges**. *Thin Solid Films* 1998, **313**:764-774.
154. Rothmund M, Schutz A, Brecht A, Gauglitz G, Berthel G, Grafe D: **Label free binding assay with spectroscopic detection for pharmaceutical screening**. *Fresenius Journal of Analytical Chemistry* 1997, **359**:15-22.
155. Schmitt HM, Brecht A, Piehler J, Gauglitz G: **An integrated system for optical biomolecular interaction analysis**. *Biosensors & Bioelectronics* 1997, **12**:809-816.
156. Hanel C, Gauglitz G: **Comparison of reflectometric interference spectroscopy with other instruments for label-free optical detection**. *Anal Bioanal Chem* 2002, **372**:91-100.
157. Ziegler C, Gopel W: **Biosensor development**. *Current Opinion in Chemical Biology* 1998, **2**:585-591.
158. Piehler J: **New methodologies for measuring protein interactions in vivo and in vitro**. *Curr Opin Struct Biol* 2005, **15**:4-14.

159. Knoll W: **Interfaces and thin films as seen by bound electromagnetic waves**. *Annu Rev Phys Chem* 1998, **49**:569-638.
160. de Fornel F: *Evanescent waves from Newtonian optics to atomic optics*. Heidelberg: Springer; 2001.
161. Cush R, Cronin JM, Stewart WJ, Maule CH, Molloy J, Goddard NJ: **The Resonant Mirror - a Novel Optical Biosensor for Direct Sensing of Biomolecular Interactions .1. Principle of Operation and Associated Instrumentation**. *Biosensors & Bioelectronics* 1993, **8**:347-353.
162. Buckle PE, Davies RJ, Kinning T, Yeung D, Edwards PR, Pollardknight D, Lowe CR: **The Resonant Mirror - a Novel Optical Sensor for Direct Sensing of Biomolecular Interactions .2. Applications**. *Biosensors & Bioelectronics* 1993, **8**:355-363.
163. Cooper MA: **Optical biosensors in drug discovery**. *Nature Reviews Drug Discovery* 2002, **1**:515-528.
164. Axelrod D, Burghardt TP, Thompson NL: **Total internal reflection fluorescence**. *Annu Rev Biophys Bioeng* 1984, **13**:247-268.
165. Thompson NL, Pearce KH, Hsieh HV: **Total internal reflection fluorescence microscopy: application to substrate-supported planar membranes**. *Eur Biophys J* 1993, **22**:367-378.
166. Thompson NL, Drake AW, Chen LX, VandenBroek W: **Equilibrium, kinetics, diffusion and self-association of proteins at membrane surfaces: Measurement by total internal reflection fluorescence microscopy**. *Photochemistry and Photobiology* 1997, **65**:39-46.
167. Thompson NL, Lagerholm BC: **Total internal reflection fluorescence: Applications in cellular biophysics**. *Current Opinion in Biotechnology* 1997, **8**:58-64.
168. Axelrod D: **Total internal reflection fluorescence microscopy in cell biology**. *Traffic* 2001, **2**:764-774.
169. Oheim M: **Imaging transmitter release. II. A practical guide to evanescent-wave imaging**. *Lasers Med Sci* 2001, **16**:159-170.
170. Toomre D, Manstein DJ: **Lighting up the cell surface with evanescent wave microscopy**. *Trends Cell Biol* 2001, **11**:298-303.
171. Mashanov GI, Tacon D, Knight AE, Peckham M, Molloy JE: **Visualizing single molecules inside living cells using total internal reflection fluorescence microscopy**. *Methods* 2003, **29**:142-152.
172. Sako Y, Uyemura T: **Total internal reflection fluorescence microscopy for single-molecule imaging in living cells**. *Cell Struct Funct* 2002, **27**:357-365.
173. Weis RM, Balakrishnan K, Smith BA, McConnell HM: **Stimulation of fluorescence in a small contact region between rat basophil leukemia cells and planar lipid membrane targets by coherent evanescent radiation**. *J Biol Chem* 1982, **257**:6440-6445.
174. Burghardt TP, Axelrod D: **Total internal reflection fluorescence study of energy transfer in surface-adsorbed and dissolved bovine serum albumin**. *Biochemistry* 1983, **22**:979-985.
175. Poglitsch CL, Thompson NL: **Interaction of antibodies with Fc receptors in substrate-supported planar membranes measured by total internal reflection fluorescence microscopy**. *Biochemistry* 1990, **29**:248-254.
176. Kalb E, Engel J, Tamm LK: **Binding of proteins to specific target sites in membranes measured by total internal reflection fluorescence microscopy**. *Biochemistry* 1990, **29**:1607-1613.

177. Buijs J, Hlady VV: **Adsorption Kinetics, Conformation, and Mobility of the Growth Hormone and Lysozyme on Solid Surfaces, Studied with TIRF**. *J Colloid Interface Sci* 1997, **190**:171-181.
178. Sund SE, Swanson JA, Axelrod D: **Cell membrane orientation visualized by polarized total internal reflection fluorescence**. *Biophys J* 1999, **77**:2266-2283.
179. Tronin A, Blasie JK: **Variable acquistion angle total internal reflection Fluorescence: A new technique for orientation distribution studies of ultrathin films**. *Langmuir* 2001, **17**:3696-3703.
180. Barzen C, Brecht A, Gauglitz G: **Optical multiple-analyte immunosensor for water pollution control**. *Biosensors & Bioelectronics* 2002, **17**:289-295.
181. Ambrose WP, Goodwin PM, Nolan JP: **Single-molecule detection with total internal reflection excitation: comparing signal-to-background and total signals in different geometries**. *Cytometry* 1999, **36**:224-231.
182. Hsieh HV, Thompson NL: **Theory for measuring bivalent surface binding kinetics using total internal reflection with fluorescence photobleaching recovery**. *Biophys J* 1994, **66**:898-911.
183. Lagerholm BC, Starr TE, Volovyk ZN, Thompson NL: **Rebinding of IgE Fabs at haptenated planar membranes: measurement by total internal reflection with fluorescence photobleaching recovery**. *Biochemistry* 2000, **39**:2042-2051.
184. Starr TE, Thompson NL: **Total internal reflection with fluorescence correlation spectroscopy: combined surface reaction and solution diffusion**. *Biophys J* 2001, **80**:1575-1584.
185. Enderlein J: **A theoretical investigation of single-molecule fluorescence detection on thin metallic layers**. *Biophys J* 2000, **78**:2151-2158.
186. Lakowicz JR: **Radiative decay engineering: biophysical and biomedical applications**. *Anal Biochem* 2001, **298**:1-24.
187. Lakowicz JR, Shen Y, D'Auria S, Malicka J, Fang J, Gryczynski Z, Gryczynski I: **Radiative decay engineering. 2. Effects of Silver Island films on fluorescence intensity, lifetimes, and resonance energy transfer**. *Anal Biochem* 2002, **301**:261-277.
188. Lakowicz JR: **Radiative decay engineering 3. Surface plasmon-coupled directional emission**. *Anal Biochem* 2004, **324**:153-169.
189. Gryczynski I, Malicka J, Gryczynski Z, Lakowicz JR: **Radiative decay engineering 4. Experimental studies of surface plasmon-coupled directional emission**. *Anal Biochem* 2004, **324**:170-182.
190. Lakowicz JR: **Radiative decay engineering 5: metal-enhanced fluorescence and plasmon emission**. *Anal Biochem* 2005, **337**:171-194.
191. Brian AA, McConnell HM: **Allogeneic stimulation of cytotoxic T cells by supported planar membranes**. *Proc Natl Acad Sci U S A* 1984, **81**:6159-6163.
192. McConnell HM, Watts TH, Weis RM, Brian AA: **Supported planar membranes in studies of cell-cell recognition in the immune system**. *Biochim Biophys Acta* 1986, **864**:95-106.
193. Thompson NL, Poglitsch CL, Timbs MM, Pisarchick ML: **Dynamics of Antibodies on Planar Model Membranes**. *Accounts of Chemical Research* 1993, **26**:568-573.
194. Sackmann E: **Supported membranes: scientific and practical applications**. *Science* 1996, **271**:43-48.

195. Starr TE, Thompson NL: **Formation and characterization of planar phospholipid bilayers supported on TiO2 and SrTiO3 single crystals**. *Langmuir* 2000, **16**:10301-10308.
196. Tien HT: **Self-Assembled Lipid Bilayers as a Smart Material for Nanotechnology**. *Materials Science & Engineering C-Biomimetic Materials Sensors and Systems* 1995, **3**:7-12.
197. Trojanowicz M, Mulchandani A: **Analytical applications of planar bilayer lipid membranes**. *Analytical and Bioanalytical Chemistry* 2004, **379**:347-350.
198. Richter RP, Maury N, Brisson AR: **On the effect of the solid support on the interleaflet distribution of lipids in supported lipid bilayers**. *Langmuir* 2005, **21**:299-304.
199. Keller CA, Kasemo B: **Surface specific kinetics of lipid vesicle adsorption measured with a quartz crystal microbalance**. *Biophysical Journal* 1998, **75**:1397-1402.
200. Richter RP, Brisson AR: **Following the Formation of Supported Lipid Bilayers on Mica: A Study Combining AFM, QCM-D, and Ellipsometry**. *Biophys J* 2005, **88**:3422-3433.
201. Radler J, Strey H, Sackmann E: **Phenomenology and Kinetics of Lipid Bilayer Spreading on Hydrophilic Surfaces**. *Langmuir* 1995, **11**:4539-4548.
202. Keller CA, Glasmastar K, Zhdanov VP, Kasemo B: **Formation of supported membranes from vesicles**. *Physical Review Letters* 2000, **84**:5443-5446.
203. Cremer PS, Boxer SG: **Formation and spreading of lipid bilayers on planar glass supports**. *Journal of Physical Chemistry B* 1999, **103**:2554-2559.
204. Schonherr H, Johnson JM, Lenz P, Frank CW, Boxer SG: **Vesicle adsorption and lipid bilayer formation on glass studied by atomic force microscopy**. *Langmuir* 2004, **20**:11600-11606.
205. Burns AR, Frankel DJ, Buranda T: **Local mobility in lipid domains of supported bilayers characterized by atomic force microscopy and fluorescence correlation spectroscopy**. *Biophys J* 2005, **89**:1081-1093.
206. Lata S, Piehler J: **Stable and functional immobilization of histidine-tagged proteins via multivalent chelator headgroups on a molecular poly(ethylene glycol) brush**. *Analytical Chemistry* 2005, **77**:1096-1105.

16. Curriculum Vitae

Name: Martynas Gavutis

Born: 11th June 1977, Vilnius Lithuania

Nationality: Lithuanian

Dissertation

Since July 2001 PhD student in AK Dr. Jacob Piehler, Institut für Biochemie, J.W.Goethe-Universität, Frankfurt (Main) Thesis: „Simultaneous fluorescence-interference detection for dissecting 2-dimensional interactions on membranes"

Undergraduate

1999-2001 Master degree in biophysics, Physics Faculty, Vilnius University, Lithuania.

Thesis: "Spectroscopic investigations of mesotetrasulphonatophenyl porphine J aggregates in polymer films"

Supervisor Prof. Ričardas Rotomskis at Biophotonics group.

1999-2000 Socrates-Erasmus scholarship for the exchange studies at the Institute of Technology, Linköping University, Sweden.

Project: "Blood antigen-antibody binding in porous silicon layers measured by spectroscopic ellipsometry"

Supervisor Prof. Hans Arwin at the Division of Applied Optics.

1995-1999 Bachelor degree in applied physics, Physics Faculty, Vilnius University, Lithuania

Thesis: "Model calculations of the penetration depth in the dye solution of the continuous and pulsed radiation",

Supervisor Prof. Ričardas Rotomskis at Biophotonics group.

Conferences:

International Symposium „Functional Membrane Proteomics – From Transport Machineries to Dynamic Assemblies and Networks", Frankfurt, Germany 2005

49th Annual Biophysical Society meeting, Long Beach, USA, 2005

Advanced Practical Course on Optical Spectroscopy in Biology, Juelich, Germany 2003

Euresco conference Bionanotechnology, Granada, Spain 2003

Annual Linz winter workshop “Advances in Single-Molecule Research for Biology & Nanoscience”, Linz, Austria, 2003

Congress & exhibition NanoBioTec 2002, Muenster, Germany 2002

Porous Semiconductors Science and Technology, Madrid, Spain, 2000.

Publications

Gavutis M, Jaks E, Lamken P and Piehler J: **Determination of the 2-dimensional interaction rate constants of a cytokine receptor complex.** *Biophysical Journal*, 2005, *accepted*

Lata S, Gavutis M and Piehler J: **Monitoring the Dynamics of Ligand-Receptor Complexes on Model Membranes.** *Submitted*

Lata S, Gavutis M, Tampé R, Piehler P: **Specific and stable fluorescence labeling of histidine-tagged proteins for studying multi-protein interactions.** *submitted*

Jaitin D, Roisman L, Jaks E, Gavutis M, Piehler J, Van der Heyden J, Uzé G, Schreiber G: **Inquiring into the differential action of interferons: an IFNα2 mutant with enhanced affinity to IFNAR1 is functionally similar to IFNβ.** *submitted*

Lamken P, Gavutis M, Peters I, Van der Heyden J, Uzé G and Piehler J: **Functional Cartography of the Ectodomain of the Type I Interferon Receptor Subunit ifnar1.** *Journal of Molecular Biology*, 2005, **350**: 476-488

Gavutis M, Lata S, Lamken P, Müller P, and Piehler J: **Lateral Ligand-Receptor Interactions on Membranes Probed by Simultaneous Fluorescence-Interference Detection.** *Biophysical Journal*, 2005, **88**: 4289–4302

Lamken P, Lata S, Gavutis M and Piehler J:**Ligand-induced Assembling of the Type I Interferon Receptor on Supported Lipid Bilayers.** *Journal of Molecular Biology,* 2004, **341**: 303-318

Arwin H, Gavutis M, Gustafsson J, Schultzberg M, Zangooie S, Tengvall P: **Protein adsorption in thin porous silicon layers.** *Physica Status Solidi A – Applied Research*, 2000, **182** (1): 515-520

Paper I

doi:10.1016/j.jmb.2004.05.059 *J. Mol. Biol.* (2004) **341**, 303–318

JMB

Available online at www.sciencedirect.com

SCIENCE DIRECT®

ELSEVIER

Ligand-induced Assembling of the Type I Interferon Receptor on Supported Lipid Bilayers

Peter Lamken†, Suman Lata†, Martynas Gavutis and Jacob Piehler*

Institute of Biochemistry
Johann Wolfgang
Goethe-University, Biocenter
N210, Marie-Curie-Straße 9
60439 Frankfurt am Main
Germany

Type I interferons (IFNs) elicit antiviral, antiproliferative and immunomodulatory responses through binding to a shared receptor consisting of the transmembrane proteins ifnar1 and ifnar2. Differential signaling by different interferons, in particular IFNαs and IFNβ, suggests different modes of receptor engagement. Using reflectometric interference spectroscopy (RIfS), we studied kinetics and affinities of the interactions between IFNs and the extracellular receptor domains of ifnar1 (ifnar1-EC) and ifnar2 (ifnar2-EC). For IFNα2, we determined a K_D value of 3 nM and 5 μM for the interaction with ifnar2-EC and ifnar1-EC, respectively. As compared to IFNα2, IFNβ formed complexes with ifnar2-EC as well as ifnar1-EC with substantially higher affinity. For neither IFNα2 nor IFNβ was stabilization of the complex with ifnar1-EC in the presence of soluble ifnar2-EC observed. We investigated ligand-induced complex formation with ifnar1-EC and ifnar2-EC being tethered onto solid-supported, fluid lipid bilayers by RIfS and total internal reflection fluorescence spectroscopy. We observed very stable binding of IFNα2 at high receptor surface concentrations with an apparent k_d value approximately 200 times lower than that for ifnar2-EC alone. The apparent k_d value was strongly dependent on the surface concentration of the receptor components, suggesting kinetic stabilization. This was corroborated by the fast exchange of labeled IFNα2 bound to the receptor by unlabeled IFNα2. Taken together, our results indicate that IFN first binds to ifnar2 and subsequently recruits ifnar1 in a transient fashion. In particular, this second step is much more efficient for IFNβ than for IFNα2, which could explain differential activities observed for these IFNs.

Keywords: type I interferon receptor; protein–protein interaction; solid-supported lipid bilayer; reflectometric interference spectroscopy; total internal reflection fluorescence spectroscopy

*Corresponding author

Introduction

Signaling induced by type I interferons (IFNs) plays a key role in host innate response to viral infection by eliciting a pleiotrophic response including antiviral, antiproliferative and immunmodulatory activities. Because of these activities, type I IFNs are attractive for clinical applications in different fields.[1] Although type I interferons are already used successfully in the treatment of several diseases, the complexity of their action interferes with a pharmacologically controlled administration. Thus, better understanding of the receptor recruitment by IFNs and the following downstream events is required for fully exploiting the therapeutical potentials of IFNs.

All type I interferons (13 different IFNαs, 1 IFNβ and 1 IFNω) exert their activity through binding to the same receptor components, ifnar1 and ifnar2.[2] Upon ligand binding, tyrosine kinases associated

† P. L. and S. L. contributed equally to this paper

Abbreviations used: IFN, human type I interferon; ifnar1-EC and ifnar2-EC, extracellular domains of the human type I interferon receptor ifnar1 and ifnar2; wt, wild-type; ifnar2-tl, tag-less ifnar2-EC; NTA, nitrilotriacetic acid; RIfS, reflectometric interference spectroscopy; FRAP, fluorescence recovery after photobleaching; TIRFS, total internal reflection fluorescence spectroscopy; MBP-H10, decahistidine-tagged maltose-binding protein; OG, Oregon green; AF, Alexa Fluor.

E-mail address of the corresponding author: j.piehler@em.uni-frankfurt.de

with the cytoplasmic domains are activated by auto-phosphorylation, followed by phosphorylation of several tyrosine residues on the receptor and other effector molecules, which are mainly members of the STAT family. It appears, however, that the function of different type I IFNs is not fully redundant, and differential signaling by different IFNs has been observed.[3–8] In particular between IFNα subtypes and IFNβ, substantial differences have been observed on the level of receptor phosphorylation[3] and STAT recruitment,[9] as well as on the level of gene induction.[10,11] As so far no further receptor component has been identified, these differences need to be explained through the mode of interaction of IFNs with the extracellular domains of ifnar1 and ifnar2 (ifnar1-EC and ifnar2-EC, respectively). Therefore, a comprehensive structural, biophysical and mechanistic picture of how the receptor domains are recruited in time and space is required for understanding the specificity of signal propagation through the membrane. In the absence of structural data, the recognition of IFNs by the receptor components has been intensively investigated by mutagenesis.[1] The high-affinity interactions between ifnar2-EC and different IFNs have been investigated in detail,[12–14] and a model for the complex between IFNα2 and ifnar2-EC based on double mutant cycle analysis has been reported.[15,16] However, the differences in affinity, binding kinetics and orientation, which have been so far observed for the interaction of IFNα2 and IFNβ with ifnar2-EC are only minute,[13,15,17] and therefore can hardly explain the functional differences. The low-affinity interaction of IFNs with ifnar1 has been much less well characterized and the K_D value was estimated to be in the micromolar range. Compared to cells expressing ifnar2 alone a 10–40-fold decrease in the K_D value has been reported. By using neutralizing antibodies, the binding site for IFNs on ifnar1 was mapped to the Ig-like domains 2 and 3 of ifnar1.[18] This observation was confirmed by several studies with bovine ifnar1,[19,20] which binds human IFNαs with high affinity. These results indicated that the ligand binding site of ifnar1 does not correspond to a classical cytokine binding module. *In vitro*, a stable ternary complex of IFNβ with ifnar1-EC and ifnar2-EC was observed by size-exclusion chromatography.[21] As no stable complex between IFNβ and ifnar1-EC was detectable under these conditions, this result indicated that cooperative interaction leads to stabilization of the ternary complex. For members of the class I cytokine family, contacts between the two extracellular receptor domains apparently contribute to the stability of the ternary complex,[22–26] and pre-association of the receptor chains has been proposed for several receptors.[25,27,28] For the IFNγ-receptor as a member of the class II cytokine receptor family, a similar mechanism was suggested recently.[29] However, the role of stem–stem contacts between the extracellular receptor domains has not been clearly resolved so far, because lateral interactions between membrane-anchored proteins are difficult to study: cellular assays with the full-length receptors do not provide the experimental control required for analyzing inter-receptor interactions properly; binding studies with the extracellular receptor domains in solution do not provide the biophysical constraints of protein–protein interaction within biological membranes such as the reduced number of degrees of freedom (reduced dimensionality) and the reduced diffusion rates.[30]

Here, we have analyzed the interactions at the extracellular domains of ifnar involved in the formation of the active ternary complex for both IFNα2 and IFNβ. We furthermore present a novel approach for studying ligand-induced receptor assembling by combining full experimental control of an *in vitro* reconstituted system with mimicking two-dimensional protein–protein interactions within the plane of the plasma membrane. Through their C-terminal histidine tags, we tethered ifnar1-EC and ifnar2-EC in an oriented manner onto supported fluid lipid bilayers containing lipids carrying high-affinity chelator head groups. We evaluated the interaction of IFNs to the receptor components reconstituted on fluid lipid bilayers by reflectometric interference spectroscopy (RIfS) and total internal reflection fluorescence spectroscopy (TIRFS). Based on these results, we discuss a biophysical model of the ternary complex formation and for differential receptor recruitment by IFNs.

Results

Expression and purification of ifnar1-EC

Ifnar1-EC with a C-terminal decahistidine-tag was expressed in *Sf*9 cells infected with a baculovirus harboring the gene of mature ifnar1-EC fused to the secretion sequence of the baculoviral protein gp67. The protein was purified to homogeneity from the supernatant by IMAC and size-exclusion chromatography (Figure 1A). In SDS-PAGE, a molecular mass of approximately 57 kDa was observed (Figure 1A), suggesting substantial glycosylation of the protein. Removal of the glycans with PNGaseF yielded a protein with an apparent molecular mass of 48 kDa (Figure 1B) corresponding to the expected molecular mass of the polypeptide chain. Under non-reducing conditions the band of ifnar1 was shifted to a lower molecular mass compared to the reduced protein, indicating internal disulfide bridge formation (Figure 1B). Glycosylated ifnar1-EC proved to be a stable protein, which was stored frozen at −80 °C. After one cycle of freezing and thawing, only insignificant loss of monomeric protein was observed by size-exclusion chromatography (Figure 1C). For all the following binding experiments, the glycosylated protein was used, because it was more stable than the deglycosylated protein.

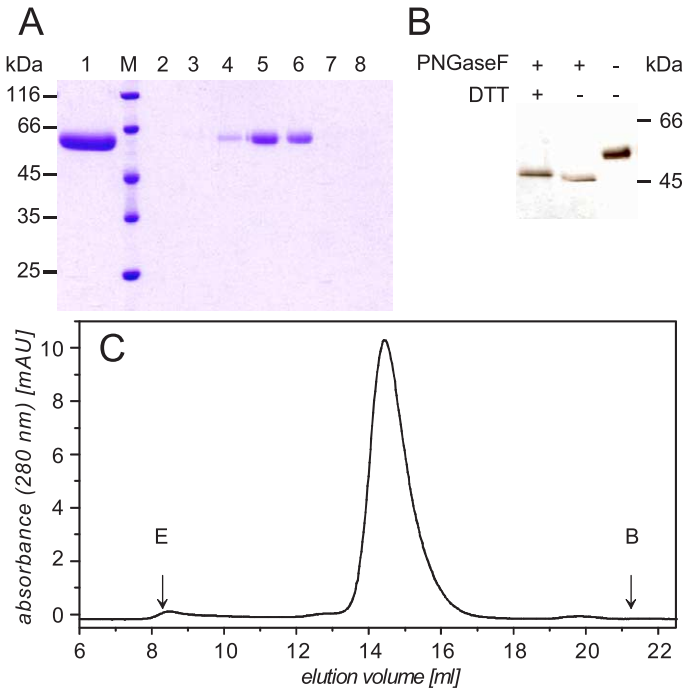

Figure 1. Purification and biochemical characterization of ifnar1-EC. A, SDS-PAGE of the purified protein: elution fraction from IMAC (lane 1) and fractions from size-exclusion chromatography (lane 2–8). B, SDS-PAGE of purified ifnar1-EC after deglycosylation with PNGaseF under non-reducing and reducing conditions in comparison to the non-deglycosylated protein. C, Size-exclusion chromatogram (Superdex 200 HR10/30) of purified ifnar1-EC after freezing and thawing (E, exclusion volume; B, bed volume).

We first characterized the interaction of ligands (IFNα2 and IFNβ with each of the receptor components (ifnar1-EC and ifnar2-EC) separately, in order to precisely determine affinities, rate constants and stoichiometries. These measurements were carried out by immobilizing either ifnar1-EC or ifnar2-EC *via* their C-terminal His-tag on the planar surface of the PEG polymer brush in an oriented fashion using high-affinity chelator head groups. Under these conditions, lateral interactions between the surface-attached proteins are minimized due to the short, covalently bound PEG chains. Protein binding was monitored label-free by RIfS detection. All binding data obtained from these measurements are summarized in Table 1.

Interaction of IFNs with ifnar2-EC

Binding of IFNα2 to immobilized ifnar2-tl has been studied before on different surfaces.[31] IFNα2 interacted specifically with ifnar2-EC immobilized *via* its C-terminal His-tag (Figure 2A) and the stoichiometry as determined from the relative binding amplitudes was 1 : 1. From concentration-dependent binding curves, a k_d value of $0.010(\pm 0.002)\ s^{-1}$, a k_a of $3(\pm 1) \times 10^6\ M^{-1}\ s^{-1}$ and a K_D of $3(\pm 1)$ nM were determined. These values are in excellent agreement with the values obtained for ifnar2-tl immobilized *via* monoclonal antibodies.[31] The association phase was significantly biased by mass transport limitation as indicated by the systematic deviation from the model (Figure 2C). Also the dissociation phase deviated significantly from a single-exponential decay indicating rebinding (Figure 2C) in agreement with that reported.[31] The interaction of IFNβ with immobilized ifnar2-EC had been investigated only at increased ionic strength in order to overcome its otherwise strong non-specific binding to the surface.[13] At the PEG polymer brush surface used in this study, no significant non-specific binding of IFNβ was detectable at physiological ionic strength after fully blocking the chelator head groups with MBP-H10 (Figure 2A). Under these conditions, IFNβ bound substantially tighter to ifnar2-EC compared to IFNα2 (Figure 2A), while from the relative signals, a 1 : 1 stoichiometry between ifnar2-EC and IFNβ was confirmed. The dissociation was very slow with an estimated k_d value of $0.0005\ s^{-1}$. From the I47A mutant of ifnar2-EC, IFNβ dissociated with a rate constant of $0.005(\pm 0.002)\ s^{-1}$ (Figure 2B). From this value, the k_d of approximately $0.0005\ s^{-1}$ was confirmed for the wild-type complex, assuming the same ten-fold difference as observed at high ionic strength.[13] Thus, the half-life of the complex with ifnar2-EC is probably about 20-fold higher for IFNβ compared to IFNα2. The observed association was strongly mass transport limited (Figure 2D), indicating that the association rate constant, k_a, is well above $5 \times 10^6\ M^{-1}\ s^{-1}$. The high k_a value can be explained by electrostatic rate enhancement, as IFNβ is positively charged and ifnar2-EC is strongly negatively charged at physiological pH.

The strong dependence of the complex stability on the ionic strength suggests that electrostatic forces also stabilize the interaction of IFNβ with ifnar2-EC. This effect, however, could also be due to rebinding on the surface, which is dependent on the k_a, value and thus also on the ionic strength. We therefore investigated the contribution of rebinding by injecting ifnar2-tl at high concentration (10 μM) during the dissociation phase (Figure 2E and F). In both cases, a significant faster

Table 1. Rate and equilibrium constants of the interaction with ifnar1-EC and ifnar2-EC determined for different IFNs and different mutants

	Ifnar2-EC			Ifnar1-EC			Ifnar2-EC/Ifnar1-EC[a]		
IFN	k_a ($M^{-1}\,s^{-1}$)	k_d (s^{-1})	K_D (nM)	k_a ($M^{-1}\,s^{-1}$)	k_d (s^{-1})	K_D (nM)	k_a ($M^{-1}\,s^{-1}$)	k_d (s^{-1})	K_D (nM)
IFNα2 wt	$(3 \pm 1) \times 10^6$	0.012 ± 0.002	3 ± 1	–	>0.5	5000 ± 2000	$(3 \pm 1) \times 10^6$	~ 0.0001	~ 0.03
IFNα2 S136C[b]	$(3 \pm 1) \times 10^6$	0.013 ± 0.002	3 ± 1		>0.5	~ 5000	$(3 \pm 1) \times 10^6$	~ 0.0001	~ 0.03
IFNα2 wt[c]	n.b.	n.b.	n.b.	–	>0.5	4000 ± 2000	n.b.	n.b.	n.b.
IFNα2 wt[d]	$(3 \pm 1) \times 10^6$	0.20 ± 0.04	60 ± 20	–	–	–	–	0.0012 ± 0.0002	–
IFNα2 R149A	–	~ 2	500 ± 100	–	>0.5	5000 ± 2000	–	0.010 ± 0.003	–
IFNβ	$>5 \times 10^6$	~ 0.001	<0.1	$(3 \pm 2) \times 10^5$	0.017 ± 0.004	50 ± 30	–	<0.0005	–
IFNβ[c]	n.b.	n.b.	n.b.	$(4 \pm 2) \times 10^5$	0.019 ± 0.004	50 ± 30	n.b.	n.b.	n.b.
IFNβ[e]	$>5 \times 10^6$	0.003 ± 0.001	<0.6	–	–	–	–	–	–
IFNβ[d]	$>5 \times 10^6$	0.005 ± 0.002	<1	–	–	–	–	<0.0005	–

Mean values and standard deviations were determined from at least three independent experiments. n.b., no binding detectable.

[a] Co-immobilized on lipid bilayers at high surface concentration.

[b] Labeled with OG-488 or AF-488 at the additional cysteine residue.

[c] In stoichiometric complex with ifnar2-tl.

[d] With the mutant ifnar2-EC I47A.

[e] At 500 mM NaCl.

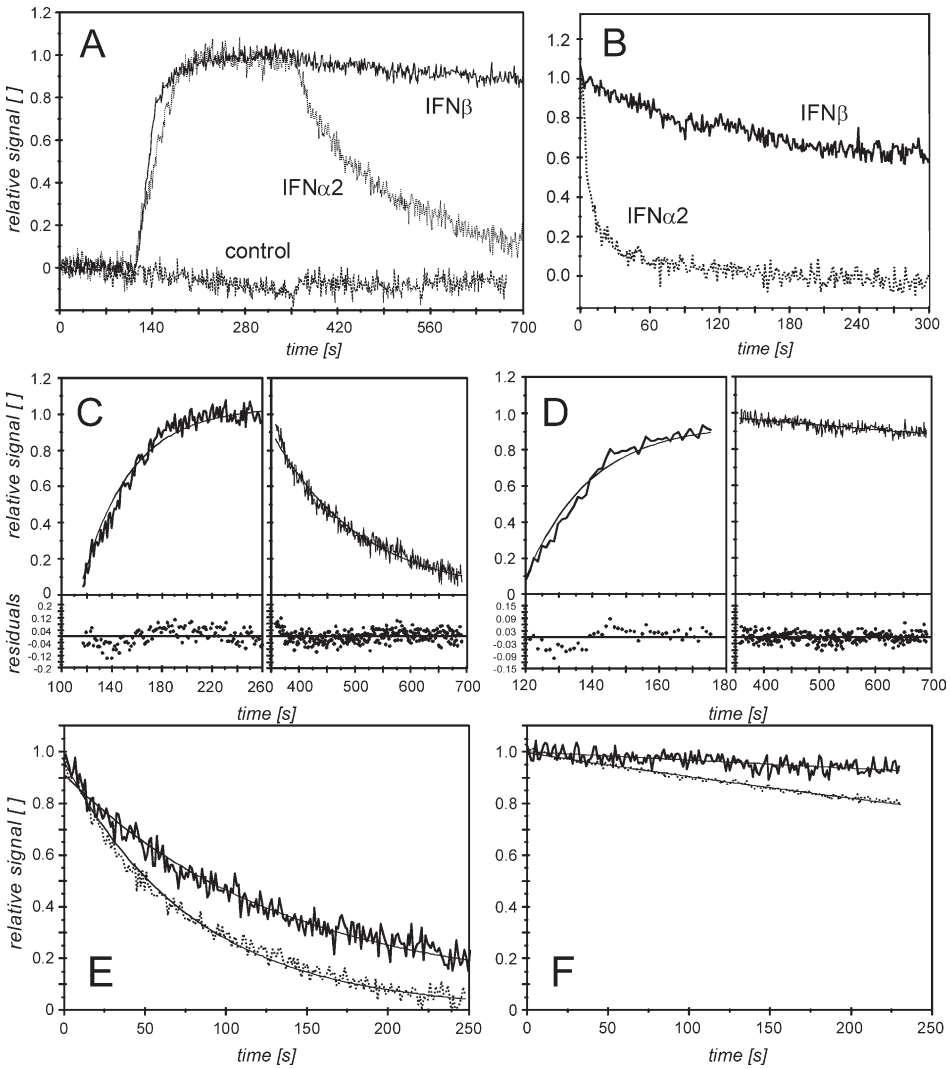

Figure 2. Interaction of IFNα2 and IFNβ with ifnar2-EC on a PEG polymer brush. A, Binding curve for 50 nM IFNα2 (·····) and 50 nM IFNβ (—) to ifnar2-EC in comparison to 50 nM IFNβ exposed to immobilized MBP-H10 (- - - -). B, Dissociation of IFNα2 (·····) and IFNβ (—) from immobilized ifnar2-EC I47A. C, Fit and residuals for association and dissociation of IFNα2 shown in A. D, Fit and residuals for association and dissociation of IFNβ shown in A. E and F, dissociation of IFNα2 (E) and IFNβ (F) from immobilized ifnar2-EC in the absence (—) and in the presence (·····) of 10 μM ifnar2-tl.

dissociation was observed resulting in corrected dissociation rate constants of 0.012(±0.003) s^{-1} for IFNα2 and ~0.001 s^{-1} for IFNβ, respectively.

Interaction of IFNs with ifnar1-EC

Binding of IFNα2 to immobilized ifnar1-EC was only detectable at concentrations above 300 nM and rapid dissociation was observed (Figure 3A). This interaction was entirely specific as confirmed by control experiments without ifnar1-EC on the surface (data not shown). From the equilibrium responses, R_{eq}, observed for IFNα2 at concentrations between 100 nM and 100 μM, titration curves were obtained (Figure 3B). A K_D value of 5(±2) μM was determined by fitting a Langmuir isotherm. Hence, the affinity of IFNα2 towards ifnar1-EC is about three orders of magnitude lower than for ifnar2-EC. The maximum binding signal, R_{max}, obtained from such titration corresponded to a 1 : 1 interaction between ifnar1-EC and IFNα2 assuming full activity of the immobilized ifnar1-EC. The same experiment was carried out with a stoichiometric complex of IFNα2 with ifnar2-tl. This complex with a life-time of ~100 s can be assumed static during the time-scale of the interaction with ifnar1-EC. Binding curves for the 0.1 μM and 10 μM IFNα2–ifnar2-tl complex are shown in Figure 3E. The relative binding signals obtained from a full titration (results not shown) confirmed a 1 : 1 stoichiometric ratio between the IFNα2–ifnar2-tl complex and immobilized ifnar1-EC. A K_D value of 4(±2) μM was obtained, which was not significantly different from the K_D determined for IFNα2 alone. This result suggests that the ternary complex of ifnar1, ifnar2 and IFNα2 is

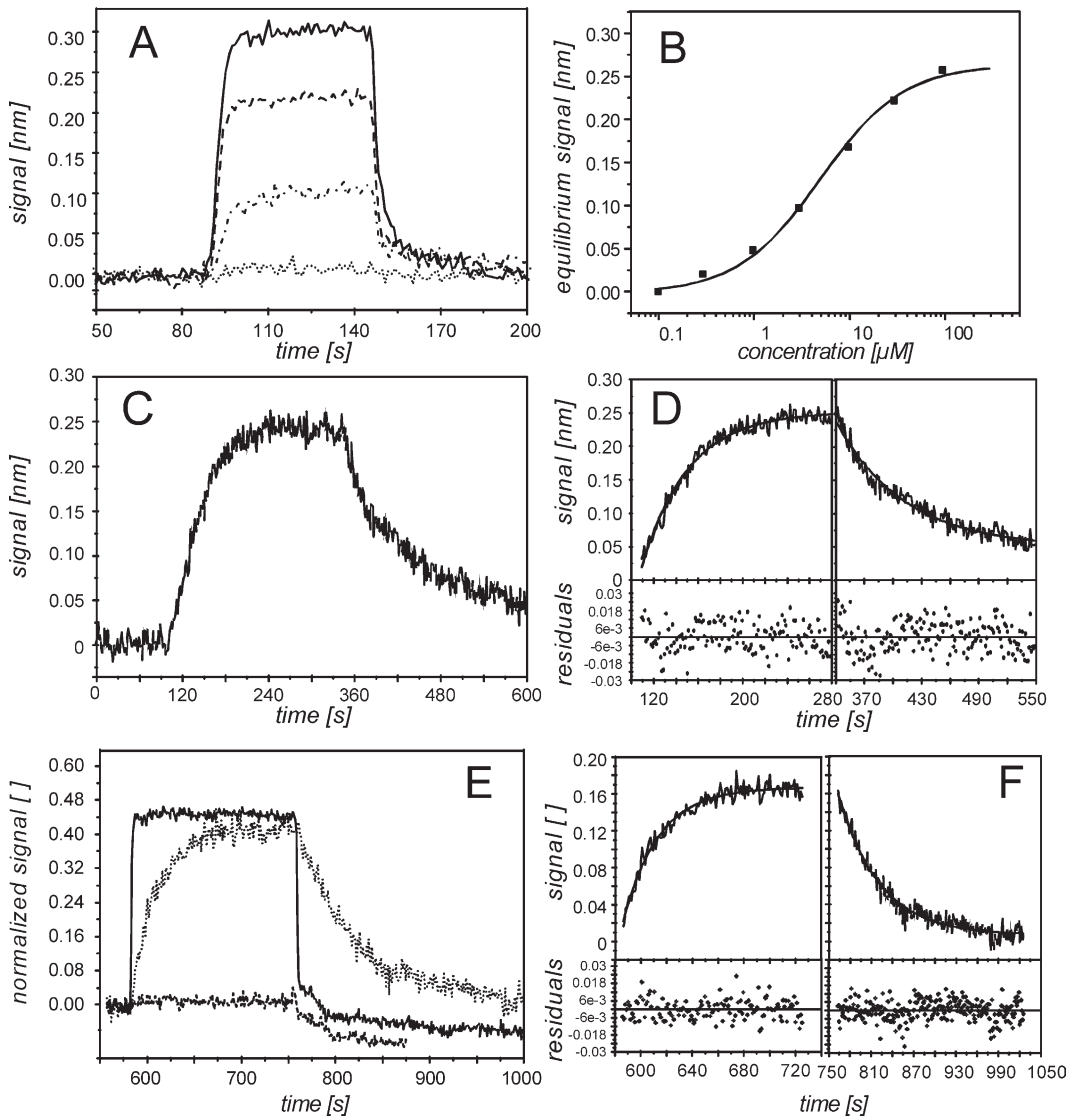

Figure 3. Binding of IFNs to immobilized ifnar1-EC on a PEG polymer brush. A, Binding of IFNα2 in various concentrations (100 nM, ·····; 1 μM, –·–·–, 10 μM, – – – –; 100 μM, —) to immobilized ifnar1-EC. B, Equilibrium response of IFNα2 binding to ifnar1-EC *versus* concentration and the fitted Langmuir isotherm. C, Binding of 50 nM IFNβ to immobilized ifnar1-EC. D, Monoexponential fit to the association and dissociation shown in C. E, Binding of 100 nM IFNβ–ifnar2-tl, 100 nM IFNα2–ifnar2-tl and 10 μM IFNα2–ifnar2-tl to immobilized ifnar1-EC in comparison (normalized to the amount of ifnar1-EC on the surface). F, Fit of single exponential models to the association and dissociation phase for the interaction of 100 nM IFNβ–ifnar2-tl with ifnar1-EC as shown in E, and the residuals of the fit.

not stabilized by additional interactions between ifnar1-EC and ifnar2-EC.

The interaction of IFNβ with immobilized ifnar1-EC was much more stable compared to the binding of the IFNα2 (Figure 3C). Association and dissociation phases were well fitted by monoexponential models (Figure 3D). From the fitting, a k_a value of $3(\pm 2) \times 10^5\ M^{-1}\ s^{-1}$ and a k_d value of $0.017(\pm 0.004)\ s^{-1}$ were obtained. The binding signals corresponded to a 1 : 1 stoichiometry between IFNβ and ifnar1-EC. Similar to IFNα2, no significant differences in the binding rates were observed for ifnar2-tl-bound IFNβ compared to free IFNβ (Figure 3E and F). Also a 1 : 1 stoichiometric ratio was confirmed. For free as well as ifnar2-tl-bound IFNβ a K_D value of 50(±30) nM was obtained. The interaction of the IFNβ–ifnar2-tl complex with ifnar1-EC was also investigated in solution by a binding inhibition assay (data not shown). The K_D value obtained from this experiment was 30(±10) nM, i.e. in good agreement with the K_D value determined for the interaction at the surface. Thus, the affinity of ifnar1-EC for IFNβ is two orders of magnitude higher than for IFNα2. Intriguingly, the association rate constant of IFNβ binding to ifnar1-EC is at least an order of magnitude lower compared to the binding to ifnar2-EC.

Complex formation on lipid bilayers

In order to analyze how the ternary complex is stabilized by lateral interaction on the membrane we investigated ternary complex formation on

solid-supported membranes. We tethered ifnar1-EC and ifnar2-EC to the surface of a solid-supported fluid lipid bilayer doped with chelator lipids using their C-terminal histidine-tags. When ifnar1-EC or ifnar2-EC were individually immobilized on solid-supported lipid bilayers, the binding curves obtained for IFNα2 and IFNβ binding to ifnar2-EC (Figure 4A and B) and ifnar1-EC (Figure 4C and D), respectively, were very similar to the corresponding measurements on the non-fluid polymer brush support. The rate and equilibrium constants obtained from these curves matched the rate constants determined from the measurements on non-fluid support. Neither for IFNα2 nor for IFNβ was significant non-specific binding detectable on the solid-supported lipid bilayers (Figure 4A, C and D).

Upon co-immobilization of ifnar1-EC and ifnar2-EC the binding kinetics of IFNα2 drastically changed (Figure 5A and B). No significant dissociation was observed within 15 minutes, and a second injection of IFNα2 did not give any significant signal (data not shown). Also the association kinetics was changed (Figure 5C–E): a constant binding rate until saturation was observed indicating highly diffusion-controlled binding. No dissociation of IFNα2 was discernible only if a 1 : 1 molar ratio for ifnar1-EC and ifnar2-EC was strictly maintained. With a molar excess of ifnar1-EC, we observed partial fast dissociation of IFNα2, and the amount of stably bound ligand corresponded to the amount of tethered ifnar2-EC (data not shown). With a molar excess of ifnar2-EC, we observed partial dissociation with a rate constant corresponding to the ifnar2–IFNα2 interaction, and the amount of stably bound ligand corresponded to the amount of ifnar1-EC on the bilayer (results not shown). These results confirmed that with IFNα2 a complex with a stoichiometry of 1 : 1 : 1 (or multiples thereof) was formed. Formation of a stable stoichiometric ternary complex was observed only on fluid supports (Figure 5B), confirming that orientation and lateral reorganization of the receptor domains were required to obtain maximum binding affinity. In order to characterize the lateral distribution of the immobilized proteins, laser scanning confocal fluorescence microscopy was carried out using ifnar2-EC-S35C labeled with OG-488 as a probe. Homogeneous lateral distribution of ifnar2-EC was observed on both polymer brush and supported membrane. The lateral diffusion of the receptor was investigated by FRAP experiments (Figure 6). No FRAP was observed for the polymer brush support (data not shown), while full FRAP was observed for the supported lipid bilayers (Figure 6A and B). For ifnar2-EC tethered to the chelator lipid, a diffusion constant of $1(\pm 0.5)\ \mu m^2/s$ was determined, which is very similar to the diffusion constant of GPI-anchored proteins in living cells.[32] No

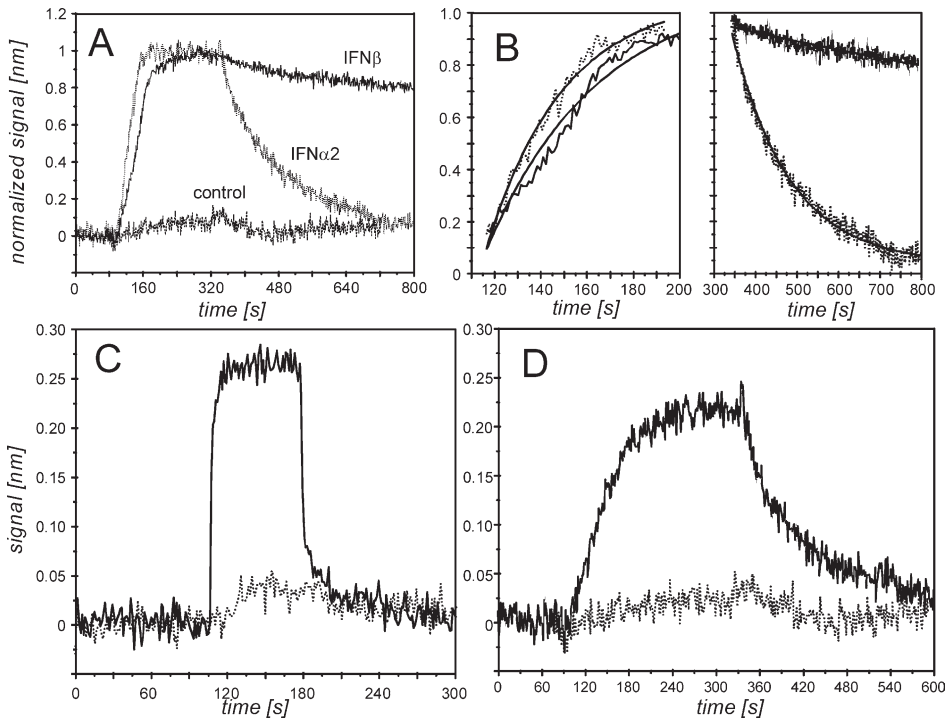

Figure 4. Ligand binding to ifnar1-EC and ifnar2-EC tethered on solid-supported lipid bilayers as detected by RIfS. A, Interaction of 50 nM IFNα2 (·····) and 50 nM IFNβ (—) with ifnar2-EC in comparison to 50 nM IFNβ exposed to a surface loaded with MBP-H10 (- - - -). B, Fit of the association and dissociation curves shown in A. C, Interaction of 10 μM IFNα2 (—) with immobilized ifnar1-EC in comparison to 10 μM IFNα2 exposed to a surface loaded with MBP-H10 (·····). D, Interaction of 100 nM IFNβ (—) with ifnar1-EC in comparison to 100 nM IFNβ exposed to a surface loaded with MBP-H10 (·····).

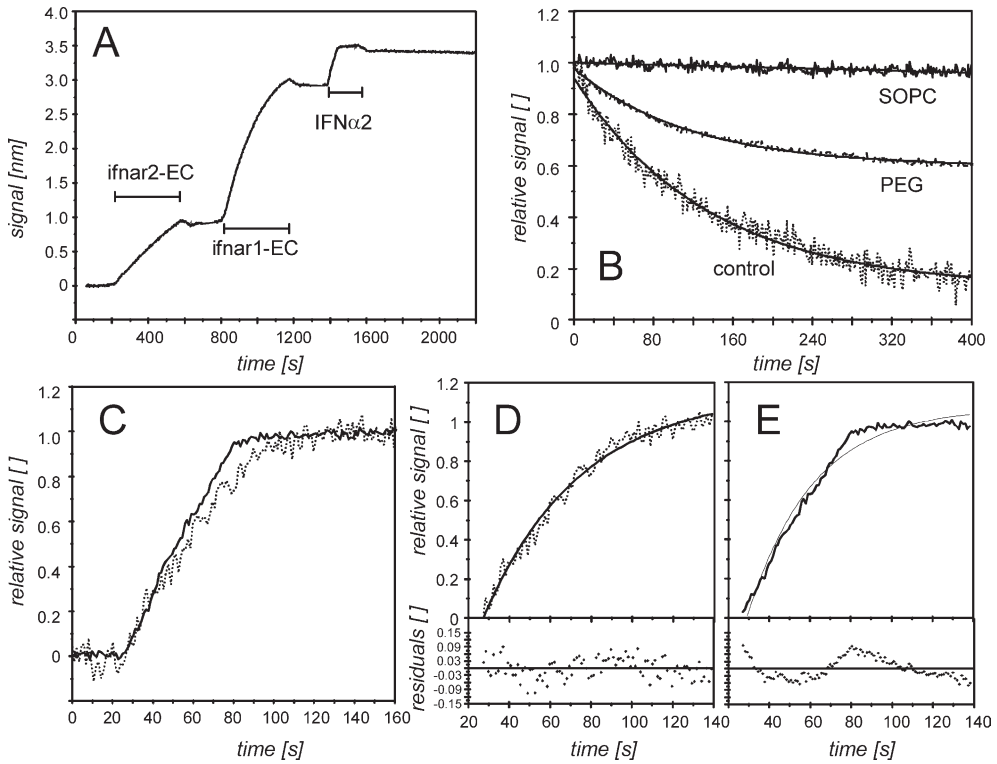

Figure 5. Ligand binding to ifnar1-EC and ifnar2-EC co-immobilized on solid-supported, fluid lipid bilayers. A, Immobilization of ifnar2-EC and ifnar1-EC in stoichiometric ratio, and interaction with 50 nM IFNα2. B, Dissociation of IFNα2 from the ternary complex with ifnar1-EC and ifnar2-EC on lipid bilayers (—) and on polymer brush support (- - - -), compared to the dissociation from ifnar2-EC alone (·····). C, Comparison of the association phases for binding of 50 nM IFNα2 to ifnar1-EC and ifnar2-EC on supported bilayers (—) and to ifnar2-EC alone (·····). D and E, Mono-exponential fit and residuals of the associations phases shown in C (with the same coding of the curves).

significant change in recovery time was observed upon co-immobilization with ifnar1, while binding of IFNα2 clearly reduced the recovery rate by a factor of 2 (Figure 6C). These results also confirmed that no substantial interaction between ifnar1-EC and ifnar2-EC takes place in the absence of the ligand.

Since for the wt proteins no dissociation from the ternary complex was observed, we investigated several mutants of ifnar2-EC and IFNα2 forming relatively less stable binary complexes with each other compared to their wild-type counterparts (Figure 7A and B). IFNα2 dissociates from ifnar2-EC I47A with a rate constant of 0.2 s^{-1} (20-fold higher than wt ifnar2-EC). Upon co-immobilization of ifnar-1EC, a k_d value of 0.0012(±0.0002) s^{-1} was observed (Figure 7C). For IFNα2 R149A (K_D, 500 nM, $k_d \approx 2\ s^{-1}$), a dissociation rate constant of 0.01(±0.003) s^{-1} in the presence of tethered ifnar1-EC was observed (Figure 7D). From these experiments it was estimated that in the presence of ifnar1-EC the apparent affinity is approximately 200-fold higher compared to the affinity towards ifnar2-EC alone.

All these measurements, however, were carried out at very high receptor surface concentrations (approximately 20–40 fmol/mm^2, i.e. 20–40% of a monolayer). The stability of the ternary complex at lower receptor concentration was studied using TIRFS because of the higher sensitivity of fluorescence detection compared to RIfS. Binding of fluorescent IFNα2 (S136C labeled with AF-488) to the receptor on lipid bilayers was measured at different surface concentrations of the receptor (Figure 8). At a high surface concentration of ifnar1-EC and ifnar2-EC, fluorescence detection principally showed similar dissociation phase as did RIfS (Figure 8A). However, a decay of the signal while rinsing was observed. This was not due to ligand dissociation, as stable binding was confirmed by simultaneous RIfS detection (data not shown), but can be ascribed to photobleaching. With a decreasing surface concentration of ifnar1-EC and ifnar2-EC we observed a decreasing stability of the ternary complex (Figure 8B). The dissociation curves were fitted by a single-exponential decay (Figure 8B and C), and increasing k_d values were obtained with decreasing surface concentrations. In Figure 8D, the dissociation rate constants were plotted as a function of receptor surface concentration, the corresponding values are listed in Table 2. At the lowest receptor surface concentration of approximately 0.3 fmol/mm^2 (~200 molecules/μm^2), the stability of the ternary complex was only three times higher than for ifnar2-EC alone. For surface concentrations of 2–4 fmol/mm^2 we determined k_d values corresponding to the affinities that have been

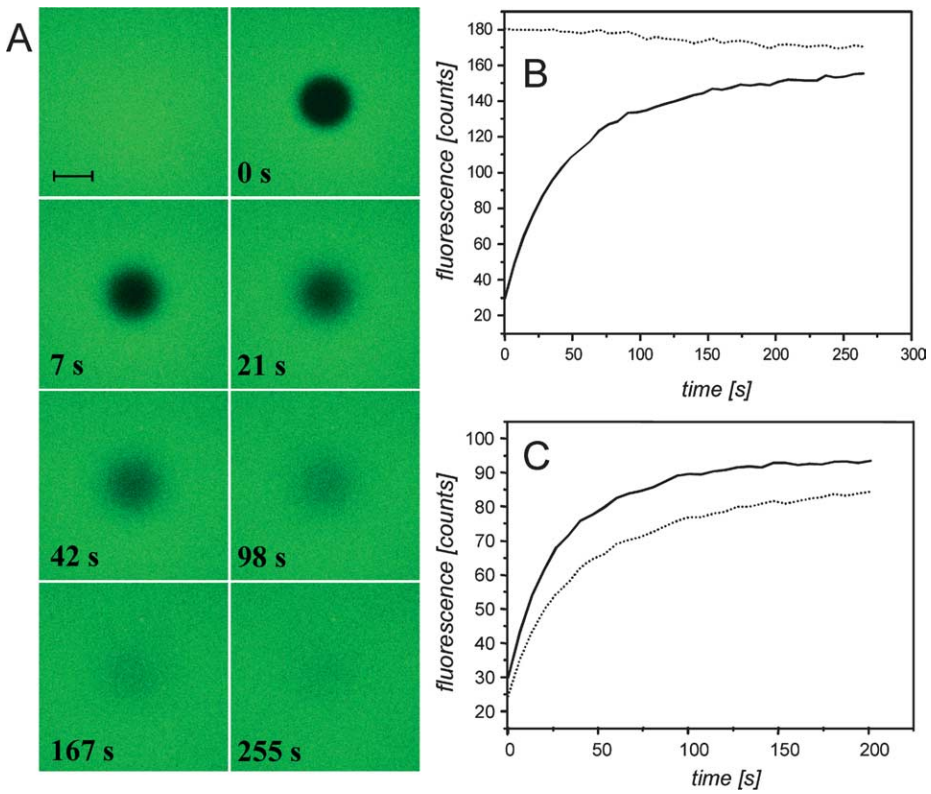

Figure 6. FRAP experiment with ifnar2-EC S35C labeled with OG488 tethered to chelator lipids in a solid-supported lipid bilayer. A, Fluorescence images of ifnar2-EC OG-488 tethered to a solid-supported lipid bilayer before and after bleaching of a circular spot (the time after bleaching is indicated in the lower left corner of each image, the bar represents 20 μm). B, Fluorescence intensity in the bleached spot as a function of time (—) compared to a non-bleached reference spot (·····). C, Recovery curves of ifnar2-EC OG-488 in the presence of ifnar1-EC before (—) and after (·····) addition of 100 nM IFNα2.

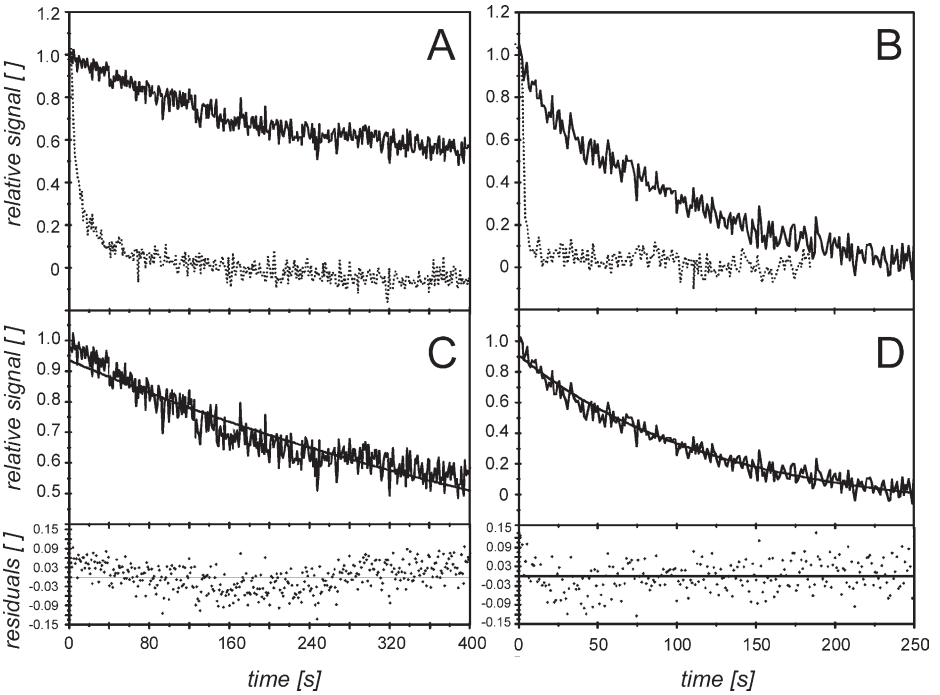

Figure 7. Dissociation of IFNα2 from both ifnar1-EC and ifnar2-EC on lipid bilayers (—) compared to ifnar2-EC alone (·····) observed for ifnar2-EC I47A with wild-type IFNα2 (A) and for wild-type ifnar2-EC with IFNα2 R149A (B). C and D, Fit of a mono-exponential decay to the dissociation from the ternary complex shown in A (C) and B (D), and the residuals.

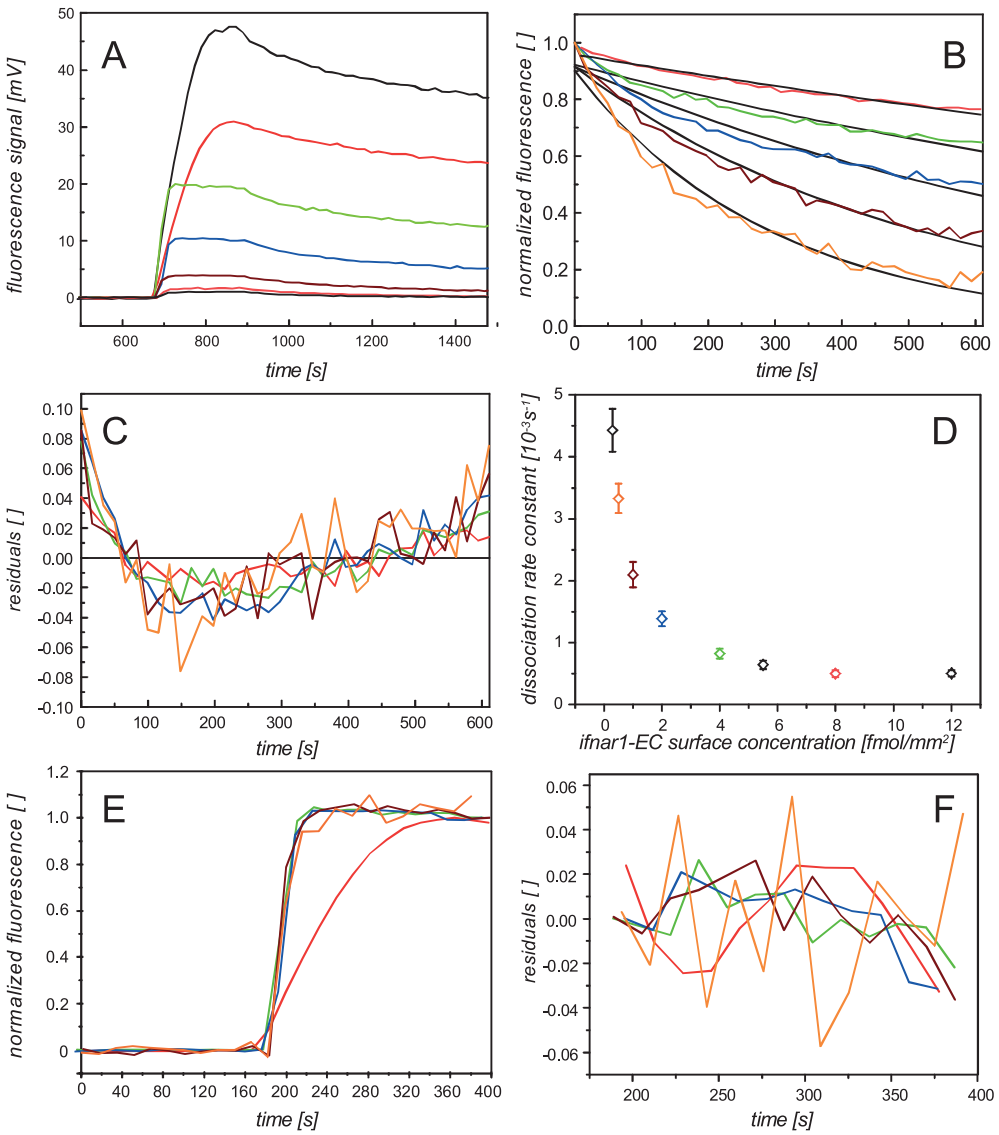

Figure 8. The IFNα2 interaction with ifnar1-EC and ifnar2-EC tethered onto supported lipid bilayers as detected by TIRFS. A, Binding of 100 nM AF-488-labeled IFNα2 at different surface concentrations of ifnar2-EC and ifnar1-EC in a stoichiometric ratio (black, 12 fmol/mm^2; red, 8 fmol/mm^2; green, 4 fmol/mm^2; blue, 2 fmol/mm^2; brown, 1 fmol/mm^2; orange, 0.5 fmol/mm^2). B, Dissociation phases of the binding curves shown in A normalized to the signal at the beginning of dissociation (same color coding as for A) including the fit curve of a mono-exponential decay (black lines). C, Residuals for fitting curves shown in B (same color coding as for A). D, Dissociation rate constant as a function of the surface concentration of the receptor. E, Association phases of binding curves shown in A normalized to the saturation signal (same color coding as for A). F, Residuals of a first-order association model fitted to the curves shown in E.

observed in binding assays with living cells.[33] The association phases of the binding curves normalized to the saturation signal are shown in Figure 8E. At receptor surface concentrations below 8 fmol/mm^2, the association curves overlayed. These curves were fitted well by a pseudo-first-order model (Figure 8F) and gave association rate constants very similar to the interaction of IFNα2 with ifnar2-EC alone (Table 2). At a higher surface concentration, significant lower association rate constants were obtained and systematic deviations from the model, as well as from the other binding curves were observed (Figure 8F). This was probably due to mass transport limitations at these high receptor surface concentrations, which have already been observed for the interaction of IFNα2 with ifnar2-EC alone.

The dependence of the complex stability on the receptor surface concentration suggested that the ternary complex is not static, but stabilized by fast re-association, the kinetics of which depends on the receptor surface concentration. This was further corroborated by the observation that stable ternary complexes were formed at low surface concentrations of ifnar2-EC but high surface concentrations of ifnar1-EC (results not shown). In

Table 2. Rate and equilibrium constants of IFNα2 binding at different stoichiometric surface concentrations of ifnar1-EC and ifnar2-EC on supported lipid bilayers

Ifnar1-EC (fmol/mm^2)	k_a (10^6 M^{-1} s^{-1})	k_d (10^{-3} s^{-1})	K_D (nM)[a]
12 ± 3	1 ± 0.3	0.5 ± 0.1	0.17 ± 0.06
8 ± 2	1 ± 0.3	0.5 ± 0.1	0.17 ± 0.06
5.5 ± 1	3 ± 1	0.6 ± 0.1	0.21 ± 0.07
4 ± 1	4 ± 1	0.8 ± 0.2	0.28 ± 0.1
2 ± 0.4	5 ± 2	1.4 ± 0.2	0.46 ± 0.16
1 ± 0.2	3.5 ± 1	2.1 ± 0.2	0.70 ± 0.24
0.5 ± 0.1	3 ± 1	3.3 ± 0.3	1.11 ± 0.4
0.3 ± 0.1	4 ± 1	4.4 ± 0.4	1.48 ± 0.5
0	4 ± 1	12 ± 1	4 ± 1.5

[a] Calculated using the average k_a of $3(\pm 1) \times 10^6$ M^{-1} s^{-1}.

order to analyze this kinetic stabilization, we challenged the apparently stable ternary complex formed with fluorescently labeled IFNα2 (S136C with OG-488) by injecting unlabeled IFNα2 or ifnar2-tl (Figure 9A). Already at a concentration of 1 μM unlabeled IFNα2, an exchange rate of 0.002 s^{-1} was observed. At the same time the total amount of bound IFN did not change as simultaneously detected by RIfS (data not shown). In contrast, no significant change in dissociation kinetics was observed when ifnar2-tl was injected, even at a concentration as high as 10 μM (Figure 9A). Furthermore, even at much lower surface concentrations of ifnar2-EC (~0.5 fmol/mm^2), fast exchange was observed in the presence of 1 μM unlabeled IFNα2 (Figure 9B). These experiments confirm that the ligand does not dissociate from the surface and re-associates (rebinding-effect), because then ifnar2-tl should interfere as efficiently as does IFNα2, and the effect should be much less pronounced at low surface concentrations. The fact that the ligand is exchanged much faster than the apparent dissociation rate furthermore corroborates the kinetic stabilization of the ternary complex.

Binding assays with ifnar1 and ifnar2 co-immobilized on lipid bilayers were also carried out with IFNβ. However, very stable binding was observed already for the interaction with ifnar2-EC alone, and thus no substantial difference in stability could be observed in the presence of ifnar1-EC. Upon challenging the ternary complex formed with IFNβ by injecting fluorescently labeled IFNα2, no exchange could be observed (data not shown), confirming the anticipated high stability of the ternary complex. Since the already formulated IFNβ could not be labeled appropriately, binding assays at low surface concentration were also not feasible.

Discussion

In this study we dissected the individual contributions of the different interactions between ifnar1-EC, ifnar2-EC and IFNs involved in formation of the ternary complex. For understanding their role for ligand-induced receptor assembling, we investigated the ternary complex formation by tethering the extracellular receptor domains in an oriented fashion on supported membranes. Based on combined fluorescence and label-free detection we studied receptor assembling on a mechanistic level, which may help to explain how differences in receptor engagement by IFNα2 and IFNβ result in differential signaling.

Interaction between ifnar1 and ifnar2

Interaction between receptor components cross-linked by binding to different sites of a ligand is the basic paradigm for cytokine receptor activation. Yet the mode of its induction is currently under controversial debate, and probably different modes apply for different systems.[34,35] Increasingly, pre-association of the receptor chains,[27,29,36] and their activation by ligand-induced conformational

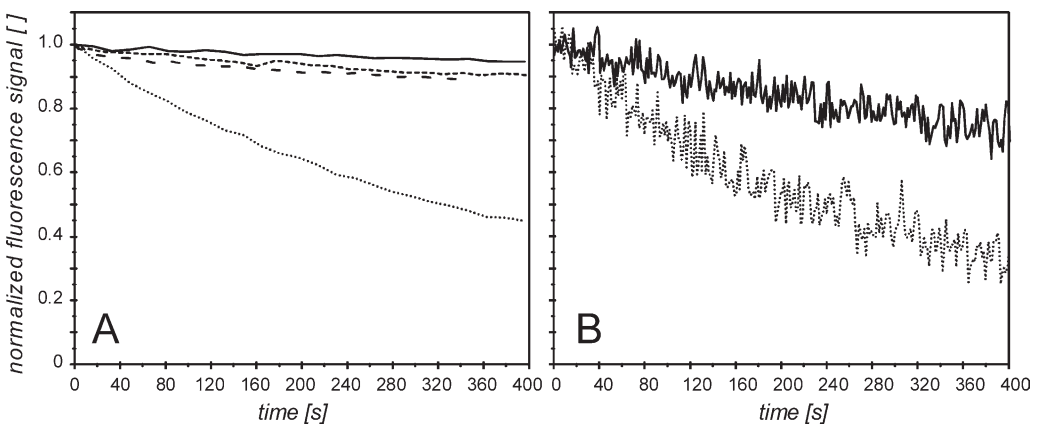

Figure 9. Chase experiments with fluorescent-labeled IFNα2 bound to ifnar2-EC and ifnar1-EC co-immobilized on supported lipid bilayers. A, Dissociation of OG-488-labeled IFNα2 (—) at high surface concentrations of both ifnar2-EC and ifnar1-EC, in the presence of 1 μM (- - - -) and 10 μM (– – – –) ifnar2-tl, and in the presence of 1 μM unlabeled IFN (·····). B, Dissociation of OG-488-labeled IFNα2 from the ternary complex at low surface concentration of ifnar2-EC in the absence (—) and in the presence (·····) of 1 μM unlabeled IFNα2.

changes have been postulated. In the case of class I cytokine receptors, namely growth hormone receptor,[37,26] interleukin-4 receptor[23] and interleukin-6 receptor,[24] stem–stem contacts between the membrane-proximal, extracellular receptor domains have been shown to be important for the formation of stable ternary complexes. Though the affinities of such receptor–receptor interactions have not been quantified yet, stabilization by cooperative inter-receptor and ligand-receptor contacts was clearly shown. Gel-filtration assays carried out with recombinant ifnar1-EC, ifnar2-EC and IFNβ indicated a similar scenario for the type I interferon receptor.[21] For both IFNα2 and IFNβ, we could clearly exclude such co-operative interaction, as we did not detect a significant difference in the affinity of ifnar1-EC for free compared to ifnar2-tl-complexed ligand. Furthermore, no direct interaction between ifnar1-EC and ifnar2-EC was detectable, neither by solid-phase detection nor by FRAP. These results suggest a different mode of interaction for this member of the class II cytokine receptor superfamily compared to the members of the class I family mentioned above. This is in good agreement with the observation that the binding site for IFNα is not located on the membrane-proximal tandem Ig-like domains, but at the hinge between the two extracellular tandem Ig-like domains of ifnar1-EC.[18,20]

Kinetic stabilization of the ternary complex with IFNα2

In order to understand the contributions of the individual interactions towards the stability of the ternary complex on the cell surface, we studied complex formation with ifnar1-EC and ifnar2-EC tethered onto solid-supported membranes. IFNα2 binding was extremely stable at high surface concentrations of ifnar1-EC and ifnar2-EC, decreasing the apparent k_d value compared to ifnar2-EC alone by approximately 200-fold. The dependence of the complex stability on the surface concentration of the receptor and the possibility of exchanging the bound ligand with much faster rates than the apparent dissociation rate constant suggest kinetic rather than static stabilization of the complex. The k_d value of $>0.5\,s^{-1}$ for the interaction between ifnar1-EC and the IFNα2–ifnar2-tl complex implies that the life-time of an individual ternary complex is of the order of a second. Since we could not observe direct interactions between ifnar2-EC and ifnar1-EC, we propose a two-step assembling mechanism as shown in Figure 10 after binding of IFNα2 to ifnar2 (k_1), ifnar1 transiently associates in a second step to the complex. Owing to the short life-time of the IFNα2–ifnar1 interaction, the complex dissociates (k_{-2}) and re-associates (k_2) in a fast manner (on a sub-second scale). Thus, depending on the receptor surface concentrations, only part of the bound ligand is involved in the ternary complex. This fraction is defined by the equilibrium dissociation constant for the interaction of the ifnar2-EC–IFN complex with ifnar1-EC on the surface $K_2 = k_{-2}/k_2$. Since direct dissociation of IFNα2 from the ternary complex is very unlikely (at least 200-fold slower than from ifnar2-EC alone), the apparent k_d value reflects the fraction of ifnar2-EC–IFNα2 not in complex with ifnar1-EC. In cellular binding assays, a 10–40-fold decrease in K_D caused by ifnar1 has been observed for IFNα2.[33] Assuming that the biophysical environment is in principle mimicked appropriately, our results have several important implications for the mechanism of receptor assembling. (i) The formation of a stable pre-formed receptor-complex by interactions mediated *via* the extracellular domains as suggested for other receptors[25,27,28] is very unlikely. (ii) The receptor components are in some way co-localized on the surface of the plasma membrane, as random distribution of several hundred receptors on the plasma membrane would not be sufficient for gaining 20–40 times increased stability. This is in line with the observation that ifnar1 and ifnar2 are located in caveolae,[38] leading to a higher effective concentration. (iii) Different receptor concentrations not only lead to different apparent binding affinities, but also different fractions of IFN involved in the ternary complex. This could explain the different actions and relative activities of IFNs on different cell types.

Differential signaling

One striking observation of this study was the much higher affinity of IFNβ compared to IFNα2 not only towards ifnar2-EC, but even more dramatically towards ifnar1-EC. This result is consistent with the observation that ifnar1 co-immunoprecipitated with ifnar2 in presence of IFNβ, but

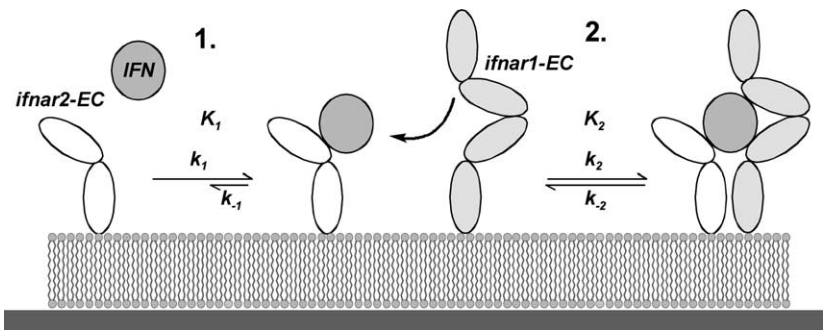

Figure 10. Scheme of a two-step formation and kinetic stabilization of the ternary complex upon IFN binding.

not IFNα2.[5,8] The higher affinity of ifnar1-EC towards ifnar2-EC and ifnar1-EC has two main consequences: first of all it implies that IFNβ binds to the cellular receptor with more than one order of magnitude higher affinity than IFNα2. For IFNα2 mutants, a clear correlation between affinity towards ifnar2-EC and anti-viral activity has been shown.[14] The antiviral activity of IFNβ is only by a factor of 2 to 4 higher than for IFNα2, and not by orders of magnitude. However, saturation of activity has also been observed for human growth hormone upon enhancing its binding affinity substantially.[39] While the reason for this saturation is not fully clear, it is plausible, that this effect is different for different types of responses. Second, the higher affinity of IFNβ towards ifnar1 implies more efficient ternary complex formation at low receptor surface concentrations and longer stability of individual ternary complexes compared to IFNα2. Such differential efficiencies in the engagement of ifnar1 (and ifnar2) by IFNβ compared to IFNα2 could then explain several features of differential signal activation by IFNs: (i) compared to IFNα, IFNβ shows additional gene activation at lower (i.e. physiological) concentrations, while at higher concentration similar activities were observed;[11] (ii) differential signaling is dependent on the cell type,[9] which may be related to (local) receptor concentrations. Further studies, and in particular binding experiments with full transmembrane proteins in living cells, will be required to test this hypothesis fully. Strikingly, the important role of the surface affinity K_2 (cf. Figure 10) for the formation of the IL4 receptor complex has been demonstrated in living cells.[40]

Materials and Methods

Materials

IFNβ (formulated Rebif 22 μg and 44 μg) was a gift from Serono GmbH, Unterschleißheim, Germany. Oregon green 488 (OG-488) maleimide and Alexa Fluor 488 (AF-488) maleimide were purchased from Molecular Probes Europe BV, Leiden, Netherlands. Synthetic stearoyl-oleoyl phosphatidylcholine (SOPC) was purchased from Avanti Polar Lipids, Alabaster, USA. The vector pACgp67B and the BaculoGold baculovirus kit were purchased from BD Biosciences GmbH, Heidelberg, Germany. The vector pMAL-c2x and PNGaseF were purchased from New England Biolabs, Frankfurt am Main, Germany.

Protein expression, purification and labeling

IFNα2, IFNα2-R149A and tag-less ifnar2-EC (ifnar2-tl) were expressed in *Escherichia coli*, refolded from inclusion bodies and purified by anion-exchange and size-exclusion chromatography as described.[41] The wt ifnar2-EC carrying a C-terminal decahistidine-tag and its mutant I47A were expressed and purified in the same manner. The ifnar2-EC mutant S35C and the IFNα2 mutant S136C were refolded and purified as the wt. After size-exclusion chromatography, the proteins were labeled by adding a threefold molar excess of OG-488 maleimide or AF-488 maleimide at 4 °C for 18 hours. Finally, they were further purified by desalting and anion-exchange chromatography. Binding experiments confirmed that the interaction properties of both proteins were not affected by mutagenesis and labeling. OG-488 and AF-488 labeled proteins showed very similar properties in terms of fluorescence intensities and bleaching rates. Ifnar1-EC with a C-terminal His-tag was cloned into the vector pACgp67B and expressed in *Sf9* insect cells using the baculovirus system (BaculoGold). The supernatant was harvested three to four days after infection and ifnar1-EC was purified by immobilized metal chelate affinity chromatography (IMAC) and size-exclusion chromatography. The protein was analytically deglycosylated using PNGaseF. MBP-H10 was expressed using the pMal-c2x vector and purified by IMAC and size-exclusion chromatography. All purified proteins were more than 95% homogeneous and monomeric as detected by non-reducing SDS-PAGE and size-exclusion chromatography.

Solid phase detection techniques

Receptor immobilization, lipid bilayer assembling and protein interactions were monitored by RIfS. This label-free detection technique monitors binding on the surface of a thin silica interference layer,[42,43] and therefore is compatible with fluorescence detection. Furthermore, background signals due to changes in the bulk refractive index as observed by evanescent field detection are much less critical in RIfS-detection.[31] Binding curves were obtained from the shift of the interference spectrum of the silica layer: a shift of 1 nm corresponds to approximately 1 ng/mm^2 protein on the surface. Measurements were carried out in a flow chamber with an acquisition rate of 1 Hz under continuous flow-through conditions as described.[31,42]

Binding of fluorescence-labeled proteins was monitored by TIRFS using a home-built setup. A 25 mW argon ion laser was used for fluorescence excitation at 488 nm. Typically a low excitation power of 2–3 μW focused onto an area of ~1–2 mm^2 was used in order to minimize photobleaching. Fluorescence was collected by an optical fiber and detected by a photomultiplier tube through a bandpass filter. The same transducer slides as for RIfS detection were used as substrates, and all processes on the surface were monitored simultaneously by single-wavelength RIfS detection at 800 nm. The combined TIRFS-RIfS set-up will be described in more detail elsewhere. Continuous flow-through conditions were maintained for all experiments. Data were acquired with a time resolution between 1.5 s and 16 s, depending on the kinetics of the process. Photobleaching was minimized by closing the shutter of the excitation source between the measurements.

Surface modification

For probing the interactions between individual proteins involved in the formation of the ternary complex, the silica surface of the transducer was modified with a two-dimensional molecular polymer brush of poly(ethylene glycol) (PEG) as described.[44] For oriented immobilization, a chelator head group carrying nitrilotriacetic acid (NTA) moieties was covalently coupled to the PEG polymer brush. This chelator head group binds decahistidine-tagged proteins with high stability

allowing complete blocking of excessive binding sites. Its synthesis and characterization will be described elsewhere.

Solid-supported lipid bilayers were obtained by vesicle fusion on the bare silica surface of the transducer as described.[45] SOPC in chloroform was mixed with 1–5 mol% of a chelator lipid based on the same chelator head group mentioned above. After removing the solvent *in vacuo* and resuspension into buffer, small unilaminar vesicles (SUV) were prepared by probe sonication. The transducer surface was incubated for 30 minutes in a freshly prepared mixture of two parts 30% (v/v) hydrogen peroxide and three parts concentrated sulfuric acid. After extensive washing with water, the transducer was mounted immediately into the flow cell. SUVs at a concentration of 250 μM were injected and bilayer formation was followed by RIfS-detection.

Binding assays

All binding assays were carried out in 20 mM Hepes (pH 7.5) and 150 mM NaCl. The chelator head groups were loaded with Ni ions by injecting 15 mM nickel(II)-chloride in running buffer. Depending on the targeted surface concentrations, the histidine-tagged receptor proteins were injected at concentrations between 2 nM and 1 μM for 100–400 s. Excessive binding sites were blocked by injecting 1 μM decahistidine-tagged maltose-binding protein (MBP-H10). Immobilized proteins were removed with a pulse of 200 mM imidazole (pH 8.0). Ligand binding experiments and their evaluation were carried out as described.[31] Protein solutions were diluted at least five-fold into the running buffer to avoid background signals. As a control for specificity, the highest protein concentration was applied either without immobilized protein or after immobilizing MBP-H10. Complex stoichiometries were estimated from the relative saturation signals taking the molecular masses of the proteins into account. In the case of rate constants below $0.3\ s^{-1}$, association and dissociation rate constants were determined by fitting a single-exponential function and assuming a 1 : 1 interaction stoichiometry. Low-affinity interactions with $k_d > 0.3\ s^{-1}$ were investigated by determining the equilibrium response at various ligand concentrations. The equilibrium dissociation constant K_D was determined from dose-response curves by fitting the Langmuir equation. For studying the interaction of complexes of IFNs and ifnar2-EC with immobilized ifnar1-EC, ifnar2-tl was added in stoichiometric amounts, and formation of the stoichiometric complex was verified by analytical gel-filtration.[41] The K_D value of the interaction of ifnar1-EC with IFNβ–ifnar2-EC complex in solution was determined by a binding inhibition assay with 20 nM IFNβ–ifnar2-EC and ifnar1-EC at concentrations between 10 nM and 1 μM. The initial slope *versus* ifnar1-EC concentration in solution was plotted and the K_D value determined by fitting the exact solution of the law of mass action as described.[46]

Fluorescence recovery after photo-bleaching (FRAP)

Fluorescence imaging and recovery experiments were carried out with a laser scanning confocal microscope (LSM 510; Zeiss, Jena) equipped with a 25 mW argon ion laser. Bilayer assembling and receptor attachment were carried out in a flow cell with automated sample handling. The ifnar2-EC mutant S35C labeled with OG-488 was immobilized as described above. A circular spot with a diameter of 20–30 μm was bleached by scanning for 9 s at 75% laser power. Immediately afterwards images were acquired at 0.1–0.4% laser power by scanning for 1.9 s with a time interval of 5–10 s. Diffusion constants were calculated from the $\tau_{1/2}$ determined from the recovery curves as described[47] using a γ-factor of 1.

Acknowledgements

IFNβ (Rebif) was provided by Dr H.-J. Obert, Serono GmbH, Unterschleißheim. The expression vectors for IFNα2 and ifnar2-EC were obtained from Gideon Schreiber, Weizmann Institute of Science. A vector containing the gene of ifnar1-EC was obtained from Gilles Uzé, CNRS Montpellier. Labeled IFNα2 was prepared by Pia Müller. We thank Bernd Otto, Fraunhofer IGB, Hannover for helpful discussions. This work was supported by the Deutsche Forschungsgemeinschaft within the Emmy-Noether Program for young investigators (PI-405/1-1,2), by the Human Frontier Science Program (RGP60/2002) and by Stiftung P.E: Kempkes (10/2000). The support from the laboratory of Robert Tampé is gratefully acknowledged, in particular the help of Eckhard Linker with insect cell culture.

References

1. Deonarain, R., Chan, D. C., Platanias, L. C. & Fish, E. N. (2002). Interferon-alpha/beta-receptor interactions: a complex story unfolding. *Curr. Pharm. Des.* **8**, 2131–2217.
2. Uze, G., Lutfalla, G. & Mogensen, K. E. (1995). Alpha and beta interferons and their receptor and their friends and relations. *J. Interferon Cytokine Res.* **15**, 3–26.
3. Abramovich, C., Shulman, L. M., Ratovitski, E., Harroch, S., Tovey, M., Eid, P. & Revel, M. (1994). Differential tyrosine phosphorylation of the IFNAR chain of the type I interferon receptor and of an associated surface protein in response to IFN-alpha and IFN-beta. *EMBO J.* **13**, 5871–5877.
4. Platanias, L. C., Uddin, S., Domanski, P. & Colamonici, O. R. (1996). Differences in interferon alpha and beta signaling. Interferon beta selectively induces the interaction of the alpha and betaL subunits of the type I interferon receptor. *J. Biol. Chem.* **271**, 23630–23633.
5. Croze, E., Russell-Harde, D., Wagner, T. C., Pu, H., Pfeffer, L. M. & Perez, H. D. (1996). The human type I interferon receptor. Identification of the interferon beta-specific receptor-associated phosphoprotein. *J. Biol. Chem.* **271**, 33165–33168.
6. Mintzer, R. J., Croze, E., Rubanyi, G. M. & Johns, A. (1998). Differential effects of IFN-beta1b on the proliferation of human vascular smooth muscle and endothelial cells. *J. Interferon Cytokine Res.* **18**, 939–945.
7. Domanski, P., Nadeau, O. W., Platanias, L. C., Fish, E., Kellum, M., Pitha, P. & Colamonici, O. R. (1998). Differential use of the betaL subunit of the type I interferon (IFN) receptor determines signalling

specificity for IFNalpha2 and IFNbeta. *J. Biol. Chem.* **273**, 3144–3147.
8. Russell-Harde, D., Wagner, T. C., Perez, H. D. & Croze, E. (1999). Formation of a uniquely stable type I interferon receptor complex by interferon beta is dependent upon particular interactions between interferon beta and its receptor and independent of tyrosine phosphorylation. *Biochem. Biophys. Res. Commun.* **255**, 539–544.
9. Grumbach, I. M., Fish, E. N., Uddin, S., Majchrzak, B., Colamonici, O. R., Figulla, H. R. *et al.* (1999). Activation of the Jak-Stat pathway in cells that exhibit selective sensitivity to the antiviral effects of IFN-beta compared with IFN- alpha. *J. Interferon Cytokine Res.* **19**, 797–801.
10. Der, S. D., Zhou, A., Williams, B. R. & Silverman, R. H. (1998). Identification of genes differentially regulated by interferon alpha, beta, or gamma using oligonucleotide arrays. *Proc. Natl Acad. Sci. USA*, **95**, 15623–15628.
11. da Silva, A. J., Brickelmaier, M., Majeau, G. R., Lukashin, A. V., Peyman, J., Whitty, A. & Hochman, P. S. (2002). Comparison of gene expression patterns induced by treatment of human umbilical vein endothelial cells with IFN-alpha 2b *versus* IFN-beta 1a: understanding the functional relationship between distinct type I interferons that act through a common receptor. *J. Interferon Cytokine Res.* **22**, 173–188.
12. Runkel, L., Pfeffer, L., Lewerenz, M., Monneron, D., Yang, C. H., Murti, A. *et al.* (1998). Differences in activity between alpha and beta type I interferons explored by mutational analysis. *J. Biol. Chem.* **273**, 8003–8008.
13. Piehler, J. & Schreiber, G. (1999). Mutational and structural analysis of the binding interface between type I interferons and their receptor ifnar2. *J. Mol. Biol.* **294**, 223–237.
14. Piehler, J., Roisman, L. C. & Schreiber, G. (2000). New structural and functional aspects of the type I interferon- receptor interaction revealed by comprehensive mutational analysis of the binding interface. *J. Biol. Chem.* **275**, 40425–40433.
15. Roisman, L. C., Piehler, J., Trosset, J. Y., Scheraga, H. A. & Schreiber, G. (2001). Structure of the interferon-receptor complex determined by distance constraints from double-mutant cycles and flexible docking. *Proc. Natl Acad. Sci. USA*, **98**, 13231–13236.
16. Chill, J. H., Quadt, S. R., Levy, R., Schreiber, G. & Anglister, J. (2003). The human type I interferon receptor. NMR structure reveals the molecular basis of ligand binding. *Structure (Camb)*, **11**, 791–802.
17. Runkel, L., De Dios, C., Karpusas, M., Baker, D., Li, Z., Zafari, M. *et al.* (2001). Mapping of IFN-beta epitopes important for receptor binding and biologic activation: comparison of results achieved using antibody- based methods and alanine substitution mutagenesis. *J. Interferon Cytokine Res.* **21**, 931–941.
18. Lu, J., Chuntharapai, A., Beck, J., Bass, S., Ow, A., De Vos, A. M. *et al.* (1998). Structure-function study of the extracellular domain of the human IFN-alpha receptor (hIFNAR1) using blocking monoclonal antibodies: the role of domains 1 and 2. *J. Immunol.* **160**, 1782–1788.
19. Goldman, L. A., Cutrone, E. C., Dang, A., Hao, X., Lim, J. K. & Langer, J. A. (1998). Mapping human interferon-alpha (IFN-alpha 2) binding determinants of the type I interferon receptor subunit IFNAR-1 with human/bovine IFNAR- 1 chimeras. *Biochemistry*, **37**, 13003–13010.
20. Cutrone, E. C. & Langer, J. A. (2001). Identification of critical residues in bovine IFNAR-1 responsible for interferon binding. *J. Biol. Chem.* **276**, 17140–17148.
21. Arduini, R. M., Strauch, K. L., Runkel, L. A., Carlson, M. M., Hronowski, X., Foley, S. F. *et al.* (1999). Characterization of a soluble ternary complex formed between human interferon-beta-1a and its receptor chains. *Protein Sci.* **8**, 1867–1877.
22. Wells, J. A. (1996). Binding in the growth hormone receptor complex. *Proc. Natl Acad. Sci. USA*, **93**, 1–6.
23. Letzelter, F., Wang, Y. & Sebald, W. (1998). The interleukin-4 site-2 epitope determining binding of the common receptor gamma chain. *Eur. J. Biochem.* **257**, 11–20.
24. Ozbek, S., Grotzinger, J., Krebs, B., Fischer, M., Wollmer, A., Jostock, T. *et al.* (1998). The membrane proximal cytokine receptor domain of the human interleukin- 6 receptor is sufficient for ligand binding but not for gp130 association. *J. Biol. Chem.* **273**, 21374–21379.
25. Livnah, O., Stura, E. A., Middleton, S. A., Johnson, D. L., Jolliffe, L. K. & Wilson, I. A. (1999). Crystallographic evidence for preformed dimers of erythropoietin receptor before ligand activation. *Science*, **283**, 987–990.
26. Bernat, B., Pal, G., Sun, M. & Kossiakoff, A. A. (2003). Determination of the energetics governing the regulatory step in growth hormone-induced receptor homodimerization. *Proc. Natl Acad. Sci. USA*, **100**, 952–957.
27. Remy, I., Wilson, I. A. & Michnick, S. W. (1999). Erythropoietin receptor activation by a ligand-induced conformation change. *Science*, **283**, 990–993.
28. Grotzinger, J. (2002). Molecular mechanisms of cytokine receptor activation. *Biochim. Biophys. Acta*, **1592**, 215–223.
29. Krause, C. D., Mei, E., Xie, J., Jia, Y., Bopp, M. A., Hochstrasser, R. M. & Pestka, S. (2002). Seeing the light: preassembly and ligand-induced changes of the interferon gamma receptor complex in cells. *Mol. Cell Proteomics*, **1**, 805–815.
30. Lenaz, G. (1987). Lipid fluidity and membrane protein dynamics. *Biosci. Rep.* **7**, 823–837.
31. Piehler, J. & Schreiber, G. (2001). Fast transient cytokine-receptor interactions monitored in real time by reflectometric interference spectroscopy. *Anal. Biochem.* **289**, 173–186.
32. Poo, H., Krauss, J. C., Mayo-Bond, L., Todd, R. F., 3rd & Petty, H. R. (1995). Interaction of Fc gamma receptor type IIIB with complement receptor type 3 in fibroblast transfectants: evidence from lateral diffusion and resonance energy transfer studies. *J. Mol. Biol.* **247**, 597–603.
33. Lim, J. K., Xiong, J., Carrasco, N. & Langer, J. A. (1994). Intrinsic ligand binding properties of the human and bovine alpha- interferon receptors. *FEBS Letters*, **350**, 281–286.
34. Frank, S. J. (2002). Receptor dimerization in GH and erythropoietin action–it takes two to tango, but how? *Endocrinology*, **143**, 2–10.
35. Sebald, W. & Mueller, T. D. (2003). The interaction of BMP-7 and ActRII implicates a new mode of receptor assembly. *Trends Biochem. Sci.* **28**, 518–521.
36. Gent, J., Van Den Eijnden, M., Van Kerkhof, P. & Strous, G. J. (2003). Dimerization and signal transduction of the growth hormone receptor. *Mol. Endocrinol.* **17**, 967–975.
37. Cunningham, B. C., Ultsch, M., De Vos, A. M., Mulkerrin, M. G., Clauser, K. R. & Wells, J. A.

(1991). Dimerization of the extracellular domain of the human growth hormone receptor by a single hormone molecule. *Science*, **254**, 821–825.
38. Takaoka, A., Mitani, Y., Suemori, H., Sato, M., Yokochi, T., Noguchi, S. *et al.* (2000). Cross talk between interferon-gamma and -alpha/beta signaling components in caveolar membrane domains. *Science*, **288**, 2357–2360.
39. Pearce, K. H., Jr, Cunningham, B. C., Fuh, G., Teeri, T. & Wells, J. A. (1999). Growth hormone binding affinity for its receptor surpasses the requirements for cellular activity. *Biochemistry*, **38**, 81–89.
40. Whitty, A., Raskin, N., Olson, D. L., Borysenko, C. W., Ambrose, C. M., Benjamin, C. D. & Burkly, L. C. (1998). Interaction affinity between cytokine receptor components on the cell surface. *Proc. Natl Acad. Sci. USA*, **95**, 13165–13170.
41. Piehler, J. & Schreiber, G. (1999). Biophysical analysis of the interaction of human ifnar2 expressed in *E. coli* with IFN alpha 2. *J. Mol. Biol.* **289**, 57–67.
42. Schmitt, H. M., Brecht, A., Piehler, J. & Gauglitz, G. (1997). An integrated system for optical biomolecular interaction analysis. *Biosens. Bioelectron.* **12**, 809–816.
43. Piehler, J., Brecht, A. & Gauglitz, G. (1996). Affinity detection of low molecular weight analytes. *Anal. Chem.* **68**, 139–143.
44. Piehler, J., Brecht, A., Valiokas, R., Liedberg, B. & Gauglitz, G. (2000). A high-density poly(ethylene glycol) polymer brush for immobilization on glass-type surfaces. *Biosens. Bioelectron.* **15**, 473–481.
45. Brian, A. A. & McConnell, H. M. (1984). Allogeneic stimulation of cytotoxic T cells by supported planar membranes. *Proc. Natl Acad. Sci. USA*, **81**, 6159–6163.
46. Piehler, J., Brecht, A., Giersch, T., Hock, B. & Gauglitz, G. (1997). Assessment of affinity constants by rapid solid phase detection of equilibrium binding in a flow system. *J. Immunol. Methods*, **201**, 189–206.
47. Axelrod, D., Koppel, D. E., Schlessinger, J., Elson, E. & Webb, W. W. (1976). Mobility measurement by analysis of fluorescence photobleaching recovery kinetics. *Biophys. J.* **16**, 1055–1069.

Edited by I. Wilson

(Received 26 January 2004; received in revised form 14 May 2004; accepted 17 May 2004)

Paper II

Lateral Ligand-Receptor Interactions on Membranes Probed by Simultaneous Fluorescence-Interference Detection

Martynas Gavutis, Suman Lata, Peter Lamken, Pia Müller, and Jacob Piehler
Institute of Biochemistry, Biocenter N210 Johann Wolfgang Goethe-University, 60439 Frankfurt am Main, Germany

ABSTRACT We describe an experimental approach for studying ligand-receptor interactions in the plane of the membrane. The extracellular domains of the type I interferon receptor subunits ifnar1-EC and ifnar2-EC were tethered in an oriented fashion onto solid-supported, fluid lipid bilayers, thus mimicking membrane anchoring and lateral diffusion of the receptor. Ligand-induced receptor assembling was investigated by simultaneous total internal reflection fluorescence spectroscopy and reflectance interferometry (RIf). Based on a rigorous characterization of the interactions of fluorescence-labeled IFNα2 with each of the receptor subunits, the dynamics of the ternary complex formation on the fluid lipid bilayer was addressed in further detail making use of the features of the simultaneous detection. All these measurements supported the formation of a ternary complex in two steps, i.e., association of the ligand to ifnar2-EC and subsequent recruitment of ifnar1-EC on the surface of the membrane. Based on the ability to control and quantify the receptor surface concentrations, equilibrium, and rate constants of the interaction in the plane of the membrane were determined by monitoring ligand dissociation at different receptor surface concentrations. Using mutants of IFNα2 binding to ifnar2-EC with different association rate constants, the key role of the association rate constants for the assembling mechanism was demonstrated.

INTRODUCTION

Lateral interactions between membrane proteins play a key role for activation and propagation of cellular signaling. These lateral interactions are not static in nature and are often triggered or stabilized by interactions with further, soluble interaction partners such as ligands, effectors, and binding proteins from the matrices adjacent to the lipid bilayer. Thus, ligand-induced interaction between two or more transmembrane proteins has been recognized as the basic principle for signal transduction through receptor tyrosine kinases, (Ullrich and Schlessinger, 1990) as well as cytokine receptors (Cunningham et al., 1991). Although recent studies have challenged this model for several cytokine receptors and more complex mechanisms for interreceptor interactions have been proposed (Gent et al., 2003; Grotzinger, 2002; Remy et al., 1999; Sebald and Mueller, 2003; Stroud and Wells, 2004), simultaneous interaction of the ligand with several transmembrane proteins is still believed to be the cause of receptor activation. The interactions involved in the formation of these complexes have been characterized in solution to much detail. To conclude their consequences for signaling, a better understanding of the biophysical principles governing ligand-induced assembling of the signaling complex on the cellular membrane is needed. After ligand binding, the subsequent interactions take place in the plane of the membrane. This reduction in dimensionality has been proposed to have important physicochemical consequences (Adam and Delbruck, 1968; Axelrod and Wang, 1994; DeLisi, 1980; Vanden Broek and Thompson, 1996; Wang et al., 1992). Therefore, lateral rate and affinity constants cannot be readily deduced from the interaction parameters determined in solution. Furthermore, the coupling of ligand binding with the lateral interactions makes deconvolution of the two processes difficult as subtle interactions undetectable in bulk phase could still affect the complex formation on the surface of the membrane.

Recently, we have established detection means for assaying the interaction of type I interferons (IFNs) with their soluble receptor domains ifnar1-EC and ifnar2-EC tethered onto solid-supported membranes (Lamken et al., 2004). Although only three components are involved, the assembly process could be considerably complicated. Thus, surface-sensitive techniques suitable for deconvoluting different facets of the assembling process in real time are required. Total internal reflection fluorescence spectroscopy (TIRFS) has been frequently used for monitoring ligand binding at surfaces and solid-supported membranes (Axelrod et al., 1984; Schmid et al., 1998; Thompson et al., 1997, 1993; Thompson and Lagerholm, 1997). High sensitivity of TIRFS makes binding events detectable even at very low surface concentrations, and provides the versatility of fluorescence

Submitted November 6, 2004, and accepted for publication February 15, 2005.

Martynas Gavutis and Suman Lata contributed equally to this article.

Address reprint requests to Jacob Piehler, Institute of Biochemistry, Biocenter N210 Johann Wolfgang Goethe-University, Marie-Curie-Straße 9, 60439 Frankfurt am Main, Germany. Tel.: 49-0-69-79829468; Fax: 49-0-69-798294695; E-mail: j.piehler@em.uni-frankfurt.de.

Abbreviations used: ifnar, human type I interferon receptor; EC, extracellular domain; IFN, human type I interferon; wt, wild-type; tl, tagless; RIf, reflectance interferometry; TIRFS, total internal reflection fluorescence spectroscopy; SPR, surface plasmon resonance; AF488, Alexa Fluor 488; OG488, Oregon Green 488.

0006-3495/05/06/4289/14 $2.00 doi: 10.1529/biophysj.104.055855

experiments. However, absolute quantification of the adsorbed molecules without a reference/standard is not possible. By exclusive detection of the fluorescent molecules, high signal/background ratios are achieved, but only a very limited picture of all binding events at the surface is obtained. As an alternative, label-free detection of surface-adsorbed molecules by optical techniques (Haake et al., 2000), e.g., surface plasmon resonance (SPR), grating couplers or resonant mirror, as well as by nonoptical techniques, e.g., quartz crystal microbalance (Marx, 2003) or surface acoustic waves (Gizeli et al., 1997) has been described. These techniques detect and quantify all adsorbed materials in real time, but lack the specificity and sensitivity of fluorescence detection. Thus, TIRFS would be ideally complemented with label-free detection. Combination of TIRFS with SPR (surface plasmon field-enhanced fluorescence spectroscopy) has been shown to be a powerful tool for characterizing processes at interfaces (Liebermann and Knoll, 2000; Neumann et al., 2002). This technique uses the same light source for fluorescence excitation as for SPR detection, thus limiting the flexibility of each technique. The metal layers required for SPR are furthermore disadvantageous due to their strongly surface distance-dependent fluorescence quenching.

Here, we describe a novel combination of TIRFS with reflectance interferometry (RIf) at a thin silica layer for studying lateral interactions at supported lipid bilayers. Spectral RIf has proven rugged and powerful for label-free detection of cytokine-receptor interactions (Piehler and Schreiber, 2001). The interaction of fluorescence-labeled IFNα2 with the extracellular domains of its receptor subunits ifnar1-EC and ifnar2-EC tethered onto solid-supported, fluid lipid bilayers containing chelator lipids (Dorn et al., 1998; Schmitt et al., 1994) was used as a model system. Based on simultaneous fluorescence and mass sensitive detection, we deconvoluted the interactions of this ligand with its receptor components on the lipid bilayer. Assuming a two-step kinetic complex assembling and disassembling model, we determined the association rate constant and the equilibrium dissociation constant of the lateral interaction of ifnar1-EC with IFNα2 bound to ifnar2-EC on the lipid bilayer surface. Further mechanistic aspects of receptor assembling were demonstrated by using mutants of IFNα2 binding to ifnar2-EC with different association rate constants.

MATERIALS AND METHODS

Proteins expression and purification

IFNα2, ifnar2-EC carrying a C-terminal decahistidine tag and tagless ifnar2-EC (ifnar2-tl) were expressed in *Escherichia coli*, refolded from inclusion bodies, and purified by ion exchange and size exclusion chromatography as described before (Piehler and Schreiber, 1999). In the structure of the ifnar2-EC-IFNα2 complex obtained by NMR and distance-constrained docking (Chill et al., 2003; Roisman et al., 2001), the residue S136 of IFNα2 was found proximal, yet not in contact with ifnar2-EC. This residue was mutated to a cysteine residue for site-specific fluorescence labeling. IFNα2-S136C, IFNα2-S136CR144A, and IFNα2-S136CM148A were refolded and purified as the wt, and labeled with Alexa Fluor 488 (AF488) maleimide or Oregon Green 488 (OG488) maleimide (both from Molecular Probes, Eugene, OR). After the labeling reaction, the labeled protein was further purified by a final step of anion exchange chromatography (HiTrap Q, Amersham Biosciences, Buckinghamshire, UK), by which the fluorescence-labeled species was further enriched. In a final desalting step (HiTrap desalting, Amersham Biosciences), residual fluorescence dye was removed. Typical labeling degrees were 60–80% as estimated from the absorbance spectra. These fluorescence-labeled IFNs will be referred to as ^{AF488}IFNα2, ^{AF488}IFNα2-M148A, and ^{OG488}IFNα2-R144A, respectively. Ifnar1-EC with a C-terminal decahistidine tag was expressed in *Sf*9 insect cells and purified from the supernatant by immobilized metal affinity chromatography and by size exclusion chromatography as described earlier (Lamken et al., 2004). All binding assays were carried out with the glycosylated protein, which had an average molecular mass of 57 kDa as determined by mass spectrometry.

Simultaneous TIRFS-RIf detection

The experimental setup was implemented as schematically shown in Fig. 1. The beam of a 488-nm Argon ion laser (162LGA/LGL, LG Laser Technologies, Kleinostheim, Germany), equipped with an electrical shutter (Uniblitz, Vincent Associates, Rochester, NY), was coupled into a 50-μm core diameter optical fiber (Ocean Optics, Duiven, The Netherlands). Excitation power was attenuated by misaligning the laser-to-fiber coupling. The light from the fiber output was focused onto the sample surface with an adjustable collimator lens (OFR-CSMA-5-VIS, Optics for Research, Verona, NJ) through a custom-made glass prism (Berliner Glas KGaA, Berlin, Germany) with a 2.8-mm hole in the center. This hole was used for attaching the fiber optics for fluorescence detection as well as for reflectance interferometry (c.f. Fig. 1 *C*) using a custom-made optical fiber bundle (Ratioplast, Löhne, Germany), which is depicted in Fig. 1 *B*. The 600-μm fiber in the center was used for fluorescence detection. After passing an infrared cutting filter (Linos Photonics, Göttingen, Germany) the appropriate spectral range was selected with a 532-nm interference filter (Edmund Optics, Blackwood, NJ) mounted in a motorized filter wheel (AB-303, CVI Laser, Albuquerque, NM) and detected by a photomultiplier module (H7711-02, Hamamatsu, Herrsching, Germany). For reflectance interferometry, the surrounding 200-μm fibers of the fiber bundle were used: half of them were combined into a fiber bundle for illumination, whereas the other half was combined into a fiber bundle for detecting the reflected light. The transducer element (10 nm Ta_2O_5 and 400 nm silica on a glass substrate, custom-made from AMP Dünnschichttechnik GmbH, Tornesch, Germany) was optimized to give a spectral interference pattern with the inflection point at 800 nm upon perpendicular illumination (Fig. 1 *D*). White light from a tungsten halogen lamp (Avantes, Boulder, CO) was monochromatized using an 800-nm interference filter (Edmund Optics) and a 780-nm-long pass filter (LOT Oriel, Darmstadt, Germany), and was coupled into the illumination fibers. The reflected light collected by the detection fibers passed a second 800-nm interference filter (Edmund Optics) and was detected with a photomultiplier tube (H7711-02, Hamamatsu). The spectral characteristics of the detection system are shown in Fig. 1 *D*, demonstrating the strict spectral separation of fluorescence and interference signals.

The transducer was mounted to a flow cell with a 1-mm wide and 100-μm deep flow channel. Sample handling was carried out in a flow-through format using a syringe pump (Microlab 541C) with two 250-μl syringes and a four-way distribution valve (MVP) (both from Hamilton, Bonaduz, Switzerland) as in principle described before (Piehler and Schreiber, 2001), which were combined with an autosampler (PS 60, MLE GmbH, Radebeul, Germany). With this system, flow rates between 1 and 500 μl/s can be employed. Sample handling and data acquisition were controlled with software written in LabVIEW (National Instruments, Munich, Germany).

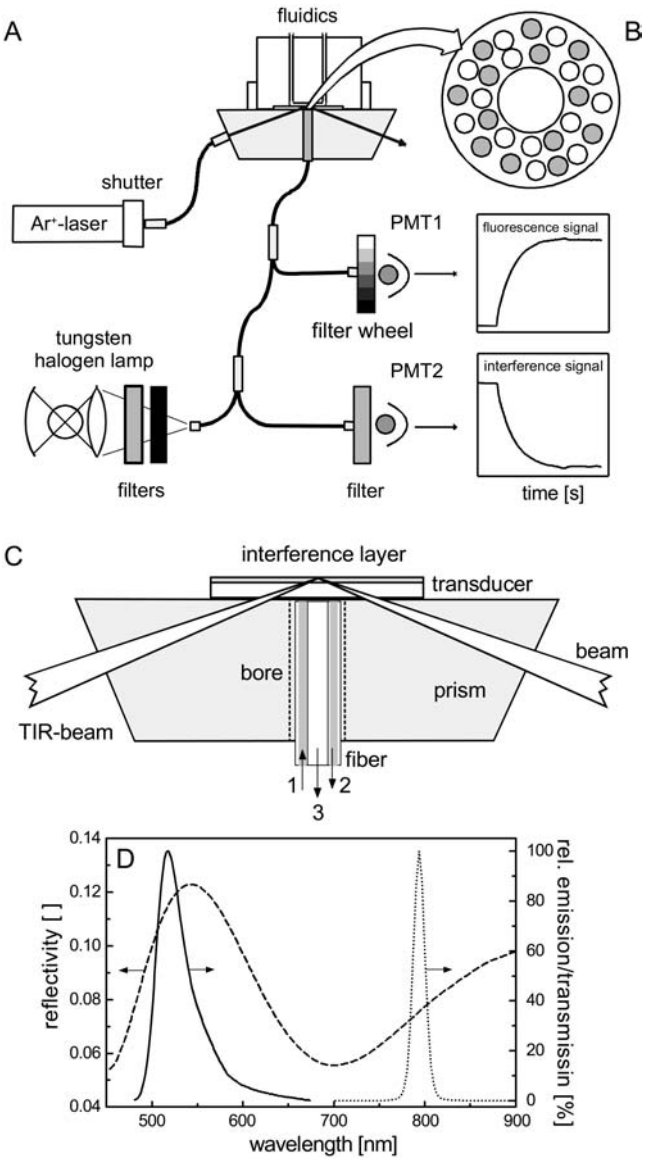

FIGURE 1 (*A*) Schematic of the setup for simultaneous TIRFS-RIf detection (details in the text). (*B*) Cross section of the fiber at the interface to the transducer: The 600-μm fiber in the center was used for fluorescence detection. The surrounding 200-μM fibers where used for RIf illumination and for RIf detection. (*C*) Enlarged view of the coupling of the light beam for fluorescence excitation into the RIf transducer, and the fibers for RIf illumination (*1*), RIf detection (*2*), and fluorescence detection (*3*). (*D*) Spectral separation of RIf and TIRFS detection: reflectivity of the RIf transducer at perpendicular illumination (*dashed line*) and transmission of the interference filter used for RIf detection (*dotted line*), in comparison to the fluorescence emission spectrum of AF488 (*solid line*).

Lipid bilayer assembling, receptor reconstitution, and binding assays

The fluorescent vesicles used for characterization of the setup were prepared by doping SOPC with the fluorescent lipids as obtained by reacting SOPE with OG488 *N*-hydroxysuccinimide ester (Molecular Probes). The lipids were homogeneously mixed in the appropriate proportion by dissolving in chloroform. The solvent was then removed in vacuo and the thin lipid film was suspended in the buffer. The translucent solution was intermittently probe sonicated in a water bath at 4°C for 15 min followed by centrifugation to obtain small unilaminar vesicles (SUV) in the supernatant. For protein tethering to the lipid membrane, the vesicles were prepared in an identical fashion as for the fluorescent vesicles, except, SOPC was doped with 5 mol% of a chelator lipid based on a novel chelator headgroup containing two NTA moieties (termed *bis*-NTA). This chelator headgroup binds decahistidine-tagged proteins with substantially increased stability compared to the conventional *mono*-NTA, and no significant dissociation of decahistidine-tagged ifnar2-EC was detectable (i.e., $k_d < 0.0005\ s^{-1}$) even at low surface concentrations of chelator headgroups (Lata and Piehler, 2005). To avoid phase segregation, this chelator lipid contained one unsaturated alkyl chain. Its synthesis and characterization will be detailed in a forthcoming article.

Before vesicle fusion, the transducer was incubated for 30 min in a freshly prepared 2:3 mixture of two parts 30% hydrogen peroxide and three parts concentrated sulfuric acid. After extensive washing with water, the transducer was dried in a nitrogen stream and mounted immediately into the flow cell. Bilayer assembling, immobilization of the receptor domains and ligand binding assays were carried out with 20 mM HEPES, pH 7.5, and 150 mM NaCl as the running buffer. Solid supported lipid bilayers were obtained by injecting SUVs at a lipid concentration of 250 μM on the surface of the transducer. Protein immobilization and binding assays were in principle carried out as described earlier (Lamken et al., 2004). For tethering the histidine-tagged proteins to the supported membranes, the chelator headgroups were loaded with Ni^{2+}-ions by injecting 10 mM nickel(II)chloride in the running buffer for 150 s followed by a 150-s injection of 200 mM imidazole to remove nonspecifically attached lipids. Depending on the targeted surface concentrations, the histidine-tagged receptor proteins were injected at concentrations between 2 nM and 1 μM for 100–400 s. For coimmobilization of ifnar1-EC and ifnar2-EC, the proteins were injected one after the other to quantify the amount of each of the receptor components. The ligand was then injected at concentrations between 100 and 200 nM for 150 s with a flow rate of 1 μl/s, followed by a wash with 10 μl/s. Maximum flow rates of 250 μl/s were applied for measurement of fast kinetics. After a set of ligand binding experiments, all attached proteins were removed by a 150-s pulse of 200 mM imidazole, and the subsequent binding assays were carried out on the same lipid bilayer.

Data evaluation

Data were analyzed using Origin (Microcal Software), Biaevaluation 2.1 (Biacore), or Berkeley Madonna (UCB) software packages. If necessary, RIf curves were corrected for a linear drift based on the signals before tethering the proteins and after regeneration with imidazole. Different models were used for data evaluation of individual ligand-receptor interaction and for ligand binding and dissociation to ifnar1-EC and ifnar2-EC coimmobilized on supported lipid bilayers.

Pseudo-first-order binding model

Ligand binding to individual receptors was fitted with standard pseudo-first-order kinetic models for association (Eq. 1) and dissociation (Eq. 2) (Eddowes, 1987):

$$R(t) = R_{eq}\left(1 - e^{-(k_a \times c + k_d) \times (t - t_0)}\right) \quad (1)$$

$$R(t) = R_0 \times e^{-k_d \times (t - t_0)}. \quad (2)$$

$R(t)$ is the signal at time t, R_{eq} is the equilibrium signal, R_0 is the signal at $t = t_0$, k_a and k_d are association and dissociation rate constants, respectively, and c is the ligand concentration. The equilibrium dissociation constant K_D was determined from the rate constants of the interaction according to Eq. 3:

$$K_D = k_d/k_a. \quad (3)$$

Ternary complex formation and dissociation

No interactions between the extracellular domains of the receptor subunits have been detectable by several techniques (Lamken et al., 2004), and therefore preassembling of the receptor could be excluded under the experimental conditions employed in this study. Furthermore, no cooperative effect of ifnar2-EC/IFN complex formation on the IFNα2-ifnar1-EC interaction has been observed (Lamken et al., 2004). Therefore, the formation and the dissociation of the ternary complex on supported lipid bilayers was modeled as a two-step process (Whitty et al., 1998) as depicted in Fig. 2. After binding ligand of IFNα2 (L) to the high-affinity receptor ifnar2-EC (R2) on the membrane surface to form the binary IFNα2-ifnar2-EC-complex (B), ifnar1-EC is recruited by lateral interaction on the surface into the ternary complex (T). The rate constants k_a^B and k_d^B are the solution association and dissociation rate constants of the IFNα2-ifnar2-EC interaction with the volume-related equilibrium constant K_D^B. The rate constants k_a^T and k_d^T are the surface association and dissociation rate constants, respectively, of the formation of the ternary complex from the binary complex and ifnar1-EC, and K_D^T the corresponding surface-related equilibrium dissociation constant. The following set of differential equations (as derived in more detail in the Appendix) was used for fitting the dissociation phase:

$$\frac{d[T]}{dt} = k_a^T \times [B] \times ([R1]_0 - [T]) - k_d^T \times [T]$$
$$\frac{d[B]}{dt} = -k_a^T \times [B] \times ([R1]_0 - [T]) + k_d^T \times [T] - k_d^B \times [B]$$
$$[S] = [T] + [B]. \quad (4)$$

$[R1]_0$ and $[R2]_0$ were initial surface concentrations of ifnar1-EC and ifnar2-EC, respectively. $[S]$ was the total surface concentration of the ligand, which was detected in a time-resolved manner by the TIRFS signal and converted into an absolute surface concentration using a calibration by RIf. Because $[T]$ and $[B]$ at $t = 0$ could not be parameterized, we assumed $[T] = [R2]_0$ and $[B] = 0$ as starting parameter for the fitting. Owing to the fast exchange kinetics, the actual values for $[T]$ and $[B]$ were reached within a few seconds—much faster than the dissociation of the ligand. The parameters $[R1]_0$ and $[R2]_0$ were estimated from the RIf signal of the respective experiment, whereas the values for k_d^B and k_d^T were taken from the binding assays with the individual receptors. The only fitted parameter was k_a^T. The surface dissociation constants K_D^T were determined from k_a^T and k_d^T, according to Eq. 3. Ligand association and ternary complex assembling kinetics was simulated using Eq. A5 using the experimentally determined parameters.

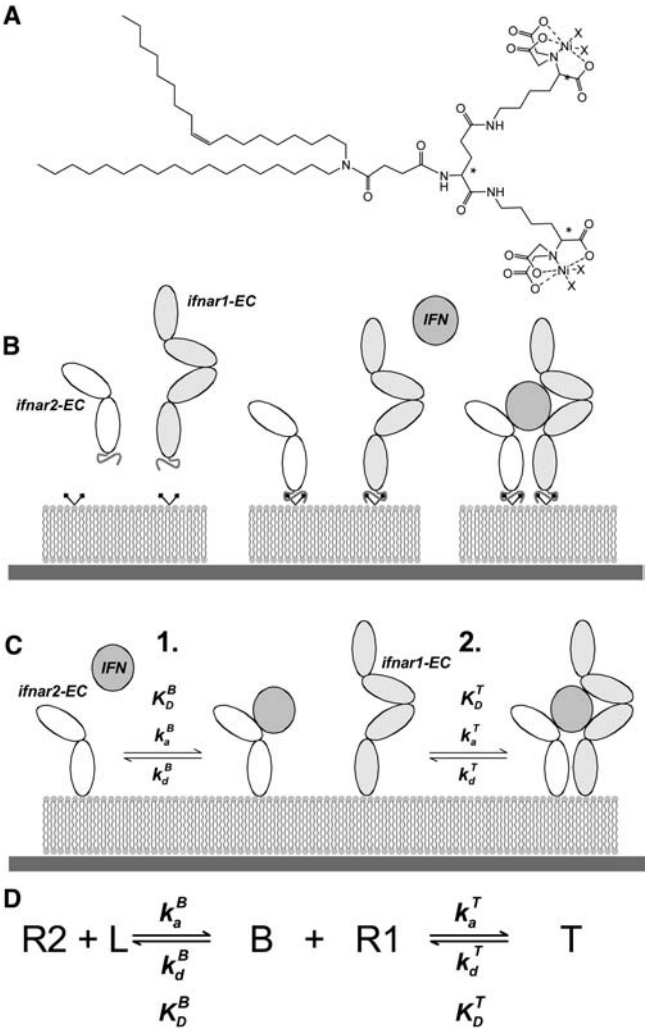

FIGURE 2 (*A*) Structure of the *bis*-NTA lipid used for tethering the extracellular receptor domains on supported lipid bilayer in a stable, yet reversible manner (*B*). (*C*) Illustration of the two-step mechanism assumed for the formation and dissociation of the ternary complex. (*D*) The corresponding interaction scheme with the identifiers used in the equations.

RESULTS

Characterization of the detection system

Solid-supported lipid bilayers are reproducibly formed by vesicle fusion on glass-type surfaces (Brian and McConnell, 1984), and have been characterized in detail with various techniques (Nagle and Tristram-Nagle, 2000; Sackmann, 1996). We therefore used lipid bilayer formation to assess the performance of TIRFS-RIf detection setup. SUVs containing OG488-labeled lipids were injected onto hydrophilic silica surfaces and fusion was monitored simultaneously on the fluorescence (TIRFS) and the interference (RIf) channels (Fig. 3 *A*). Upon a complete bilayer formation, a total decrease of (6.7 ± 0.2) % in the light intensity was measured in the RIf channel. Assuming a surface density of 5 ng/mm^2 for a lipid bilayer (Keller and Kasemo, 1998), the RIf signal was calibrated to a mass loading of 0.7 ng/mm^2 per percentage decrease in intensity. By comparing the signals obtained for vesicle fusion by RIf and by spectral RIf, for which the mass sensitivity has been determined with radioactively labeled proteins (Hanel and Gauglitz, 2002), this mass sensitivity was also confirmed for proteins (data not shown). For clarity sake, the RIf signal converted into surface mass loading will be shown in the measurements to follow (Fig. 3 *B*). Based on this calibration, a typical rms noise of 10 pg/mm^2 was determined for the RIf signal at a data acquisition rate of 1 Hz. This value is ~5× higher than the rms noise of optimized spectral RIf systems under similar conditions of data acquisition (Piehler and Schreiber, 2001). In contrast to the unaltered RIf signal, the fluorescence signal for a full bilayer

varied with the molar fraction of the fluorescent lipids in the vesicles (Fig. 3 *C*). At concentrations below 1 mol%, the signal observed for a full lipid bilayer linearly correlated with the fraction of the labeled lipids. Assuming an area of 70 Å^2 per lipid molecule (Nagle and Tristram-Nagle, 2000), a detection limit of ~0.1 fmol/mm^2 was reached with an excitation power of ~3 μW/mm^2 (Fig. 3 *D*). Consequently, by increasing the excitation power, considerably lower surface concentrations than ~0.1 fmol/mm^2 should be detectable. Yet all further experiments were carried out at this low a power so that the binding curves were least biased by photobleaching. For the same reason, shutter-triggered data collection was applied while monitoring slow dissociation processes. An important feature of this setup is that the two optical techniques are spectrally separated: the light intensity of the RIf channel was several orders of magnitude higher than the typical fluorescence intensity, yet no cross talk between the channels was detected. This holds true also for yellow-fluorescent dyes, which were also successfully used with this setup using a frequency-doubled Nd-YAG laser (532 nm) for excitation (data not shown).

To assess the ability of measuring transient interactions by TIRFS, the contribution of the background fluorescence from the bulk was investigated by injecting OG488 dye at different concentrations (Fig. 4 *A*). These experiments were carried out on solid-supported lipid bilayers containing chelator lipids. The signal from bulk fluorescence was above the noise level at dye concentrations of 200 nM and higher. The signals were fully transient and their amplitudes correlated linearly with the dye concentrations (Fig. 4 *A*). We used the dye injections to estimate the upper limit of the determinable rate constants. For the rise as well as the decay of the concentration in the flow cell, rate constants of ~5 s^{-1} were obtained by fitting monoexponential curves (Fig. 4 *B*).

IFNα2 interaction with ifnar2-EC and ifnar1-EC

The interaction of wild-type IFNα2 with its receptor subunits ifnar1-EC and ifnar2-EC was previously described in detail (Lamken et al., 2004). Here, we used the IFNα2 mutant S136C with an additional cysteine, to which the fluorophore AF488 was coupled site specifically (^{AF488}IFNα2). To exclude that these modifications of the protein affected its binding properties, we characterized the interaction with each of the receptor subunits. The interaction parameters obtained from these measurements are summarized in Table 1. Fig. 5 shows TIRFS and RIf signals during the course of a typical binding assay that includes the following main steps: bilayer formation by fusion of vesicles containing 5% *bis*-NTA lipids (*1*); tethering of the high-affinity receptor component ifnar2-EC through their C-terminal decahistidine tags (*4*); binding of the fluorescently labeled ligand (*5*), and removal of the bound proteins with imidazole (*6*). Each of these steps was monitored quantitatively by RIf, confirming stable tethering of ifnar2-EC. The binding of the labeled ligand, was also detected on the TIRFS channel with substantially higher signal/noise ratio in comparison to the RIf channel. An overlay of the signals obtained by TIRFS and by RIf for the injection of ^{AF488}IFNα2 is shown in Fig. 6 *A*. For both the association and the dissociation phase, very similar shapes of TIRFS and RIf signals were observed. The dissociation curves were fitted by a monoexponential decay (Eq. 2) yielding a dissociation rate constant k_d of (0.010 ± 0.002) s^{-1} for both signals. An association rate constant k_a of ~3 × 10^6 M^{-1}s^{-1} estimated from a monoexponential fit of the association phase (Eq. 1). Both k_a and k_d obtained for the ^{AF488}IFNα2 were in good agreement with the data obtained with wild-type IFNα2 (Lamken et al., 2004; Piehler and Schreiber, 2001) under similar experimental conditions, confirming that the mutation and the coupling of a fluorophore

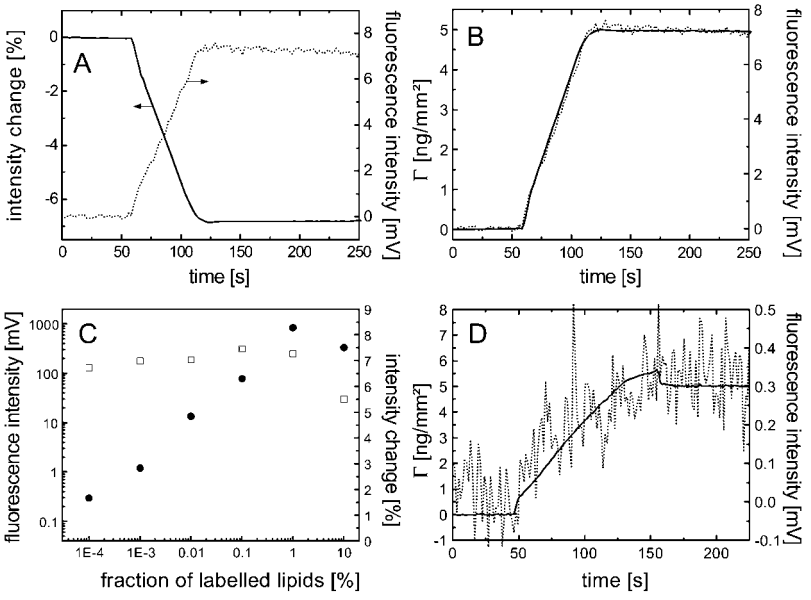

FIGURE 3 Characterization of simultaneous TIRFS-RIf detection. (*A*) Fusion of unilaminar vesicles containing fluorescently labeled lipids simultaneously detected by RIf (*solid line*) and TIRFS (*dotted line*). (*B*) Overlay of the curves shown in panel *A* after RIf intensity change was converted into surface mass deposition. (*C*) RIf (□) and TIRFS (●) signals observed for a full lipid bilayer at different fractions of labeled lipids. (*D*) RIf (*solid line*) and TIRFS (*dotted line*) signals at a fraction of 10^{-4}% fluorescent lipids.

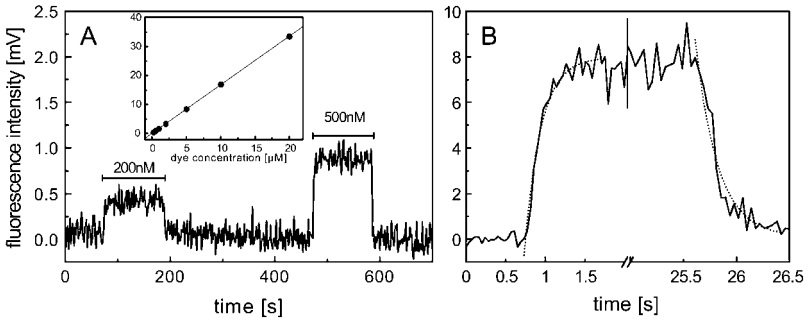

FIGURE 4 Background signals and time resolution. (*A*) Background fluorescence signals from OG488 dye in solution. The inset shows the linear dependence of the signal on the fluorophore concentration. (*B*) Concentration profile obtained from bulk fluorescence measurements and fit of the rise and decay phases by monoexponential functions.

did not affect the binding properties. However, the association and dissociation curves indicated mass transport effects, which have been frequently observed for interactions at the solid-liquid interface at high surface concentrations (Glaser, 1993; Lagerholm and Thompson, 1998; Schuck and Minton, 1996). Therefore, ligand binding at lower surface concentration of ifnar2-EC was investigated (Fig. 6 *B*), which was possible because of the higher signal/noise ratio of fluorescence detection. At ifnar2-EC surface concentrations below 150 pg/mm^2 (6 fmol/mm^2), association and dissociation phases basically unbiased by mass transport limitation were observed. Furthermore, dissociation of ^{AF488}IFNα2 in the presence of 1 μM IFNα2 was measured (Fig. 6 *C*), which gave a very similar dissociation curve as obtained at low ifnar2-EC surface concentrations (Fig. 6 *D*). From these experiments, an average k_d of 0.013 $\pm$ 0.002 s^{-1} was determined for the molecular interaction of ^{AF488}IFNα2 with ifnar2-EC. Furthermore, a strict 1:1 interaction between ifnar2-EC and IFNα2 on the lipid bilayer was confirmed. No differences in binding properties were observed between ^{AF488}IFNα2 and ^{OG488}IFNα2 (data not shown).

For the interaction of IFNα2 with ifnar1-EC, a K_D of 5 μM has been previously determined, which is three orders of magnitude higher than the K_D of the interaction of IFNα2 with ifnar2-EC (Lamken et al., 2004). Dissociation of the ligand was too fast to be resolved by RIf. Owing to a higher signal/noise ratio, dissociation of ^{AF488}IFNα2 from ifnar1-EC could be resolved by TIRFS detection at low receptor surface concentration (i.e., unbiased by rebinding). To minimize background signals, the ligand was injected at a concentration of 200 nM. The fluorescence signal upon ligand injection is shown in (Fig. 6 *C*). From these experiments, a k_d of (1 $\pm$ 0.3) s^{-1} was determined by fitting Eq. 2. Thus, the IFNα2-ifnar1-EC complex is ~100-fold less stable than the IFNα2-ifnar2-EC complex (Fig. 6 *D*). The k_a could not be reliably determined from these curves. However, a similar K_D of ~5 μM was concluded for ^{AF488}IFNα2 as for wild-type IFNα2 by comparing the equilibrium amplitudes determined by RIf at different ligand concentrations (data not shown). From these values, a k_a of ~2 $\times$ 10^5 M^{-1}s^{-1} was estimated for this interaction using Eq. 3. Thus, the ligand binds >10 times faster to ifnar2-EC than to ifnar1-EC. The same binding experiment was carried out with ^{AF488}IFNα2 in stoichiometric complex with ifnar2-tl (data not shown). A dissociation rate constant of ~1 s^{-1} was determined, confirming the similar affinity of IFNα2 and the IFNα2-ifnar2-EC complex for ifnar1-EC (Lamken et al., 2004). Thus, the interaction of ifnar2-EC with IFNα2 does not significantly affect the binding affinity of IFNα2 toward ifnar1-EC. The same binding experiments were carried out with the fluorescence labeled mutants ^{AF488}IFNα2-M148A and ^{OG488}IFNα2-R144A, which bind with altered affinity to ifnar2-EC. Also for these proteins, the S136C mutation and coupling of the fluorophore did not affect the binding properties (see below).

Ligand-induced receptor assembling

To study ligand-induced receptor assembling, both ifnar2-EC and ifnar1-EC were tethered sequentially to the lipid bilayer. The absolute amounts tethered to the surface were quantified by RIf detection. Then, 100 nM ^{AF488}IFNα2 was injected for ensuring maximum coverage of the high-affinity component ifnar2-EC, and the interaction was monitored simultaneously by RIf and TIRFS. A set of experiments with different absolute and relative surface concentrations of ifnar2-EC and ifnar1-EC is shown in Fig. 7. At high surface concentrations of both the receptor components in stoichiometric amounts (~12 fmol/mm^2), ligand dissociated very slowly (Fig. 7 *A*). When the surface concentrations of both receptor components were reduced by a factor of ~6, considerably faster dissociation was observed (Fig. 7 *B*). However, when only the surface concentration of ifnar2-EC was low (~2 fmol/mm^2), and the surface concentration of ifnar1-EC was high (~12 fmol/mm^2), the ligand dissociated at a comparably slow rate (Fig. 7 *C*). With a stoichiometric excess of ifnar2-EC on the surface, a biphasic decay with a high offset of stable-bound IFNα2 was observed (Fig. 7 *D*). The k_d of the faster decay matched the k_d of the IFNα2-ifnar2-EC interaction, whereas the remaining amount of IFNα2 confirmed a 1:1:1 stoichiometry of the complex of IFNα2 with ifnar2-EC and ifnar1-EC. The association phases for these experiments are compared in Fig. 7 *E*. Again, mass transport limitation was observed at high surface concentrations of ifnar2-EC (>4 fmol/mm^2). At low surface concentrations, the association phase perfectly matched the

TABLE 1 Parameters of the interaction with ifnar2-EC and ifnar1-EC for IFNα2 and the mutants used in this study

	Ifnar2-EC			Ifnar1-EC		
IFNα2*	k_a [$M^{-1}s^{-1}$]	k_d [s^{-1}]	K_D [nM]	k_d [s^{-1}]	K_D [μM]	k_a [$M^{-1}s^{-1}$]
wt	$(3 \pm 1) \times 10^6$	0.013 ± 0.002	4 ± 2	1 ± 0.3	~5	$\sim 2 \times 10^5$
M148A	$(3 \pm 1) \times 10^6$	0.3 ± 0.05	100 ± 40	1 ± 0.3	~5	$\sim 2 \times 10^5$
R144A	$(3 \pm 1) \times 10^5$	0.04 ± 0.005	130 ± 50	0.9 ± 0.3	~5	$\sim 2 \times 10^5$

*All species carried the S136C mutation and were site-specifically labeled with OG488 or AF488.

association observed for ifnar2-EC alone, and the same k_a was obtained by fitting Eq. 1.

The striking differences in the dissociation kinetics observed in these experiments support a kinetic stabilization of the ternary complex, and underscore the importance of quantifying receptor surface concentrations. The dynamic nature of the ternary complex was furthermore corroborated by challenging the ternary complex formed with ^{AF488}IFNα2 with unlabeled IFNα2 (Fig. 8 *A*). This experiment was carried out at relatively low receptor surface concentration, thus excluding bias of the dissociation kinetics by rebinding. Fast exchange of the labeled ligand was observed with much higher rate constant than the dissociation of the unchallenged ligand. Chasing with tagless ifnar2-EC did not accelerate ligand dissociation (data not shown), excluding that this effect was due to rebinding. We explain this fast exchange of the ligand by additional binding of the unlabeled ligand to unoccupied receptor subunits, which could even be detected by RIf (Fig. 8 *B*). This fast ligand exchange strongly supports a dynamic equilibrium between ternary and binary complexes.

Interaction in plane of the membrane

With stoichiometric amounts of ifnar1-EC and ifnar2-EC, we assumed a simplified two-step mechanism for receptor formation and dissociation as depicted in Fig. 2 because of the higher affinity and association rate constants of IFNα2 binding to ifnar2-EC. Under these conditions, the rate of ligand dissociation from the surface in the presence of ifnar1-EC is a probe of the dynamic equilibrium between binary (ifnar2-EC/IFNα2) and ternary complex on the membrane. We therefore determined this surface dissociation constant of this lateral interaction by evaluating ligand dissociation at various stoichiometric surface concentrations of ifnar2-EC and ifnar1-EC at stoichiometric ratio. For calculating the signals into surface concentrations, the fluorescence signal was calibrated against the mass-sensitive signal. A linear correlation of the maximum ligand binding fluorescence signals with the receptor surface concentration as determined by RIf was observed (Fig. 9 *A*). This calibration allowed: i), conversion of the fluorescence signals, as observed during ligand binding and dissociation, into mass loading (Fig. 9 *B*), and ii), precise assessment of absolute receptor surface concentrations even at low surface coverage. To determine the association rate constant k_a^T of the interaction of ifnar2-EC-bound IFNα2 with ifnar1-EC on the bilayer surface, Eq. 4 was fitted to the ligand dissociation phase with k_a^T as the only fitting parameter, whereas all the other parameters were fixed at the values determined in the previous measurements: k_d^B was parameterized with the rebinding-corrected k_d of the ifnar2-EC-IFNα2 interaction (0.013 s^{-1}); k_d^T was parameterized with the k_d of the interaction of the ligand with ifnar1-EC from solution (1 s^{-1}), assuming that tethering the complex on the membrane did not affect the complex lifetime. The receptor surface concentrations $[R1]_0$ and $[R2]_0$ were determined directly from the RIf signals. Despite the constrained parameterization, very good agreement of the fit was observed for all the measured curves (Fig. 9, *C* and *D*), which was significantly better than a monoexponential fit (Lamken et al., 2004). The k_a^T determined at different surface concentrations and the corresponding surface dissociation constant K_D^T are listed in Table 2. Strikingly, similar values for k_a^T were obtained for all dissociation curves, resulting into an average k_a^T of (16.5 ± 1.6) $mm^2fmol^{-1}s^{-1}$ or ~ 0.027 $\mu m^2 molecules^{-1}s^{-1}$. From the surface rate constants, a surface equilibrium dissociation constant K_D^T of 0.061 ± 0.006 $fmol/mm^2$ or ~ 36 $mol/\mu m^2$ was determined using Eq. 3.

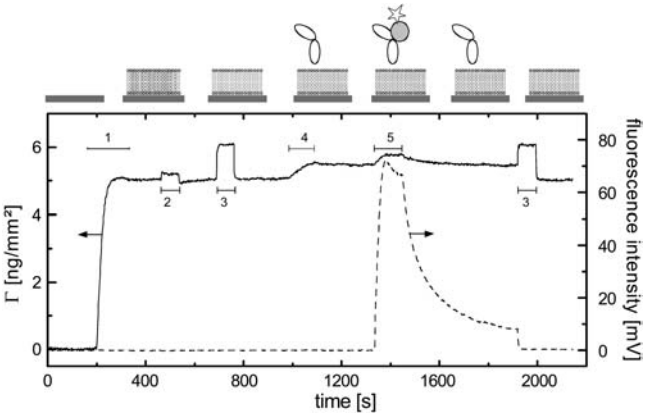

FIGURE 5 Course of a typical binding experiment on supported lipid bilayers as detected by RIf (*solid line*) and TIRFS (*dashed line*). Injection of (*1*) SOPC SUVs, (*2*) 10 mM nickel(II)chloride, (*3*) 200 mM imidazole, (*4*) 300 nM ifnar2-H10, and (*5*) 100 nM ^{AF488}IFNα2.

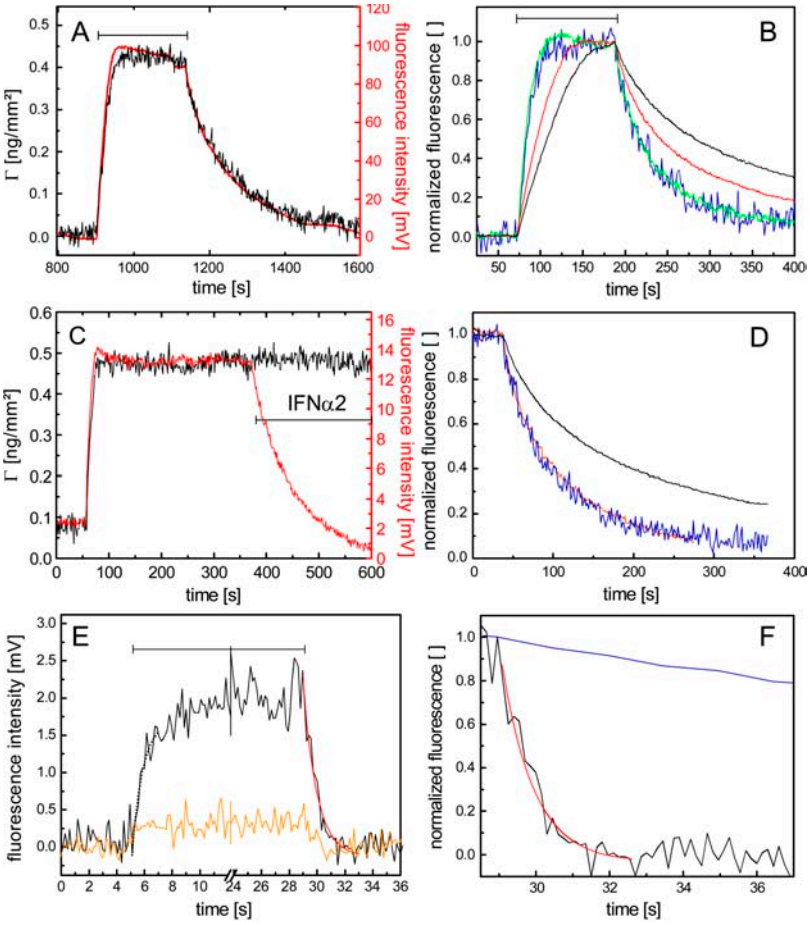

FIGURE 6 Interaction of ^{AF488}IFNα2 separately with each of the receptor subunits ifnar2-EC (*A–D*) and ifnar1-EC (*E* and *F*) tethered to supported lipid bilayers. (*A*) Ligand binding (100 nM) to ifnar2-EC and dissociation as detected simultaneously by TIRFS (*red*) and RIf (*black*). (*B*) Interaction of 100 nM ligand with ifnar2-EC at different ifnar2-EC surface concentrations (20 pg/mm^2, *blue*; 150 pg/mm^2, *green*; 500pg/mm^2, *red*; and 1000 pg/mm^2, *black*) as detected by TIRFS. The signals were normalized to the maximum signal, which at this ligand concentration corresponds to R_{max}. (*C*) Chasing of ^{AF488}IFNα2 bound to ifnar2-EC by injection of 1 μM unlabeled IFNα2 as detected by RIF TIRFS (*red*) and RIf (*black*). (*D*) Comparison of the dissociation curves at high ifnar2-EC surface concentration (*black*), at low ifnar2-EC surface concentration (*blue*), and for chasing with unlabeled IFNα2 (*orange*). (*E*) Binding of 200 nM ^{AF488}IFNα2 with (*black*) and without (*orange*) immobilized ifnar1-EC, and the fit of the dissociation curve (*red*). (*F*) Comparison of the dissociation of IFNα2 from ifnar1-EC (*black*) including the fit curve (*red*) with the dissociation from ifnar2-EC (*blue*).

The roles of the association rate constants

Based on these results we simulated the assembling kinetics at different receptor surface concentrations (Fig. 10 *A*) and different stabilities of the ligand complex with ifnar2-EC (Fig. 10 *B*). These simulations showed that ligand association to ifnar2-EC is the rate-determining step in ternary complex assembling (Fig. 10 *A*). Consequently, assembling mechanism should be primarily determined by the faster association of the ligand to ifnar2-EC compared to ifnar1-EC, and not by the stability of the complex with ifnar2-EC (Fig. 10 *B*). Owing to the principle of microscopic reversibility, this faster interaction of the ligand with ifnar2-EC should also dictate the dissociation mechanism. To test this hypothesis, the dissociation from the ternary complex was probed with the mutants IFNα2-M148A and IFNα2-R144A. These mutants bind ifnar2-EC with 25–30-fold lower affinity than the wild type, but with very different rate constants (Piehler et al., 2000): for IFNα2-M148A, the k_a is unchanged compared to the wild type, whereas for IFNα2-R144A, the k_a is decreased by one order of magnitude. These mutants were site-specifically fluorescence labeled with AF488 (M148A) and OG488 (R144A) through the S136C mutation as the wild-type protein (^{AF488}IFNα2-M148A and ^{OG488}IFNα2-R144A, respectively), and the interaction with ifnar2-EC was characterized by TIRFS-RIf detection. The dissociation of these IFNα2 mutants from ifnar2-EC are compared in Fig. 11 *A*. The rate constants obtained for the mutants (Table 1) were in good agreement with the published values, while binding to ifnar1-EC was unchanged compared to the wild type (data not shown).

With ifnar2-EC and ifnar1-EC coimmobilized on lipid bilayers, for both ^{OG488}IFNα2-R144 and ^{AF488}IFNα2-M148A significantly faster ligand dissociation compared to ^{AF488}IFNα2 was observed (Fig. 11 *B*). For ^{AF488}IFNα2-M148A, however, the dissociation at different receptor surface concentrations was still fitted well by the same model and the stringent parameterization as used for ^{AF488}IFNα2 (Fig. 11, *C* and *D*). Moreover, a surface association rate constant k_a^T of (18 $\pm$ 1) mm^{2}fmol^{-1}s^{-1} was obtained, resulting into a surface equilibrium dissociation constant K_D^T of 0.056 $\pm$ 0.004 fmol/mm^2 (i.e., 33 molecules/μm^2). These values are in very good agreement with the values obtained for ^{AF488}IFNα2. In contrast, considerable systematic deviation of the fit was obtained for ^{OG488}IFNα2-R144A (Fig. 11, *E* and *F*), and a significantly lower k_a^T of (9 $\pm$ 1) mm^{2}fmol^{-1s-1} was obtained, resulting into a higher apparent K_D^T of 0.11 $\pm$ 0.01 fmol/mm^2. (i.e., 67 molecules/μm^2). We conclude from these results that the model shown in Fig. 2 holds true only for the

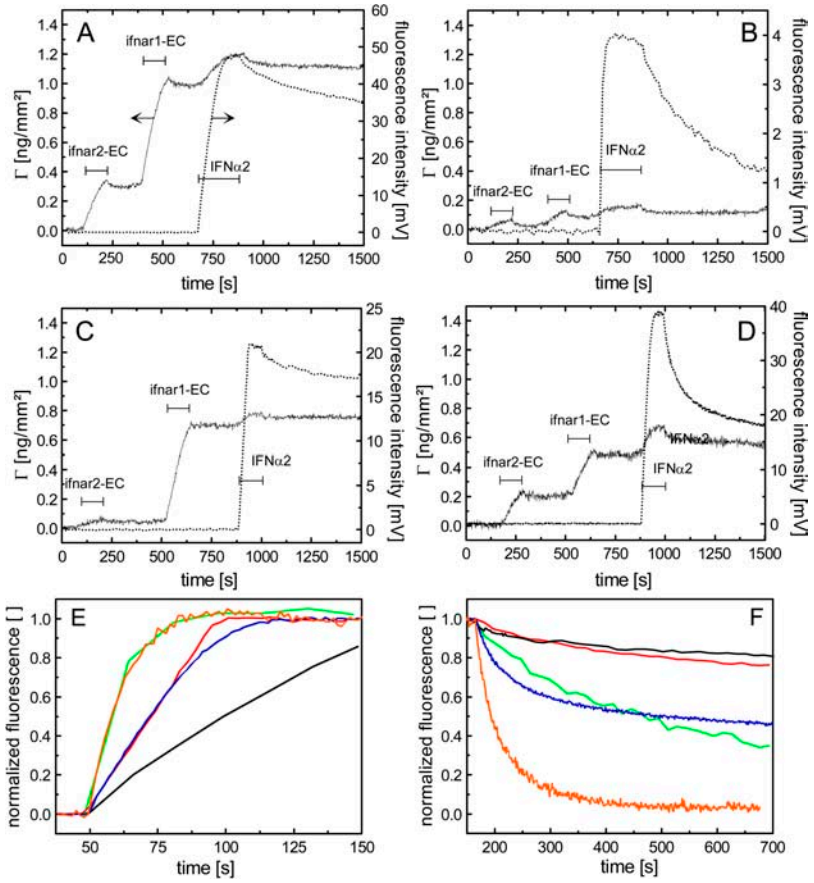

FIGURE 7 Interaction of 100 nM ^{AF488}IFNα2 with ifnar1-EC and ifnar2-EC coimmobilized onto supported lipid bilayers at different absolute and relative amounts. The signals detected by TIRFS (*dotted line*) and by RIf (*solid line*) during sequential tethering of ifnar2-EC and ifnar1-EC followed by injection of the ligand are shown in panels *A–D*. (*A*) Ifnar2-EC (25 kDa) and ifnar1-EC (57 kDa) (12 fmol/mm^2 of both). (*B*) Ifnar2-EC and ifnar1-EC (2 fmol/mm^2 of both). (*C*) Ifnar2-EC (2 fmol/mm^2)and ifnar1-EC (10 fmol/mm^2). (*D*) Ifnar2-EC (8 fmol/mm^2)and ifnar1-EC (5 fmol/mm^2). (*E* and *F*) Fluorescence traces of association (*E*) and dissociation (*F*) of ^{AF488}IFNα2 shown in panels *A* (*black*), *B* (*green*), *C* (*red*), and *D* (*blue*), in comparison to the interaction with ifnar2-EC alone (*orange*).

case that the k_a of the interaction with ifnar2-EC substantially exceeds the k_a the interaction with ifnar1-EC.

DISCUSSION

Simultaneous TIRFS-RIf detection

Precise quantification of the interacting species is a key requirement for studying biomolecular interactions in a quantitative manner. For studying protein-protein interaction on solid supported membranes, we incorporated label-free detection by RIf into a prism-based TIRFS setup. Mass-sensitive detection by RIf enabled for monitoring and quantifying all binding events on the surface including lipid bilayer fusion and receptor reconstitution, thus adding important features in comparison to exclusive fluorescence detection: i), fluorescence labeling of several components can be avoided, reducing signal cross talk and possible effects on protein function; ii), surface concentrations are directly determined and their changes are monitored, which is extremely important in case of sensitive multicomponent surface architectures; iii), straightforward calibration of fluorescence signals with respect to surface coverage. The RIf transducer element—a silica layer on top of a glass substrate—is fully transparent and does not quench surface-proximal fluorophores, unlike noble metal surfaces required for detection by SPR, and therefore is ideally compatible with TIRFS. At the same time, its silica surface is ideally suited for preparing solid-supported fluid lipid bilayers. RIf detection is based on directional reflection, providing several advantages over other detection techniques (Hanel and Gauglitz, 2002): i), compared to evanescent field interrogation, background signals due to changes in the refractive index or buffer properties are much lower; ii), strict mass sensitivity independent on the distance from the surface or changes in shear forces; iii), simple and rugged fiber-based interrogation with no moving parts. Fluorescence excitation and emission were kept independent of RIf illumination by implementing monochromatic RIf detection in the near infrared region. Thus, we realized a simple and rugged setup for simultaneous mass sensitive and fluorescence detection without compromising the flexibility of either technique. Complete spectral separation of the two techniques proved valuable as high-power illumination for optimum RIf detection could be applied without photobleaching the fluorophores absorbing in the visible region. By further optimizing the detection, the rms noise of the RIf signal of currently 10 pg/mm^2 could be improved down to 1–2 pg/mm^2, which is comparable to spectral RIf detection (Hanel and Gauglitz, 2002). No significant cross talk be-

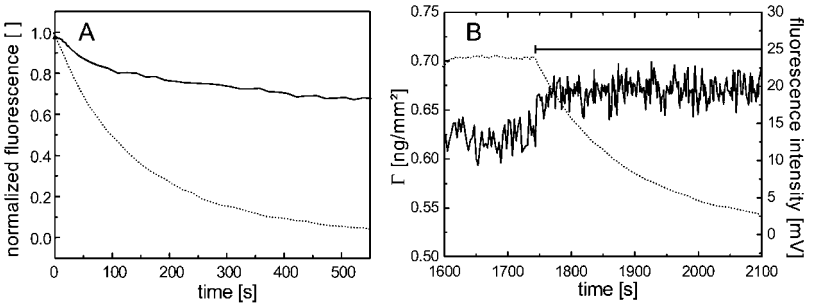

FIGURE 8 Ligand exchange in the ternary complex. Ternary complex was formed with 2 fmol/mm^2 ifnar2-EC and 10 fmol/mm^2 ifnar1-EC tethered on the lipid bilayer, followed by an injection of 100 nM ^{AF488}IFNα2. (*A*) Decay of the fluorescence signal in absence (*solid line*) and in presence (*dotted line*) of 10 μM unlabeled IFNα2. (*B*) Fluorescence (*dotted line*) and interference (*solid line*) signals during injection of 10 μM unlabeled IFNα2. Additional binding of the nonlabeled IFNα2 during this injection was detected by RIf.

tween the two techniques was detectable: fluorescence excitation with different excitation sources and different excitation power was possible without compromising RIf detection (data not shown). Vice versa, the performance of the TIRFS setup was completely independent of RIf illumination. Even at a low excitation power (2–3 μW/mm^2) a detection limit of 10^7 fluorophores/mm^2 (i.e., 10 fluorophores/μm^2) was reached, and thus fluorescence detection could be carried out without significantly photobleaching the flurophores.

Ligand-induced receptor assembling

We have applied simultaneous TIRFS-RIf detection for measuring ligand-receptor interactions within the plane of the membrane. The extracellular domains of the two subunits of the type I interferon receptor were tethered via C-terminal histidine tags in an oriented fashion onto supported lipid bilayers using chelator lipids (Dorn et al., 1998; Schmitt et al., 1994). Here, we used *bis*-NTA chelator headgroups, which bind decahistidine-tagged proteins very stably (Lata and Piehler, 2005), ensuring that the interacting proteins were tightly tethered to the membrane. Thus, oriented anchoring and lateral diffusion of the receptor in the plasma membrane was mimicked while the receptor surface concentrations could be varied in a straightforward manner. Homogeneous distribution of ifnar2-EC tethered on these bilayers, and fast lateral diffusion with a diffusion coefficient of 1 μm^2/s has been previously shown by laser scanning microscopy (Lamken et al., 2004). This is comparable to the local receptor mobility on the plasma membrane as determined by single particle tracking (Ritchie et al., 2003). The formation of a complete lipid bilayer and its integrity during the experiments was monitored by RIf, thus ensuring full experimental control. Furthermore, the amounts of ifnar2-EC and ifnar1-EC tethered to the bilayers were quantified in each binding experiment. Site-specifically fluorescence-labeled IFNα2-S136C was used to dissect and study the interactions involved in ternary complex formation by monitoring ligand binding simultaneously by TIRFS and

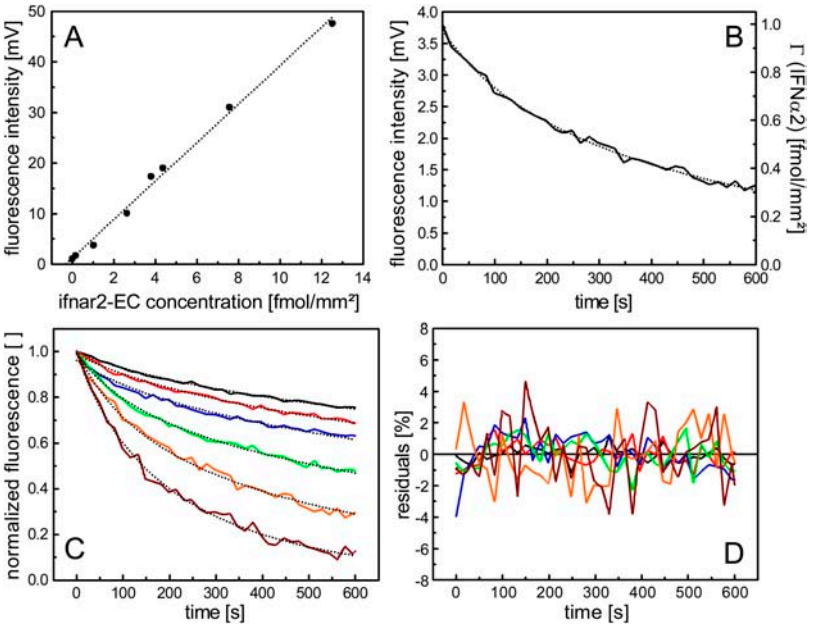

FIGURE 9 Evaluation of ligand dissociation kinetics from the ternary complex at different receptor surface concentrations. (*A*) Correlation between saturation ligand binding signals (fluorescence) and molar surface concentration of ifnar2-EC as determined from the RIf signal. (*B*) Dissociation phase at a receptor surface concentration of 1 fmol/mm^2: fluorescence signal correlated with the mass loading (*solid line*) and fit of Eq. 4 (*dotted line*). (*C*) Normalized dissociation phase (*solid line*) at different receptor surface concentrations (*black*, 12 fmol/mm^2; *red*, 8 fmol/mm^2; *blue*, 4 fmol/mm^2; *green*, 2 fmol/mm^2; *orange*, 1 fmol/mm^2; *brown*, 0.3 fmol/mm^2) with fit curves (*dotted line*). (*D*) Residuals from the curves shown in panel *C* (same color coding as in *C*).

TABLE 2 Surface association rate constants k_a^T and surface dissociation constants K_D^T determined from the fit of the ligand dissociation kinetics from the ternary complex

IFNα2	ifnar1 [fmol/mm^2]	k_a^T [mm^{2}fmol^{-1}s^{-1}]	K_D^T [fmol/mm^2]
wt	12.0	19.2	0.076
	7.8	16.8	0.047
	4.7	17.7	0.040
	3.8	16.6	0.063
	2.2	14.8	0.087
	1.0	15.5	0.085
	0.3	14.7	0.069
	Average	16 ± 2	0.061 ± 0.006
M148A	16.0	18.0	0.056
	7.4	19.0	0.053
	2.2	17.5	0.057
	Average	18 ± 1	0.056 ± 0.004
R144A	8.5	8.2	0.12
	3.9	8.5	0.12
	1.6	9.8	0.10
	Average	9 ± 1	0.11 ± 0.01

RIf. Although the interaction properties of this ligand were very similar to the interaction properties previously determined for wild-type IFNα2 (Lamken et al., 2004), we furthermore succeeded to determine the rate constants of the very transient interaction with ifnar1-EC by fluorescence detection. All results supported the previously proposed two-step assembling mechanism of the ternary complex and a dynamic equilibrium between binary and ternary complex on the membrane. Furthermore, possible cooperative effects in the ternary complex, which have been observed for other cytokine-receptor complexes, could not be detected for the IFNα2-ifnar interactions.

We used ligand dissociation kinetics for probing this dynamic equilibrium between binary and ternary complex. We assumed ligand association to ifnar2-EC as the first step (Fig. 2), thus simplifying the mathematical treatment compared to the general model (Thompson and Axelrod, 1983). The possibility of i), readily varying the receptor surface concentrations by reversible tethering, and ii), quantifying absolute surface concentrations by RIf turned out to be of key importance. Thus, we were able to precisely parameterize the system. The ligand dissociation kinetics was fitted well by the model with a single parameter being adjusted: the association rate constant k_a^T of the interaction between the IFNα2-ifnar2-EC complex and ifnar1-EC in plane of the membrane. Despite this very constrained fitting procedure, this k_a^T turned out to be independent on the surface concentration of the receptor subunits. Even for the IFNα2-mutant M148A, which dissociated from ifnar2-EC nearly as fast as from ifnar1-EC, the ligand dissociation kinetics was properly described by the model. Strikingly, a very similar k_a^T was obtained for this mutant, confirming that the IFNα2-ifnar1-EC interaction was probed by ligand dissociation. In the case of the IFNα2-mutant R144A with a similar k_a toward ifnar2-EC and ifnar1-EC, however, the model did not properly fit the observed dissociation kinetics, and a significantly lower k_a^T was obtained as compared to IFNα2 wild type and IFNα2-M148A. These two mutants, which bind ifnar2-EC with very similar affinity, impressively demonstrate the role of the association rate constants for the assembling mechanism and the dynamics of the ternary complex on the membrane.

Interaction in two and three dimensions

The interaction of IFNα2 with ifnar1-EC in solution and on the surface can be compared based on these results: the equilibrium dissociation constant of 36 mol/μm^2 as determined for the interaction on the surface corresponds to a K_D of 5 μM (or 3000 mol/μm^3) with the ligand in solution. At the concentrations corresponding to these respective K_D, the same numbers of association events per time unit take place on the surface as in solution, assuming the same dissociation rate constants. The average distance between the molecules at these concentrations are ~200 nm on the membrane and ~100 nm in solution. Under these conditions, the probability of random collision between the two particles should be 10–100-fold higher in solution than on the membrane as estimated by the collision laws for diffusion in three and two dimensions (Hardt, 1979) taking the different diffusion coefficients in solution (~100 μm^2/s, (Kreuz and Levy, 1965) and on the membrane (1 μm^2/s) into account. Collisions must, therefore, be 10–100 times more productive when the proteins are tethered to the membrane. This substantially higher efficiency could be ascribed to a longer

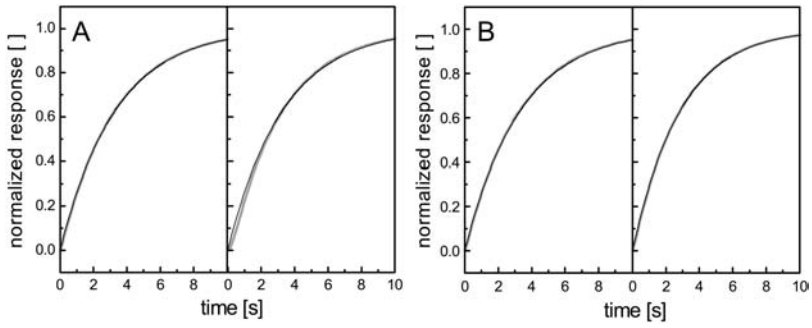

FIGURE 10 Simulation of ligand association and ternary complex formation kinetics based on the experimental rate constants of the interaction with ifnar1-EC on the membrane (ligand concentration of 100 nM). For comparison, all curves were normalized to the equilibrium signal. (*A*) Comparison of the ligand association kinetics (*black*) and the ternary complex formation (*gray*) at different receptor surface concentrations (*left*, 10 fmol/mm^2; *right*, 1 fmol/mm^2). (*B*) Comparison of the ligand association kinetics (*black*) and the ternary complex formation (*gray*) at different stabilities of the ligand interaction with ifnar2-EC (*left*, 0.01 s^{-1}; *right*, 1 s^{-1}).

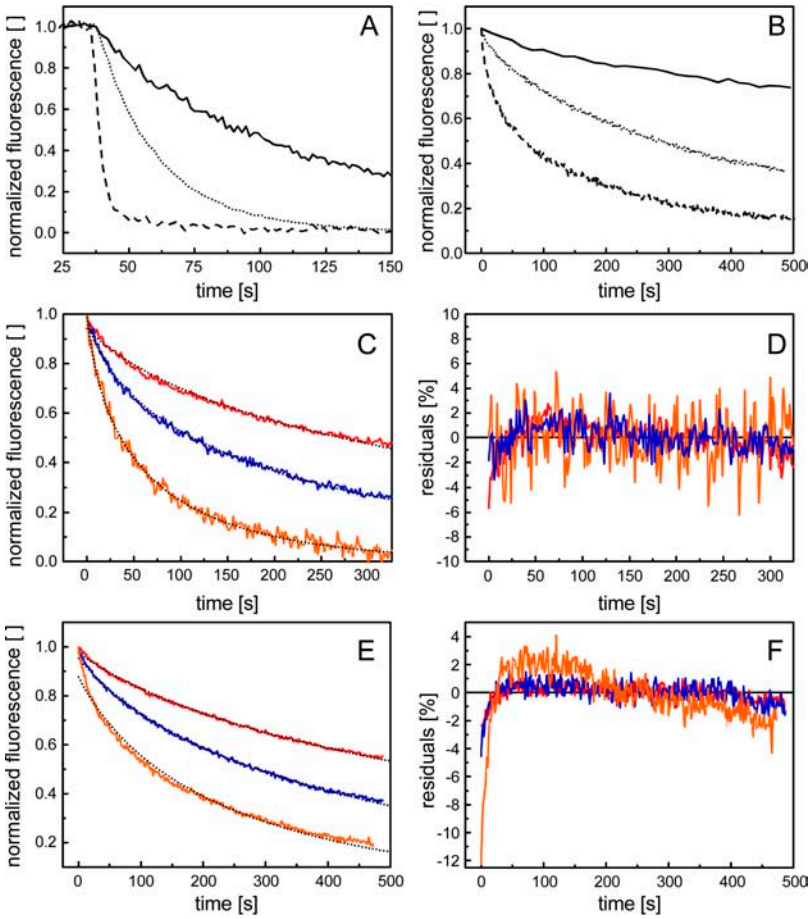

FIGURE 11 Binary and ternary complex formation analyzed for the IFNα2 mutants M148A and R144A. (*A*) Dissociation of ^{OG488}IFNα2-R144A (*dotted line*) and ^{AF488}IFNα2-M148A (*dashed line*) from ifnar2-EC in comparison to ^{AF488}IFNα2 (*solid line*) as detected by TIRFS. (*B*) Dissociation of ^{OG488}IFNα2-R144A (*dotted line*) and ^{AF488}IFNα2-M148A (*dashed line*) from ifnar2-EC and ifnar1-EC (both 5–7 fmol/mm^2) in comparison to ^{AF488}IFNα2 (*solid line*) as detected by TIRFS. (*C*) Normalized dissociation phases for ^{AF488}IFNα2-M148A at different receptor surface concentrations (*red*, 16 fmol/mm^2; *blue*, 7.4 fmol/mm^2; *orange*, 2.2 fmol/mm^2) with fit curves (*dotted line*). (*D*) Residuals from the curves shown in panel *C* (same color coding). (*E*) Normalized dissociation phases for ^{OG488}IFNα2-R144A at different receptor surface concentrations (*red*, 8.5 fmol/mm^2; *blue*, 3.9 fmol/mm^2; *orange*, 1.6 fmol/mm^2) with fit curves (*dotted line*). (*F*) Residuals from the curves shown in panel *E* (same color coding).

lifetime of the encounter complex due to slower diffusion in the membrane (Gutfreund, 1995), suggesting that a decrease in collision rate on the membrane is essentially compensated by an increase in successful collisions. Furthermore, preorientation of the membrane-tethered proteins should also contribute to higher encounter efficiency.

Receptor recruitment on the plasma membrane

Our data also implicate functional consequences, as the surface equilibrium and rate constants determine the formation and the lifetime of the ternary signaling complex. The apparent ligand dissociation rate constant (and also the apparent equilibrium dissociation constant) can be used for assessing the equilibrium on the cellular plasma membrane. Thus, 10–20% free binary complex can be estimated for IFNα2 by comparing our results with published cellular binding data (Cutrone and Langer, 1997). Indeed, very similar numbers were concluded from cellular binding data for the IL-4-receptor (Whitty et al., 1998), where the binding affinities are well comparable to the IFNα2-ifnar interaction (Letzelter et al., 1998). A surface equilibrium constant of 36 mol/μm^2, however, is not sufficient for such effective recruitment in case that the typically few 1000 receptors are uniformly distributed on the total cell surface ($\sim$1–10 mol/μm^2). This suggests preorganization of the receptor proteins at higher local concentration within membrane domains, which have been shown to play an important role in cytokine signaling (Sehgal, 2003; Takaoka et al., 2000). The efficiency of ternary complex formation and its dynamics could well be an important parameter determining the responsiveness of different cell types. Differential responsiveness of different cells types toward different IFNs could also be explained in terms of the efficiency of recruiting ifnar1, because very different affinities have been observed for IFNα2 and IFNβ (Lamken et al., 2004).

APPENDIX

The proposed assembling mechanism shown in Fig. 2 can be described by the following set of differential equations:

$$\frac{d[T]}{dt} = k_a^T[B][R1] - k_d^T[T]$$
$$\frac{d[B]}{dt} = -k_a^T[B][R1] + k_d^T[T] - k_d^B[B] + k_a^B[R2][L], \qquad \text{(A1)}$$

where $[B]$ and $[T]$ are the surface concentrations of the binary and the ternary complex, respectively; $[R1]$ and $[R2]$ are the surface concentrations of free

ifnar1-EC and ifnar2-EC, respectively; $[L]$ is the (volume) concentration of the free ligand; k_a^B and k_d^B are the association and the dissociation rate constant of ifnar2-EC-IFNα2 complex formation; k_a^T and k_d^T are the surface association and dissociation rate constants of the interaction of ifnar1-EC with the ifnar2-EC-IFNα2 complex on the surface. The total surface-bound ligand is monitored, i.e., the sum of both complexes $[S]$:

$$[S] = [T] + [B]. \tag{A2}$$

The total amount of ifnar2-EC on the membrane $[R2]_0$ is given by the sum of the amount of free ifnar2-EC, the binary complex and the ternary complex:

$$[R2]_0 = [R2] + [B] + [T]. \tag{A3}$$

The total amount of ifnar1-EC $[R1]_0$, is given by the sum of the amounts of free ifnar1-EC and the ternary complex.

$$[R1]_0 = [R1] + [T]. \tag{A4}$$

$[R1]$ and $[R2]$ from Eqs. A2 and A3 are inserted into Eq. A1:

$$\begin{aligned}
\frac{d[T]}{dt} &= k_a^T \times [B] \times ([R1]_0 - [T]) - k_d^T \times [T] \\
\frac{d[B]}{dt} &= -k_a^T \times [B] \times ([R1]_0 - [T]) + k_d^T \times [T] \\
&\quad - k_d^B \times [B] + k_a^B \times ([R2]_0 - [T] - [B]) \times [L] \\
[S] &= [T] + [B].
\end{aligned} \tag{A5}$$

During dissociation ligand concentration equals 0, $[L] = 0$ and Eq. A5 can be simplified to

$$\begin{aligned}
\frac{d[T]}{dt} &= k_a^T \times [B] \times ([R1]_0 - [T]) - k_d^T \times [T] \\
\frac{d[B]}{dt} &= -k_a^T \times [B] \times ([R1]_0 - [T]) + k_d^T \times [T] - k_d^B \times [B] \\
[S] &= [T] + [B].
\end{aligned} \tag{A6}$$

We gratefully acknowledge support from the laboratory of Robert Tampé.

This work was supported by the Deutsche Forschungsgemeinsch (Emmy-Noether-Program Pi 405/1, project Pi 405/2, and the SFB 628), and by the Human Frontier Science Program (RGP60/2002).

REFERENCES

Adam, G., and M. Delbruck. 1968. Reduction of dimensionality in biological diffusion processes. *In* Structural Chemistry and Molecular Biology. N. Davidson, editor. W. H. Freeman, New York, NY. 198–215.

Axelrod, D., T. P. Burghardt, and N. L. Thompson. 1984. Total internal reflection fluorescence. *Annu. Rev. Biophys. Bioeng.* 13:247–268.

Axelrod, D., and M. D. Wang. 1994. Reduction-of-dimensionality kinetics at reaction-limited cell surface receptors. *Biophys. J.* 66:588–600.

Brian, A. A., and H. M. McConnell. 1984. Allogeneic stimulation of cytotoxic T cells by supported planar membranes. *Proc. Natl. Acad. Sci. USA.* 81:6159–6163.

Chill, J. H., S. R. Quadt, R. Levy, G. Schreiber, and J. Anglister. 2003. The human type I interferon receptor. NMR structure reveals the molecular basis of ligand binding. *Structure (Camb).* 11:791–802.

Cunningham, B. C., M. Ultsch, A. M. De Vos, M. G. Mulkerrin, K. R. Clauser, and J. A. Wells. 1991. Dimerization of the extracellular domain of the human growth hormone receptor by a single hormone molecule. *Science.* 254:821–825.

Cutrone, E. C., and J. A. Langer. 1997. Contributions of cloned type I interferon receptor subunits to differential ligand binding. *FEBS Lett.* 404:197–202.

DeLisi, C. 1980. The biophysics of ligand-receptor interactions. *Q. Rev. Biophys.* 13:201–230.

Dorn, I. T., K. Pawlitschko, S. C. Pettinger, and R. Tampe. 1998. Orientation and two-dimensional organization of proteins at chelator lipid interfaces. *Biol. Chem.* 379:1151–1159.

Eddowes, M. J. 1987. Direct immunochemical sensing: basic chemical principles and fundamental limitations. *Biosensors.* 3:1–15.

Gent, J., M. Van Den Eijnden, P. Van Kerkhof, and G. J. Strous. 2003. Dimerization and signal transduction of the growth hormone receptor. *Mol. Endocrinol.* 17:967–975.

Gizeli, E., M. Liley, C. R. Lowe, and H. Vogel. 1997. Antibody binding to a functionalized supported lipid layer: a direct acoustic immunosensor. *Anal. Chem.* 69:4808–4813.

Glaser, R. W. 1993. Antigen-antibody binding and mass transport by convection and diffusion to a surface: a two-dimensional computer model of binding and dissociation kinetics. *Anal. Biochem.* 213:152–161.

Grotzinger, J. 2002. Molecular mechanisms of cytokine receptor activation. *Biochim. Biophys. Acta.* 1592:215–223.

Gutfreund, H. 1995. Kinetics for the Life Sciences: Receptors, Transmitters and Catalysts: Cambridge University Press, Cambridge, UK.

Haake, H. M., A. Schutz, and G. Gauglitz. 2000. Label-free detection of biomolecular interaction by optical sensors. *Fresenius J. Anal. Chem.* 366:576–585.

Hanel, C., and G. Gauglitz. 2002. Comparison of reflectometric interference spectroscopy with other instruments for label-free optical detection. *Anal. Bioanal. Chem.* 372:91–100.

Hardt, S. L. 1979. Rates of diffusion controlled reactions in one, two and three dimensions. *Biophys. Chem.* 10:239–243.

Keller, C. A., and B. Kasemo. 1998. Surface specific kinetics of lipid vesicle adsorption measured with a quartz crystal microbalance. *Biophys. J.* 75:1397–1402.

Kreuz, L. E., and A. H. Levy. 1965. Physical properties of chick interferon. *J. Bacteriol.* 89:462–469.

Lagerholm, B. C., and N. L. Thompson. 1998. Theory for ligand rebinding at cell membrane surfaces. *Biophys. J.* 74:1215–1228.

Lamken, P., S. Lata, M. Gavutis, and J. Piehler. 2004. Ligand-induced assembling of the type I interferon receptor on supported lipid bilayers. *J. Mol. Biol.* 341:303–318.

Lata, S., and J. Piehler. 2005. Stable and functional immobilization of histidine-tagged proteins via multivalent chelator head-groups on a molecular poly(ethylene glycol) brush. *Anal. Chem.* 77:1096–1105.

Letzelter, F., Y. Wang, and W. Sebald. 1998. The interleukin-4 site-2 epitope determining binding of the common receptor gamma chain. *Eur. J. Biochem.* 257:11–20.

Liebermann, T., and W. Knoll. 2000. Surface-plasmon field-enhanced fluorescence spectroscopy. *Colloids Surf. A.* 171:115–130.

Marx, K. A. 2003. Quartz crystal microbalance: a useful tool for studying thin polymer films and complex biomolecular systems at the solution-surface interface. *Biomacromolecules.* 4:1099–1120.

Nagle, J. F., and S. Tristram-Nagle. 2000. Structure of lipid bilayers. *Biochim. Biophys. Acta.* 1469:159–195.

Neumann, T., M. L. Johansson, D. Kambhampati, and W. Knoll. 2002. Surface-plasmon fluorescence spectroscopy. *Adv. Funct. Mater.* 12:575–586.

Piehler, J., L. C. Roisman, and G. Schreiber. 2000. New structural and functional aspects of the type I interferon-receptor interaction revealed by comprehensive mutational analysis of the binding interface. *J. Biol. Chem.* 275:40425–40433.

Piehler, J., and G. Schreiber. 1999. Biophysical analysis of the interaction of human ifnar2 expressed in E-coli with IFN alpha 2. *J. Mol. Biol.* 289:57–67.

Piehler, J., and G. Schreiber. 2001. Fast transient cytokine-receptor interactions monitored in real time by reflectometric interference spectroscopy. *Anal. Biochem.* 289:173–186.

Remy, I., I. A. Wilson, and S. W. Michnick. 1999. Erythropoietin receptor activation by a ligand-induced conformation change. *Science.* 283:990–993.

Ritchie, K., R. Iino, T. Fujiwara, K. Murase, and A. Kusumi. 2003. The fence and picket structure of the plasma membrane of live cells as revealed by single molecule techniques (Review). *Mol. Membr. Biol.* 20:13–18.

Roisman, L. C., J. Piehler, J. Y. Trosset, H. A. Scheraga, and G. Schreiber. 2001. Structure of the interferon-receptor complex determined by distance constraints from double-mutant cycles and flexible docking. *Proc. Natl. Acad. Sci. USA.* 98:13231–13236.

Sackmann, E. 1996. Supported membranes: scientific and practical applications. *Science.* 271:43–48.

Schmid, E. L., A. P. Tairi, R. Hovius, and H. Vogel. 1998. Screening ligands for membrane protein receptors by total internal reflection fluorescence: the 5-HT3 serotonin receptor. *Anal. Chem.* 70:1331–1338.

Schmitt, L., C. Dietrich, and R. Tampe. 1994. Synthesis and characterization of chelator-lipids for reversible immobilization of engineered proteins at self-assembled lipid interfaces. *J. Am. Chem. Soc.* 116: 8485–8491.

Schuck, P., and A. P. Minton. 1996. Analysis of mass transport-limited binding kinetics in evanescent wave biosensors. *Anal. Biochem.* 240: 262–272.

Sebald, W., and T. D. Mueller. 2003. The interaction of BMP-7 and ActRII implicates a new mode of receptor assembly. *Trends Biochem. Sci.* 28: 518–521.

Sehgal, P. B. 2003. Plasma membrane rafts and chaperones in cytokine/STAT signaling. *Acta Biochim. Pol.* 50:583–594.

Stroud, R. M., and J. A. Wells. 2004. Mechanistic diversity of cytokine receptor signaling across cell membranes. *Sci. STKE.* 2004:re7.

Takaoka, A., Y. Mitani, H. Suemori, M. Sato, T. Yokochi, S. Noguchi, N. Tanaka, and T. Taniguchi. 2000. Cross talk between interferon-gamma and -alpha/beta signaling components in caveolar membrane domains. *Science.* 288:2357–2360.

Thompson, N. L., and D. Axelrod. 1983. Immunoglobulin surface-binding kinetics studied by total internal reflection with fluorescence correlation spectroscopy. *Biophys. J.* 43:103–114.

Thompson, N. L., A. W. Drake, L. Chen, and W. Vanden Broek. 1997. Equilibrium, kinetics, diffusion and self-association of proteins at membrane surfaces: measurement by total internal reflection fluorescence microscopy. *Photochem. Photobiol.* 65:39–46.

Thompson, N. L., and B. C. Lagerholm. 1997. Total internal reflection fluorescence: applications in cellular biophysics. *Curr. Opin. Biotechnol.* 8:58–64.

Thompson, N. L., K. H. Pearce, and H. V. Hsieh. 1993. Total internal reflection fluorescence microscopy: application to substrate-supported planar membranes. *Eur. Biophys. J.* 22:367–378.

Ullrich, A., and J. Schlessinger. 1990. Signal transduction by receptors with tyrosine kinase activity. *Cell.* 61:203–212.

Vanden Broek, W., and N. L. Thompson. 1996. When bivalent proteins might walk across cell surfaces. *J. Phys. Chem.* 100:11471–11479.

Wang, D., S. Y. Gou, and D. Axelrod. 1992. Reaction rate enhancement by surface diffusion of adsorbates. *Biophys. Chem.* 43:117–137.

Whitty, A., N. Raskin, D. L. Olson, C. W. Borysenko, C. M. Ambrose, C. D. Benjamin, and L. C. Burkly. 1998. Interaction affinity between cytokine receptor components on the cell surface. *Proc. Natl. Acad. Sci. USA.* 95:13165–13170.

Paper III

doi:10.1016/j.jmb.2005.05.008 J. Mol. Biol. (2005) 350, 476–488

JMB

Available online at www.sciencedirect.com

SCIENCE DIRECT®

ELSEVIER

Functional Cartography of the Ectodomain of the Type I Interferon Receptor Subunit ifnar1

Peter Lamken[1], Martynas Gavutis[1], Imke Peters[1], José Van der Heyden[2] Gilles Uzé[2] and Jacob Piehler[1]*

[1]*Institute of Biochemistry Johann Wolfgang Goethe-University, Frankfurt am Main, Germany*

[2]*UMR 5124, CNRS Montpellier, France*

**Corresponding author*

Ligand-induced cross-linking of the type I interferon (IFN) receptor subunits ifnar1 and ifnar2 induces a pleiotrophic cellular response. Several studies have suggested differential signal activation by flexible recruitment of the accessory receptor subunit ifnar1. We have characterized the roles of the four Ig-like sub-domains (SDs) of the extracellular domain of ifnar1 (ifnar1-EC) for ligand recognition and receptor assembling. Various sub-fragments of ifnar1-EC were expressed in insect cells and purified to homogeneity. Solid phase binding assays with the ligands IFNα2 and IFNβ revealed that all three N-terminal SDs were required and sufficient for ligand binding, and that IFNα2 and IFNβ compete for this binding site. Cellular binding assays with different fragments, however, highlighted the key role of the membrane-proximal SD for the formation of an *in situ* IFN–receptor complex. Even substitution with the corresponding SD from homologous cytokine receptors did not restore high-affinity ligand binding. Receptor assembling analysis on supported lipid bilayers *in vitro* revealed that the membrane-proximal SD controls appropriate orientation of the receptor on the membrane, which is required for efficient association of ifnar1 into the ternary complex.

Keywords: cytokine receptor; type I interferon receptor; protein–protein interaction; solid-supported membrane; total internal reflection fluorescence spectroscopy

Introduction

Type I interferons (IFNs) elicit a potent, pleiotrophic antiviral, antiproliferative and immunmodulatory response as an innate first-line defense against viral infection. All human type I IFNs (12 IFNα subtypes and several allelic variants, 1 IFNβ,1 IFNε, 1 IFNκ and 1 IFNω[1]) exert activity through binding to the same receptor components, ifnar1 and ifnar2.[2] It appears, however, that the function of these different IFNs is not fully redundant, but that differential signaling by different IFNs can be observed.[3–9] In particular between the IFNα subtypes and IFNβ, substantial differences have been observed on the level of receptor phosphorylation[3] and effector recruitment,[10] as well as on the level of gene induction.[11] As no further receptor component has yet been identified, these differences need to be explained through the mode of interaction of IFNs with the extracellular domains of ifnar1 (ifnar1-EC) and ifnar2 (ifnar2-EC). The high-affinity interactions between the ifnar2-EC and different IFNs have been investigated in detail,[9,12–14] and a model for the complex between IFNα2 and ifnar2-EC, based on double mutant cycle analysis, has been reported.[15,16] However, the structural differences which have been identified for the interaction of ifnar2-EC with IFNα2 and IFNβ are only minute,[13–15] and therefore cannot explain their functional differences.

The interaction between ifnar1 and IFN has been reported to be of much lower affinity, and its contribution towards complex formation is less well characterized. Cellular binding and activity

Abbreviations used: IFN, human type I interferon; EC, extracellular domains; EGFP, enhanced green fluorescent protein; STAT, signal transducer and activator of transcription; CBM, cytokine binding module; IMAC, immobilized metal affinity chromatography; mAb, monoclonal antibody; RIf, reflectance interference; H10, decahistidine; DT, double-tagged; SD, Ig-like sub-domain; SEC, size-exclusion chromatography; TIRFS, total internal reflection fluorescence spectroscopy.

E-mail address of the corresponding author: j.piehler@em.uni-frankfurt.de

assays are limited by the fact that the properties of cell surface receptor such as affinity and competition are dominated by the (high-affinity) interaction with ifnar2. Sequence alignment has predicted that ifnar1-EC is composed of four Ig-like domains,[17] suggesting two potential cytokine binding modules, but so far only 1:1:1 complex stoichiometries have been detected both *in vivo*[18] and *in vitro*.[19,20] Time-resolved binding assays have detected very transient binding of IFNα2 to ifnar1-EC with a dissociation constant K_D of 5 μM, while for IFNβ a considerably lower K_D value of 50 nM was determined.[20] Furthermore, no contacts between ifnar1-EC and ifnar2-EC stabilizing the ternary complex have been detected.[20] The binding site for IFNs was mapped to the Ig-like domains 2 and 3 by using neutralizing antibodies against ifnar1-EC.[21] These studies also indicated differential recognition of IFNα2 and IFNβ by ifnar1. The important role of domains 2 and 3 for ligand binding was confirmed by direct *in vivo* binding assays with bovine ifnar1, which binds human IFNαs with high affinity.[22] Several residues on these two domains critical for binding IFNα2 have been identified.[23,24] These results indicated that the ligand-binding site of ifnar1 does not correspond to a classical cytokine binding module and a more complex architecture of the functional complex. Cellular binding assays, however, could neither clearly define which of the Ig-like domains of ifnar1-EC form the binding site for different IFNs, nor resolve the role of different ligand–receptor stoichiometries. Therefore, more detailed characterization of the interaction of ifnar1 with different IFNs is crucial for a better understanding of differential receptor recruitment.

We have used subfragments of ifnar1-EC containing different Ig-like domains for confining the binding site for type I IFNs. The proteins were expressed, purified and characterized in detail. Binding of IFNα2 and IFNβ was studied *in vitro* by solid phase detection; namely, reflectance interference (RIf) and total internal reflection fluorescence spectroscopy (TIRFS) in different assay formats. Furthermore, ternary complex assembly was investigated for different ifnar1 constructs in living cells, and by ligand dissociation measurements *in vitro* on supported lipid bilayers.

Results

Expression and purification of ifnar1-EC and its subfragments

For identification of the Ig domains required for ligand binding, ifnar1-EC with a C-terminal decahistidine-tag (SD1234-H10) and with N and C-terminal decahistidine-tag (SD1234-DT), as well as the subfragments H10-SD123, SD234-H10, H10-SD12 and SD34-H10 (Figure 1(a)) were expressed in *Sf*9 insect cells. All proteins were secreted into the medium and efficiently purified by immobilized metal affinity chromatography (IMAC). In the subsequent size exclusion chromatography (SEC) all proteins eluted within a single protein peak, while only minor quantities of higher molecular mass aggregates were observed. An SDS-PAGE and the SEC chromatograms of the purified proteins (both carried out under non-reducing conditions) are shown in Figure 1. In all cases, homogeneity was >95% as judged by SDS-PAGE (Figure 1(b)) and analytical SEC (Figure 1(c)). For all species the yield of purified protein was 0.5–2 mg from 200 ml of cell culture. The proteins, stored at physiological pH and ionic strength, were stable (monomeric) for several weeks at 4 °C. Upon shock-freezing in liquid nitrogen and thawing, more than 90% of the monomeric protein was retained for all species as determined by analytical SEC.

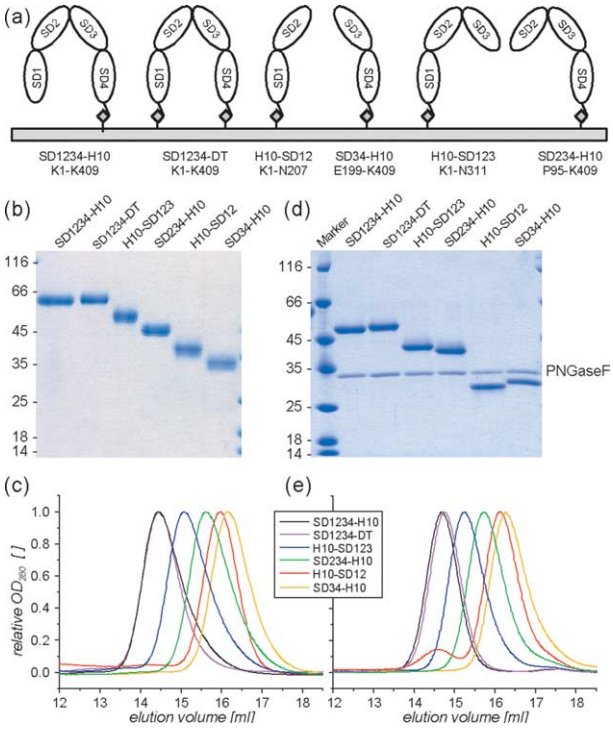

Figure 1. Purification of ifnar1-EC and the subfragments. (a) Schematic of the ifnar1-EC fragments used for localizing the IFN binding site, and their attachment to surfaces *via* N and C-terminal H10-tags. (b) SDS-PAGE of the purified subfragments after purification by immobilized metal affinity chromatography and size-exclusion chromatography. (c) Analytical SEC of the purified subfragments on a Superdex 200 HR10/30 column. (d) SDS-PAGE of the purified subfragments after deglycosylation with PNGaseF. (e) Analytical SEC of the purified subfragments after deglycosylation with PNGaseF under native conditions.

All ifnar1-EC fragments were glycosylated and properly folded

Yields, stability and monomeric nature of the subfragments under non-reducing conditions

Table 1. Properties of the ifnar1-EC fragments used for defining the IFN binding site

Name	SD1234-H10	SD1234-DT	H10-SD12	SD34-H10	H10-SD123	SD234-H10
Sequence[a]	K1-K409	K1-K409	K1-N207	E199-K409	K1-N311	P95-K409
H10-tag[b]	C	C, N	N	C	N	C
Total no. of aa	424	436	224	226	326	325
Glycos. sites[c]	9	9	5	4	7	5
MM (expected) (kDa)	49.0	50.6	25.8	26.2	37.9	37.4
MM (found)[d] (kDa)	57.3	–	31.1	29.4	45.3	42.2
MM (deglyc.)[e] (kDa)	49	50	29	30	40	39
β-Sheet/α-helix/RC[f]	84/2/14	78/2/20	70/4/26	77/01/22	76/3/21	75/2/23

[a] First and last amino acid (aa) according to the predicted mature sequence of ifnar1.
[b] Terminus, to which the decahistidine-tag was fused.
[c] Potential glycosylation sites as predicted by the NetNGlyc 1.0 server.
[d] Mean mass determined by MALDI-MS.
[e] Estimated from SDS-PAGE.
[f] As determined by circular dichroism spectroscopy.

indicated appropriate folding, which was further corroborated by a more detailed protein-biochemical analysis. Since the proteins were expressed and secreted in eukaryotic cells, glycosylation of some of the overall nine potential glycosylation sites of ifnar1-EC was expected (Table 1). Accordingly, the apparent molecular mass observed in SDS-PAGE was substantially higher than the expected mass for all proteins (Table 1): for SD1234-H10 and SD1234-DT a single, yet broadened band corresponding to a molecular mass of approximately 57 kDa was observed in SDS-PAGE (Figure 1(b)) compared to 49 kDa expected for the polypeptide chain. For the subfragments, similar shifts as well as band broadening and even multiple bands were observed (Figure 1(b)). To confirm glycosylation the proteins were deglycosylated in analytical amounts using PNGaseF. The SDS-PAGE analysis of deglycosylated SD1234-H10, SD1234-DT and their subfragments is shown in Figure 1(d). For all proteins the apparent molecular mass shifted to the expected mass (Figure 1(d) and Table 1). A similar, yet less pronounced effect was observed in analytical SEC (Figure 1(e)). The rather broad, asymmetric peaks observed for the glycosylated proteins (Figure 1(c)) became more sharp and symmetric, and slightly shifted towards higher elution volumes after deglycosylation (Figure 1(e)). No significant differences were observed in the elution volumes of SD1234-H10 and SD1234-DT. In contrast H10-SD123 eluted with substantially higher apparent molecular mass than SD234-H10, despite the very similar molecular mass observed in SDS-PAGE (Figure 1(d)). This difference suggests a different spatial arrangement or a different flexibility of the three Ig-like domains in these two proteins. Also between H10-SD12 and SD34-H10, a small, but reproducible and significant shift was observed, indicating different organization of the Ig-like domains within these two potential CBMs. Under non-reducing conditions the band of the different ifnar1-EC species was shifted to a lower molecular mass compared to the reduced proteins (data not shown) indicating internal disulfide bridge formation. The anticipated secondary structure of mainly β-sheet (70–84%) was furthermore confirmed for all subfragments by circular dichroism spectroscopy (Table 1) corroborating appropriate folding of the protein.

The three N-terminal domains of ifnar1-EC are required for IFN binding

For all the following binding experiments the glycosylated proteins were used because they were more stable than the deglycosylated ones. We probed the interaction of IFNα2 and IFNβ with the immobilized subfragments by solid phase detection. The proteins were immobilized on a polymer brush *via* their H10-tags using high-affinity multivalent chelator head groups providing oriented and homogeneous attachment.[25] Both ifnar1-EC and ifnar2-EC fully retained their ligand binding activity on these surfaces and non-specific binding of IFNα2 and IFNβ to these surfaces was shown to be negligible upon blocking excess binding sites with histidine-tagged maltose-binding protein.[20,25] For ifnar1-EC (SD1234-H10) K_D values of 5 μM and 50 nM were found for the interaction with IFNα2 and IFNβ, respectively, while a 1:1 stoichiometry was indicated by the relative amplitudes.[20] Virtually the same equilibrium dissociation constants were obtained for IFNα2 and IFNβ in complex with tag-less ifnar2-EC, implying that the interactions of IFNs with ifnar1-EC and ifnar2-EC are non-cooperative.[20] In order to exclude that the additional N-terminal decahistidine-tag of SD1234-DT affected the interaction with IFNs, ligand binding assays with SD1234-DT tethered onto surfaces through both histidine-tags (Figure 1(a)) were carried out. The reduced surface binding capacity observed for SD1234-DT compared to SD1234-H10, as well as imidazole-induced dissociation experiments (data not shown) confirmed that indeed both histidine-tags were involved in tethering the protein to the surface. Binding of IFNα2 and IFNβ to immobilized SD1234-DT is shown in Figure 2. The K_D value of the interaction with IFNα2 was determined from the equilibrium response, while the rate constants of the interaction

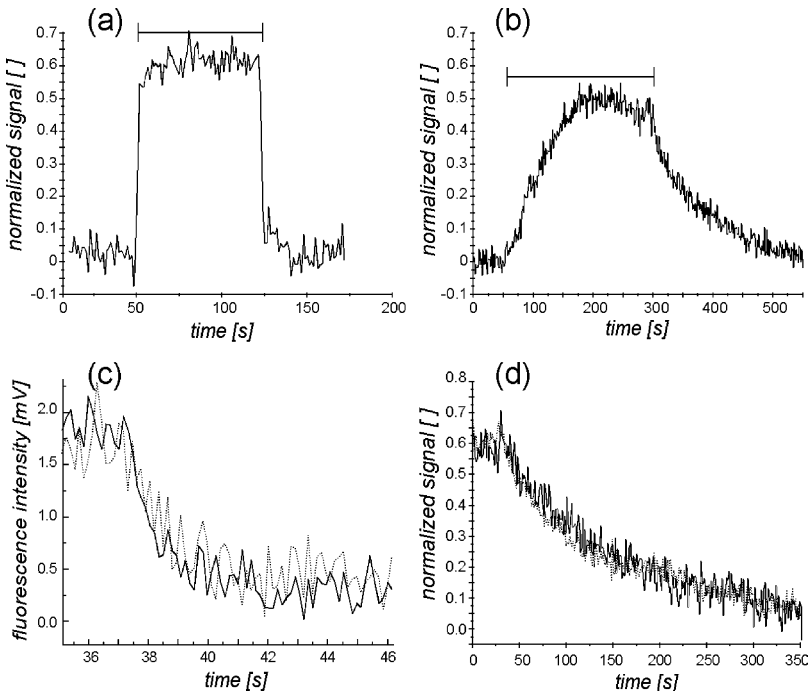

Figure 2. (a) and (b) Binding of (a) 1 μM IFNα2 and (b) 100 nM IFNβ to SD1234-DT immobilized on a polymer brush surface as detected by RIfS (the bar marks the injection period). SD1234-DT was site-specifically tethered to the surface through interaction of its histidine-tags with covalently attached multivalent chelator head groups. (c) Dissociation of ^{AF488}IFNα2 (200 nM) from SD1234-DT (—) as detected by TIRFS in comparison to the same experiment carried out with SD1234-H10 (···). (d) Dissociation of IFNβ (100 nM) from SD1234-DT (—) in comparison to the same experiment carried out with SD1234-H10 (···).

with IFNβ were determined by fitting exponential functions to association and dissociation phase of the binding curves. Furthermore, the k_d value of the dissociation of IFNα2 from immobilized SD1234-DT was determined by total internal reflection fluorescence spectroscopy. IFNα2-S136C site-specifically labeled with the fluorescence dye Alexa Fluor 488 (^{AF488}IFNα2) was used, which was shown to interact with ifnar2-EC and ifnar1-EC as wild-type IFNα2.[26] All equilibrium dissociation constants and rate constants obtained for IFNα2 and IFNβ (Table 2) were in agreement with the values observed for SD1234-H10.

In the same manner, binding of IFNα2 and IFNβ was assessed for the subfragments. Up to concentrations of 10 μM IFNα2 and 200 nM IFNβ, no specific binding was detectable for H10-SD12 and SD34-H10, as well as SD234-H10 (Figure 3(a)–(c)). Thus, the K_D values of these subfragments were >100 μM for IFNα2 and >2 μM for IFNβ. In contrast, uncompromised binding of both IFNs was observed for H10-SD123 (Figure 3(a)–(c)). The interaction constants determined from these curves were very similar to the values observed for SD1234-H10 (Table 2). Furthermore, H10-SD12 and SD34-H10 were co-immobilized in stoichiometric amounts onto solid-supported, fluid lipid bilayers in order to allow simultaneous interaction with the ligand (Figure 3(d)). Still, neither for IFNα2 (Figure 3(e)) nor for IFNβ (Figure 3(f)) was significant binding detectable, indicating that the linkage between H10-SD12 and SD34-H10 is required for the formation of an intact binding site. In order to confirm that loss of binding activity was not due to denaturation of the protein during immobilization on the surface we devised another assay to assess binding. Ifnar2-EC was immobilized on the surface and followed by

Table 2. Affinities and rate constants of the interaction with IFNα2 and IFNβ determined for different ifnar1-EC constructs

Ifnar1	IFNα2			IFNβ			IFNα2 (L30A)/ ifnar2-EC[a]
Fragment	k_a (M^{-1} s^{-1})[b]	k_d (s^{-1})	K_D (μM)[c]	k_a ($M^{-1}s^{-1}$)	k_d (s^{-1})	K_D (nM)[d]	k_d (s^{-1})
SD1234-H10	~2×10^5	1.0±0.3	~5	(3±2)×10^5	0.015±0.005	50±20	~0.0001 (0.015±0.003)
SD1234-DT	~2×10^5	1.0±0.3	~6	(3±2)×10^5	0.015±0.005	50±20	~0.0001 (0.017±0.004)
H10-SD123	~2×10^5	1.3±0.4	~8	(3±2)×10^5	0.020±0.006	70±20	~0.0002 (0.025±0.003)

[a] Ifnar1-EC constructs co-immobilized with ifnar2-EC on fluid lipid bilayers at high surface concentrations (20–40 fmol/mm^2).
[b] Calculated from k_d and K_D.
[c] Determined from equilibrium response.
[d] Calculated from k_a and k_d.

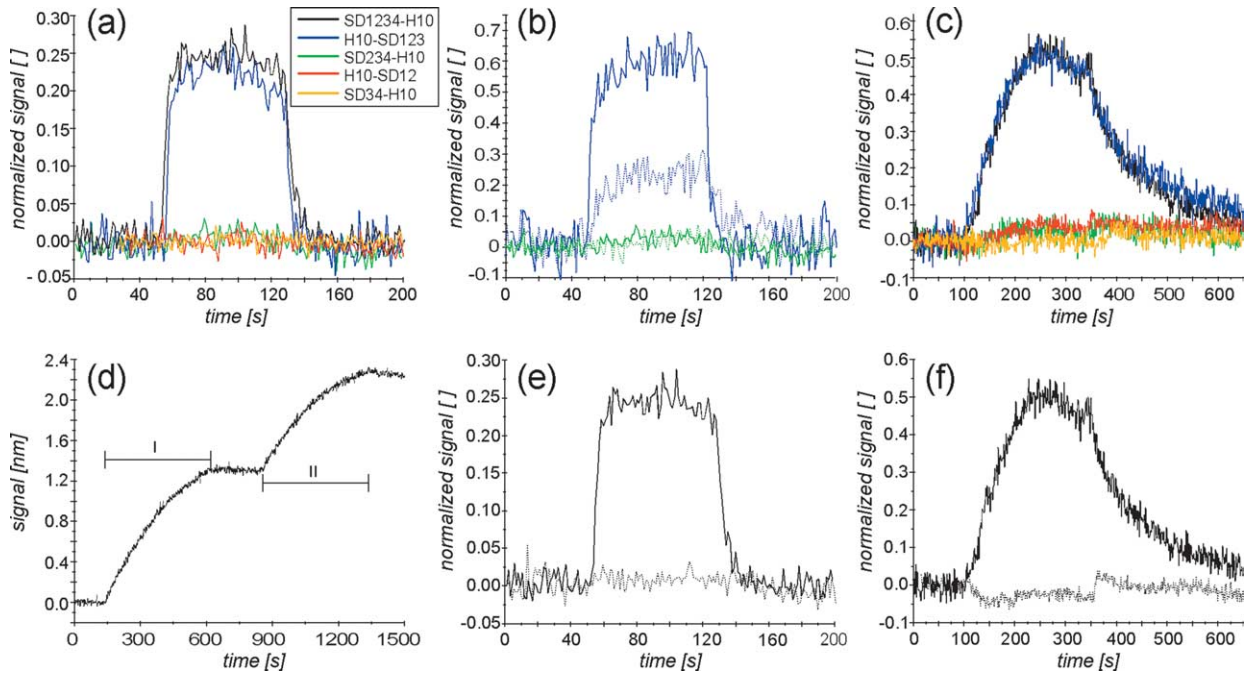

Figure 3. Binding of IFNα2 and IFNβ to the different subfragments immobilized on the transducer surface. (a) Response during injection of 1 μM IFNα2 to SD1234-H10, H10-SD123, H10-SD234, H10-SD12, SD34-H10 in comparison (color coding as shown in the inset). Signals were normalized to the molar surface concentration of the immobilized protein. (b) Response during injection of 1 μM (···) and 10 μM (—) IFNα2 onto H10-SD123 and SD234-H10 in comparison. (c) Response during injection of 50 nM IFNβ onto SD1234-H10, H10-SD123, SD234-H10, H10-SD12, SD34-H10 in comparison (same color coding as in (a)). (d) Co-immobilization of H10-SD12 (I) and SD34-H10 (II) on solid-supported lipid bilayers. (e) Response during injection of 1 μM IFNα2 onto H10-SD12 and SD34-H10 co-immobilized (···) on solid-supported lipid bilayers in comparison to SD1234-H10 (—). (f) The same experiment as shown in (e) carried out with 50 nM IFNβ.

binding of IFNβ, which binds nearly irreversibly to ifnar2-EC (Figure 4(b)). Subsequently, binding of SD1234-H10 and the subfragments to ifnar2-EC-bound IFNβ was studied (Figure 4(b)). In Figure 4(c) binding of the subfragments is compared with binding of SD1234-H10. Again, specific binding was only detectable for the subfragment H10-SD123. All these experiments confirmed that the N-terminal Ig-like domains 1, 2 and 3 on a single polypeptide chain were required for the formation of an intact binding site for IFNα2 and IFNβ.

IFNα2 and IFNβ bind competitively to ifnar1-EC

Since the analysis of different subfragments did not indicate different binding domains in ifnar1-EC

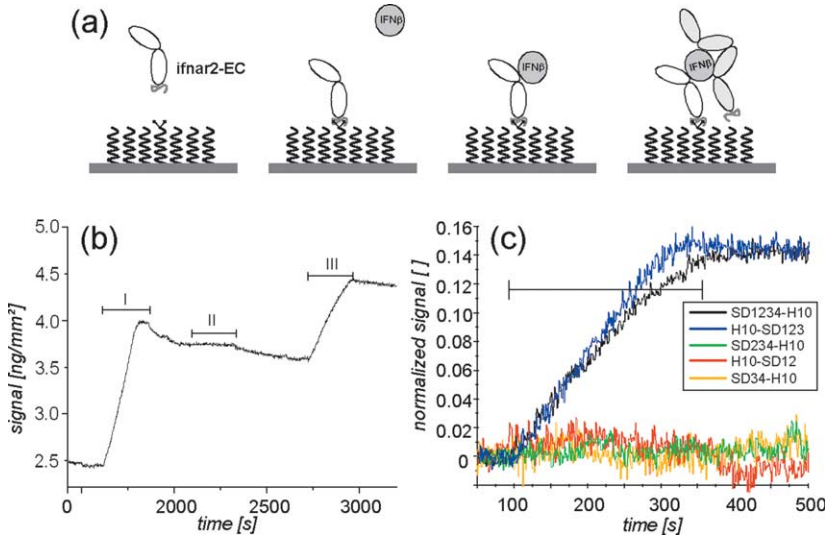

Figure 4. Binding of ifnar1-EC species to the complex of immobilized ifnar2-EC and IFNβ. (a) Schematic of the sandwich assay: after immobilization of ifnar2-EC excess chelators are blocked with MBP-H10 (not shown); then, IFNβ binds irreversibly to ifnar2-EC, followed by binding of the respective ifnar1-EC variant. (b) Typical binding of IFNβ (I) to immobilized ifnar2-EC, followed by an injection of 50 nM H10-SD12 (II) and of 50 nM SD1234-H10 (III). (c) Binding curves for SD1234-H10 and the subfragments in comparison (50 nM each; the color coding is shown in the inset).

for both IFNα2 and IFNβ, we investigated whether these two IFNs actually bind competitively to an overlapping epitope. Binding of ^{AF488}IFNα2 was monitored in real-time by simultaneous TIRFS-RIf detection, which combines label-free detection with fluorescence detection.[26] Both the fluorescence and the mass-sensitive signal monitored in real-time during a typical experiment are shown in Figure 5(a): after immobilization of ifnar1-EC, first 1 μM ^{AF488}IFNα2 was injected, followed by an injection of 1 μM ^{AF488}IFNα2 mixed with 100 nM unlabeled IFNβ. Subsequently, only 100 nM IFNβ was injected for comparison. The fluorescence signals during the first two injections are compared in Figure 5(b). Fast, transient binding of IFNα2 was detectable in the fluorescence channel with a similar characteristic as observed for unlabeled IFNα2, as shown in Figure 3(a). The sensitivity of Rif detection is too low to detect binding at this IFNα2 concentration, because of the rather low surface concentration of SD1234-H10 used for these measurements. When IFNα2 was injected together with IFNβ a decay of the fluorescence signal after the initial fast rise was observed (Figure 5(a) and (b)). This transient binding of IFNα2 during injection may be ascribed to labeled IFNα2 being exchanged for unlabeled IFNβ, which binds more stably to ifnar1-EC. IFNα2 binds much faster than IFNβ because of its higher concentration in the mixture and the similar association rate constants of IFNα2 and IFNβ.[26] Binding of IFNβ with its typical association and dissociation characteristics was simultaneously detectable on the RIf-channel (Figure 5(a)). For the injection of IFNβ without IFNα2 a very similar binding curve was detected for IFNβ on the Rif channel while no signal was detectable on the fluorescence channel. More detailed analysis of the binding curves at different concentrations confirmed that the rate constants of the interaction did not change, corroborating competitive binding of IFNα2 and IFNβ to ifnar1-EC. The same experiment was carried out with H10-SD123 immobilized on the surface. A comparison of the curves for 1 μM IFNα2 in the presence and absence of 100 nM IFNβ is shown in Figure 5(c). Very similar shapes of the curves as for ifnar1-EC were obtained, confirming that IFNα2 and IFNβ bind to an overlapping epitope formed by the three N-terminal Ig-like domains of ifnar1-EC.

Ternary complex formation on supported lipid bilayers

The direct interaction assays revealed that the binding affinity towards IFNα2 and IFNβ decreased by a factor of more than 20 in cases H10-SD12, SD34-H10 and SD234-H10, while nearly full binding affinity was maintained for H10-SD123. Owing to the already low affinity of IFNs towards ifnar1-EC, the residual binding affinity could not be established by these assays. Furthermore, the effects of subdomain deletion on ternary complex formation remained unclear. We therefore investigated ligand binding to ifnar2-EC co-immobilized with ifnar1-EC or its subfragments onto a solid-supported, fluid lipid bilayer (Figure 6(a)). It was shown that with stoichiometric amounts of ifnar2-EC and SD1234-H10 at high surface concentrations (~25–50 fmol/mm^2) IFNα2 binds at least 100 times stronger than to ifnar2-EC alone.[20] The course of a

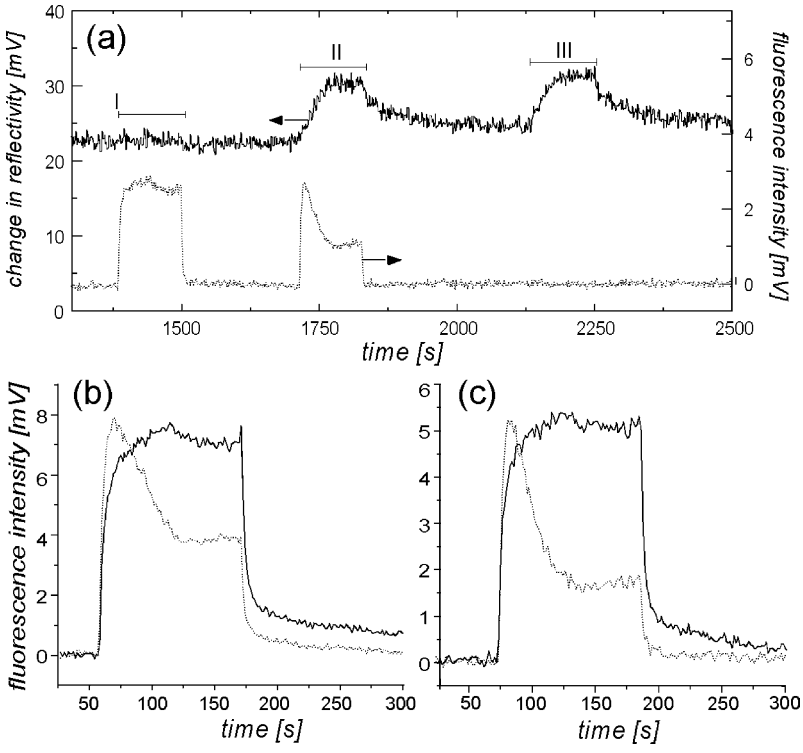

Figure 5. Competition of IFNα2 and IFNβ for the ifnar1-EC binding site. (a) Interference signal (—) and fluorescence signal (···) during injection of ^{AF488}IFNα2 (1 μM) alone (I), mixed with 100 nM IFNβ (II) and injection of IFNβ alone (III) on immobilized SD1234-H10. (b) Overlay of the fluorescence signals of injections I (—) and II (···). (c) Overlay of the fluorescence signals of injections I (—) and II (···) for the same experiment carried out with immobilized H10-SD123.

typical binding experiment with SD1234-H10 is shown in Figure 6(b). After tethering ifnar2-EC and ifnar1-H10 in stoichiometric amounts, diffusion-controlled association of IFNα2 was observed and no significant dissociation from the ternary complex (Figure 6(c)). The dissociation curves of IFNα2 from ifnar2-EC co-immobilized with different ifnar1-EC variants is compared in Figure 6(d). In the case of SD1234-DT, the ligand dissociation kinetics were indistinguishable from the kinetics observed for SD1234-H10 (Figure 6(d)), suggesting that the formation of the ternary complex was not affected by the additional tethering through the N-terminal His-tag. For the subdomains H10-SD12, SD34-H10 (data not shown) and SD234-H10 (Figure 6(d)) no significant difference in the dissociation kinetics was observed compared to the dissociation from ifnar2-EC alone. Also upon co-immobilization of H10-SD12 and SD34-H10 with ifnar2-EC, no change in the dissociation kinetics was observed (Figure 6(d)). This binding assay is even more sensitive to low affinities, since the ligand is captured by the high-affinity interaction with ifnar2-EC, and a subtle lateral interaction on the surface would be reflected by a decrease in the dissociation rate constant. From these assays, a loss of affinity by more than two orders of magnitude can be concluded for the subfragments H10-SD12, SD34-H10 and SD234-H10. In contrast, a strong decrease in the apparent k_d value was observed for SD123 co-immobilized with ifnar2-EC (Figure 6(d)), almost as strong as for ifnar1-EC. A k_d value of $0.0002\ s^{-1}$ was estimated by an exponential fit, i.e. two orders of magnitude slower than the dissociation from ifnar2-EC alone. The stability of the ternary complex formed upon co-immobilization with ifnar2-EC was compared in more detail for the variants SD1234-H10, SD1234-DT and H10-SD123 applying the IFNα2 mutant L30A, which binds ~500 times weaker to ifnar2-EC ($k_d \sim 5\ s^{-1}$). The

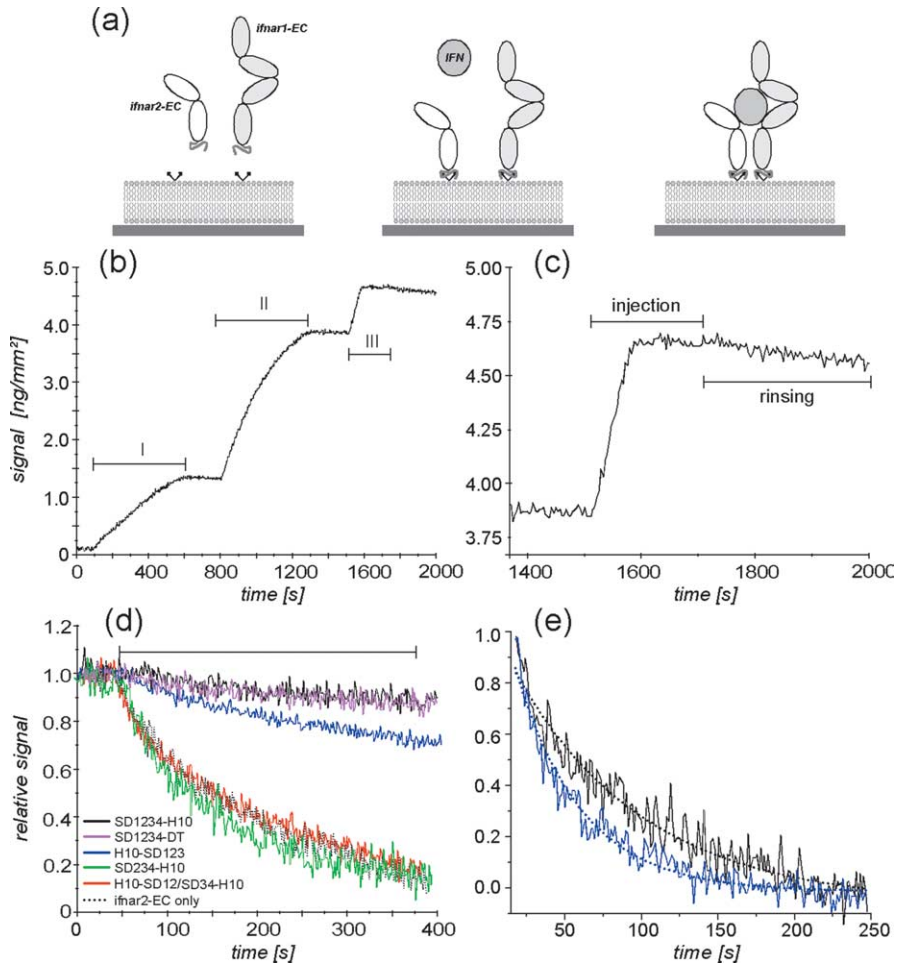

Figure 6. IFNα2 binding to ifnar2 co-immobilized with different ifnar1 subfragments onto solid-supported lipid bilayers. (a) Schematic of the assay: ifnar2-EC and ifnar1-EC were sequentially tethered onto the supported lipid bilayer in a stoichiometric ratio, followed by injection of the ligand. (b) Binding of IFNα2 at high, stoichiometric receptor surface concentrations of ifnar2-EC and SD1234-H10 as detected by RIfS. (c) IFNα2 binding and dissociation as shown in (b). (d) Dissociation kinetics for SD1234-H10 (black), SD1234-DT (magenta), H10-SD123 (blue), SD234-H10 (green) and H10-SD12/SD34-H10 (red) co-immobilized with ifnar2-EC (⋯) in comparison to the dissociation from ifnar2-EC alone. (e) Dissociation of IFNα2-L30A from SD1234-H10 (black) and H10-SD123 (blue) co-immobilized with ifnar2-EC. The dotted lines are the mono-exponential fits of these curves.

curve observed for SD1234-DT (data not shown) was indistinguishable from the curve obtained for SD1234-H10 (Figure 6(e)) with a k_d value of 0.015 s^{-1}. In the case of H10-SD123, slightly faster dissociation was observed ($k_d = 0.025\ s^{-1}$). Thus, only small differences in ternary complex stability were observed for H10-SD123 compared to SD1234-H10 at these high receptor surface concentrations, confirming that ternary complex formation was possible without SD4.

No high-affinity binding of IFNα2 to ifnar1 variants without SD4 *in vivo*

In cells ifnar1 has been shown to increase the apparent binding affinity by tenfold to 20-fold compared to ifnar2 alone,[18,27] which is ascribed to the formation of the ternary signaling complex. In order to study the effect of sub-domain deletion on ternary complex formation *in vivo*, ligand binding was analyzed in HEK293T cells overexpressing ifnar2 with different constructs of ifnar1-EC fused to the ifnar1 transmembrane and cytoplasmic domains (TMCD). The binding of IFNα2 and ifnar1 surface expression was quantified by fluorescence-assisted cell sorting (FACS) (Figure 7). Ifnar1 and the fragments were overexpressed by one to two orders of magnitude higher than endogenous ifnar1 without significantly affecting the expression level of overexpressed ifnar2 (Figure 7(a)). The amount of ligand bound to the cell surface receptor was quantified by FACS using ^{AF488}IFNα2. The amount of receptors presented at the cell surface was determined by FACS using monoclonal antibodies. A linear increase in ligand binding was observed with increasing cell surface concentration of wild-type ifnar1. As expected, for SD234-TMCD no increase in ligand binding was detectable, but also for SD123-TMCD no high-affinity ligand binding was observed (Figure 7(b)). In order to exclude that steric hindrance due to direct linkage of SD3 to the plasma membrane was responsible for this effect, two constructs were made, where SD4 of ifnar1 was substituted by the corresponding domains from two other class II cytokine receptors: the IL10 receptor 2 chain (SD123IL10R2D2-TMDC) and the interferon λ receptor (SD123LRD2-TMDC). However, high-affinity ligand binding could not be recovered with these receptor proteins (Figure 7(b)) suggesting that SD4 has an important function for the assembling of the ternary complex *in vivo*.

Orientation of ifnar1 affects ternary complex assembling

In order to better understand this role of SD4, we studied ternary complex assembly with several ifnar1-EC fragments and variants in more detail *in vitro*. SD123LRD2 with a C-terminal H10-tag (SD123LRD2-H10), as well as SD1234 with an N-terminal H10-tag (H10-SD1234) and SD123 with a C-terminal H10-tag (SD123-H10) (Figure 8(a)) were expressed in *Sf*9 insect cells and purified to homogeneity. As expected from the previous analysis, direct binding of IFNα2 and IFNβ was unaltered compared to SD1234-H10 for these proteins (data not shown). Ternary complex assembling was studied by TIRFS-RIf detection with ^{AF488}IFNα2 at receptor surface concentrations of ~3 fmol/mm^2 of the ifnar1-EC construct. This surface concentration is representative for the cell surface receptor density,[20] and more than one order of magnitude lower than the receptor surface concentrations used in the ternary complex formation assays described above. A comparison of ligand dissociation curves for different fragments is shown in Figure 8(b). For SD1234-H10, significantly faster ligand dissociation was observed compared to the curve shown in Figure 6(b), as expected for less efficient kinetic stabilization at these lower receptor surface concentrations.[20,26] Under the same conditions, substantially faster dissociation was observed for SD123LRD2-H10 than for SD1234-H10, in agreement with the low affinity observed for this variant on the cell surface. The dissociation kinetics, however, was still four to five times slower than from ifnar2-EC alone, indicating that the ternary complex still assembled, yet with a much lower efficiency. In order to test the role of orientation on surface affinity, we investigated ligand dissociation from ternary complexes formed

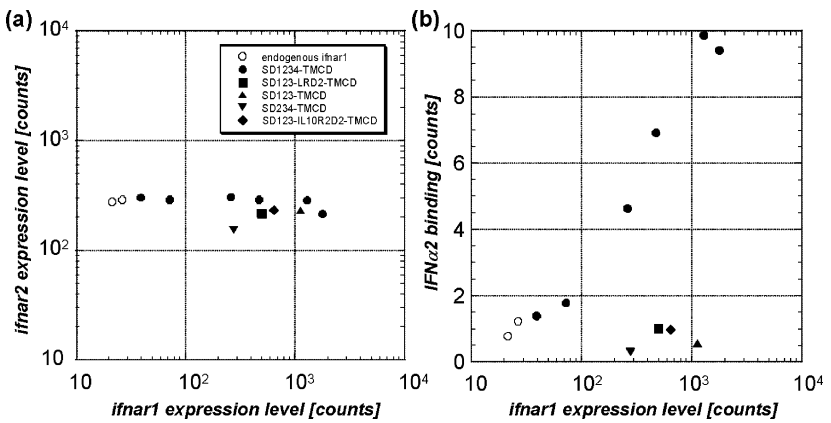

Figure 7. Cell surface binding of IFNα2 on HEK293T cells overexpressing ifnar2 and different amounts of ifnar1. HEK293T cells were co-transfected with plasmids encoding EGFP, ifnar2 and ifnar1. The EGFP positive population was analyzed in FACS for (a) the cell surface expression level of ifnar1 and ifnar2 and (b) for specific binding of ^{AF488}IFNα2. The binding of ^{AF488}IFNα2 is expressed relative to the binding level measured on cells transfected with EGFP and ifnar2 alone (open circles).

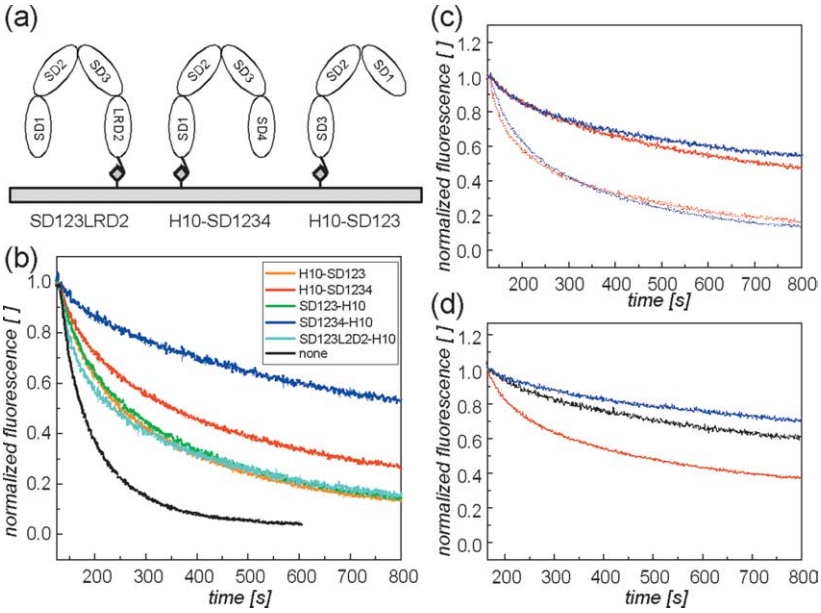

Figure 8. (a) Schematic of the constructs SD123LRD2-H10, H10-SD1234 and H10-SD123 and their attachment to the lipid bilayer. (b) Dissociation of IFNα2 from ifnar2-EC co-immobilized with different constructs of ifnar1-EC on lipid bilayers (receptor surface concentration ~3 fmol/mm^2). (c) Dissociation of IFNα2 from ifnar2-EC co-immobilized with H10-SD123 (red) and SD123LRD2-H10 (blue) at different surface concentrations (continuous line: ~7 fmol/mm^2; dotted line: ~3 fmol/mm^2). (d) Dissociation of IFNα2 from ifnar2-EC co-immobilized with SD1234-H10 (blue), H10-SD1234 (red), and SD1234-DT (black) on supported lipid bilayers (receptor surface concentration ~4 fmol/mm^2).

with H10-SD1234, SD123-H10 and H10-SD123 under the same conditions (i.e. receptor surface concentrations). Strikingly, also for H10-SD1234, substantially faster ligand dissociation from the ternary complex was observed than for SD1234-H10. For both H10-SD123 and SD123-H10 ligand dissociation from the ternary complex was similarly fast as observed for SD123LRD2-H10. However, by increasing the receptor surface concentration, the decrease in ligand binding affinity could be compensated (Figure 8(c)). Interestingly, tethering ifnar1-EC through both the N and C terminus onto the membrane (SD1234-DT) had only a minor effect on ligand dissociation (Figure 8(d)). Taken together, these results indicate that SD4 and its anchoring to the lipid bilayer plays a key role for the efficiency of ifnar1 recruitment into the ternary complex without being responsible for ligand recognition.

Discussion

Characterization of the binding site of human ifnar1 *in vivo* has been hampered by the extremely low affinity towards its ligands: the high-affinity interaction with ifnar2 dominates binding to the cellular receptor, while binding to ifnar1 alone is too transient to be detectable. Thus, structure–function studies of IFN recognition by ifnar1-EC *in vivo* were performed either in the presence of ifnar2-EC,[21,24] or with bovine ifnar1, which binds human IFNαs with much higher affinity.[22,23] We analyzed for the first time ligand binding to different subfragments of human ifnar1-EC *in vitro* in order to dissect contributions towards ligand recognition and ternary complex assembly. The architecture of ifnar1-EC with its four Ig-like domains suggests potentially two cytokine binding modules. By direct ligand binding assays we could clearly show that these potenial CBMs, SD12 and SD34, separately do not interact with IFNα2 or with IFNβ. Even when co-immobilized on a fluid support, which allowed lateral rearrangements, the binding site was not restored. Hence, the covalent linkage between SD2 and SD3 is absolutely critical for ligand binding. Out of the two subfragments containing three Ig-like domains (i.e. with an intact linkage between SD2 and SD3) SD123 retained nearly full ligand-binding activity while no ligand binding was detectable for SD234. Interestingly, SD123 and SD234 also appeared to be different in their apparent molecular size in SEC, indicating an asymmetric architecture of the four Ig-like domains of ifnar1 and not simply two, linked symmetric CBMs. No differences in terms of subdomains required for ligand recognition were found for IFNα2 and IFNβ, which have been suggested to bind to different epitopes on ifnar1.[21] By direct competition experiments we could show that the binding sites of IFNα2 and IFNβ are at least overlapping, if not congruent.

SD4 does not seem to play a substantial role for ligand recognition, and is also not required for ternary complex formation with ifnar2-EC. In cells, however, no high-affinity ligand-binding site was observed in the absence of SD4 or when it was exchanged by a corresponding domain of homologous cytokine receptors. More detailed analysis of these constructs *in vitro* indicated that ternary complex formation is still possible, but recruitment efficiency is substantially impaired if SD4 is absent or exchanged. Strikingly, the orientation of ifnar1-EC was shown to play a key role for stable complex formation on supported lipid bilayers, as tethering of ifnar1-EC only at the N-terminal domain significantly decreased the stability of the ternary complex. We have recently shown that

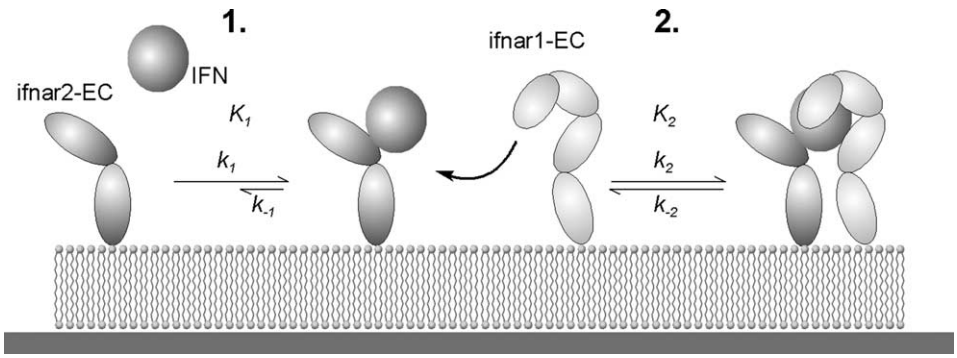

Figure 9. Kinetically controlled two-step receptor assembling mechanism, and the role of the appropriate orientation of ifnar1-EC. Recruitment of ifnar1 into the ternary complex depends on the (surface) affinity constant K_2 and the receptor surface concentration. Reduced complex stability without SD4 anchored to the membrane suggests that K_2 depends on the orientation of the receptor.

IFN-induced receptor assembling occurs in two steps as depicted in Figure 9, and that the equilibrium dissociation constant of the ifnar1/IFNα2 interaction at the surface (K_2) governs kinetic stabilization of the ifnar2/IFNα2 complex.[20,26] The decrease of ligand binding stability observed for N-terminally attached or impaired ifnar1 constructs reflects a decrease in K_2. We ascribe this drop in surface binding affinity to a decrease in the surface association rate constant k_2; recently, we have shown that this association rate on the membrane is enhanced by tenfold to 100-fold in terms of successful collisions compared to the interaction in solution,[26] which can be ascribed to pre-orientation of the interaction sites. Non-optimal orientation of the ligand binding site of ifnar1 on the membrane probably reduces the rate of productive collisions, and thus reduces the surface association rate constant and the surface affinity constant. While this effect was clearly detectable by mimicking membrane anchoring of the receptors *in vitro*, it could contribute even stronger in the case of the probably much more rigidly oriented transmembrane proteins on the cell surface. This could explain the complete loss of a high-affinity binding observed for the chimeric ifnar1 constructs in living cells. Strikingly, these effects only play a role if K_2 limits ternary complex formation (i.e. at low receptor surface concentrations). This is very likely to be the case for the IFNα2–ifnar complex[20] and has been shown to be the case for the IL4 receptor *in vivo*.[28] We suggest that SD4 plays a key role for properly orientating the binding site of ifnar1 at SD123 on the membrane for highly efficient collision with the ifnar2–IFNα2 complex. Appropriate orientation apparently is finely adjusted for different members of the class II cytokine receptor family, as exchange of homologous domains abolished high-affinity ligand binding. For some cytokine receptors orientation of the extracellular domains have been shown to be critical for signal activation.[29,30] We have provided evidence that an appropriate orientation of the interaction sites on the membrane is crucial for efficient receptor assembling. This insight is particularly important for the *de novo* design of cytokine-like molecules for therapeutic application.

Materials and Methods

Protein expression and purification

IFNα2 and ifnar2-EC were expressed in *Escherichia coli*, refolded from inclusion bodies and purified by anion-exchange and size-exclusion chromatography as described.[31] The IFNα2 mutant S136C was site-specifically labeled with Alexa Fluor 488 (AF488) maleimide (Molecular Probes), and was further purified by desalting and a final step of anion-exchange chromatography. Ifnar1-EC and its subfragments and variants (Figure 10(a)) were expressed in insect cells using the baculovirus system. The gene of mature ifnar1-EC (GenBank accession number NM_000629; amino acids from KNL until TSK) with an additional stretch of nucleotides coding for a C-terminal decahistidine-tag (SD1234-H10) was cloned into the transfer vector pAcGP67B (BD Biosciences) *via* the BamHI and PstI restriction sites. An additional N-terminal extension ADLGS is expected from the cleavage site of the gp67 secretion sequence in the vector. SD1234-DT was obtained by inserting a linker coding for an H10-tag at the N terminus of SD1234-H10 into the BamHI site, resulting in a total N-terminal extension of ADLGSH_{10}RS. This linker was designed so that only the N-terminal BamHI site was retained. The subfragments were subcloned based on this SD1234-DT construct. Baculoviruses were obtained by co-transfection with linearized baculoviral DNA (BaculoGold, BD Biosciences) into *Sf*9 cells. For protein expression, fresh *Sf*9 cell cultures (200 ml) were infected with the respective baculovirus. The supernatant was harvested three to four days after infection, adjusted to TBS (20 mM Tris (pH 8.0), 200 mM sodium chloride) and thoroughly dialyzed against the same buffer. After centrifugation, the supernatant was applied to a 5 ml chelating Sepharose column (HiTrap chelating; Amersham Biosciences) loaded with Zn^{2+}. After washing with TBS, the proteins were eluted with a gradient from 0 mM to 500 mM imidazole in TBS. Pooled fractions were further purified by size-exclusion chromatography in TBS (Superdex 200-16/60; Amersham Biosciences).

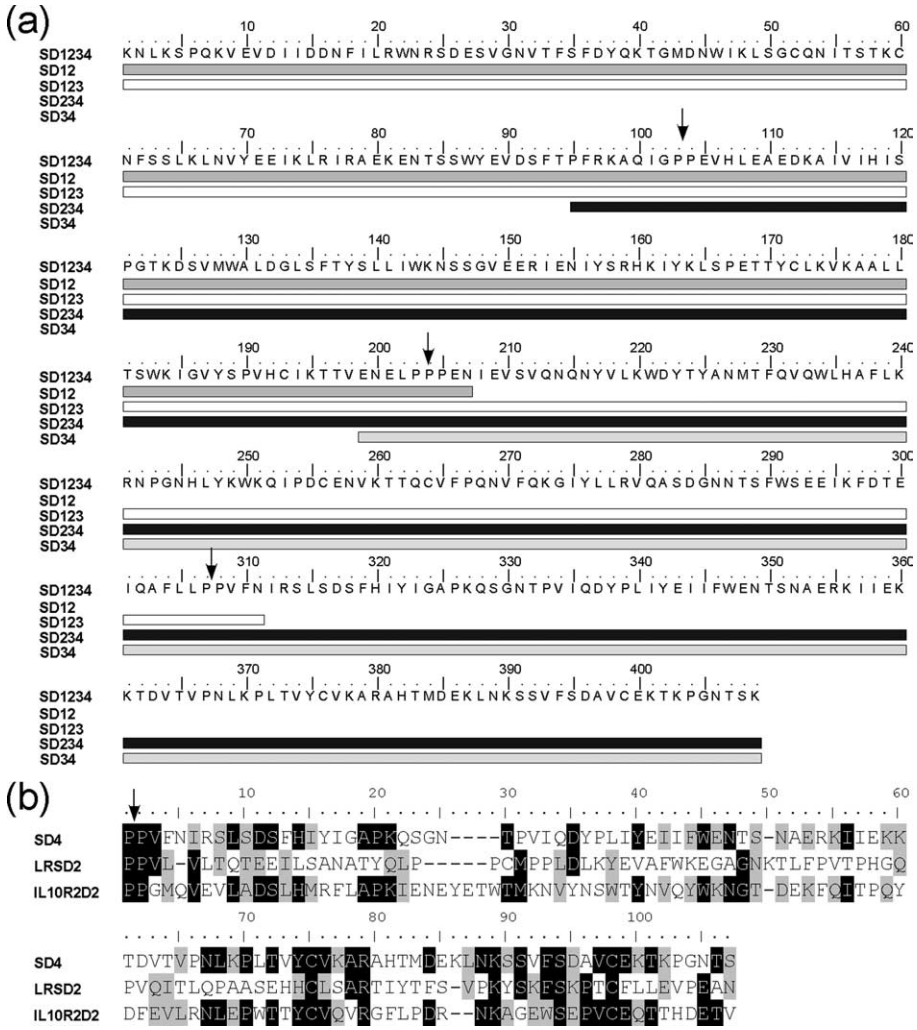

Figure 10. (a) Sequence of ifnar1-EC and the different subfragments, which were expressed and purified. The arrows indicate the three proline-rich regions of the transition between two Ig-like domains. (b) Sequence alignment of SD4 of ifnar1-EC with LRD2 and IL10R2D2.

Protein biochemistry

Proteins were deglycosylated at room temperature on an analytical scale using PNGaseF (New England Biolabs) according to the manufacturer's instructions at room temperature. Analytical size-exclusion chromatography was carried out with a Superdex 200 HR10/30 column (Amersham Biosciences) with TBS as the running buffer. Typically, 500 µl of a 2 µM protein solution was injected. For circular dichroism spectroscopy, proteins at 20 µM–40 µM concentration were extensively dialyzed against 20 mM phosphate (pH 8), 150 mM sodium fluoride. Circular dichroism spectra were recorded at 22 °C on a Jasco J-810 circular dichroism spectrometer equipped with a Jasco PTC-423S Peltier temperature control system using quartz cuvettes with 0.2 mm path lengths. The secondary structure composition was calculated using the estimation software Jasco Spectra Manager version 1.53.00.

In vitro binding assays by solid phase detection

Label-free binding assays by reflectometric interference spectroscopy (RIfS) were carried out as described[20,32] using a home-built set-up.[33] Simultaneous total internal reflection fluorescence spectroscopy (TIRFS) and reflectance interference (RIf) detection were carried out as described.[26] All measurements were carried out in HBS (20 mM Hepes (pH 7.5), 150 mM NaCl). For monitoring the interaction with IFNα2 and IFNβ, ifnar1-EC and its derivatives were immobilized onto PEG-modified surfaces using multivalent chelators for stable immobilization as described.[20,25] Excess coordination sites were blocked with decahistidine-tagged maltose-binding protein (MBP-H10) to avoid non-specific binding. Ternary complex formation was measured with ifnar2-H10 and the ifnar1-EC proteins tethered onto supported lipid bilayers *via* chelator lipids as described.[20,26] Ternary complex assembly at high receptor surface concentrations was probed by RIfS using IFNα2 as a ligand. Ternary complex assembly at low receptor surface concentrations was probed by TIRFS using ^{AF488}IFNα2 as a ligand.

Construction of plasmids encoding transmembrane ifnar1 variants

Ifnar1 cDNA (GenBank accession number NM_000629) was inserted into an expression vector after the SRα

promoter. The deletion or substitution of subdomains (SD) was carried out with a PCR-based site-directed mutagenesis kit ExSite (Stratagene). Ifnar1 deletion mutants SD123-TMCD and SD234-TMCD lack amino acid residues P307 to S408 or K1 to P104, respectively. Substitution mutant SD123-LRD2-TMCD was derived from the deletion mutant SD123-TMCD by insertion of the amino acid sequence P127 to N226 from the human IFN-λ receptor (IL28R1; GenBank accession number AAN28266), at the site of the SD4 in ifnar1 wild-type (Figure 10(b)). Amino acids P115 to V218 from the human IL10R2 (GenBank accession number AAP7216) were inserted at the same position in mutant SD123-IL10R2D2 (Figure 10(b)). Numbering of IFN-λ receptor and IL10R2 includes the leader peptide.

Cell cultures and transfection

HEK293T cells were cultured in DMEM with 10% (v/v) fetal calf serum (FCS) and transfected by the use of Lipofectamine (Invitrogen). The total amount of transfected DNA (1.22 μg/500,000 cells in 9.6 cm^2) was maintained constant with the empty expression vector. EGFP and ifnar2 expression plasmids were transfected at 1/50 and 1/12, respectively, of the total DNA. In order to get different ifnar1 expression levels, the ifnar1 plasmids were co-transfected at 1/1.1 to 1/120 of the total DNA.

FACS assays

Receptor levels at the cell surface and ligand binding was measured by fluorescence-assisted cell sorting (FACS). Cells were detached with PBS 0.5 mM EDTA 48 hours after transfection and collected in the same buffer containing 3% FCS. Cells were incubated at 6 °C in 5 nM ^{AF488}IFNα2 with or without a 30 times molar excess of unconjugated IFNα2. After 90 minutes cells were pelleted by centrifugation and fixed with 4% (v/v) paraformaldehyde (Becton Dickinson). Amplification was achieved by the binding of rabbit anti-Alexa IgG (Molecular Probes), followed by biotinylated donkey anti-rabbit (Jackson ImmunoResearch) and streptavidin-allophycocyanin conjugate (SAv-APC) (Pharmingen). Detached cells were incubated with monoclonal antibody (mAb) EA12[34] for quantification of ifnar1 or with mAb D5 for quantification of ifnar2 (both D5 and EA12 were a generous gift of from Dr L. Runkel). The signal was amplified with biotinylated rat anti-mouse IgG (Jackson ImmunoResearch) and SAv-APC. Fluorescence was measured in a FacsCalibur dual laser FACS system (BD Biosciences). EGFP fluorescence was captured in FL1 and APC fluorescence in FL4. Cells were gated for single cells by FCS and SSC and for high expression of EGFP. Results are expressed as the mean APC fluorescence of gated cells.

Acknowledgements

IFNβ (Rebif) was generously provided by Dr Garth Virgin, Serono GmbH, Unterschleißheim. We thank Christian Schlörp for experimental support, Suman Lata for providing bis-NTA chelator lipids and Dr Laura Runkel (Biogen Inc.) for the gift of anti-ifnar1 and anti-ifnar2 monoclonal antibodies. The hospitality and the support from the laboratory of Robert Tampé are gratefully acknowledged, in particular excellent technical assistance by Eckhard Linker with insect cell culture. This work was supported by grants to J.P. by the DFG (Emmy-Noether Program Pi 405/1 and SFB 628), as well as by a grant to J.P and G.U. by the Human Frontier Science Program (RGP60/2002).

Supplementary Data

Supplementary data associated with this article can be found, in the online version, at doi:10.1016/j.jmb.2005.05.008

References

1. Pestka, S., Krause, C. D. & Walter, M. R. (2004). Interferons, interferon-like cytokines, and their receptors. *Immunol. Rev.* **202**, 8–32.
2. Uze, G., Lutfalla, G. & Mogensen, K. E. (1995). Alpha and beta interferons and their receptor and their friends and relations. *J. Interferon Cytokine Res.* **15**, 3–26.
3. Abramovich, C., Shulman, L. M., Ratovitski, E., Harroch, S., Tovey, M., Eid, P. & Revel, M. (1994). Differential tyrosine phosphorylation of the IFNAR chain of the type I interferon receptor and of an associated surface protein in response to IFN-alpha and IFN-beta. *EMBO J.* **13**, 5871–5877.
4. Domanski, P., Nadeau, O. W., Platanias, L. C., Fish, E., Kellum, M., Pitha, P. & Colamonici, O. R. (1998). Differential use of the betaL subunit of the type I interferon (IFN) receptor determines signaling specificity for IFNalpha2 and IFNbeta. *J. Biol. Chem.* **273**, 3144–3147.
5. Platanias, L. C., Uddin, S., Domanski, P. & Colamonici, O. R. (1996). Differences in interferon alpha and beta signaling. Interferon beta selectively induces the interaction of the alpha and betaL subunits of the type I interferon receptor. *J. Biol. Chem.* **271**, 23630–23633.
6. Croze, E., Russell-Harde, D., Wagner, T. C., Pu, H., Pfeffer, L. M. & Perez, H. D. (1996). The human type I interferon receptor. Identification of the interferon beta-specific receptor-associated phosphoprotein. *J. Biol. Chem.* **271**, 33165–33168.
7. Mintzer, R. J., Croze, E., Rubanyi, G. M. & Johns, A. (1998). Differential effects of IFN-beta1b on the proliferation of human vascular smooth muscle and endothelial cells. *J. Interferon Cytokine Res.* **18**, 939–945.
8. Russell-Harde, D., Wagner, T. C., Perez, H. D. & Croze, E. (1999). Formation of a uniquely stable type I interferon receptor complex by interferon beta is dependent upon particular interactions between interferon beta and its receptor and independent of tyrosine phosphorylation. *Biochem. Biophys. Res. Commun.* **255**, 539–544.
9. Deonarain, R., Chan, D. C., Platanias, L. C. & Fish, E. N. (2002). Interferon-alpha/beta-receptor interactions: a complex story unfolding. *Curr. Pharm. Des.* **8**, 2131–2137.
10. Grumbach, I. M., Fish, E. N., Uddin, S., Majchrzak, B., Colamonici, O. R., Figulla, H. R. *et al*. (1999). Activation of the Jak-Stat pathway in cells that exhibit

selective sensitivity to the antiviral effects of IFN-beta compared with IFN-alpha. *J. Interferon Cytokine Res.* **19**, 797–801.
11. da Silva, A. J., Brickelmaier, M., Majeau, G. R., Lukashin, A. V., Peyman, J., Whitty, A. & Hochman, P. S. (2002). Comparison of gene expression patterns induced by treatment of human umbilical vein endothelial cells with IFN-alpha 2b vs. IFN-beta 1a: understanding the functional relationship between distinct type I interferons that act through a common receptor. *J. Interferon Cytokine Res.* **22**, 173–188.
12. Runkel, L., Pfeffer, L., Lewerenz, M., Monneron, D., Yang, C. H., Murti, A. *et al*. (1998). Differences in activity between alpha and beta type I interferons explored by mutational analysis. *J. Biol. Chem.* **273**, 8003–8008.
13. Piehler, J. & Schreiber, G. (1999). Mutational and structural analysis of the binding interface between type I interferons and their receptor ifnar2. *J. Mol. Biol.* **294**, 223–237.
14. Piehler, J., Roisman, L. C. & Schreiber, G. (2000). New structural and functional aspects of the type I interferon–receptor interaction revealed by comprehensive mutational analysis of the binding interface. *J. Biol. Chem.* **275**, 40425–40433.
15. Roisman, L. C., Piehler, J., Trosset, J. Y., Scheraga, H. A. & Schreiber, G. (2001). Structure of the interferon–receptor complex determined by distance constraints from double-mutant cycles and flexible docking. *Proc. Natl Acad. Sci. USA*, **98**, 13231–13236.
16. Chill, J. H., Quadt, S. R., Levy, R., Schreiber, G. & Anglister, J. (2003). The human type I interferon receptor. NMR structure reveals the molecular basis of ligand binding. *Structure (Camb.)*, **11**, 791–802.
17. Bazan, J. F. (1990). Structural design and molecular evolution of a cytokine receptor superfamily. *Proc. Natl Acad. Sci. USA*, **87**, 6934–6938.
18. Cohen, B., Novick, D., Barak, S. & Rubinstein, M. (1995). Ligand-induced association of the type I interferon receptor components. *Mol. Cell. Biol.* **15**, 4208–4214.
19. Arduini, R. M., Strauch, K. L., Runkel, L. A., Carlson, M. M., Hronowski, X., Foley, S. F. *et al*. (1999). Characterization of a soluble ternary complex formed between human interferon-beta-1a and its receptor chains. *Protein Sci.* **8**, 1867–1877.
20. Lamken, P., Lata, S., Gavutis, M. & Piehler, J. (2004). Ligand-induced assembling of the type I interferon receptor on supported lipid bilayers. *J. Mol. Biol.* **341**, 303–318.
21. Lu, J., Chuntharapai, A., Beck, J., Bass, S., Ow, A., De Vos, A. M. *et al*. (1998). Structure-function study of the extracellular domain of the human IFN-alpha receptor (hIFNAR1) using blocking monoclonal antibodies: the role of domains 1 and 2. *J. Immunol.* **160**, 1782–1788.
22. Goldman, L. A., Cutrone, E. C., Dang, A., Hao, X., Lim, J. K. & Langer, J. A. (1998). Mapping human interferon-alpha (IFN-alpha 2) binding determinants of the type I interferon receptor subunit IFNAR-1 with human/bovine IFNAR-1 chimeras. *Biochemistry*, **37**, 13003–13010.
23. Cutrone, E. C. & Langer, J. A. (2001). Identification of critical residues in bovine IFNAR-1 responsible for interferon binding. *J. Biol. Chem.* **276**, 17140–17148.
24. Cajean-Feroldi, C., Nosal, F., Nardeux, P. C., Gallet, X., Guymarho, J., Baychelier, F. *et al*. (2004). Identification of residues of the IFNAR1 chain of the type I human interferon receptor critical for ligand binding and biological activity. *Biochemistry*, **43**, 12498–12512.
25. Lata, S. & Piehler, J. (2005). Stable and functional immobilization of histidine-tagged proteins via multivalent chelator head-groups on a molecular poly(ethylene glycol) brush. *Anal. Chem.* **77**, 1096–1105.
26. Gavutis, M., Lata, S., Lamken, P., Müller, P. & Piehler, J. (2005). Lateral ligand–receptor interactions on membranes probed by simultaneous fluorescence-interference detection. *Biophys. J.* [doi:10.1529/biophysj.104.055855].
27. Cutrone, E. C. & Langer, J. A. (1997). Contributions of cloned type I interferon receptor subunits to differential ligand binding. *FEBS Letters*, **404**, 197–202.
28. Whitty, A., Raskin, N., Olson, D. L., Borysenko, C. W., Ambrose, C. M., Benjamin, C. D. & Burkly, L. C. (1998). Interaction affinity between cytokine receptor components on the cell surface. *Proc. Natl Acad. Sci. USA*, **95**, 13165–13170.
29. Syed, R. S., Reid, S. W., Li, C., Cheetham, J. C., Aoki, K. H., Liu, B. *et al*. (1998). Efficiency of signalling through cytokine receptors depends critically on receptor orientation. *Nature*, **395**, 511–516.
30. Stroud, R. M. & Wells, J. A. (2004). Mechanistic diversity of cytokine receptor signaling across cell membranes. *Sci. STKE 2004*, **re7**.
31. Piehler, J. & Schreiber, G. (1999). Biophysical analysis of the interaction of human ifnar2 expressed in E-coli with IFN alpha 2. *J. Mol. Biol.* **289**, 57–67.
32. Piehler, J. & Schreiber, G. (2001). Fast transient cytokine–receptor interactions monitored in real time by reflectometric interference spectroscopy. *Anal. Biochem.* **289**, 173–186.
33. Schmitt, H. M., Brecht, A., Piehler, J. & Gauglitz, G. (1997). An integrated system for optical biomolecular interaction analysis. *Biosens. Bioelectron.* **12**, 809–816.
34. Goldman, L. A., Zafari, M., Cutrone, E. C., Dang, A., Brickelmeier, M., Runkel, L. *et al*. (1999). Characterization of antihuman IFNAR-1 monoclonal antibodies: epitope localization and functional analysis. *J. Interferon Cytokine Res.* **19**, 15–26.

Edited by I. B. Holland

(Received 5 March 2005; received in revised form 29 April 2005; accepted 4 May 2005)

Paper IV

Monitoring the dynamics of ligand-receptor complexes on model membranes

Suman Lata, Martynas Gavutis, Jacob Piehler*

Goethe University Frankfurt/Main, Institute of Biochemistry, Marie-Curie-Straße 9, 60439 Frankfurt/Main, Germany

RECEIVED DATE (automatically inserted by publisher); j.piehler@em.uni-frankfurt.de

Ligand-induced receptor oligomerization has been shown to be a general principle for signal propagation across the plasma membrane common to many cell surface receptors.[1] Reduction in dimensionality upon ligand binding onto the membrane has been proposed to have important physicochemical consequences on receptor recruitment and signaling efficiency.[2-4] Therefore, elucidation of the biophysical mechanisms governing the dynamics of ligand-receptor complexes on membranes is a prerequisite for understanding and for systematic manipulation of signal activation. Owing to a lack of suitable experimental tools, however, the 2-dimensional interaction kinetics of ligand-receptor complexes with appropriately mimicked biophysical constraints including membrane anchoring and membrane fluidity has hardly been studied quantitatively. Here, we describe an *in vitro* approach for determining a 2-dimensional dissociation rate constant of a cytokine-receptor complex.

Chelator lipids incorporated into lipid bilayers have been shown to be powerful tools for tethering histidine-tagged proteins onto solid-supported membranes in an oriented and reversible fashion.[5] A drawback of the traditional chelator lipids based on a single nitrilotriacetic acid (NTA) moiety, however, is its low intrinsic affinity towards the oligohistidine-tag, leading to transient and ill-defined attachment.[6,7] Measurement of 2-dimensional interactions kinetics between membrane-anchored proteins requires stable tethering of a receptor ectodomain by a single histidine-tag, and therefore tethering through traditional chelator lipids is not appropriate.

Recently, we have reported molecularly stable tethering by multivalent chelator head groups.[8] Here, we have synthesized a lipid-analogue based on a chelator head group comprising two NTA moieties (*bis*-NTA), which binds histidine tagged proteins with multivalent interactions (Figure 1a). High mobility in the membrane was ensured by conjugating *bis*-NTA to a saturated and an unsaturated alkyl chain (octadec-9-enyl-octadecylamine). This *bis*-NTA lipid was incorporated into silica-supported, fluid lipid bilayers (Figure 1b). Thus, interactions at the bilayer surface can be studied by surface-sensitive detection while maintaining lateral mobility of proteins attached to the *bis*-NTA head group. This experimental approach was employed to explore the dynamics of ligand-induced ternary complex formation of the type I interferon (IFN) receptor. The extracellular domains of the receptor subunits ifnar1 and ifnar2 fused to a C-terminal decahistidine-tag (ifnar1-H10 and ifnar2-H10, respectively) were tethered onto solid-supported membranes (Figure 1b), and complex formation upon binding of the ligand IFNα2 was monitored in real time by fluorescence and mass-sensitive detection. The dynamics of the ternary complex in plane of the membrane was probed by a pulse-chase approach based on fluorescence resonance energy transfer (FRET) between IFNα2 and ifnar2-H10 (Figure 1c,d).

The interaction of IFNα2 with the two receptor subunits has been studied in detail earlier, and a two-step assembling mechanism was established.[10]

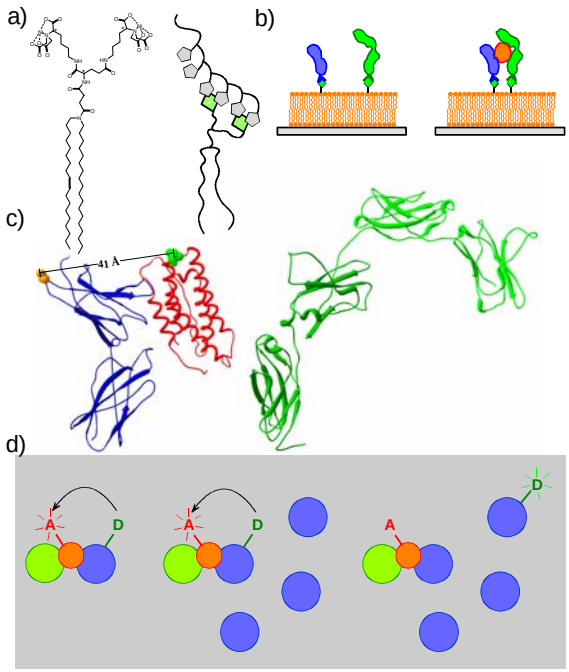

Figure 1 The chemical structure and schematic representation of *bis*-NTA lipid (a), which binds histidine-tagged proteins by multivalent interaction. b) Silica-supported lipid bilayers doped with *bis*-NTA lipid were used for stable and controllable tethering of ifnar2-H10 (blue) and ifnar1-H10 (green), and ternary complex formation was induced by binding of IFNα2 (orange). c) Structure of ifnar2-EC (blue) in complex with IFNα2 (red) and a model of ifnar1-EC (green). The residues mutated for labeling are colored in orange (ifnar2-EC) and green (IFNα2). d) Principle of surface kinetics measurements by FRET (top view onto the membrane): Donor fluorescence from ifnar2-H10 (blue) is quenched upon ternary complex formation with acceptor-labeled IFNα2 (orange) and unlabeled ifnar1-H10 (green). Upon pulse-chasing the ternary complex by tethering rapidly an excess of unlabeled ifnar2-H10 to the membrane, donor-labeled ifnar2-H10 is competed out of the complex, leading to a recovery of the donor fluorescence.

Here, ligand interaction with ifnar2-H10 was monitored by FRET using simultaneous total-internal reflection fluorescence spectroscopy and reflectance interference (TIRFS-RIf) detection.[9] The interaction of IFNα2 S136C site-specifically labeled with Cy3 (^{Cy3}IFNα2) with membrane-tethered ifnar2-H10 S35C site-specifically labeled with Alexa Fluor 488 (^{AF488}ifnar2-H10) is shown in Figure 2a. Ligand binding was detected by a drop in the donor fluorescence signal due to FRET from ^{AF488}ifnar2-H10 to

bound ^{Cy3}IFNα2. During ligand dissociation, the fluorescence signal recovered, confirming ligand-specific fluorescence quenching. As the interaction between IFNα2 and ifnar2-H10 at surfaces was shown to be strongly biased by mass transport limitation,[9] ligand dissociation unbiased by rebinding was measured by pulse-chasing the receptor-ligand complex with 1 µM non-labeled IFNα2 in solution, and by tethering an excess of non-labeled ifnar2-H10 to the surface (Figure 2b). Similar dissociation kinetics with a k_d of 0.05 ±0.005 s^{-1} was observed.

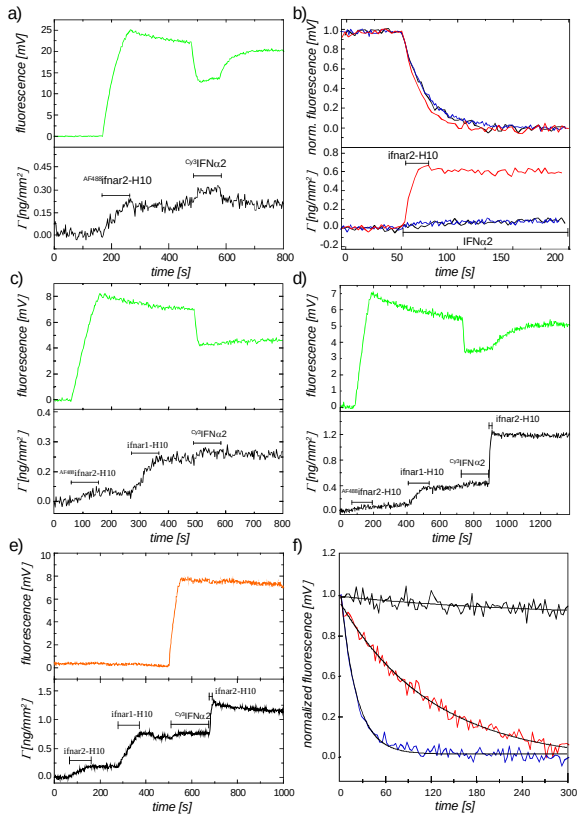

Figure 2 Surface kinetics measurements by FRET. a) Donor fluorescence detected by TIRFS (upper panel) and mass signal detected by RIf (lower panel) for tethering of ^{AF488}ifnar2-H10 (60 nM) onto lipid bilayer followed by binding of ^{Cy3}IFNα2 (100 nM). b) Dissociation of ^{Cy3}IFNα2 from ^{AF488}ifnar2-H10 upon chasing with IFNα2 (black) and upon a pulse-chase injection of ifnar2-H10 (red) as monitored by FRET (top panel: normalized fluorescence curves; bottom curves: mass deposition as detected by RIf). For comparison, the dissociation of ^{Cy3}IFNα2 from ifnar2-H10 upon chasing with IFNα2 as detected by direct excitation of Cy3 is shown. c) Interaction of ^{Cy3}IFNα2 with ^{AF488}ifnar2-H10 and ifnar1-H10 tethered in stoichiometric amounts onto the lipid bilayer as detected by donor quenching. d) Binding of ^{Cy3}IFNα2 (100 nM) to ^{AF488}ifnar2-H10 and ifnar1-H10 tethered in stoichiometric amounts onto the lipid bilayer followed by a pulse chase injection of ifnar2-H10. e) Binding of ^{Cy3}IFNα2 (detected by direct excitation of Cy3) to ifnar2-H10 and ifnar1-H10 tethered in stoichiometric amounts followed by a pulse chase injection of ifnar2-H10. f) Comparison of the exchange kinetics as detected by the pulse-chase experiment shown in d) (red) with the dissociation of ^{Cy3}IFNα2 from ^{AF488}ifnar2-H10 alone as shown in b) (blue) and the dissociation of ^{Cy3}IFNα2 from the ternary complex as shown in e) (black).

Based on the FRET between ^{Cy3}IFNα2 and ^{AF488}ifnar2-H10, the formation and the dynamics of the ternary complex with ifnar1-H10 tethered onto the bilayer were studied. Ifnar1-H10 binds IFNα2 with a very low affinity (~5 µM) and a k_d of ~1 s^{-1}.[9] Previous extensive binding studies have shown that the interaction of IFNα2 with ifnar1-H10 is independent on the interaction with ifnar2.[10] After sequentially tethering ^{AF488}ifnar2-H10 and ifnar1-H10 onto the lipid bilayer in a 1:1 molar ratio, ^{Cy3}IFNα2 was injected, and the interaction with ^{AF488}ifnar2-H10 was monitored by FRET (Figure 2c). Dissociation of the ligand was very slow compared to the interaction with ifnar2-H10 alone, which can be ascribed to the formation of a ternary complex by simultaneous interaction of IFNα2 with ifnar2-H10 and ifnar1-H10. This ternary complex, however, is in dynamic equilibrium with the binary complexes of IFNα2 with each of the receptor subunits. In order to probe the surface kinetics of the interaction with ifnar2-H10, the ternary complex was pulse-chased by tethering a 10-fold excess of non-labeled ifnar2-H10 over ^{AF488}ifnar2-H10 onto the surface within ~10 s (Figure 2d). Under these conditions, the rise in fluorescence intensity indicated ^{AF488}ifnar2-H10 dissociation from ^{Cy3}IFNα2. No ligand, however, dissociated from the surface under these conditions as confirmed in a control experiment with direct excitation of Cy3 (Figure 2e). Thus, the change in fluorescence was solely due to exchange of ^{OG488}ifnar2-H10 in the ternary complex by unlabeled ifnar2-H10, confirming the dynamic nature of the ternary complex. The kinetics monitored by donor fluorescence recovery therefore represents the dissociation kinetics of the ^{AF488}ifnar2/^{Cy3}IFNα2 complex in plane of the membrane. Strikingly, significantly slower dissociation was observed under these conditions with a k_d of 0.012 ± 0.003 s^{-1} (Figure 2f). The reasons for the slower dissociation could be slower diffusion of the proteins in the membrane, the reduced degree of freedom affecting the reaction coordinate or cooperative interaction with ifnar1-H10. Further studies are required to resolve this issue decisively.

The substantial effect of protein tethering to the membrane on the dissociation kinetics, however, highlights the key importance of mimicking the properties of the membrane for studying ligand-receptor dynamics. Here, we have succeeded to directly determine the dissociation rate constant of an important cytokine-receptor complex in plane of the membrane. The novel, high-affinity *bis*-NTA lipid provided the key prerequisites of such an endeavor: stable tethering of the proteins to the membrane in an oriented manner, and the possibility to rapidly change the receptor surface concentration. In combination with powerful surface-sensitive techniques for controlling and probing interaction this provides means for experimentally addressing the role of lateral interaction at the membrane in signaling processes.

Ackknowledgement. We thank Robert Tampé for hosting and supporting our group. This work was supported by the DFG within the Emmy-Noether program for young investigators (Pi 405/1) and the research grant Pi 405/2, and by the BMBF (0312005A).

Supporting information available: Description of the synthesis of the *bis*-NTA lipid, description of the binding assays.

References

(1) Ullrich, A.; Schlessinger, J. *Cell* **1990**, *61*, 203-212.
(2) Adam, G.; Delbruck, M. In *Structural Chemistry and Molecular Biology*; Davidson, N., Ed.; W. H. Freeman and Company, 1968, pp 198-215.
(3) DeLisi, C. *Q Rev Biophys* **1980**, *13*, 201-230.
(4) Axelrod, D.; Wang, M. D. *Biophys J* **1994**, *66*, 588-600.
(5) Busch, K.; Tampe, R. *J Biotechnol* **2001**, *82*, 3-24.
(6) Dorn, I. T.; Neumaier, K. R.; Tampe, R. *Journal of the American Chemical Society* **1998**, *120*, 2753-2763.
(7) Lata, S.; Piehler, J. *Anal Chem* **2005**, *77*, 1096 -1105.
(8) Lata, S.; Reichel, A.; Brock, R.; Tampé, R.; Piehler, J. *J Am Chem Soc* **2005**, ASAP. DOI: 10.1021/ja050690c
(9) Gavutis, M.; Lata, S.; Lamken, P.; Müller, P.; Piehler, J. *Biophys J* **2005**, *88*, 4289-4302.
(10) Lamken, P.; Lata, S.; Gavutis, M.; Piehler, J. *J Mol Biol* **2004**, *341*, 303-318.

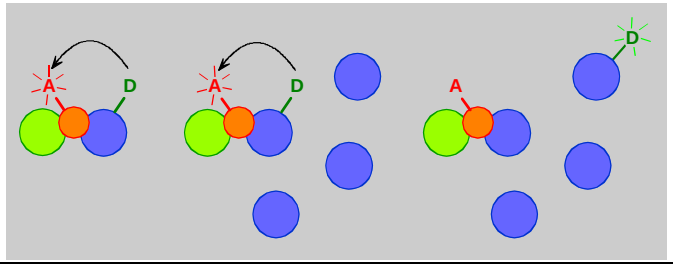

Abstract. Ligand-induced cross-linking of cell surface receptors is a basic paradigm of signal activation by many transmembrane receptors. After ligand binding, the receptor complexes formed on the membrane are dynamically maintained by 2-dimensional protein-protein interactions on the membrane. The biophysical principles governing the dynamics of such interactions have not been understood, mainly because measurement of lateral interactions on membranes so far has not been experimentally addressed. Here, we describe a generic approach for measuring 2-dimensional dissociation rate constants *in vitro* using a novel high-affinity chelator lipid for reconstituting a ternary cytokine-receptor complex on solid-supported membranes. While monitoring the interaction between the ligand and one of the receptor subunits on the membrane by fluorescence resonance energy transfer, the equilibrium on the surface was perturbed by rapidly tethering a large excess of the unlabeled receptor subunit. Exchange of labeled by un-labeled protein in the ternary complex was detected as a recovery of the donor quenching. Since the dissociation of the ligand-receptor complex in plane of the membrane was the rate-limiting step under these conditions, the 2-dimensional rate constant of this process was determined. Strikingly, the 2-dimensional dissociation was much slower than ligand dissociation into solution, suggesting that membrane tethering significantly affects the dissociation process. This result highlights the importance of studying ligand-receptor complexes tethered to membranes for understanding the principles governing signal activation by ligand-induced receptor assembling.

Paper V

Determination of the 2-dimensional interaction rate constants of a cytokine receptor complex

Martynas Gavutis, Eva Jaks, Peter Lamken, Jacob Piehler*

*Corresponding author:
Institute of Biochemistry, Biocenter N210
Johann Wolfgang Goethe-University
Marie-Curie-Straße 9
60439 Frankfurt am Main
Phone: +49 (0)69 79829468
Fax: +49 (0)69 798294695
E-mail: j.piehler@em.uni-frankfurt.de

Keywords

Reduction of dimensionality; solid-supported lipid bilayer; protein-protein interaction; type I interferon receptor; total internal reflection fluorescence spectroscopy; reflectance interference.

Abbreviations

FRET, fluorescence resonance energy transfer; ifnar, type I interferon receptor; IFN, type I interferon; RIf reflectance interferometry; TIRFS, total internal reflection fluorescence spectroscopy; EC, ectodomain; H10, decahistidine-tag; tl, tag-less.

Abstract

Ligand-receptor interactions within the plane of the plasma membrane play a pivotal role for transmembrane signaling. The biophysical principles of protein-protein interactions on lipid bilayers, though, have hardly been experimentally addressed. We have dissected the interactions involved in ternary complex formation by ligand-induced cross-linking of the subunits of the type I interferon (IFN) receptor ifnar1 and ifnar2 *in vitro*. The extracellular domains ifnar1-EC and ifnar2-EC were tethered in an oriented manner on solid-supported lipid bilayers. The interactions of IFNα2 and several mutants, which exhibit different association and dissociation rate constants towards ifnar1-EC and ifnar2-EC, were monitored by simultaneous label-free detection and surface-sensitive fluorescence spectroscopy. Surface dissociation rate constants were determined by measuring ligand exchange kinetics, and by measuring receptor exchange on the surface by fluorescence resonance energy transfer. Strikingly, approximately 3-times lower dissociation rate constants were observed for both receptor subunits compared to the dissociation in solution. Based on these directly determined surface dissociation rate constants, the surface association rate constants were assessed by probing ligand dissociation at different relative surface concentrations of the receptor subunits. In contrast to the interaction in solution, the association rate constants depended on the orientation of the receptor components. Furthermore, the large differences in association kinetics observed in solution were not detectable on the surface. Based on these results, the key roles of orientation and lateral diffusion on the kinetics of protein interactions in plane of the membrane are discussed.

Introduction

Protein-protein interactions within the plane of cellular membranes play a key role for many biological processes and in particular for transmembrane signaling. These lateral interactions are not static and are typically triggered or stabilized by interactions with further interaction partners such as ligands, effectors and binding proteins from the matrices adjacent to the lipid bilayers. A prominent example is the ligand-induced cross-linking of receptor tyrosine kinases (1,2) and cytokine receptors (3), where 2-dimensional interaction between receptor subunits have been recognized to be important for regulating signaling (4-7). The fundamental importance of such coupled interactions for cell-surface receptor activation has stimulated numerous theoretical studies (8-13). The underlying concept of these models is the reduction in dimensionality upon ligand binding to a membrane anchored receptor (14). The binding of ligands to individual surface receptors can be determined by standard techniques, and rate constants and equilibrium constants are measured in the same units as for interaction in solution. In the second step, however, lateral interactions take place in the plane of the membrane, i.e. in two instead of three space dimensions. For several reasons, the kinetic parameters of these interactions cannot be readily deduced from the rate constants of the same interaction in solution: (i) Anchoring of the proteins into the membrane reduces the translational and rotational freedom, and results in a preferred orientation of the interaction partners to each other along the normal of the surface. Hence, the reaction diagram and the reaction coordinate of the interaction are different from the interaction in solution. (ii) Lateral and rotational diffusion of the membrane-anchored protein is much slower than in solution, while the dynamics of the amino acid side chains mediating the interaction between the proteins are not affected. The consequences of these constraints have been subject of numerous speculations and theoretical consideration, but to date only very few semi-quantitative (4) or quantitative (15,16) experimental approaches towards characterizing 2-dimensional interactions on membranes have been reported.

Recently, we have reported an experimental approach for reconstituting and analyzing membrane-anchored proteins on solid-supported lipid bilayers. The extracellular receptor domains of the type I interferon (IFN) receptor subunits ifnar1 (ifnar1-EC) and ifnar2 (ifnar2-EC) were tethered in an oriented manner onto solid-supported lipid bilayers providing well-defined and homogeneous diffusion kinetics. The interaction of the membrane-anchored receptor subunits with the ligand IFNα2 was studied by using simultaneous surface-sensitive fluorescence and interference detection (17). This approach enables to monitor and vary the concentrations of the receptor subunits on the lipid bilayer, and the absolute surface concentrations can be quantified. A rigorous analysis of all possible interactions between the three partners established ternary complex formation by independent interaction of ifnar1 and ifnar2 with the ligand IFNα2 (17,18). A general mechanism describing the two possible pathways of ternary complex formation and dissociation is depicted in Figure 1. Altogether, 4 separate interactions have to be considered: two of them (described by K_1 and K_4) involve ligand binding from solution to the surface receptor subunits. The affinity of IFNα2 towards ifnar2-EC (K_1: 5 nM) is about three orders of magnitude higher than the affinity towards ifnar1-EC (K_4: ~5µM) (18). In contrast, the interactions of the binary complexes on the surface with the second receptor subunits (described by K_2 and K_3) are 2-dimensional interactions. Despite its inherent 3-body complexity, several striking features make this interaction a particularly suitable system for studying surface interactions: First, the receptor subunits interact independent from each other with the ligand, and do not interact with each other as proposed for other cytokine receptors. Second, only a heterodimeric ternary complex was detectably involving ifnar2-EC, ifnar1-EC and IFNα2 in a 1:1:1 stoichiometry. Thus, the surface interaction is triggered by a ligand binding from solution and the equilibria K_2 and K_3

between binary and ternary complex on the surface K_2 and K_3 can be probed by the dissociation kinetics of the ligand from the surface (17). Since receptor surface concentrations can be absolutely quantified in the reconstituted system, this provides the means for determining the equilibrium dissociation constants of these 2-dimensional interactions.

Because ligand binding to ifnar2-EC (k_1) is at least 10-times faster than to ifnar1-EC (k_4), pathway 1 has been assumed to be substantially favored both for formation and for the dissociation of the ternary complex at stoichiometric surface concentrations of the receptor subunits. For an IFNα2 mutant with reduced k_1, however, pathway 2 has been proposed to considerably contribute, which may hold true also for other members of the type I IFN family (17). Here, we have employed the features of this system to explore the biophysical principles governing protein interactions in plane of biological membranes. By using different chasing and pulse-chasing assays, as well as IFN-mutants with different affinities and different association and dissociation rate constants of the interaction with ifnar1-EC and ifnar2-EC, each of the 2-dimensional rate constants of the two interaction pathway depicted in Figure 1 were determined. Furthermore, the role of electrostatic rate enhancement and the relative orientation of the receptor subunits on the surface association rate constants were investigated. Based on these data, we compare the determinants of protein interaction kinetics in 3 and 2 dimensions.

Materials and Methods

Protein expression and purification

IFNα2, IFNα2 HEQ, ifnar2-EC with a C-terminal decahistidine-tag (ifnar2-H10), ifnar2-H10 I47A and tag-less ifnar2-EC (ifnar2-tl) were expressed in Escherichia coli, refolded from inclusion bodies and purified by anion-exchange and size-exclusion chromatography as described (19). For site-specific labeling, an additional cysteine was introduced by the mutations S136C (IFNα2) and S35C (ifnar2-H10). These proteins were expressed, refolded and purified as the wild-type proteins. After size exclusion chromatography, these proteins were incubated with a 3-fold excess of Alexa Fluor 488 (AF488) maleimide or Oregon Green 488 (OG488) maleimide as FRET donors, and Alexa Fluor 568 (AF568) maleimide as an FRET acceptor (all from Molecular Probes, Eugene, OR). After the labeling reaction, the proteins were further purified by anion exchange chromatography. Binding experiments confirmed that the interaction properties of both proteins were not affected by mutagenesis or labeling. Ifnar1-EC with a C-terminal decahistidine tag (Ifnar1-H10) and with a N-terminal decahistidine tag (H10-ifnar1) were expressed in Sf9 insect cells, and purified from the supernatant by immobilized metal affinity chromatography followed by size exclusion chromatography as described earlier (20).

Simultaneous fluorescence interference detection

Two dimensional interactions were detected with a home-built set-up for simultaneous reflectance interferometry (RIf) and total internal reflection fluorescence spectroscopy (TIRFS) detection as described previously in more detail (17). An argon ion laser was used for fluorescence excitation at 488 nm at an excitation power of 2–3 µW focused onto an area of 1 mm² in order to minimize photo-bleaching. Fluorescence was collected by an optical fiber and detected by a photomultiplier tube through bandpass filters. FRET measurements with donor and acceptor fluorescence detection were carried out by changing the emission filters by means of a filter wheel. Mass deposition onto the surface was monitored simultaneously by RIf detection at 800 nm. Both TIRFS and RIf were acquired with a time resolution of 1.2-1.5 s. Sample handling was carried out in a flow-through format using a

syringe pump as described (21). With this system, flow rates between 1 and 500µl/s can be employed. Sample handling and data acquisition were controlled with software written in LabVIEW (National Instruments).

Lipid bilayer assembling, receptor reconstitution and binding assays

The transducer surface was incubated for 30 min in a freshly prepared mixture of two parts 30% (v/v) hydrogen peroxide and three parts concentrated sulfuric acid. After extensive washing with water, the transducer was dried in a nitrogen stream and mounted immediately into the flow cell. Solid supported lipid bilayers were prepared by fusion of small unilamelar vesicles (SUVs) obtained by probe sonication. Synthetic stearoyl-oleoyl phosphatidylcholine (SOPC, Avanti Polar Lipids, Alabaster, AL) lipids were doped with 5 mol% lipid containing *bis*-NTA chelator head (17). The unsaturated alkyl chain of both matrix and chelator lipid prevented phase segregation and ensured bilayer fluidity.

All binding studies were carried out with 20 mM HEPES, pH 7.5, and 150 mM NaCl as the running buffer. Solid-supported lipid bilayers were obtained by injecting SUVs at a lipid concentration of 250 µM on the surface of the transducer. Protein immobilization and binding assays were in principle carried out as described earlier (18). For tethering the histidine-tagged proteins to the supported membranes, the chelator head groups were loaded with Ni^{2+} ions by injecting 10 mM nickel(II)chloride in the running buffer for 150 s and conditioned by a 150 s injection of 200 mM imidazole. Depending on the targeted surface concentrations, the his-tagged proteins were sequentially injected at concentrations between 2 nM and 1 µM for 20–60 s. The ligand was then injected at a concentration of 50 nM for 150-300 s with a flow rate of 1 µl/s, followed by a buffer wash with 10 µl/s or injection of 2 µM ifnar2-tl, 1 µM IFNα2 or 1 µM IFNα2 HEQ at a flow rate of 1µl/s for 300-450 s. For pulse-chase experiments 1µM ifnar2-H10 was injected for 20 s, followed by a buffer wash with a flow rate of 10µl/s. After a set of ligand binding experiments, all attached proteins were removed by a 150 s pulse of 200 mM imidazole, and the subsequent binding assays were carried out on the same lipid bilayer.

Data evaluation

Binding curves were analyzed using Origin (Microcal Software, Northampton, MA) or Berkeley Madonna (UCB, Berkeley, CA) software packages. If necessary, RIf curves were corrected for a linear drift based on the signals before tethering the proteins and after regeneration with imidazole. Two different models were used to evaluate ligand dissociation curves. Dissociation rate constants were obtained by fitting a mono-exponential function:

$$R(t) = R_0 \cdot e^{-k_d \cdot (t - t_0)} \qquad \text{(Equation 1)}$$

2-dimensional association rate constants were determined by fitting a two step dissociation model describing one of the two pathways shown in Figure 1 as in principle described before (17). For determination of k_2 (pathway 1), the following set of differential equations was fitted:

$$\begin{aligned} \frac{d[T]}{dt} &= k_2 \cdot [B2] \cdot ([R1]_0 - [T]) - k_{-2} \cdot [T] \\ \frac{d[B2]}{dt} &= -k_2 \cdot [B2] \cdot ([R1]_0 - [T]) + k_{-2} \cdot [T] - k_{-1} \cdot [B2] \\ [S] &= [T] + [B2], \text{with } T_{t=0} = [R1]_0, [B2]_{t=0} = 0 \end{aligned} \qquad \text{(Equation 2)}$$

For determination of k_3 (pathway 2), the following set of differential equations was fitted:

$$\frac{d[T]}{dt} = k_3 \cdot [B1] \cdot ([R2]_0 - [T]) - k_{-3} \cdot [T]$$
$$\frac{d[B1]}{dt} = -k_3 \cdot [B1] \cdot ([R2]_0 - [T]) + k_{-3} \cdot [T] - k_{-4} \cdot [B1] \quad \text{(Equation 3)}$$
$$[S] = [T] + [B1], \text{ with } T_{t=0} = [R2]_0, [B1]_{t=0} = 0$$

$[R1]_0$ and $[R2]_0$ were initial surface concentrations of ifnar1-EC and ifnar2-EC, respectively, which were determined from the RIf signals. [S] was the total surface concentration of the ligand, which was detected in a time-resolved manner by the TIRFS signal and converted into a absolute surface concentration using a calibration by RIf. The 2-dimensional dissociation rate constants k_{-2} and k_{-3}, respectively, were determined independently by chasing experiments. The respective 2-dimensional association rate constant was the only parameter varied in the fitting procedure.

Simulations

Ligand dissociation kinetics through both pathways was numerically simulated using the following set of differential equations:

$$\frac{d[T]}{dt} = k_2 \cdot [B2] \cdot ([R1]_0 - [T] - [B1]) - k_{-2} \cdot [T] + k_3 \cdot ([B1] \cdot ([R2]_0 - [T] - [B2]) - k_{-3} \cdot [T])$$
$$\frac{d[B2]}{dt} = -k_2 \cdot [B2] \cdot ([R1]_0 - [T] - [B1]) + k_{-2} \cdot [T] - k_{-1} \cdot [B2]$$
$$\frac{d[B1]}{dt} = -k_3 \cdot [B1] \cdot ([R2]_0 - [T] - [B2]) + k_{-3} \cdot [T] - k_{-4} \cdot [B1]$$
$$\frac{d[p1]}{dt} = k_{-1} \cdot [B2], \frac{d[p2]}{dt} = k_{-4} \cdot [B1] \quad \text{(Equation 4)}$$
$$[S] = \frac{[T] + [B2] + [B1]}{[T]_{t=0}}$$

with the initial conditions: $[T]_{t=0} = 2\,\text{fmol/mm}^2, [B2]_{t=0} = 0, [B1]_{t=0} = 0$. For the total surface concentrations of the receptor subunits, 2 or 22 fmol/mm² were assumed.

The populations of pathway 1 and pathway 2 were simulated according to the equations

$$path1 = \frac{[T]_{t=0} - p1}{[T]_{t=0}}$$
$$path2 = \frac{[T]_{t=0} - p2}{[T]_{t=0}} \quad \text{(Equation 5)}$$

Results

The interaction kinetics of ifnar2-EC and ifnar1-EC with IFNα2 has been previously studied in detail, and numerous mutants with different interaction rate constants have been described (18,22-25). Here, we used several mutants of IFNα2 and ifnar2-EC, as well as different variants of ifnar1-EC. The rate constants of the mutants applied for further characterization of the 2-dimensional interaction involved in ternary complex formation were verified by ligand binding assays with the site-specifically fluorescence labeled IFNα2 species using TIRFS detection (Table 1).

Pathways of receptor assembling and dissociation

IFN-induced two-step assembling and dissociation of the ternary complex with ifnar1-EC and ifnar2-EC can occur by two different pathways (Figure 1). For the interaction of IFNα2 with ifnar2-EC and ifnar1-EC at stoichiometric concentration, pathway 1 has been considered to determine both complex formation and dissociation, because of the faster association rate constant k_1 compared to k_4 (17). This holds obviously true for the complex formation, since ligand binding from solution is the rate-limiting step of the assembling process (17), which is ~10-fold faster to ifnar2-EC than to ifnar1-EC. Dissociation of the ternary complex, however, is determined by the 2-dimensional rate constants k_2, k_{-2}, k_3 and k_{-3}, which have been assumed to scale relatively as the corresponding rate constants in solution. This assumption was qualitatively tested by rapidly changing the receptor surface concentration after formation of a stoichiometric ternary complex (Figure 2). Ifnar1-EC and ifnar2-EC carrying a C-terminal decahistidine-tag (ifnar1-H10 and ifnar2-H10) were site-specifically tethered in stoichiometric concentrations onto silica-supported lipid bilayers doped with *bis*-NTA lipids. The dissociation kinetics of fluorescence-labeled IFNα2 (^{AF488}IFNα2) was monitored before and after tethering additional ifnar1-H10 onto the membrane (Figure 2B, C). As expected, slower ligand dissociation kinetics was observed upon loading additional ifnar1-H10, indicating a shift of the equilibrium K_2 towards the ternary complex (cf. Figure 1). Surprisingly, however, a similar effect was observed when the ifnar2-H10 surface concentration was rapidly increased under the same conditions (Figure 2D, E). Since only pathway 2 depends on the surface concentration of ifnar2, this result indicates that this pathway is significantly involved in the dissociation of the ternary complex. Properly describing the receptor dynamics therefore requires dissection of all four 2-dimensional rate constants involved in ternary complex formation.

2-dimensional dissociation kinetics measured by FRET

The dissociation rate constant of the 2-dimensional interaction between ifnar2-H10 and the IFNα2 complexed by ifnar1-H10 was directly measured using a pulse chase approach, which is schematically depicted in Figure 3A. After ternary complex formation of ^{AF568}IFNα2 with ^{AF488}ifnar2-H10 and ifnar1-H10, a substantial excess of unlabeled ifnar2-H10 was rapidly tethered onto the membrane, and the exchange of ^{AF488}ifnar2-H10 from ternary complex with unlabeled ifnar2-H10 was monitored by the decaying FRET between ^{AF568}IFNα2 and ^{AF488}ifnar2-H10. A typical experiment is shown in Figure 3B. Donor fluorescence from ^{AF488}ifnar2-H10 was quenched upon ternary complex formation with acceptor-labeled ^{AF568}IFNα2, which was accompanied by an increase in sensitized fluorescence. During rinsing, slow recovery of the donor fluorescence and likewise and decay of the acceptor fluorescence due to ligand dissociation was observed. Upon pulse-chasing the ternary complex by rapidly tethering an excess of unlabeled ifnar2-H10 onto the membrane, much faster recovery of the donor fluorescence and decay of the acceptor fluorescence where

observed. Under these conditions, ligand dissociation was hardly detectable (Figure 3C and Figure 2D), confirming that indeed the kinetics of the exchange of ^{AF488}ifnar2-H10 against unlabelled ifnar2-H10 on the surface was monitored by FRET. The normalized traces for donor and acceptor fluorescence were in excellent agreement (Figure 3C). The rate constant of this exchange is determined by the 2-dimensional dissociation rate constant of the ifnar2-H10/IFNα2 complex k_{-3}, which is the rate-limiting step in this process. The rate constants obtained by a mono-exponential fit to the two FRET signals were in good agreement and an average k_{-3} of 0.007 ± 0.001 s^{-1} was determined from multiple experiments at different receptor surface concentrations. Strikingly, k_{-3} is ~3-times lower than the k_{-1} of 0.02 s^{-1} for the dissociation of IFNα2 from ifnar2-H10 into solution (cf. Figure 3C and Table 1). Extensive ligand binding studies with the soluble receptors domains have excluded cooperative binding of the receptor subunits to IFNα2. Thus, the difference between k_{-1} and k_{-3} results from anchoring the complex onto the membrane.

Determination of 2-dimensional rate constants by ligand chasing

In order to confirm this effect on the dissociation kinetics, the 2-dimensional dissociation rate constants were assessed by ligand chasing experiments. The principle of this assay is depicted in Figure 4A. Here, a high excess of ifnar1-EC compared to ifnar2-H10 was tethered onto the membrane, and the ternary complex was formed by injecting ^{AF488}IFNα2. The excess of ifnar1-H10 remained free due to the low affinity of wild-type IFNα2 to ifnar1-H10 and its fast dissociation from ifnar1-H10 (k_d: ~1 s^{-1}). By injection of 1 µM unlabeled IFNα2 HEQ, which binds to ifnar1-H10 with 20-fold higher affinity (25), these free ifnar1-EC molecules are rapidly saturated with ligand. The labeled ligand in the ternary complex is first exchanged against unlabeled IFNα2 HEQ by 2-dimensional dissociation of the ifnar2-H10/IFNα2 interaction, followed by dissociation from excess ifnar1-H10 into solution (cf. Figure 4A). Because of the fast dissociation of labeled IFNα2 from excess ifnar1-H10 into solution, the rate-limiting step of this exchange process is the dissociation of the ifnar1-H10/IFNα2 complex from ifnar2-H10, which is again the 2-dimensional dissociation rate constant k_{-3}. A typical course of such an experiment is shown in Figure 4B. After tethering the receptor subunits in appropriate surface concentrations, ^{AF488}IFNα2 was injected and spontaneous dissociation was monitored. Fast dissociation from excess ifnar1-H10 within a few seconds was followed by very slow dissociation (comparable to the ligand dissociation kinetics in Figure 2A after loading excess of ifnar1-H10). The same injection of ^{AF488}IFNα2 was repeated, but ligand dissociation was monitored in presence of tag-less ifnar2-EC (ifnar2-tl) in order to suppress mass-transport dependent rebinding (26,27), which has to be considered at these receptor surface concentrations. After the third injection of ^{AF488}IFNα2, unlabeled IFNα2 HEQ was injected and the exchange kinetics was monitored. Rapid saturation of the excess ifnar1-H10 by binding of IFNα2 HEQ was verified by the RIf signal. The normalized dissociation curves are compared in Figure 4C with the ligand dissociation from ifnar2-H10 into solution. Again, substantially slower 2-dimensional dissociation of ifnar2-H10 from IFNα2 bound to ifnar1-H10 was observed compared to the 3-dimensional dissociation. A rate constant k_{-3} of $(0.0044 \pm 0.001)^{s-1}$ was obtained, which is in good agreement with the value obtained by pulse-chasing with ifnar2-H10.

From the spontaneous ligand dissociation kinetics, the 2-dimensional association rate constant was determined, assuming that dissociation through pathway 1 can be neglected at this high excess of ifnar1-EC. Since spontaneous dissociation was indeed biased by rebinding (Figure 4C), the dissociation curve in presence of 2 µM ifnar2-tl was used. A 2-step dissociation model (equation 3) was fitted taking into account the appropriate 2- and 3-dimensional rate constants k_{-3} and k_{-4}, respectively, as well as the surface concentration of

ifnar2-H10 as quantified from the RIf signal. A 2-dimensional association rate constant k_3 of 3.3×10^{16} $mm^2mol^{-1}s^{-1}$ was obtained from the fit. Thus, a 2-dimensional equilibrium dissociation constant (K_3) of 0.004 fmol/mm² or 2.3 molecules/µm² was obtained for the IFNα2/ifnar2 interaction.

The same experiment was carried out with the ifnar2-H10 mutant I47A, which binds IFNα2 with ten-fold lower affinity, but with the same association rate constant. Much faster spontaneous ligand dissociation from the ternary complex was observed at similar receptor surface concentrations used for wt ifnar2-H10 (Figure 4D). Upon chasing with IFNα2 HEQ, the labeled ligand was exchanged within a few 10 seconds. Comparison of 2- and 3-dimensional dissociation kinetics (Figure 4E), however, again yielded a ~2-fold lower rate constant for the interaction in plane of the membrane ($k_{-3} = 0.11s^{-1}$) compared to the dissociation of the ligand from the surface ($k_{-1} = 0.2s^{-1}$). In contrast, the 2-dimensional association rate constant k_{-3} obtained from fitting the spontaneous dissociation kinetics with a 2-step dissociation model (Equation 3) was 2.8×10^{16} $mm^2mol^{-1}s^{-1}$, i.e. very similar to the k_3 obtained for the interaction of IFNα2 with wild-type ifnar2-H10 interaction. These consistent results confirmed that the surface dissociation kinetics is affected by tethering the receptor subunits to the membrane, and the robustness of the experimental approach to determine 2-dimensional rate constants.

The 2-dimensional interaction involved in pathway 2 was furthermore characterized by applying the IFNα2 mutant R144A (data not shown), which binds ifnar2-H10 with a 10-fold lower association rate constant than wild-type IFNα2 (cf. Table 1). Again, ~3-times slower dissociation in plane of the membrane ($k_{-3} = 0.012s^{-1}$) was observed compared to the dissociation from the surface ($k_{-1} = 0.044s^{-1}$). More importantly, however, a slower 2-dimensional association rate constant ($k_3 = 9.1\times10^{15}$ $mm^2mol^{-1}s^{-1}$) was obtained, which was ~3-fold slower than the 2-dimensional association rate constant of wild-type IFNα2. Thus, the 10-fold difference of the k_a in solution was not maintained on the membrane surface, suggesting that the slower diffusion on the membrane may affect association kinetics.

The 2-dimensional rate constants of pathway 1

In order to determine the 2-dimensional rate constants of the interaction between ifnar1-H10 and IFNα2 in the ternary complex we studied the ligand dissociation pathway 1 by a similar set of experiments. In order to ensure that 2-dimensional dissociation is rate limiting, ifnar2-H10 I47A was used in combination with IFNα2 HEQ, which dissociates from ifnar1-EC with a rate constant of 0.05 s^{-1}. The ligand chasing experiment were carried out at an excess of ifnar2-H10 I47A, and wild-type IFNα2 was used for chasing (Figure 5A). A typical experiment is shown Figure 5B: After formation of the ternary complex with ^{AF488}IFNα2 HEQ, spontaneous dissociation was monitored in presence of 2 µM ifnar2-tl to suppress rebinding of the ligand. After a second injection of ^{AF488}IFNα2 HEQ, ligand exchange in presence of unlabeled wild-type IFNα2 was monitored. In Figure 5C, the dissociation kinetics in plane of the membrane is compared with the dissociation from the surface. Again, significantly lower dissociation rate constant was obtained for 2-dimensional dissociation (k_{-2}: $0.026s^{-1}$) was observed compared to the dissociation into solution (k_{-4}: $0.047s^{-1}$). Based on this 2-dimensional dissociation rate constant, the spontaneous ligand dissociation kinetics was fitted by a 2-step model (Equation 2). A 2-dimensional association rate constant of 1.3×10^{16} $mm^2mol^{-1}s^{-1}$ was obtained for the interaction of IFNα2 HEQ with ifnar1-H10 (k_2). These measurements were also carried out with different combinations of wild-type and mutant IFNα2 and ifnar2-H10. All results are summarized in Table 2. In all combinations, similar values of $\sim1\times10^{16}$ $mm^2mol^{-1}s^{-1}$ were obtained for k_2, very similar to the k_3 obtained for IFNα2 R144A. Interestingly, also the 3-dimensional association rate constants k_1 and k_4 are

very similar for this mutant (cf. Table 1). Furthermore, a ~2.5-fold lower k_{-2} compared to k_2 was confirmed for all combinations, confirming the decrease in the dissociation rate constant by tethering the complex onto the surface. Based on these consistent observations, we estimated a k_{-2} of 0.4 s^{-1} for wild-type IFNα2.

The role of orientation in 2-dimensional interactions

Orientation and flexibility of membrane-anchored proteins have been suggested to be key parameters in the kinetics of 2-dimensional interactions on membranes. In order to study the role of orientation on ternary complex formation, we tethered ifnar1-EC through an N-terminal decahistidine tag (H10-ifnar1) onto the membrane. For this protein, very similar rate constants as for ifnar1-H10 were obtained by conventional ligand binding assays (Table 1). The 2-dimensional rate constants were determined using ligand chasing experiments as described above. The results are summarized in Table 2. No significant effect on the surface dissociation rate constants k_{-2} and k_{-3} was observed upon changing the orientation of ifnar1-EC. The effect on the 2-dimensional association rate constants, however, was substantial: for k_2 (pathway 1), a ~3-fold decrease was observed compared to the rate constant obtained with ifnar1-H10. For k_3 (pathway 2), the effect was even stronger with a ~5-fold decrease compared to the rate constant obtained with ifnar1-H10. Thus, we could demonstrate the key role of receptor orientation on surface association kinetics and affinity by mimicking oriented attachment to the membrane *in vitro*.

Population of the dissociation pathways

Based on the experimentally determined rate constants, the population of the two dissociation pathways was compared at experimentally relevant receptor surface concentrations by numerically simulating ligand dissociation (Equation 4 and 5). The ligand dissociation curves for both pathways together and individually are compared for the wild-type proteins and two mutants in Figure 6. At stoichiometric concentration of the receptor subunits, pathway 1 is clearly dominant in case of the wt proteins (Figure 6A), and also for ifnar2-I47A (Figure 6B). However, a substantial contribution of pathway 2 to ligand dissociation is observed, which is in line with the only ~3-fold higher 2-dimensional association rate k_3 compared to k_2. For IFNα2 R144A ($k_3 \approx k_2$), both pathways are similarly populated at stoichiometric receptor concentrations, confirming the key role of the relative surface 2-dimensional association rate constants on the dissociation pathway. At 10-fold excess of ifnar2 or ifnar1, only pathway 1 or pathway 2, respectively, is responsible for ligand dissociation.

Discussion

Cellular signaling by cytokine receptors is initiated by ligand-mediated cross-linking of two or more receptor subunits. Thus, the 2-dimensional interactions between the ligand and its cognate receptor subunits determine the dynamics of the receptor complex on the plasma membrane, which has been proposed to play a critical role for signaling and its regulation . Here, we have for the first time parameterized the rate constants of a ternary cytokine-receptor complex on model membranes. By exchange experiments based on chasing the ternary complex with additional receptor or ligand, we succeeded to reliably determine the 2-dimensional dissociation rate constants. The two possible pathways were studied separately by using excess concentrations of one of the receptor subunits. Based on several mutants and variants of the interacting proteins, the effect of different rate constants and protein orientation on the complex dynamics was studied. Thus, we have identified several critical features of 2-dimensional interactions on membrans, which cannot be readily concluded from solution binding assays. The first surprising observation was that the dissociation rate constants were generally 2-3-fold lower for the interaction in plane of the membrane

compared to the interaction in solution. This difference was not due to cooperative binding of the receptor subunits, which was confirmed by extensive ligand binding studies. Surface anchoring limits the degree of freedom, which may affect the reaction coordinate, but the dissociation kinetics in plane of the membrane was hardly significantly affected by the orientation of ifnar1-EC. The environment of the interaction interface is not affected by membrane anchoring, but the separation of the interaction partners by lateral diffusion, is ~100-fold slower on the membrane than in solution, which may account for the slower dissociation. Furthermore, more efficient rebinding of the membrane-anchored proteins prior to full dissociation may be caused by reducing rotational freedom. The first explanation implies that the dynamics of ligand-receptor complexes may depend on the diffusion properties of the receptor in the membrane, which are known to be locally rather variable due to the microdomain structure of the plasma membrane. By partitioning of receptor complexes in microdomains with low fluidity such as caveolae, which has been reported for several tyrosine kinases and cytokine receptors (28,29) including ifnar (30), the stability of oligomeric complexes would be substantially enhanced. This could be a simple mechanism for increasing receptor recruitment efficiency at low receptor surface concentration. However, more detailed analysis of the dependence of the 2-dimensional k_d on membrane fluidity would be required, as well as confirmation for other ligand-receptor complexes.

Assessment of the association rate constants in plane of the membrane and towards the receptor subunits revealed further striking features of interactions on membranes. More than 10-fold faster association of IFNα2 with ifnar2 compared to ifnar1-EC suggested that pathway 1 dominates both formation and dissociation of the ternary complex. On the membrane, though, a less than 3-fold difference in the 2-dimensional association rate constants was observed. For the IFNα2 mutant R144A, which binds to ifnar2-EC with a 10-fold lower association rate constant than wild-type IFNα2, similar 2-dimensional association rate constants were obtained for both pathways. It was shown earlier that the association kinetics of IFNα2 to ifnar2 is accelerated by electrostatic attraction (19). Electrostatic association rate enhancement has been explained by a stabilization of the encounter complex and by steering of the proteins into appropriate orientations (31-34). Our results suggest that this electrostatic rate enhancement is not as effective on the membrane. This could be ascribed to changed electrostatic properties by tethering the interacting proteins onto the membrane. Another reason could be that the association kinetics is limited by the slower diffusion on the membrane. While electrostatic steering did not seem to be as important as in solution, receptor orientation was shown to strongly affect the 2-dimensional association rate constants. Interestingly, even more similar values were observed for both k_2 and k_3 upon tethering ifnar1-EC through the N-terminus. Compared to the rate constants obtained with ifnar1-EC tethered in its natural orientation both k_2 and k_3 were substantially decreased. Orientation has been proposed to play a key role for 2-dimensional interactions on membranes (35); the strong effect, though, is somewhat surprising because tethering through the histidine tag to the membrane is expected to provide substantial flexibility, which should counteract pre-orientation. Furthermore, ifnar1-EC comprising four Ig-like domains is probably rather flexible in itself. However, our results suggest that steering of association by oriented anchoring in the membrane is more critical for 2-dimensional association kinetics than electrostatic steering. We have shown here that membrane anchoring through histidines can in principle mimic some determinant of ligand-receptor interaction on membranes. The importance of lateral diffusion kinetics, orientation and flexibility underscore the importance of assessing transmembrane proteins interactions under conditions, which mimic the properties of membrane anchoring even more appropriately.

Acknowledgement

This project was supported by the DFG (Pi 405/1, Pi 405/2 and SFB 628), and by the HSFP (RGP60/2002). The plasmid for expression of IFNα2 HEQ was obtained from Dr. Gideon Schreiber, Rehovot. The hospitality and the support from the laboratory of Robert Tampé are gratefully acknowledged.

References

1. Schlessinger J. 1988. Signal transduction by allosteric receptor oligomerization. Trends Biochem Sci 13(11):443-7.
2. Ullrich A, Schlessinger J. 1990. Signal transduction by receptors with tyrosine kinase activity. Cell 61(2):203-12.
3. Cunningham BC, Ultsch M, De Vos AM, Mulkerrin MG, Clauser KR, Wells JA. 1991. Dimerization of the extracellular domain of the human growth hormone receptor by a single hormone molecule. Science 254(5033):821-5.
4. Whitty A, Raskin N, Olson DL, Borysenko CW, Ambrose CM, Benjamin CD, Burkly LC. 1998. Interaction affinity between cytokine receptor components on the cell surface. Proc Natl Acad Sci U S A 95(22):13165-70.
5. Schlessinger J. 2000. Cell signaling by receptor tyrosine kinases. Cell 103(2):211-25.
6. Sebald W, Mueller TD. 2003. The interaction of BMP-7 and ActRII implicates a new mode of receptor assembly. Trends Biochem Sci 28(10):518-21.
7. Stroud RM, Wells JA. 2004. Mechanistic diversity of cytokine receptor signaling across cell membranes. Sci STKE 2004(231):re7.
8. DeLisi C, Chabay R. 1979. The influence of cell surface receptor clustering on the thermodynamics of ligand binding and the kinetics of its dissociation. Cell Biophys 1(2):117-31.
9. DeLisi C. 1981. The effect of cell size and receptor density on ligand--receptor reaction rate constants. Mol Immunol 18(6):507-11.
10. McCloskey MA, Poo MM. 1986. Rates of membrane-associated reactions: reduction of dimensionality revisited. J Cell Biol 102(1):88-96.
11. Axelrod D, Wang MD. 1994. Reduction-of-dimensionality kinetics at reaction-limited cell surface receptors. Biophys J 66(3 Pt 1):588-600.
12. Kholodenko BN, Hoek JB, Westerhoff HV. 2000. Why cytoplasmic signalling proteins should be recruited to cell membranes. Trends Cell Biol 10(5):173-8.
13. Perelson AS, Delisi C. 1980. Receptor Clustering on a Cell-Surface .1. Theory of Receptor Cross-Linking by Ligands Bearing 2 Chemically Identical Functional-Groups. Mathematical Biosciences 48(1-2):71-110.
14. Adam G, Delbruck M. 1968. Reduction of dimensionality in biological diffusion processes. In: Davidson N, editor. Structural Chemistry and Molecular Biology: W. H. Freeman and Company. p 198-215.
15. Dustin ML, Ferguson LM, Chan PY, Springer TA, Golan DE. 1996. Visualization of CD2 interaction with LFA-3 and determination of the two-dimensional dissociation constant for adhesion receptors in a contact area. J Cell Biol 132(3):465-74.
16. Yang T, Baryshnikova OK, Mao H, Holden MA, Cremer PS. 2003. Investigations of bivalent antibody binding on fluid-supported phospholipid membranes: the effect of hapten density. J Am Chem Soc 125(16):4779-84.
17. Gavutis M, Lata S, Lamken P, Müller P, Piehler J. 2005. Lateral ligand-receptor interactions on membranes probed by simultaneous fluorescence-interference detection. Biophys J 88(6):4289-302.
18. Lamken P, Lata S, Gavutis M, Piehler J. 2004. Ligand-induced assembling of the type I interferon receptor on supported lipid bilayers. J Mol Biol 341(1):303-18.

19. Piehler J, Schreiber G. 1999. Biophysical analysis of the interaction of human ifnar2 expressed in E-coli with IFN alpha 2. Journal of Molecular Biology 289(1):57-67.
20. Lamken P, Gavutis M, Peters I, Van der Heyden J, Uze G, Piehler J. 2005. Functional cartography of the extracellular domain of the type I interferon receptor subunit ifnar1. Journal of Molecular Biology 350(3):476-88.
21. Piehler J, Schreiber G. 2001. Fast transient cytokine-receptor interactions monitored in real time by reflectometric interference spectroscopy. Analytical Biochemistry 289(2):173-186.
22. Piehler J, Roisman LC, Schreiber G. 2000. New structural and functional aspects of the type I interferon- receptor interaction revealed by comprehensive mutational analysis of the binding interface. Journal of Biological Chemistry 275(51):40425-40433.
23. Piehler J, Schreiber G. 1999. Mutational and structural analysis of the binding interface between type I interferons and their receptor ifnar2. Journal of Molecular Biology 294(1):223-237.
24. Roisman LC, Jaitin D, Baker DP, Schreiber G. 2005. Mutational analysis of the IFNAR1 binding site on IFNalpha2 reveals the architecture of a weak ligand-receptor binding-site. submitted.
25. Jaitin D, Roisman LC, Jaks E, Gavutis M, Piehler J, Van der Heyden J, Uze G, Schreiber G. 2005. An IFNalpha2 mutant endowed with highly enhanced binding affinity to IFNAR1 is functionally similar to IFNbeta. submitted.
26. Schuck P, Minton AP. 1996. Analysis of mass transport-limited binding kinetics in evanescent wave biosensors. Anal Biochem 240(2):262-72.
27. Schuck P. 1996. Kinetics of ligand binding to receptor immobilized in a polymer matrix, as detected with an evanescent wave biosensor. I. A computer simulation of the influence of mass transport. Biophys J 70(3):1230-49.
28. Le Roy C, Wrana JL. 2005. Clathrin- and non-clathrin-mediated endocytic regulation of cell signalling. Nat Rev Mol Cell Biol 6(2):112-26.
29. Rao R, Logan B, Forrest K, Roszman TL, Goebel J. 2004. Lipid rafts in cytokine signaling. Cytokine Growth Factor Rev 15(2-3):103-10.
30. Takaoka A, Mitani Y, Suemori H, Sato M, Yokochi T, Noguchi S, Tanaka N, Taniguchi T. 2000. Cross talk between interferon-gamma and -alpha/beta signaling components in caveolar membrane domains. Science 288(5475):2357-60.
31. Schreiber G, Fersht AR. 1996. Rapid, electrostatically assisted association of proteins. Nat Struct Biol 3(5):427-31.
32. Sheinerman FB, Norel R, Honig B. 2000. Electrostatic aspects of protein-protein interactions. Curr Opin Struct Biol 10(2):153-9.
33. Selzer T, Schreiber G. 2001. New insights into the mechanism of protein-protein association. Proteins 45(3):190-8.
34. Schreiber G. 2002. Kinetic studies of protein-protein interactions. Curr Opin Struct Biol 12(1):41-7.
35. Berg OG. 1985. Orientation constraints in diffusion-limited macromolecular association. The role of surface diffusion as a rate-enhancing mechanism. Biophys J 47(1):1-14.

Tables

Table 1 Parameters of the individual interactions between IFNα2 and the receptor subunits.

IFNα2	Ifnar2-H10			Ifnar2-H10 I47A			Ifnar1-H10/H10-ifnar1		
	k_a (k_1) [$M^{-1}s^{-1}$]	k_d (k_{-1}) [s^{-1}]	K_D (K_1) nM	k_a (k_1) [$M^{-1}s^{-1}$]	k_d (k_{-1}) [s^{-1}]	K_D (K_1) nM	k_a (k_4) [$M^{-1}s^{-1}$]	k_d (k_{-4}) [s^{-1}]	K_D (K_1) nM
wt	3×10^6	0.02	7	3×10^6	0.2	70	2×10^5	1	5000
R144A	3×10^5	0.044	150	3×10^5	0.5	1700	2×10^5	1	5000
HEQ	3×10^6	0.02	7	3×10^6	0.2	70	2×10^5	0.05	250

In brackets, the identifier of the constants as introduced in Figure 1 are given. All IFNα2 species were site-specifically fluorescence labeled with OG488 or AF488 by incorporating the additional mutation S136C.

Table 2 2-dimensional interaction rate constants determined for different combinations of receptor and ligand variants

	Pathway 1			Pathway 2		
Ifnar2-H10/IFNα2/ ifnar1-EC	k_2 [$mm^2fmol^{-1}s^{-1}$]	k_{-2} [s^{-1}]	K_2 [$fmol/mm^2$]	k_3 [$mm^2fmol^{-1}s^{-1}$]	k_{-3} [s^{-1}]	K_3 [$fmol/mm^2$]
I47A/wt/C-term [a]	16.5 ± 3.3	~0.4 [c]	0.024	28.2 ± 5.1	0.11 ± 0.02	0.004
I47A/R144A/C-term [a]	9.6±2.0	~0.4 [c]	0.042	11.3±2.2	0.2±0.02	0.018
wt/R144A/C-term [a]	9.1 ± 1.8	~0.4 [c]	0.044	9.1±2.0	0.012±0.001	0.0013
wt/wt/C-term [a]				33±5.5	0.0044±0.001	0.00013
wt/HEQ/C-term [a]					0.004	
I47A/HEQ/C-term [a]	13.1±2.8	0.026±0.002	0.002			
wt/wt/N-term [b]				5.2±1.2	0.007±0.002	0.0014
I47A/wt/N-term [b]	4.0 ± 0.8	~0.4[c]	0.100	5.0±1.0	0.070±0.005	0.014
I47A/HEQ/N-term [b]	4.0 ± 0.9	0.033±0.004	0.008			

[a] ifnar1-EC tethered to the membrane by a C-terminal H10-tag. [b] ifnar1-EC tethered to the membrane by a N-terminal H10-tag; [c] estimated by comparison with IFNα2 HEQ.

Legends to figures

Figure 1 Schematic of the dynamic equilibria of solution and surface interactions involved in the 2-step formation and dissociation of the ternary IFN-receptor complex on a membrane (details in the text).

Figure 2 Relevance of the two possible dissociation pathways of the ternary complex. (A) Schematic of the experiments: ternary complex on fluid lipid membrane was formed by sequential tethering of ifnar2-H10 (1) and ifnar1-H10 (2) in stoichiometric amounts, followed by binding ^{AF488}IFNα2 to form the ternary complex (3). After the second injection of ^{AF488}IFNα2, additional ifnar1-H10 (top) or ifnar2-H10 (bottom) was rapidly tethered onto the membrane, and dissociation was monitored (4). (B) Course of a typical experiment as monitored by simultaneous TIRFS (top) and RIf (bottom) detection with addition loading of ifnar1-H10. (C) Overlay of ligand dissociation curves with (red) and without (black) free ifnar1-H10 on the membrane. (D) Course of a typical experiment as monitored by simultaneous TIRFS (top) and RIf (bottom) detection with addition loading of ifnar2-H10. (E) Overlay of ligand dissociation curves with (red) and without (black) free ifnar2-H10 on the membrane.

Figure 3 Monitoring 2-dimensional dissociation kinetics by pulse-chasing the ternary complex. (A) Principle of surface dissociation rate constant determination as detected by FRET: The ternary complex on fluid lipid membrane is formed by sequential injection of ^{AF488}ifnar2-H10 (1), ifnar1-H10 (2) and ^{AF568}IFNα2 (3). Equilibrium is then perturbed by rapidly tethering an excess of non-labeled ifnar2-H10 onto the membrane (4), which exchanges the labeled ifnar2-H10 in the ternary complex (5). (B) Course of a typical experiment monitoring donor fluorescence (green) and acceptor (red trace) fluorescence by TIRFS and the mass loading by RIf (black). (C) Comparison of the surface dissociation rates from donor (green) and acceptor (red) channels with the dissociation of ^{AF568}IFNα2 from ifnar2-H10 alone (blue). A control experiment carried out the same way, but with unlabeled ifnar2-H10 in (1) and with direct excitation of ^{AF568}IFNα2 confirmed negligible ligand dissociation from the surface (black). The residuals from monoexponential curve fits are shown in the bottom.

Figure 4 Determination of 2-dimensional dissociation rate constants by ligand chasing. (A) Schematic of the assay: Ternary complex on fluid lipid membrane was formed by sequential injection of ifnar2-H10 (1), a large excess of ifnar1-H10 (2) and ^{AF488}IFNα2 (3). The excess of ifnar1 was then loaded with an unlabeled competitor (4), which binds ifnar1 with high affinity (IFNα2 HEQ) and exchanged the labeled ligand in the ternary complex (5). (B) Typical experiment carried out with the wild-type proteins as detected by TIRFS (green) and by RIf (black). After the second injection of ^{AF488}IFNα2, 2 µM ifnar2-tl was injected to eliminate rebinding. After the third injection of ^{AF488}IFNα2, 1 µM unlabeled IFNα2 HEQ was injected. (C) Overlay of the normalized ^{AF488}IFNα2 dissociation curves from B: spontaneous dissociation during washing with buffer (black) and with 2µM ifnar2-tl (red), as well as dissociation while chasing with IFNα2 HEQ (green). Dissociation from

ifnar2-H10 alone is shown for comparison (blue). The residuals from the curve fits are shown in the bottom. (D) Same experiment as in B carried out with ifnar2-H10 I47A. (E) Overlay of the dissociation curves from D (same color coding as in C) with comparison of ^{AF488}IFNα2 dissociation from ifnar2-H10 I47A alone (blue). The residuals from the curve fits are shown in the bottom.

Figure 5 Determination of 2-dimensional rate constants for pathway 1. (A) Schematic of the assay: ternary complex on fluid lipid membrane was formed by sequential injection of ifnar1-H10 (1), excess ifnar2-H10 I47A (2) and ^{AF488}IFNα2 HEQ (3). Upon loading the excess binding sites of ifnar2-H10 with unlabeled IFNα2 (4), labeled IFNα2 in the ternary complex was exchanged (5). (B) Course of a typical experiment as detected by TIRFS (green) and RIf (black). During spontaneous ligand dissociation, 2 μM ifnar2-tl was maintained in the background in order to eliminate rebinding. After the second injection of ^{AF488}IFNα2 HEQ 1 μM unlabeled IFNα2-wild-type was injected. (C) Overlay of the normalized dissociation curves: spontaneous dissociation from the ternary complex (red) and ligand exchange kinetics washing with 1μM IFNα2 HEQ (green). Dissociation from Ifnar1-H10 alone is shown for comparison (blue). The residuals from the curve fits are shown in the bottom.

Figure 6 Population of the dissociation pathways under different conditions. Ligand dissociation was numerically simulated based on the experimentally determined 2- and 3-dimensional rate constants for the following species of ifnar2/IFNα2/ifnar1: wt/wt/wt (A); I47A/wt/wt (B); wt/R144A/wt (C). In all cases, 2 fmol/mm² of both ifnar2 and ifnar1 were assumed to form ternary complex under three different condition: no excess of either of the receptor subunits (top panel), with an excess of 20 fmol/mm² ifnar1 (middle panel), and with an excess of 20 fmol/mm² ifnar2 (bottom panel).

Figures

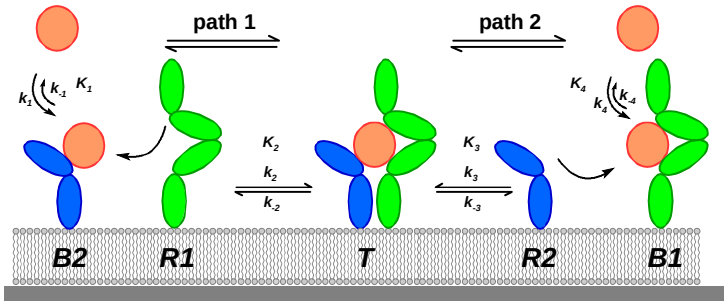

Figure 1

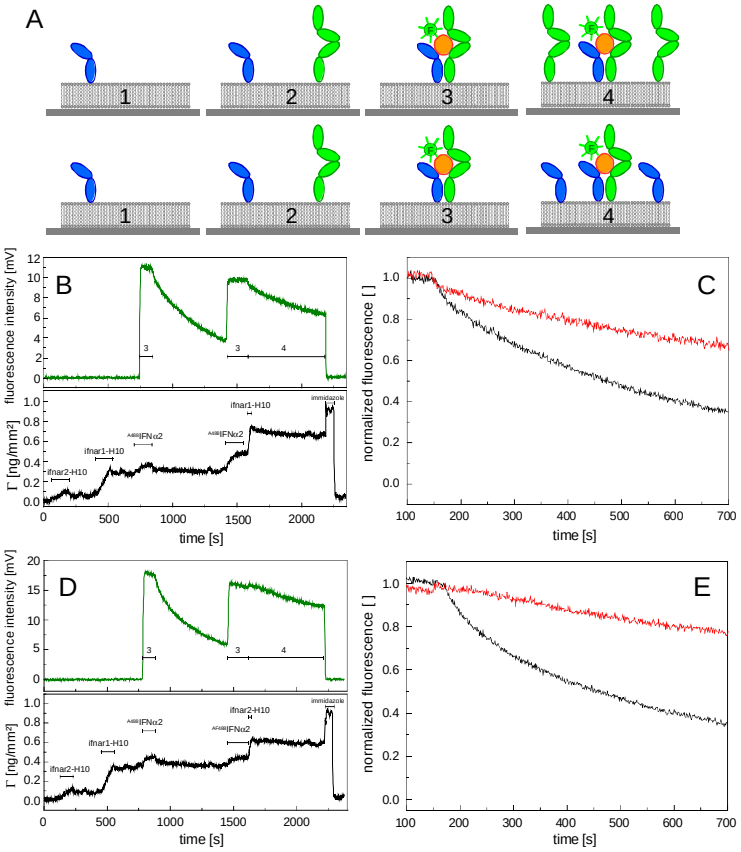

Figure 2

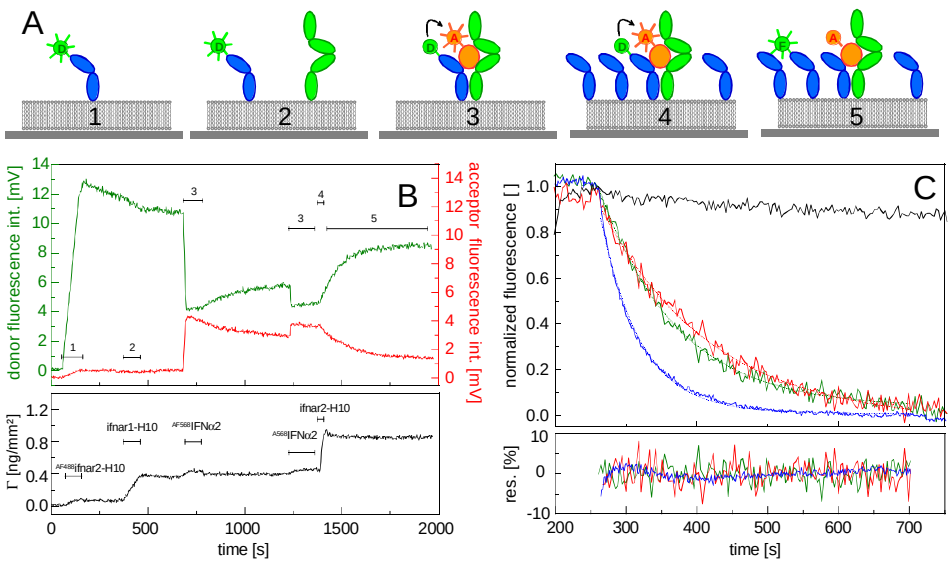

Figure 3

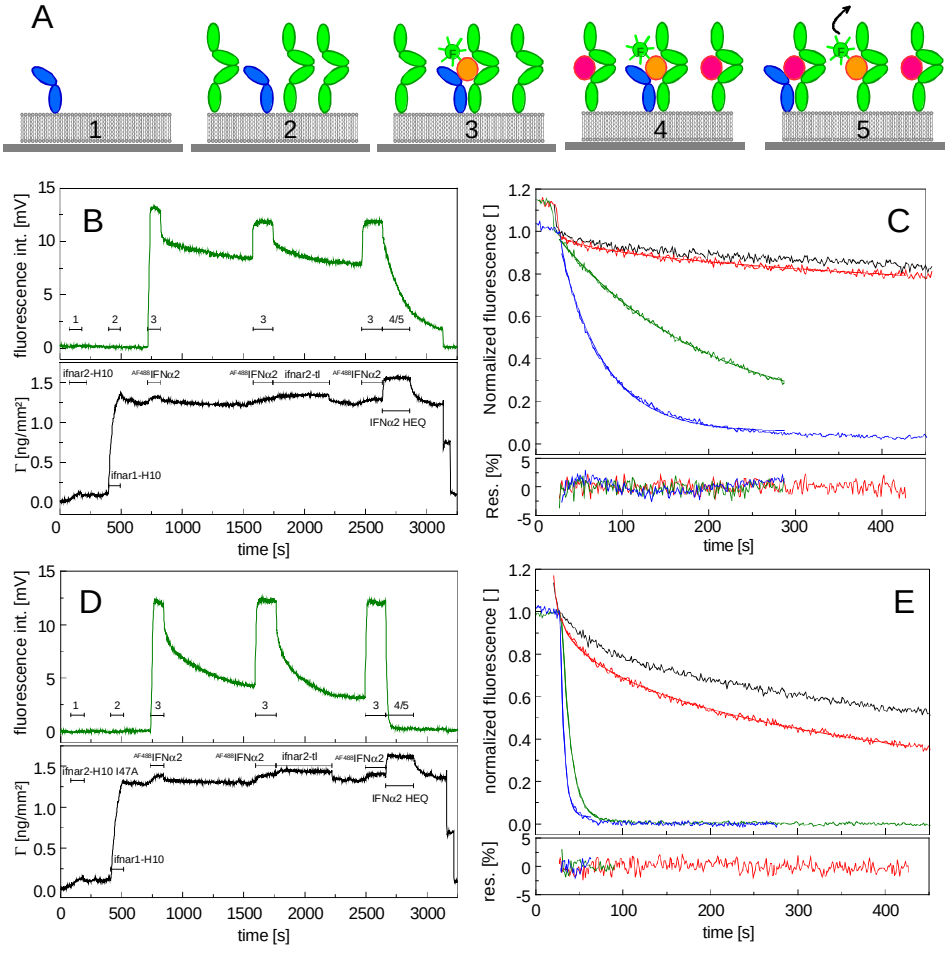

Figure 4

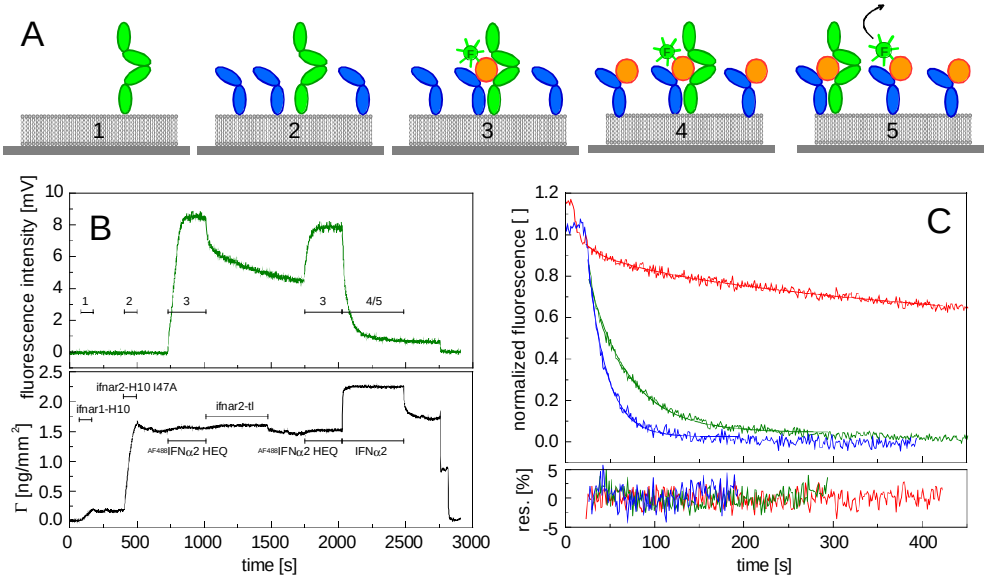

Figure 5

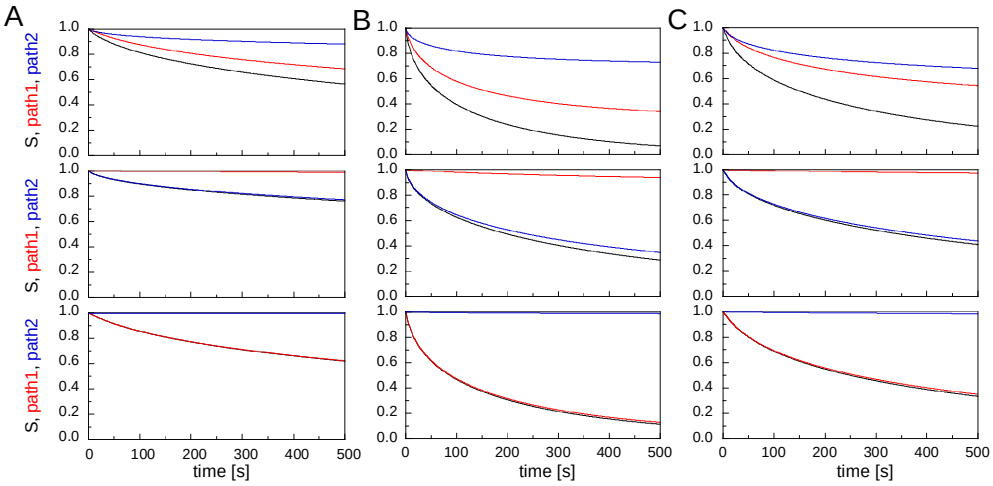

Figure 6